THE VALIDATION AND IMPROVEMENT OF ROUTE-BASED ROAD WEATHER FORECASTS

by

DAVID STUART HAMMOND

A thesis submitted to
The University of Birmingham
for the degree of
DOCTOR OF PHILOSOPHY

School of Geography, Earth & Environmental Sciences
The University of Birmingham
January 2011

ABSTRACT

This thesis aims to develop the foundations for a new validation strategy for route-based road weather forecasts that will enable validation of route-based models at a vastly improved spatial and temporal resolution, and in doing so provide a tool for rapid appraisal of new model parameterisations. A validation strategy that uses clustering techniques to create clusters of forecast points with similar geographical and infrastructure characteristics is presented, as well as two methodologies for de-parameterising key geographical and infrastructure parameters in the *ENTICE* route-based model that are currently not measured at the spatial scale demanded by a route-based forecast. The proposed validation strategy facilitates the analysis of forecast statistics at the cluster level, which is shown to provide a more representative measure of the model's spatial forecasting ability. The majority of thermal variations around the study route are well represented by the clustering solutions, presenting the opportunity for new sampling strategies with the potential to validate forecasts at a vastly improved spatial and temporal resolution. De-parameterisation of the road construction and surface roughness parameters within the *ENTICE* model using Ground Penetrating Radar and airborne LIDAR data has been shown to significantly improve the spatial forecasting ability of *ENTICE*, with the model changes leading to refinement of the clustering solution which enables it to better capture the physical relationship between road surface temperature and the geographical and infrastructure parameters around the study route. Suggestions for future research are provided along with a blueprint for the future of route-based road weather forecasts.

ACKNOWLEDGMENTS

Firstly, I must acknowledge the financial support of Weather Services International and the University of Birmingham for funding this project. This thesis is in many ways a continuation of the work started by Dr Lee Chapman over a decade ago, whose supervision, advice and friendship over the past 3 years has been greatly appreciated. A big thank you must also go to Professor John E. Thornes for his supervision over the past 6 years including the KTP project with Campbell Scientific. I've now been associated with the University of Birmingham for 7 years, firstly as an MSc student, then as a KTP research associate, and finally as a doctoral researcher, and over this time I've made many new friends. A big thank you to all the friends I've had the pleasure of knowing during my years at Birmingham.

A few people at Birmingham who deserve a special mention include Richard Johnson for his expert workmanship in designing a mobile infrared sensor mount out of a bike rack, Jill Crossman for assisting with GPR data collection (at very short notice!) and Kevin Burkhill for his continual assistance with drawings. Thank you also to the editors and anonymous referees involved in the peer review of papers submitted from this thesis, whose comments and suggestions for improvement have helped to refine this final work.

During the writing of this thesis many hours were spent working at home, and special thanks have to go to Max for the many afternoon walks which came as a welcome distraction. Finally, thank you to my wife, Laura, whose constant support over the past 3 years has not gone unnoticed.

10 January 2011

CONTENTS PAGE

LIST OF FIGURES

LIST OF TABLES

LIST OF ABBREVIATIONS AND SYMBOLS

AADT	Annual Average Daily Traffic
ANOVA	Analysis of Variance
BADC	British Atmospheric Data Centre
CSC	Clustering Similarity Coefficients
DEM	Digital Elevation Model
DSM	Digital Surface Model
DTM	Digital Terrain Model
ESA	European Space Agency
EWMA	Exponentially Weighted Moving Average
FHWA	Federal Highway Administration
FSL	Forecast Systems Laboratory
GIS	Geographical Information System
GPD	Geographical Parameter Database
GPR	Ground Penetrating Radar
GPRS	General Packet Radio Service
GPS	Global Positioning System
GSM	Global System for Mobile Communications
IP	Internet Protocol
LIDAR	Light Detection and Ranging
MDSS	Maintenance Decision Support System
METRo	Model of the Environment and Temperature of the Roads
MIDAS	Motorway Incident Detection and Automatic Signalling
MORST	Met Office Road Surface Temperature Model
NWP	Numerical Weather Prediction
PCA	Principal Components Analysis
RCTM	Road Condition and Treatment Module
RMSE	Root Mean Square Error
RST	Road Surface Temperature
RWFS	Road Weather Forecast System
RWIS	Road Weather Information System
SD	Standard Deviation
TM	Thermal Mapping
TSC	Traffic Similarity Coefficients
UK	United Kingdom

US	United States
USB	Universal Serial Bus
VDT	Vehicle Data Translator
VFM	View Factor Mapping
VII	Vehicle Integrated Infrastructure
XML	Extensible Markup Language
β	Bias
σ_β	Standard deviation of bias
ε	Surface emissivity
ε_{sky}	Effective emissivity of the sky
ρ	Air density
Γ	Dry adiabatic lapse rate
α	Albedo
a	Adiabatic exchange coefficient
σ	Stefan Boltzmann constant
ψ_s	Sky view factor
c	Speed of light in free space (m s^{-1})
C	Heat capacity of air
cal cm^{-1} sec^{-1} °C	Calorie (IT) per centimetre per second per degree Celsius
d	Thermal diffusivity
d'	Bulk adiabatic diffusivity
d_i	Thickness of ith layer
$\varepsilon_{r,i}$	Dielectric constant of ith layer
E	Surface energy flux
H	Sensible heat flux to air
I_{net}	Net rate of loss of energy
k	von Kármán constant
K_s	Thermal conductivity of soil
LE	Latent heat flux
L	Latent heat of evaporation
MHz	Megahertz
ns	Nanosecond
P_m	Percentage of modelled values within ±1°C of actual values
P_{rm}	Percentage of residual modelled values within ±1°C of residual actual values
Q_{FV}	Waste heat from vehicles
Q	Beam radiation

q	Diffuse radiation
q_2	Absolute humidity at Z_2
q_0	Surface wetness
R^2	Coefficient of determination
R_i	Richardson number
R_n	Net Radiation
S	Heat flux to soil
T_{sky}	Sky Temperature
T_0	Surface Temperature
T_{sky}	Radiation temperature of sky hemisphere
t_i	Two-way travel time
μm	Micrometre
U	Wind speed (m s^{-1})
u_*	Friction velocity (m s^{-1})
Z_0	Roughness Length
Z_0^{eff}	Effective Roughness Length
Z_2	Height of air thermal damping depth
Z_s	Thermal damping depth of soil

MATHEMATICAL DESCRIPTION OF *ENTICE* ROUTE-BASED FORECAST STATISTICS

ENTICE Route-based forecast Bias (β) is calculated as follows:

$$\beta = \frac{1}{n}\sum_{i=1}^{n}(Tm_i - Ta_i)$$

where Tm_i is the modelled temperature at the *i*th forecast point, Ta_i the actual surface temperature at the *i*th forecast point obtained from thermal mapping data, and *n* is the total number of forecast points along the study route (2261) or within a cluster (variable) dependent on whether entire route or cluster statistic.

ENTICE Route-based forecast standard deviation of Bias (σ_β) is calculated as follows:

$$\sigma_\beta = \sqrt{\frac{1}{n}\sum_{i=1}^{n}\left((Tm_i - Ta_i) - \frac{\sum_{i=1}^{n}(Tm_i - Ta_i)}{n}\right)^2}$$

where Tm_i is the modelled temperature at the *i*th forecast point, Ta_i the actual surface temperature at the *i*th forecast point obtained from thermal mapping data, and *n* is the total number of forecast points along the study route (2261) or within a cluster (variable) dependent on whether entire route or cluster statistic.

ENTICE root mean square error (*RMSE*) is calculated as follows:

$$RMSE = \sqrt{\frac{1}{n}\sum_{i=1}^{n}(Tm_i - Ta_i)^2}$$

where Tm_i is the modelled temperature at the *i*th forecast point, Ta_i the actual surface temperature at the *i*th forecast point obtained from thermal mapping data, and *n* is the total number of forecast points along the study route (2261) or within a cluster (variable) dependent on whether entire route or cluster statistic.

Percentage of *ENTICE* modelled values within ± 1°C of actual values (*Pm*) is calculated as follows:

For $i = 1{:}n$

If

$$|Tm_i - Ta_i| \leq 1$$

Then

$$N_i = 1$$

Else

$$N_i = 0$$

End If

$$Pm = \sum_{i=1}^{n} \frac{N_i}{n} \times 100$$

where Tm_i is the modelled temperature at the *i*th forecast point, Ta_i the actual temperature at the *i*th forecast point obtained from thermal mapping data, and *n* is the total number of forecast points around the study route (2261) or within a cluster (variable) dependent on whether entire route or cluster statistic.

Percentage of *ENTICE* residual modelled values within ± 1°C of residual actual values (*Prm*) is calculated as follows:

For $i = 1{:}n$

$$Trm_i = Tm_i - \left(\frac{1}{n}\sum_{i=1}^{n} Tm_i\right) \qquad and \qquad Tra_i = Ta_i - \left(\frac{1}{n}\sum_{i=1}^{n} Ta_i\right)$$

If

$$|Trm_i - Tra_i| \leq 1$$

Then

$$N_i = 1$$

Else

$$N_i = 0$$

End If

$$Prm = \sum_{i=1}^{n} \frac{N_i}{n} \times 100$$

where Trm_i is the residual modelled temperature at the *i*th forecast point, Tm_i the modelled temperature at the *i*th forecast point, Tra_i the residual actual temperature at the *i*th forecast point, Ta_i the actual temperature at the *i*th forecast point obtained from thermal mapping data, and *n* is the total number of forecast points around the study route (2261) or within a cluster (variable) dependent on whether entire route or cluster statistic.

INPUTS TO THE *ENTICE* MODEL

Temporal Data	**Meteorological Data***	**Geographical Data**	**Pre-coded constants**
Angle of declination	RST at noon	Latitude	Thermal conductivity of asphalt
Radius vector	Air temperature[1]	Altitude	Thermal conductivity of concrete
Date	Dew-point[1]	CAPI	Thermal Conductivity of soil
	Wind-Speed[1]	Sky-view factor	Thermal diffusivity of asphalt
	Rainfall[1]	Screening matrix	Thermal diffusivity of concrete
	Cloud cover[2]	Road type[3]	Thermal diffusivity of soil
	Cloud type[2]	Landuse[4]	Road damping depth

*Meteorological inputs remain the same as those used by Thornes (1984) and Chapman (2002).

[1]Nine values at 12:00, 15:00, 18:00, 21:00, 00:00, 03:00, 06:00, 09:00, 12:00.

[2]Eight values averaged over the periods 12:00-15:00, 15:00-18:00, 18:00-21:00, 21:00-00:00, 00:00-03:00, 03:00-06:00, 06:00-09:00, 09:00-12:00.

[3]Road type (used to estimate road construction in original *ENTICE* model) is replaced by road construction measurements calculated from GPR data (Chapter 3).

[4]Landuse (used to estimate Z_0 in original *ENTICE* model) is replaced by Z_0^{eff} estimates calculated from airborne LIDAR data (Chapter 4).

1. INTRODUCTION

1.1 Winter Road Maintenance

Adverse winter weather conditions have a major impact on the safety and operation of a nation's road network, affecting driver behaviour, vehicle performance, surface friction and the roadway infrastructure. To alleviate this impact, winter road maintenance is common practice for many countries around the world that experience winter climates. In the United States (US) for example, adverse weather and the associated poor roadway conditions are responsible for approximately 1.5 million vehicle crashes per year leading to 7,400 fatalities (Figure 1.1) and 554 million vehicle-hours of delay, with associated economic costs reaching into the billions of dollars (Drobot et al. 2010).

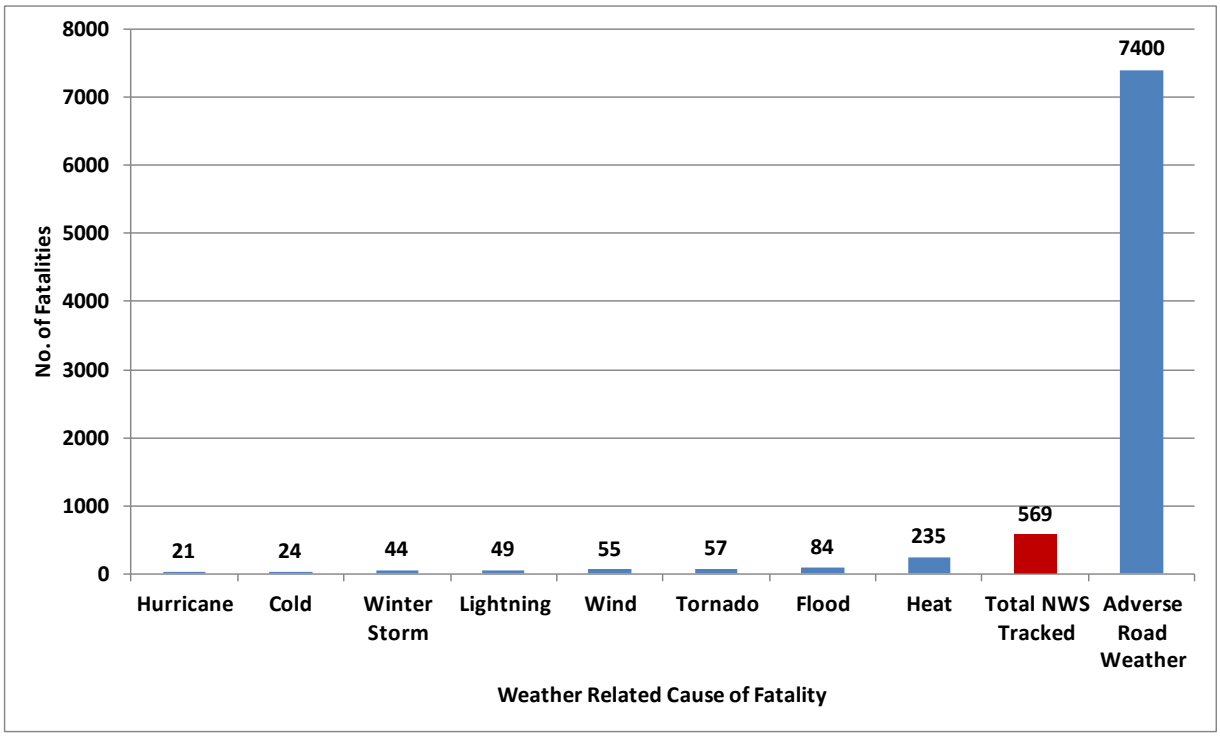

Figure 1.1 Average annual weather related fatalities in the US, based on data from the National Center for Atmospheric Research, Boulder, Colorado (Drobot et al. 2010).

In marginal winter environments, the largest potential savings to be made in winter maintenance focus upon the prediction of ice formation, and 0°C is an important threshold in this respect. As well as determining the possibility of frost or ice formation on the road surface, the air temperature determines whether or not precipitation is likely to fall as snow. Ice is also at it most slippery at 0°C (Figure 1.2), so marginal winter environments such as the United Kingdom (UK) where the road surface temperature (RST) commonly fluctuates around 0°C often present a greater problem to the highway engineer than roads with temperatures well below zero (Thornes 1991).

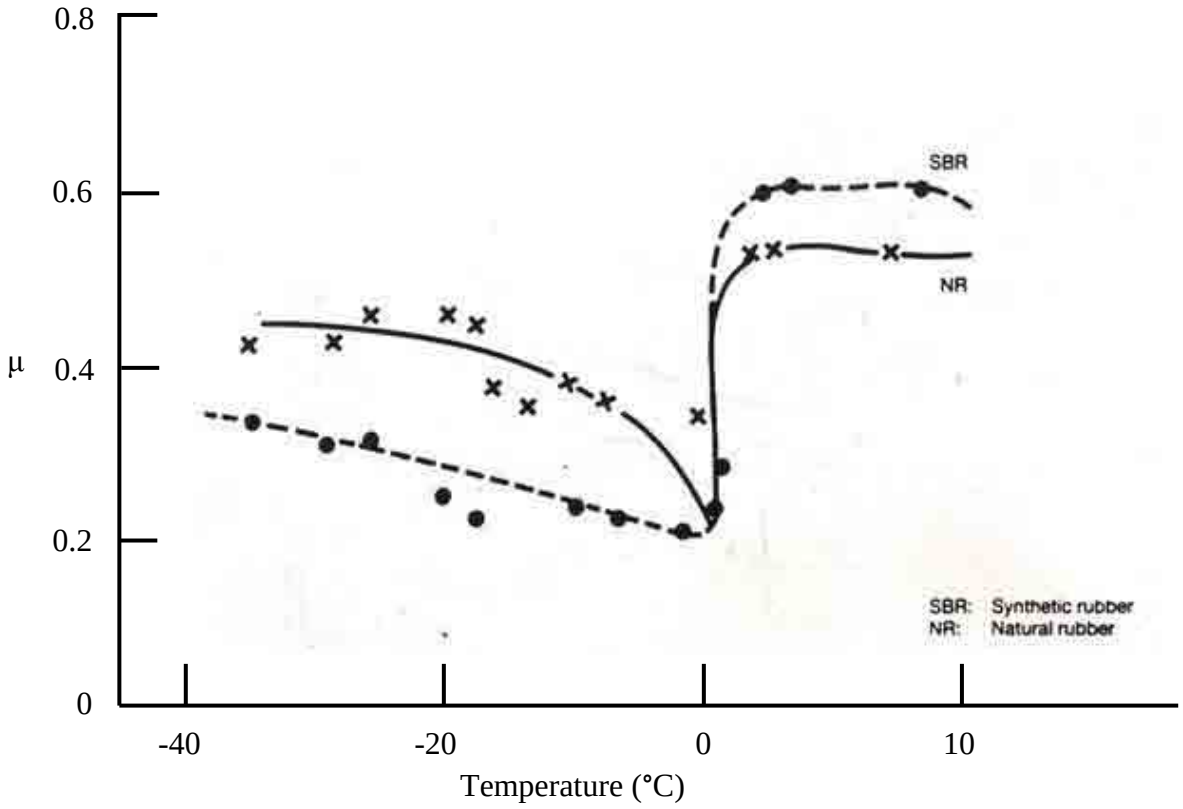

Figure 1.2 Skid resistance as a function of temperature (Moore 1975).

In the mid-1990's the costs of winter road maintenance in the UK were estimated to exceed £140 million each year (Cornford & Thornes 1996), although the total costs were more likely in excess of £200 million with the additional damage caused to vehicles and infrastructure through salt corrosion (Thornes 1996). The high costs of salting, particularly when using newer molasses doped salts such as Safecote (http://www.safecote.com/) that require larger upfront expenditure (albeit with greater long term savings), mean that winter maintenance engineers often face a difficult decision of whether or not to salt, and the wrong decision can be a costly mistake since four times more salt is required to melt snow and ice than to prevent its initial formation. Conversely, if salt is spread too soon then traffic and precipitation may disperse the salt before it has had time to take effect (Thornes, 1991), leading to dangerous driving conditions. Nowadays, winter maintenance engineers use information from road weather forecasts to aid such winter maintenance decisions, with modern route-based forecasts (Chapman & Thornes 2006) and decision support systems (Petty & Mahoney 2008) providing the winter maintenance engineer with the tools required to make informed treatment decisions that ensure the safety of the travelling public with the most efficient use of resources.

In 2001 it was estimated that more than £2 million of the UK's annual winter maintenance budget is spent on road weather forecasts (Thornes & Stephenson 2001), but the subsequent decade has since seen significant reductions to winter maintenance budgets in the UK, forcing highway engineers to re-evaluate their winter maintenance operations in an effort to reduce costs in line with budgetary demands. Furthermore, with the new UK coalition government focused on reducing the national deficit over the coming years, the strain on local government finances will be tighter than ever, and winter maintenance engineers will be looking to get better value for money and increased efficiency from their winter maintenance services. Even with the severe UK winters of 2008/09 and 2009/10, social research carried out by the Local Government Association in the UK in mid-January 2010 revealed a general understanding

amongst the British public that the occurrence of particularly severe winters is believed to be sufficiently rare that it might be uneconomic for local authorities to make excessive preparations for such occurrences (Quarmby et al. 2010). Furthermore, the climate research team at the Met Office Hadley Centre are predicting that the general effect of climate change will be to gradually but steadily reduce the probability of severe winters in the UK, which currently stands at a probability of 1 in 20. Consequently, the Winter Resilience Review commissioned by the UK Department for Transport suggests that in the future there will be a higher risk that local authorities and the public will be less experienced and capable of coping with extreme winter events when they do occur (Quarmby et al. 2010). Hence, given the almost inevitable budgetary constraints and the likelihood of increased complacency within the winter maintenance industry (and the wider pubic), the need for more cost effective, efficient and accurate road weather forecasts has perhaps never been greater than it is at present.

1.2 The History of Road Weather Information Systems

Road weather forecasting has experienced significant changes over the past 30 years. From the early days of road danger warnings through to the current first generation of route-based forecasting techniques, the main aim has always been to reduce costs without compromising safety, and this will continue to be the case as local authorities are increasingly under pressure to reduce their winter maintenance costs. Figure 1.3 outlines the significant changes that have occurred in road weather forecasting in the UK over the past 30 years:

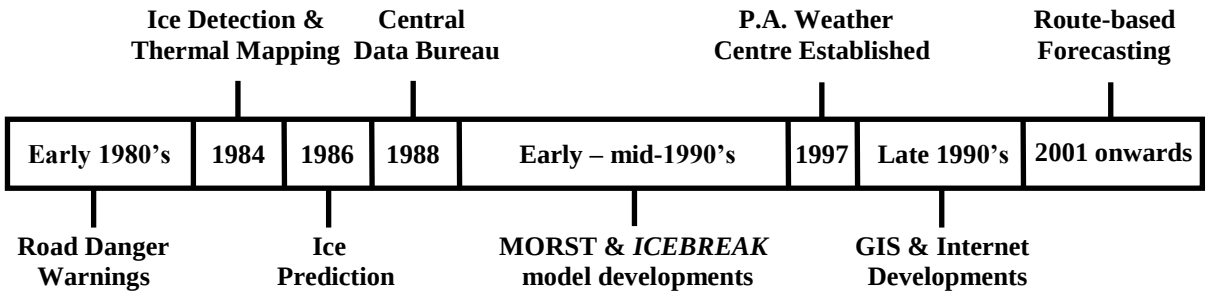

Figure 1.3 Significant events in the history of UK road weather forecasting.

1.2.1 Road danger warnings

Prior to the development of Road Weather Information Systems (RWIS) in the mid-1980's, road weather forecasting in the UK consisted of simple road danger warnings issued by the Met Office to advise motorists of potentially dangerous driving conditions. A typical road danger warning would read:

"Road surface temperatures are expected to fall below zero around midnight leading to icy patches on roads." (Thornes 1985)

The production and use of these warnings was subject to a number of errors (Figure 1.4), including meteorological errors in the forecast, geographical errors across the local road network, and judgement errors by the maintenance engineer (Thornes 1985). These errors, coupled with the extremely vague advice for treating roads given in the Department of Transports code of practice for the winter maintenance of motorways and trunk roads (Department of Transport 1984), often left winter maintenance engineers having to make awkward decisions regarding road treatments with a minimal amount of information to aid their decisions.

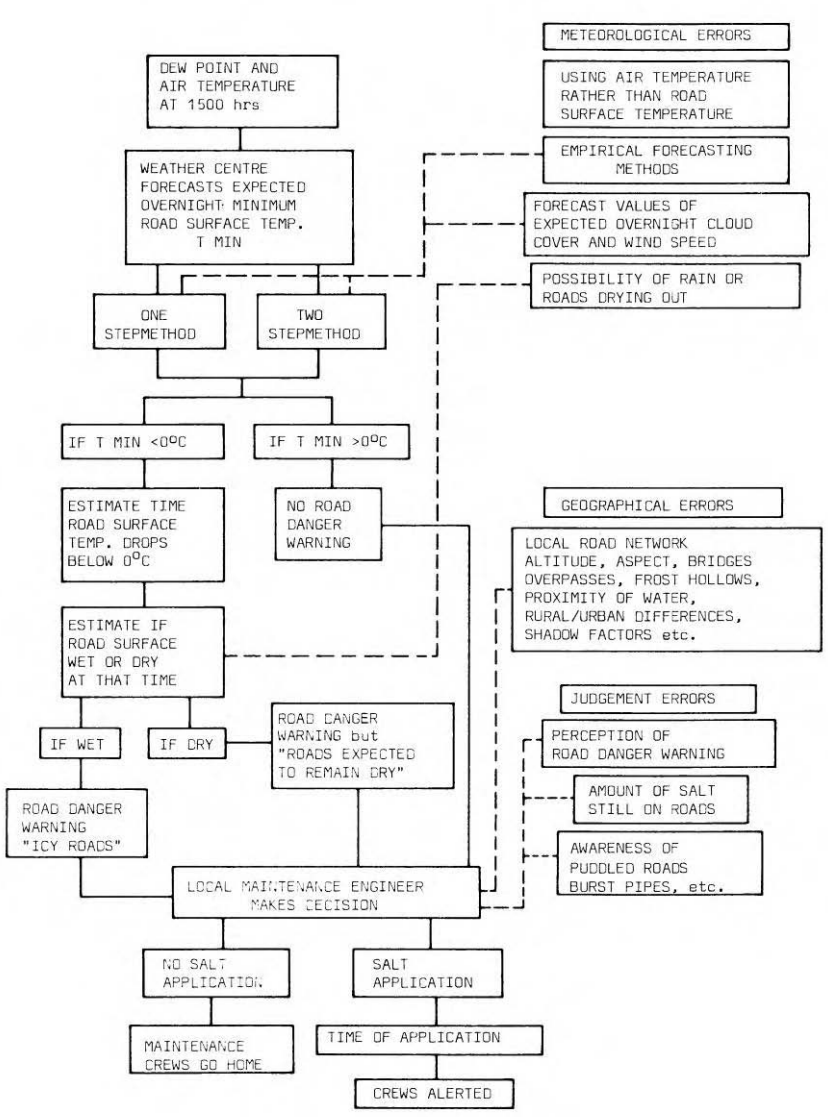

Figure 1.4 Possible sources of error in the forecast and treatment of icy roads using road danger warnings (Thornes 1985).

1.2.2 Ice detection

In the early 1980's the first automatic road weather stations, known as outstations or environmental sensor stations, were introduced onto the road network (Figure 1.5). Outstations provide measurements of key meteorological and road surface parameters including RST, air temperature, dew point, precipitation and wind speed and direction. Sensors embedded in the road surface provided winter maintenance engineers with up to date information on the current state of the roads, enabling ice formation to be more easily detected. These sensors alone however were somewhat insufficient since they had no

forecasting ability and were extremely localised in their measurements, to the extent that a poorly located outstation could lead to over salting of large areas of the road network if located in a cold spot or, more dangerously, too little salt being spread if located in a warm spot.

Figure 1.5 A Vaisala Road Surface Analyser (ROSA) outstation monitoring road surface and atmospheric conditions.

To resolve some of these issues a technique known as thermal mapping was developed by the University of Birmingham and commercialised through a spin-out company Thermal Mapping International (Thornes 1985). Thermal mapping is the process of measuring the spatial variation of nocturnal RST along a road network (Thornes 1991). The technique is performed using a vehicle mounted infrared thermometer which measures RST at a fixed spatial resolution. The infrared thermometer measures the energy flux density (E) emitted by the road surface which, according to the Stefan Boltzmann law, is proportional to the fourth power of its absolute temperature (Liou 2002). Given the energy flux density from the surface, RST is calculated through simple manipulation of the Stefan Boltzmann equation:

$$E = \varepsilon \sigma T_0^4 \quad (1.1)$$

where T_0 is the RST, σ is the Stefan Boltzmann constant ($5.67E^{-8}$) and ε is the emissivity of the road surface.

As well as thermal interpolation, thermal mapping quickly became the standard method for identifying the optimum locations for installing outstations, and for deciding the number of outstations required to give adequate coverage of the road network. Outstations started to be strategically located to enable the climatic variability in a particular 'climate zone' to be measured. Climate zones are simply a classification of a geographical area into a series of locations that experience a similar regional climate, such as urban centres, upland rural regions and coastal districts (Chapman & Thornes 2006).

Originally, thermal mapping data was displayed as a thermal fingerprint (Figure 1.6) showing RST as a pattern of temperature variations along the route (Shao et al. 1996). The amplitude of the thermal fingerprint displays the departure of RST from an averaged value against distance for each route (Shao et al. 1997). The extent of RST variation along a route, and thus the amplitude of the thermal fingerprint, is controlled by atmospheric stability, with the greatest variations being observed during stable conditions associated with anticyclonic weather patterns (Thornes 1991). To account for these variations, thermal mapping surveys are usually performed under a variety of synoptic weather conditions to ensure all different levels of atmospheric stability are covered. Shao et al (1996) have shown that under a certain weather condition the spatial variation of RST along a route appears in a consistent pattern. This consistency enables thermal mapping surveys to be conducted under a few selected weather conditions. In the UK, the terms extreme, intermediate and damped have been widely used for the stability classification of thermal fingerprints, which are quantified through analysis of the average wind speed and cloud cover during the 12-hour period preceding the survey.

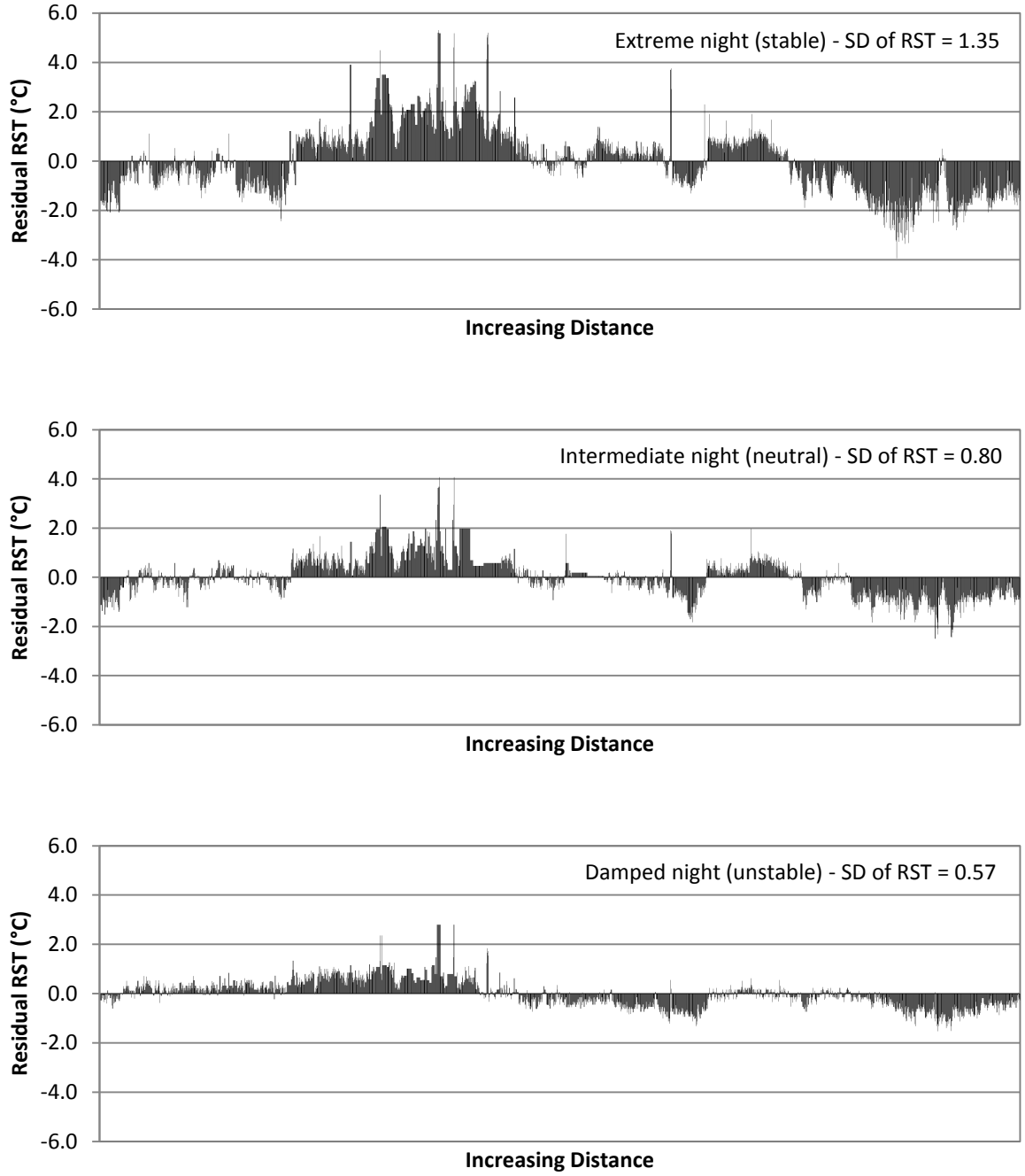

Figure 1.6 Thermal fingerprints showing the variation in residual (average) road surface temperature for the same route at different levels of atmospheric stability.

Once a sample of thermal fingerprints has been collected for a particular road network, thermal maps for each stability class are drawn up which represent the average spatial variations of minimum RST under different weather conditions. Initially the production of thermal maps from a combination of fingerprints was a time consuming exercise, but nowadays with the advancements in computer processing and software, thermal maps can

easily be plotted in a GIS (Geographical Information System) (Figure 1.7). Based on both thermal maps and a numerical model forecast at reference sites, the likelihood of ice or frost forming on different parts of a road network can then be determined.

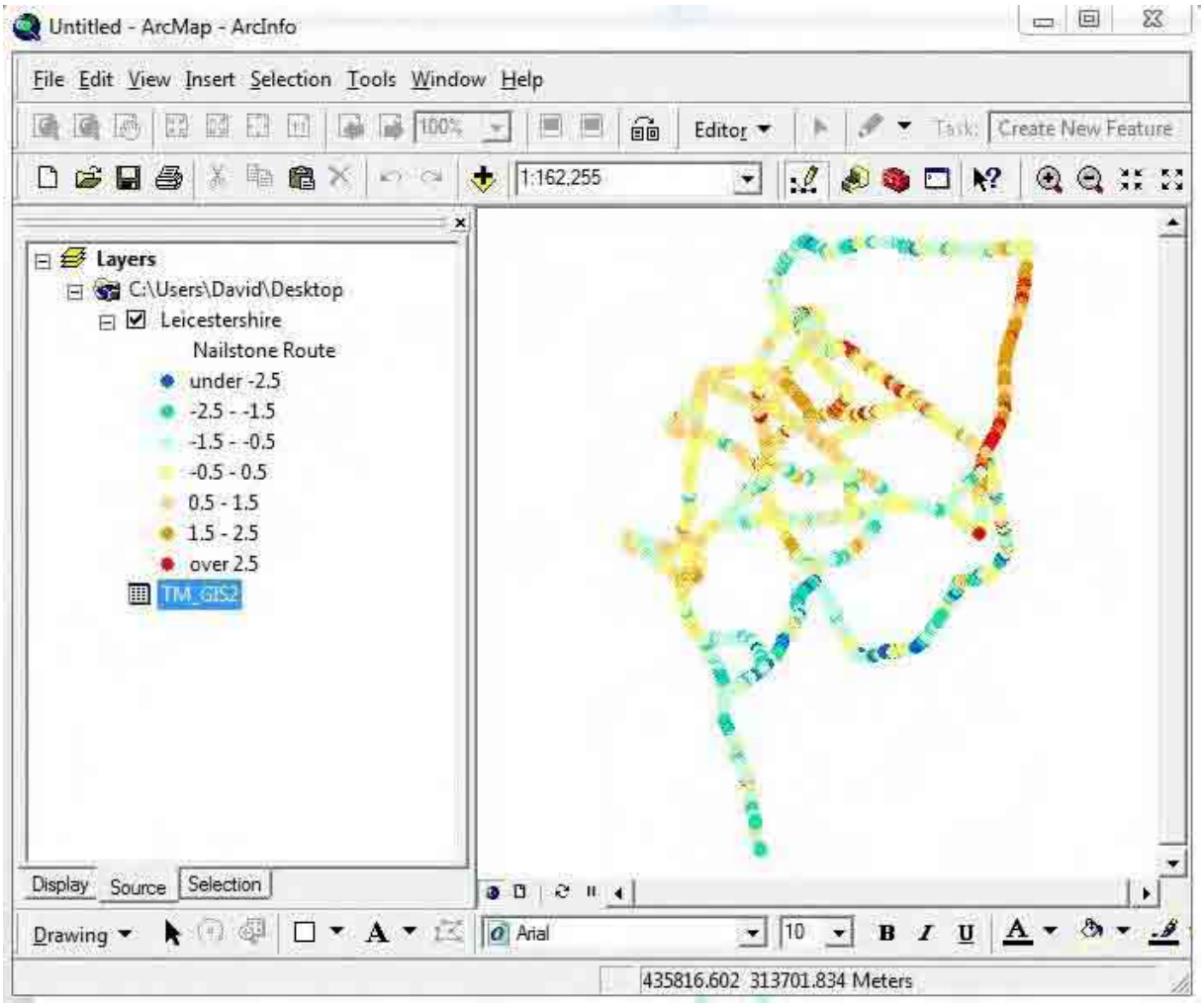

Figure 1.7 Thermally mapped data plotted in a GIS environment (Leicestershire, 10/02/08).

With the value that thermal mapping clearly added to a road weather forecast, it quickly became the standard methodology used in most countries for thermal interpolation between forecast sites. However, the technique is subject to a number of random and systematic errors that are widely discussed in the road weather literature (Thornes 1991; Shao & Lister 1995; Shao et al. 1996; Chapman & Thornes 2006) and relate largely to the repeatability of thermal mapping surveys. Changing surface emissivity, atmospheric absorption, poor equipment

calibration and poor measurement of distance are just some of the sources of error that can occur during a thermal mapping survey. A more detailed analysis of these and other errors associated with thermal mapping can be found in Chapter 2.

1.2.3 Ice prediction

Numerical road weather prediction models were first developed during the late 1970s, but it wasn't until the mid-1980s that they began to be used operationally for road weather forecasting. To provide a predictive dimension to the sensor information obtained from outstations, a road weather prediction model based upon the zero-dimensional energy balance approach was developed and integrated into an ice prediction strategy (Thornes 1984). The model simulated the surface temperature and energy regime of a selected site based upon equilibrium temperature theory, which states that if a given set of astronomical-temporal, atmospheric and surface boundary conditions exist, there is only one surface temperature which will balance the energy conservation equation across the surface of the earth (Outcalt 1972). The original temporal component of the model developed by Myrup (1969) was later modified by Outcalt (1971) to produce numerical stability, convergence with available field data and increased flexibility by increasing the number of environmental variables considered in the model. The model was based on the energy conservation law (Equation 1.2), where the sum of net radiation flux (R_n), latent heat flux (LE), sensible heat flux (H) and heat flux to soil (S) is zero, i.e.,

$$R_n + LE + H + S = 0 \tag{1.2}$$

At any point in time this equation must balance, and as each term is a function of surface temperature, there is one, and only one, surface temperature that balances the equation, known as the equilibrium surface temperature. Outcalt (1972) expanded the terms in Equation (1.2) to further define R_n, H, LE and S as follows:

$$R_n = (1-\alpha)(Q+q) + \varepsilon_{sky}\sigma T_{sky}^4 - \varepsilon\sigma T_0^4 \quad (1.3)$$

where α is the surface albedo, Q is beam solar radiation, q is diffuse solar radiation, ε_{sky} is the effective emissivity of the sky (assumed to be unity), σ is the Stefan Boltzman constant, T_{sky} is the sky temperature, T_0 is the surface temperature, and ε is the emissivity of the surface.

$$H = RCK[T_2 - \Gamma Z_2 - T_0] \quad (1.4)$$

where R is a stability correction factor (see section 4.2), C is the heat capacity of air, K is the adiabatic estimate of the turbulent transfer coefficient whereby $K = (k^2 U_2 \rho)/[ln\ Z_2/Z_0]^2$ (Myrup 1969), k is von Karmen's constant, U_2 is the wind speed at air thermal damping depth of Z_2, ρ is air density, Z_0 is roughness length, Z_2 is the height of air thermal damping depth, T_2 is the temperature at Z_2, Γ is the dry adiabatic lapse rate, and T_0 is the surface temperature.

$$LE = RLK[q_2 - q_0] \quad (1.5)$$

where L is the latent heat of evaporation, q_2 is the absolute humidity at Z_2, and q_0 is surface wetness.

$$S = \frac{K_s}{\left(\frac{Z_s}{2}\right)}[T_n - T_0] \quad (1.6)$$

where K_s is the thermal conductivity of soil, Z_s is the thermal damping depth of soil, and T_n is the temperature at depth $Z/2$ calculated via a finite-difference solution of the Fickian diffusion equation, whereby:

$$T_n(I) = T_n(I-1) + \{d[T_s - 2T_n(I-1) + T_0(I-1)]/(Z_s/2)^2\}\Delta t \qquad (1.7)$$

where I is Δt (the time increment considered), d is the thermal diffusivity and T_s is the temperature at depth Z_s.

Despite the practical difficulties in observing and interpreting the energy balance of an urban area, numerous observational campaigns have been undertaken actively during the past three decades, focussing mainly on the energy balance of temperate western cities (Nunez & Oke 1977; Cleugh & Oke 1986; Grimmond 1992; Grimmond & Oke 1995; Grimmond & Oke 1999a) and to a lesser extent in tropical areas, e.g. Mexico (Oke et al. 1999) and Asia (Yoshida et al. 1991). A number of studies have shown that the geometry of urban street canyons reduces the reflected radiant energy leaving a canyon due to multiple reflections that occur within the canyon (Aida, 1982, cited in Offerle et al. 2007; Kondo et al. 2001; Harman et al. 2004). Recently, research has shown that while sensible heat fluxes from roof tops dominate daytime surface atmosphere heat exchanges, stored heat released from the urban fabric of street canyons can help maintain neutral to unstable conditions over dense urban areas during the nocturnal period (Christen & Vogt 2004; Grimmond et al. 2004; Salmond et al. 2005; Offerle et al. 2006). Indeed, the representation of urban surface fluxes in energy balance models has received great attention over the past decade in an attempt to improve numerical weather prediction and air pollution dispersion models (Masson 2000; Best 2005; Brown et al. 2008b). Numerical modelling and wind tunnel experiments have shown that the differential heating of surfaces within a street canyon can influence the flow pattern, with thermal impacts on the flow regime greatest when wind speeds are weak (Offerle et al. 2007). Numerous simulated small-scale flows within the canopy layer (Sini et al. 1996; Baik & Kim 1999) have revealed a flow structure consisting of two counter-rotating cells caused by heating of the windward or leeward wall, and where surface heating is introduced multiple

vortex development is found (Kim & Baik 2001). Hence, the overall complexity of urban surfaces means that the energy balance shown in Equation (1.2) cannot be resolved for every point on the urban surface, but instead requires approximation.

Thornes (1984) modified Outcalt's model to predict RST iteratively over a 24 hour period, based solely on the input of meteorological data. Using the twelve noon measured values of RST and wetness along with air temperature, humidity, wind speed and cloud cover, the model forecasted the RST and wetness for the next 24 hours, using forecast values for the meteorological parameters at 1500, 1800, 0000, 0600 and 1200 hours. The forecast model was run twice to produce an optimistic and pessimistic forecast, with the difference between them giving the winter maintenance engineer a better idea of the confidence in the model (Thornes 1985). The forecast was issued in the form of a RST forecast curve (Figure 1.8), from which early decisions could be made by the engineers regarding the treatment of the road network, with thermal maps used to extrapolate the forecast data between outstations.

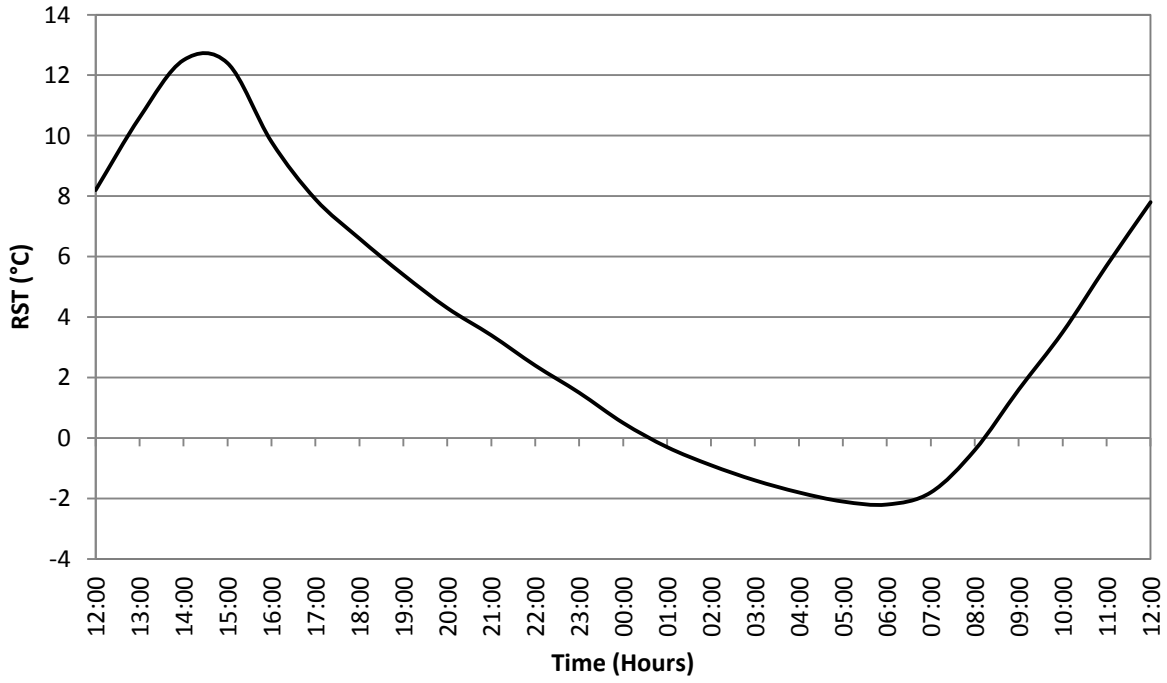

Figure 1.8 Example RST forecast curve.

In 1986 the Department of Transport specified the National Ice Prediction network based around RWIS. RWIS comprise of several components which are used to predict the variation in RST around a road network. In the original network architecture (Figure 1.9), a local authority instation would interrogate each of the outstations along their road network via the public switched telephone network and collect and store the measured data. This data was then forwarded to the Met Office where it was inserted with other forecast data into their own numerical road weather prediction model (Rayer 1987). The resulting ice prediction forecast was sent back to the local authority instation where it was made available to the winter maintenance engineer to aid them in their decision making.

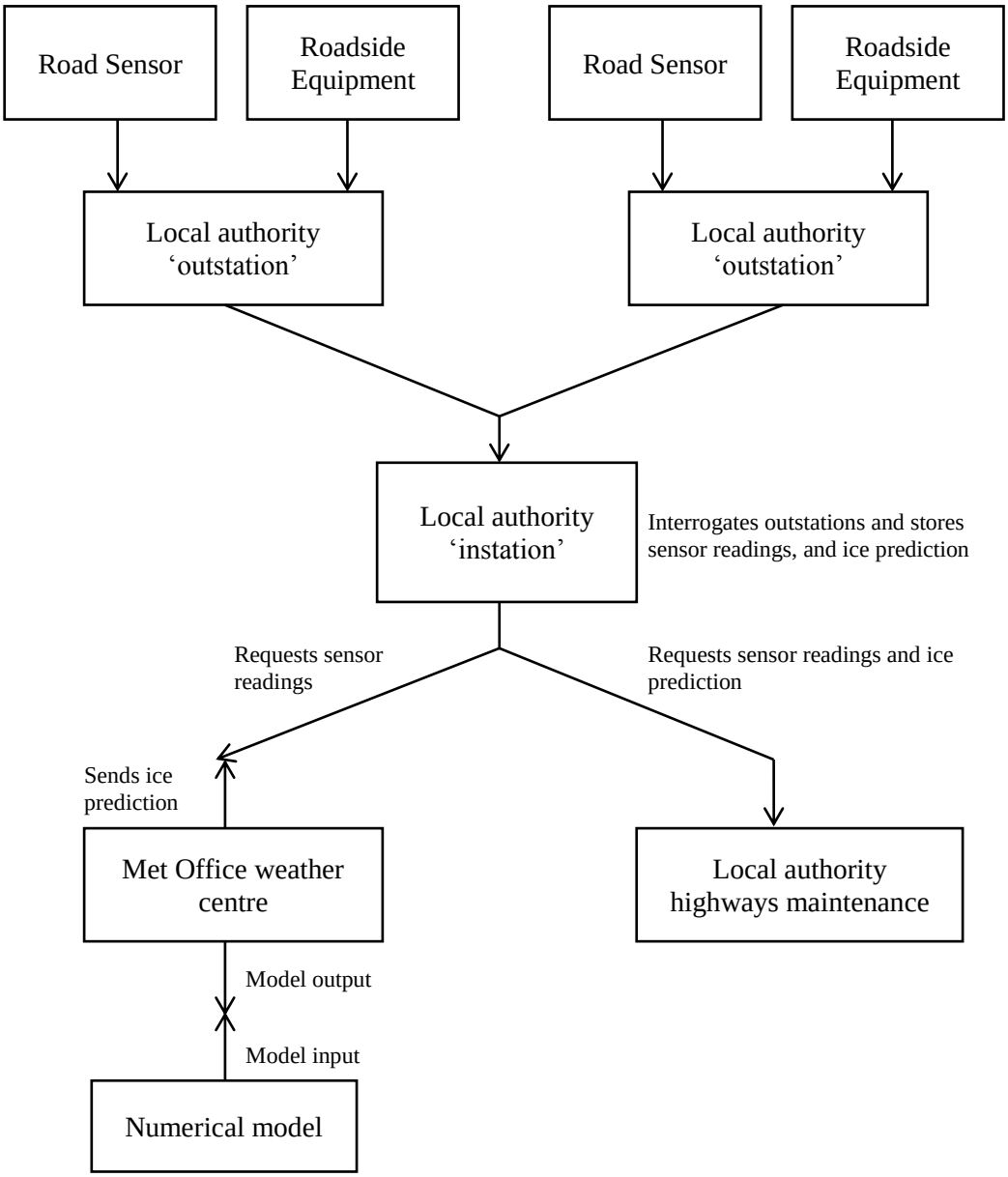

Figure 1.9 Schematic of the National Ice Prediction Network (Rayer 1987).

In 1988 the architecture of the UK National Ice Prediction network changed somewhat with the development of a central bureau service for data collection and archiving. With the bureau service, local authorities were no longer responsible for interrogating their outstations, as this was all controlled centrally from within the bureau. Once collected, data was validated before being sent to a forecast provider to be inserted into a road weather prediction model. The resulting forecast was then sent to the bureau where it was disseminated to the relevant local authority winter maintenance engineer. This bureau structure is still in use today, although

technological advancements have helped to improve efficiency and reduce costs. For example, mobile GSM and GPRS communications are increasingly being utilised to transfer outstation data to a central bureau, and with advancements in solar power technology the outstations themselves can now be located in more remote locations where mains power is unavailable, thus increasing coverage around the road network. Perhaps the most noticeable advancement however is the increasing efficiency with which forecasts are now disseminated to the winter maintenance engineer. With the use of web servers for hosting forecast and sensor data, dissemination of this data has become an automated process and winter maintenance engineers now have access to forecast and actual sensor data 24 hours and day during the winter season via the internet.

Numerical prediction of ice and frost has been accepted by both winter maintenance engineers and meteorologists as an appropriate and valuable technique for winter road maintenance. Road weather models provide winter maintenance engineers with advance knowledge of where and when ice or frost is likely to occur, enabling them to better plan salting strategies. The technique enables highway authorities to maintain or improve already established road safety standards, whilst also reducing the huge costs associated with salt usage, labour and equipment, and the damage caused to the environment (Shao & Lister 1996). A survey in the mid-1990's commissioned by the UK Met Office found that approximately £170 million and up to 50 lives have been saved each year in the UK since the introduction of a road ice prediction system (Thornes, 1994).

The last decade of the twentieth century saw a great deal of research focused towards improving the accuracy of road weather prediction models, much of which was prompted by the rapid increase in the processing capabilities of computers. In the early 1990's there were two road weather models in commercial use in the UK: the Met Office Road Surface Temperature model (MORST) (Rayer 1987; Thompson 1988), and Vaisala's *ICEBREAK* model (Shao 1990), both of which have undergone continuous developments as the

processing capabilities of computers has increased. Data input into the MORST model was streamlined with the inclusion of a mesoscale model, which provided the benefit of being less pessimistic than the numerical equivalent, thus reducing model bias (Astbury 1996). The coarse scale of the model however caused problems since interpolation of the data for forcing the RST model could lead to errors in representivity (Maisey et al. 2000). For example, smaller topographical variables were sometimes disregarded, and grid-points of the mesoscale model did not always coincide with the outstation sites used by the original model (Thornes & Shao 1992). To overcome this, Thornes & Shao (1992) recommended linearly combining grid-points to provide a better data input set together with an averaging template of several days to correct for systematic error. With the obvious inadequacies of the mesoscale model in driving the MORST model, in the mid to late 1990's the Met Office developed a high resolution Site Specific Forecast Model which uses high resolution (25 metre horizontal) land use data to estimate localised surface fluxes, the incorporation of which has shown significant improvements over the mesoscale model for site specific forecasting and helped to improve road weather forecasts internationally (Maisey et al. 2000).

The *ICEBREAK* model has also been continuously developed to the point where it is now fully automated and can be used for three hourly nowcasting, with no external meteorological input data required other than automatically collected sensor measurements of RST, air temperature, dew point and wind speed from the forecast site (Shao & Lister 1996). The application of a three-layer neural network trained by an error-back propagation algorithm has further increased the accuracy of nowcasts by reducing the root mean square error (RMSE) of temperature forecasts and increasing the accuracy of frost-ice prediction, particularly at problematic sites where complex environmental conditions and underlying nonlinear mechanisms are unresovlable by operational numerical models (Shao 1998).

In 1997 PA Weather Centre (now MeteoGroup UK), a joint venture between the Press Association and Dutch weather forecasting company Meteo Consult, was established and

started supplying forecasts to a wide range of clients including some in the road industry. The Press Association road forecast model has since been developed to produce site forecast graphs using a statistical approach in combination with traditional energy balance equations (http://www.meteogroup.co.uk/).

A number of other models remain in development around the world, most notably the RWFS (Road Weather Forecast System) in the US which was developed as part of a five year Federal Highway Administration (FHWA) program, initiated in 1999, to explore the applicability of technologies developed at national research laboratories to the problem of winter road maintenance (Schultz 2005). The first specific goal was to develop an automated decision support system to generate snow ploughing and roadway chemical application guidance for use by state departments of transport, which led to the development of the Maintenance Decision Support System (MDSS) (Mahoney et al. 2005). In the MDSS prototype architecture, the gridded outputs from an ensemble of mesoscale model forecasts generated by the National Oceanic and Atmospheric Administration's Forecast Systems Laboratory (FSL) are transmitted in real time to the Research Applications Laboratory at the National Centre for Atmospheric Research. Here, the FSL models are ingested along with a large scale lateral boundary model into the RWFS, where they are combined with a Road Condition and Treatment Model (RCTM) which is the central component of the MDSS. The function of the RCTM is to produce road condition forecasts and treatment recommendations (Petty & Mahoney 2008), using the Model of the Environment and Temperature of the Roads (METRo) (Crevier & Delage 2001; Linden & Drobot 2010) to generate predictions of pavement conditions, with treatment recommendations constructed using current and forecasted atmospheric and road condition information (Petty & Mahoney 2008).

A restriction of all the road weather models discussed thus far is that they only produce RST forecasts for the outstations from which meteorological data are obtained, with thermal mapping required to extrapolate this forecast data around a road network. Alternative methods

to thermal mapping have been proposed, most notably the use of empirical local climatological and statistical models to predict spatial variations of RST in a road network (Bogren et al. 1992; Gustavsson & Bogren 1993). Such models are in commercial use in Sweden and have helped to demonstrate the influence of geographical factors (Bogren & Gustavsson 1991; Bogren et al. 2000a) and meteorological parameters (Gustavsson et al. 1998; Bogren et al. 2000b) on RST. However, local statistical models require a large number of observations to obtain reliable statistical relationships, and any such model derived in one area will usually require major modification before it can be applied to another area (Shao et al. 1997). With such doubts on the accuracy and general applicability of statistics-based climatological models, thermal mapping has until recently remained the standard methodology used in most countries for describing and displaying variations in RST between forecast sites.

This first generation of RWIS described thus far relies largely on methods and tools developed in the 1980s, but as technology has progressed and the processing capabilities of computers has increased, it is now being superseded by a new generation of RWIS capable of forecasting for individual salting routes, rather than traditional site specific forecasts which rely on interpolation by thermal mapping.

1.2.4 Route-based forecasting

Within a climate zone there usually exists at least one outstation, and the weather recorded at this outstation is assumed to be representative of the climate zone as a whole. Chapman & Thornes (2001a; 2001b) use this assumption to hypothesise that if the regional climate is constant, any variation in climate and RST across the climate zone is controlled by the variation in geographical parameters. They further suggest that by measuring local variations in geography and modelling the impact of these variations on RST, accurate ‘virtual’ forecasts can be created away from the road weather outstation, thus enabling route-based forecasts to

be produced. Such an approach enables the thermal projection of RST across the road network entirely by model predictions without the need for thermal maps.

Chapman et al. (2001b) developed an improved road weather prediction model (*ENTICE*) based around the Thornes (1984) model, with an added high resolution, site-specific spatial component to predict local variations in RST over both time and space. The spatial component of *ENTICE* is driven by a Geographical Parameter Database (GPD) consisting of several geographical parameters that have been widely proven to influence RST. In a pilot study in the West Midlands, UK, *ENTICE* was shown to be able to explain up to 72% of the variation in RST purely by thermally projecting surface temperature using geographical variables (Chapman et al. 2001b). A later study by Chapman & Thornes (2006), again in the West Midlands, found that *ENTICE* could explain up to 74% of the variation in RST in urban areas and up to 58% in rural areas.

The ability to thermally project RST across a road network entirely by model predictions raises the question of whether thermal mapping is still a required component of RWIS. The requirement of thermal mapping as a forecasting tool has diminished as the predictive ability of numerical models has improved, and this is likely to continue as more local authorities start to use route-based forecasting solutions within their winter maintenance strategies. However, the development of route-based forecasting has brought with it a new challenge relating to the validation of the forecasts – How can a route-based forecast be validated? Whilst traditional site specific forecasts can be validated against sensor data from outstations located at the forecast sites, no such data exists for verifying the thermal projections of RST between outstation locations in a route-based forecast. Chapman et al. (2001b) and Chapman & Thornes (2006) used data acquired from thermal mapping surveys as a means of testing the predictive ability of the *ENTICE* route-based forecasting model, which suggests that the future role of thermal mapping within the framework of route-based forecasting could be that of a validation tool. However, whilst the results obtained using thermal mapping data to

validate the *ENTICE* model were generally good (up to 74% of thermal variations around the route explained by the model), these results were based on average statistics for an entire study route and provide no indication of the variation in model performance around the route. Hence, the current methodology of using 'entire route' statistics obtained from the averaging of thermal mapping data is clearly too simplistic and needs to be changed. The increased resolution of route-based RST forecasts requires validation at a whole new spatial scale that up until now has never been required for road weather forecasts. Clearly route-based forecasting is a significant step forward, but it is still a relatively new concept to some local authorities, many of whom do not yet have the confidence to be able to selectively salt their road network based solely on model predictions. In order to build this confidence, more attention needs to be focused towards improving the validation strategy for route-based forecasts, which possibly represents one of the biggest challenges currently facing the road weather research community.

1.3 Aims and Objectives

1.3.1 Aims

This thesis has two main aims. The first of these is to develop the foundations for a new validation strategy for route-based road weather forecasts that will potentially enable validation at the full spatial and temporal resolution of the model. Such a technique must be capable of identifying variations in spatial model performance to enable weaknesses in the forecast model to be more easily identified and resolved. Moreover, it is intended that the new validation strategy be used as a consistent methodology for identifying whether new model parameterisations (whenever proposed) improve the overall spatial forecasting performance compared to existing parameterisations. Since *ENTICE* assumes that the local geography and road infrastructure are the main influence on thermal variations within a climate zone, it is imperative that we also get better control over the geographical and infrastructure parameters that are currently inadequately parameterised in the model. Hence, the second aim of the thesis is to improve the accuracy of the *ENTICE* route-based forecast model by de-parameterising key geographical and infrastructure parameters within the model that are currently not measured at the spatial scale demanded by a route-based forecast.

1.3.2 Objectives

These aims will be achieved through the following objectives:

1. To critically review existing road weather validation techniques as tools for verifying route-based road weather forecasts.
2. From the outcome of (1), devise a new methodology to facilitate validation of the *ENTICE* model at a spatial scale previously unseen with route-based forecasts.
3. Investigate new techniques to remove geographical and infrastructure parameterisations in the *ENTICE* model, namely:

i. Road construction re-parameterisation through the use of Ground Penetrating Radar technology.

ii. Surface roughness (land use) re-parameterisation using airborne LIDAR data.

4. To use the validation strategy devised in (2) as a new methodology for testing whether the changes to geographical and infrastructure parameterisation improve the overall spatial forecasting performance of the *ENTICE* model.
5. Make recommendations for the future of route-based forecasting

The road weather market in the UK is currently in a transition phase with an increasing number of local authorities changing to a route-based forecasting system, and it is hoped that the results of this thesis will have a positive impact on a number of different fronts. Increased model performance will help to increase overall confidence in route-based forecasting, which is crucial if local authorities are ever to adopt selective salting strategies that require the confidence to simply treat one section of road and risk leaving another warmer section untreated. Economically, the realisation of selective salting should bring huge financial savings to local authorities as the efficiency of winter maintenance operations improves, and with increased confidence in the model local authorities should also be more receptive to the idea of optimising their salting routes (Handa et al. 2007), a strategy which offers the potential for even greater financial savings. Furthermore, increased forecast accuracy should lead to better treatment decisions which will ultimately help to reduce the number of weather-related road traffic accidents that occur each year. From an environmental perspective, improvements to route-based forecast accuracy will ultimately result in smaller quantities of de-icing material being required to treat road networks, reducing the levels of salt and associated additives entering water courses via road runoff. Finally, from a modelling perspective, although this research is being conducted using the *ENTICE* route-based forecast model, the

validation strategy and any newly proposed model parameterisations will be relevant to any spatial road weather model.

CHAPTER ONE SUMMARY

The development of route-based road weather models was the first real innovation in road weather forecasting in over a decade and was long overdue. The technique of route-based forecasting enables the thermal projection of RST around a road network at a high spatial resolution entirely by model predictions. However, the increased resolution of route-based forecasts requires validation at a whole new spatial scale that up until now has never been required for road weather forecasts. The improved spatial scale of route-based forecasts also places an increasing demand on measurement requirements in order to fully account for the variations in geographical and infrastructure parameters which influence thermal variations around a route, some of which are not currently measured at the spatial scale demanded by a route-based forecast. This thesis aims to address these issues, starting with the development a new validation strategy in the following chapter.

2. A NEW VALIDATION STRATEGY FOR ROUTE-BASED ROAD WEATHER FORECASTS

The road weather industry is becoming an increasingly commercial environment, and users of road weather forecasts are continually having to prove that they are getting value for money from their winter maintenance expenditure (Thornes & Stephenson 2001). The quality and/or value of weather forecasts has received much attention in the literature (Mylne 1999; Thornes 1995; Thornes & Proctor 1999; Stephenson 2000), and as route-based forecasting techniques have led to significant increases in the spatial resolution of road weather forecasts, model validation along the entire length of a route is now a real necessity. Validation loosely refers to the process of assessing whether a design, procedure or process is correct and satisfies specified requirements (Edwards et al. 2002). The traditional methods of validation for road weather forecasting, which are discussed in the following section, no longer satisfy the increased spatial demands of route based forecasts, and as will become apparent through the remainder of this chapter, the aim of this part of the research is to develop a streamlined methodology for calculating route-based model performance at a much greater spatial resolution than is currently feasible, hence improving route-based forecast model validation.

2.1 Existing Validation Techniques

2.1.1 Road outstations

Since the development of ice prediction strategies in the mid-1980s, road weather outstations have provided the main source of validation data for site specific forecasts produced by road weather prediction models. However, with the emergence of route-based forecasting as the standard methodology for delivering winter maintenance services in the UK, the limitations of road outstation data are becoming increasingly apparent. Even with careful design and

installation and assuming good sensor calibration, embedded road sensors only provide a spot measurement of RST and are therefore unable to provide information on the spatial variation of RST around a road network. This severely limits their use as a validation tool for route-based forecasts, although instances occur where spot measurements of RST could provide useful information. In the UK, road outstations are strategically located to enable climatic variability to be measured, but some countries take a more pessimistic approach and specifically locate outstations at the coldest locations around a road network to give a 'worst case' scenario. Cold spots or thermal singularities such as frost hollows and bridge decks are some of the most difficult locations for road weather models to resolve (Shao 1998), and outstations located at these problematic sites could provide useful spot measurements for validation in a route-based forecast model. However, in countries such as the UK outstations are rarely located at such problematic sites, and to do so now would require large amounts of investment that few highway authorities can afford given the large costs of installing new road outstations and the continual pressures winter maintenance managers face to reduce expenditure. A more realistic alternative could involve the installation of low cost remote infrared temperature sensors for monitoring RST at problematic forecast sites that are recognised thermal singularities.

2.1.2 Remote infrared temperature sensors

Recently developed remote infrared surface temperature sensors from established instrument manufacturers such as Vaisala (Cyclo) and Campbell Scientific (IRIS; Figure 2.1) provide low cost alternatives to traditional road outstations and have a number of advantages over their predecessors that facilitates their use as a validation tool. Such sensors utilise modern solar power technology and remote GSM/GPRS communications which significantly reduces installation costs as no fixed power and communication lines are required. Whilst many traditional outstations are now equipped with mobile communications, their locations are generally restricted to sites with mains power due to the high power consumption of

embedded surface sensors and an increasing demand for outstation cameras capable of live video streaming over IP networks. This gives low power remote infrared sensors a distinct advantage for route-based forecast validation since a much greater network coverage is possible, making it feasible to install one or more sensors on every forecast route at a reasonably low cost. These sensors also have the added advantage of measuring RST over a larger surface area compared to the spot measurements of embedded surface sensors, making them less susceptible to erroneous measurements and providing a more realistic indication of the average RST at a particular site.

Figure 2.1 An IRIS remote infrared temperature sensor monitoring road surface temperatures at the Eurotunnel freight terminal in Folkestone, UK. Photograph courtesy of Campbell Scientific Ltd.

Remote infrared sensors can be susceptible to measurement errors due to traffic, however, and whilst sensors have traffic filtering algorithms programmed into the systems, the effectiveness of these algorithms under heavy traffic conditions is somewhat unknown and requires further study. Furthermore, these sensors contain algorithms to account for the increased effects of atmospheric radiation on RST under clear sky conditions when other infrared sensors are often inaccurate, but these algorithms contain certain assumptions that can sometimes lead to measurement errors since neither sensor directly measures the actual sky temperature for inclusion into its algorithms. Surface emissivity is another potential source of error for remote infrared sensors. Emissivity is defined as 'the ratio of the total radiant energy emitted per unit time per unit area of a surface at a specified wavelength and temperature to that of a blackbody under the same conditions' (Oke 1992). Tabulated values give an emissivity for concrete of 0.92-0.94 and 0.967 for asphalt, but the apparent emissivity of a road surface will vary according to surface state and the view angle of the sensor (Gustavsson 1999). Remote infrared sensors are usually pre-calibrated for specific surface types based on tabulated emissivity values, but any changes to the apparent emissivity are not accounted for and will affect the accuracy of temperature readings.

Despite these potential errors, an increasing number of highway authorities around the world are using remote infrared sensors as a low cost alternative to increase coverage of their road network between existing road outstation locations, mainly attracted by the lower purchase and installation costs and the greater network coverage that these sensors offer. However, as with traditional road outstations, remote infrared sensors are unable to provide information on the spatial variation of RST around a road network, and although their low cost provides an opportunity to instrument the network at a greater resolution, this will still be significantly coarser than the forecast points used in a route-based forecasting service. Ultimately, this would require thousands of infrared sensors to be installed around the road network which is clearly impractical. As a validation tool for problematic forecast sites around salting routes

however, remote infrared sensors have several benefits over traditional outstations, and could potentially be used for verifying specific forecast points around a route.

2.1.3 Thermal mapping

Whilst road outstations and remote infrared sensors are unable to verify the spatial variation of RST around a road network, one existing technique does fulfil this requirement. The technique of thermal mapping has been used in applied road climatological studies since the mid-1970s, but it wasn't until the mid-1980s that the use of thermal mapping became common practice in winter road maintenance. The technique played a key role in the progression from basic ice detection systems to ice prediction, and more than 20 years on the same technique could have an equally important role to play in the progression from climatic domain to route-based forecasts. Thermally mapping the road network with a vehicle mounted infrared temperature sensor provides a data set describing the spatial variation of RST around the road network (Shao et al. 1997), precisely what is required for verifying a route-based forecast. It is well documented that the technique of thermal mapping is subject to a number of random and systematic errors (Table 2.1), but under strict quality control many of the errors can be minimised or eliminated altogether. For example, distance errors due to differences in tyre pressures, cornering at different angles and variations in speedometer accuracy between vehicles have now been eradicated by fixing the exact location of each reading with GPS (Chapman et al. 2001a). Other errors, however, are less easy to resolve, and Table 2.1 provides a summary of the main errors currently associated with thermal mapping. These are divided into two types of error. The first of these is random errors that are caused by unknown and unpredictable changes in the measurement, which are changes that may occur in the measuring equipment or in the environmental conditions. The second type of error is systematic errors caused by the measuring equipment, which usually result in some form of bias in the sensor measurements rather than a random fluctuation.

Table 2.1 Potential sources of error in thermal mapping (adapted from Thornes (1991) and Chapman et al. (2005).

Random errors due to unknown and unpredictable changes	**Systematic errors from the measuring equipment**
Varying road surface emissivity	Temperature range of instrument exceeded
Atmospheric absorption & attenuation	Contaminated optics
Signal noise	Sensor angle
Narrow sensor waveband	Variations between sensors due to tolerance
Lane changes due to slow moving vehicles	
Unstable sensor body temperature	

The greatest source of random error during a thermal mapping survey is the emissivity of the road surface, which will vary according to the road surface material and, to a lesser extent, road surface state. Despite these variations, for the purposes of thermal mapping surface emissivity is typically held constant at 0.95 (Sugrue 1983). Road surface temperatures calculated from the surface energy flux density (E) using the Stefan-Boltzmann law are extremely sensitive to even the smallest change in emissivity. Gustavsson (1999) estimates that a 10% change in emissivity from 0.95 to 0.85 will cause an infrared detector to under read surface temperature by approximately 8°C when E = 300 Wm^{-2}. Thornes (1991) puts this temperature difference at a more conservative 5°C, which given the variation in emissivity between concrete and asphalt surfaces of up to 4% can lead to a potential error around a survey route of approximately ±2°C. Another important parameter affecting surface emissivity is road surface state. Measurements using an infrared sensor have shown that calculated RST on an asphalt surface can vary by approximately 0.8°C depending on whether the surface is dry or moist (Gustavsson 1999), which restricts the periods over which thermal mapping surveys can be conducted to situations with constant surface status, otherwise it can

be difficult to interpret the temperature recordings collected. Atmospheric absorption is another potential source of random error in thermal mapping (Thornes 1991), preventing all of the radiation from the surface reaching the sensor. However, well designed infrared sensors are sensitive to a specific waveband between 8 and 14 μm known as the atmospheric window (Liou 2002), where radiation from the Earth is almost completely reflected with little atmospheric attenuation, so errors due to absorption should be minimal with a well-designed sensor and can be further avoided by positioning the sensor close to the road surface. Alongside this, good calibration is required to compensate for the narrow waveband of most infrared sensors which only transmit part of the infrared spectrum, and even more desirable is individual sensor calibration, which will also eradicate random errors between sensors due to component tolerances.

A further source of random error in thermal mapping, and one which can easily be overlooked, is that caused by an unstable sensor body temperature. Modern infrared sensors utilise a thermopile detector which detects the presence of thermal radiation, consisting of a number of thermocouples connected in series. One set of thermocouple junctions is exposed to the radiation source (i.e. the road surface in the case of thermal mapping) and is heated by it, whilst the other set is shielded from the radiation. A highly polished metal cone concentrates the radiation onto the exposed junctions, which are coated with lamp-black to enhance the efficiency with which the radiation is absorbed. The output from the thermopile detector is a voltage proportional to the thermal energy balance between itself and the surface it is detecting. Taking Equation 2.1, the rate at which a unit surface area of a road surface receives radiation from surrounding objects at temperature T_0 is σT_0^4, and the net rate of loss of energy by the road surface is given by I_{net}, as shown in Equation 2.1:

$$I_{net} = \varepsilon\sigma\left(T^4 - T_0^4\right) \tag{2.1}$$

where T is the surface temperature observed by the detector and T_0 the temperature of the detector usually measured by an internal thermistor (Liou 2002).

The voltage output by the infrared sensor is proportional to this thermal energy balance, so the maintenance of a stable body temperature is essential for accurate measurements to be made. In addition, infrared sensors are calibrated in such a way that increased accuracy is achieved with smaller temperature differences between the sensor and the target surface. As such, the positioning of an infrared sensor on a vehicle should be carefully considered to minimise random errors relating to the thermal energy balance, and systematic errors such as signal noise from vehicle emitted radiation or contaminated sensor optics due to dirt and condensation. The angle at which the sensor is mounted on the vehicle is also important since it will influence how much radiation received by the sensor originates from the road surface and how much comes from surrounding objects and the atmosphere (Gustavsson 1999). To minimise the influence of surrounding objects and the atmosphere, the infrared sensor should be mounted in a nadir position. In addition, apparent emissivity has been shown to change with view angle (Scott 1986; Lagourade et al. 1995), with detailed studies over an asphalt surface showing an 8% decrease in apparent emissivity with a view angle of 45° (Bergendahl 1998 cited in Gustavsson 1999). However, this variation is much greater than those found in other studies, and Gustavsson (1999) suggests further work is required in this area to understand fully the effects of varying view angle on RST.

The use of thermal mapping as a validation tool for route-based forecasts is by no means a new idea. The technique was first used for such purposes by Chapman et al. (2001a; 2001b), and Weather Services International have successfully used the technique to verify their OpenRoute™ route-based forecasting service, driven by the *ENTICE* model, during the 2006/07 and 2007/08 winter seasons (White 2007). In its current form however, thermal mapping is a time consuming and costly exercise. The large extent of some highway authority road networks means that a single complete survey covering all salting routes can often take

several nights to complete given the time restrictions imposed on surveys by daylight and traffic loads. Research has shown that traffic is a major source of potential error in thermal mapping surveys (Prusa et al. 2002; Chapman & Thornes 2005), with heat fluxes from vehicles having the effect of increasing RST which consequently impacts on the timing of thermal mapping runs. Chapman & Thornes (2005) suggest limiting thermal mapping surveys to the few hours before sunrise on weekends to avoid 'snapshot' data collected at any other time which they argue will not be representative of minimum temperatures. Whilst this may be a somewhat histrionic approach, it emphasises the fact that thermal mapping surveys are restricted to a small time window, during which it is impossible to survey the full spatial and temporal resolution of a route-based forecast. This somewhat limits the usefulness of thermal mapping as a suitable long term validation technique for route-based forecasts. Given the time constraints associated with thermal mapping surveys and the growing demand for validation data as increasing numbers of highway authorities use route-based forecasting services, the time appears to have come for a new validation technique to be developed. Any new technique will need to be both robust and reliable, whilst at the same time offering a rapid and cost effective solution for the forecast provider, but unless a new technique allowing validation at the full spatial and temporal resolution can be found, compromises will have to be made.

2.2 Data Reduction

From the review of existing validation techniques, it is clear that no one technique provides the answer to verifying a route-based forecast. Clearly validation cannot be achieved using regression analysis on thermal mapping data since the aim is to verify rather than predict RST, with the latter undertaken using heat balance models. The main problem is the vast number of points that need to be validated, and a sensible approach is somehow to reduce the number of points needing to be validated to provide a more manageable dataset. An obvious

solution would be simply to reduce the resolution of the route-based forecast, say from 50 metres to 100 metres. This would immediately halve the number of forecast points needing to be validated, but would bring no operational benefit to the forecast provider since it would still require the same mileage of road network to be driven for thermal mapping validation. Additionally, any reduction in the resolution of the route-based forecast can be seen as a reduction in the quality of the forecast since it reduces the ability to be able to identify and model small scale thermal singularities around the road network such as bridges and areas prone to katabatic drainage. In an environment of increasing litigation there is an argument to be made that even a resolution of 50 m is insufficient since RST has been shown to vary by over 1.5°C at the sub-metre scale (Chapman & Thornes 2008). Clearly an alternative methodology is required in order to reduce the number of points needing to be validated without compromising on the quality of the route-based forecast being delivered.

2.2.1 Techniques for data reduction

Numerous statistical techniques are available for the purposes of data reduction, and many of these can be categorised under the general headings of Factor Analysis or Clustering. The most common form of Factor Analysis for achieving data reduction uses principal components extraction and is commonly referred to as Principal Components Analysis (PCA). The central idea of PCA is to describe a dataset consisting of a large number of variables by means of only a few variables, while retaining as much of the variability present in the original dataset as possible (Preisendorfer 1988). PCA is commonly used in the field of geographical sciences where an abundance of instrumentation often enables numerous system variables to be measured and large sample sizes to be collected. When more than two or three variables are being measured, it can often become difficult to visualise their relationships. However, in data sets with many variables, groups of variables are often associated and co-vary together, since more than one variable might be measuring the same driving principle

governing the behaviour of the system. In many systems there are only a few such driving forces, even though an abundance of instrumentation enables you to measure many system variables. PCA is a quantitatively rigorous method of simplifying a dataset by replacing a group of variables with a new set of variables (axes) called principal components, each treated as a single axis in space. Each principal component is a linear combination of the original variables, but all the components are orthogonal to each other so are uncorrelated. The full set of principal components explains all of the variance in the original set of variables.

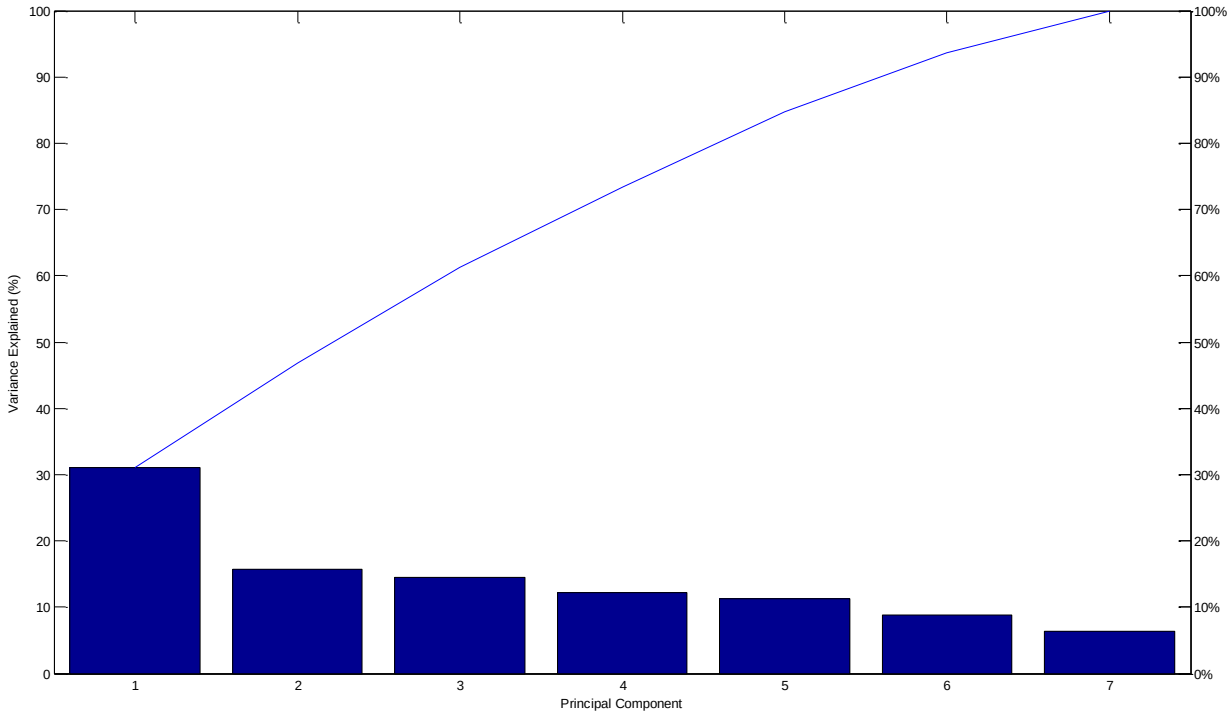

Figure 2.2 Example Pareto chart for showing the variance explained by each principal component.

The percentage of variance explained by each principal component is best viewed using a Pareto chart (Figure 2.2) where the principal components are arranged and plotted in descending order, with an accompanying line graph showing the accumulative variance. The first principal component accounts for as much of the total variance in the dataset as possible, with the second principal component accounting for as much of the remaining variance as

possible whilst being uncorrelated with the first component, continuing in this way until there are as many components as original variables. It is commonplace for the sum of the variances of the first few principal components to explain the majority of the total variance of the original data, with the remaining components accounting for only a small part of the total variance and thus being unimportant. By examining plots of the main principal components of a dataset it is possible to identify the dominant patterns of spatial variability in the data to develop a deeper understanding of the driving forces that generated the original data.

Clustering can most easily be defined as the grouping of similar objects using data from the objects (Seber 2004). It is a general term which encompasses a number of different algorithms and methods for organising datasets into groups in such a way that the degree of association between two objects is greatest if they belong to the same group and minimal otherwise. The goals of cluster analysis are varied and include widely different activities such as hypothesis generation, identification of 'natural' groups of like objects to form the first stage of a stratified sampling strategy, and the development of classification schemes such as the classification of plants and animals (taxonomy) or diseases (Seber 2004). Clustering techniques have been applied to a wide variety of research problems in numerous subject areas including archaeology, anthropology, agriculture, economics, education, geography, geology, linguistics, market research, genetics, medicine, psychology, psychiatry and sociology, and Hartigan (1975) provides an extensive summary of numerous published studies reporting the results of cluster analyses.

Seber (2004) identifies three main types of clustering: Hierarchical clustering, Partitioning and Overlapping clusters. In hierarchical clustering the clusters are themselves grouped into other clusters, with the process being repeated at different levels to form a tree of clusters often referred to as a dendrogram. The cluster tree can be constructed using either a bottom-up agglomerative approach involving a series of successive fusions of *n* objects into clusters, or from the top down using a divisive method which partitions the total set of *n* objects into

increasingly smaller clusters (Seber 2004). Within partitioning methods of clustering, objects are partitioned into non-overlapping clusters, the number of which is usually determined in advance. Although there are numerous partitioning methods of clustering, K-means is perhaps the most commonly used. The K-means analysis procedure assigns objects to clusters based on distance from pre-assigned cluster centres, the locations of which are updated based on the mean values of the objects in each cluster. Overlapping clusters, sometimes referred to as Clumping, are rarely used and intended for situations where it is more meaningful to allow a certain degree of overlap between clusters (Seber 2004). Such an example would be in linguistics, where words can have several meanings and may belong to several groups. Overlapping methods of clustering, however, are generally more computationally complex and the results more difficult to interpret (Sneath & Sokal 1973), leaving hierarchical and partitioning methods of clustering as the preferred options for multivariate analysis.

2.2.2 Data reduction in the *ENTICE* route-based forecast model

2.2.2.1 Building the *ENTICE* GPD

The spatial modelling approach used in the *ENTICE* route-based forecast model is driven by a GPD consisting of several geographical and infrastructure parameters listed in Table 2.2. Construction of the *ENTICE* GPD firstly requires View Factor Mapping (VFM) surveys to be undertaken, where sky view factor (ψ_s) data are collected in real-time using a patented method first developed by Chapman & Thornes (2004). This technique uses a feed-forward back-propagation artificial neural network to calculate ψ_s by proxy by measuring the number of tracked and visible satellites in the Global Positioning System (GPS) network and the quality of incoming signal to noise ratios from the satellites. The equipment used in a VFM survey consists of a Navman GPS development unit with a roof mounted antenna connected to a laptop computer via USB connection, both powered from a 12V DC in-car cigarette lighter via a 12V DC to 230V AC 150W power invertor. Bespoke logging software is used to initiate

the logging of GPS positional and proxy ψ_s data which is automatically appended to a database file every second. With the positional and ψ_s data being logged, a survey route is driven and to ensure optimum GPS positional fix throughout the survey, driving speed along the route is restricted to a maximum of 50 mph.

Table 2.2 Meteorological, geographical and road infrastructure parameters used to drive the *ENTICE* road weather prediction model (Chapman et al. 2001a).

Meteorological Parameters	**Geographical Parameters**	**Road Parameters**
Solar radiation	Latitude	Depth of construction
Terrestrial radiation	Altitude	Thermal conductivity
Air temperature	Topography	Thermal diffusivity
Cloud cover and type	Screening	Emissivity
Wind speed	Sky View Factor *(ψ_s)*	Albedo
Humidity / dew-point	Landuse	Traffic
Precipitation	Topographic exposure	

Altitude, slope and aspect data for each forecast point are obtained from a high resolution digital elevation model (DEM) using GIS software, and road type data are derived from Ordnance Survey® Meridian™ data. A proxy classification of land use density is obtained via a spatial density analysis of vector road data using the method described by Chapman & Thornes (2006) to locate dense areas of the road network, with the assumption that more heavily urbanised areas have a denser road network than suburban and rural areas. Traffic density is parameterised through use of a general traffic algorithm (Chapter 6) described by Chapman (2002) that introduces a slight temperature bias dependent on land use and road type classifications and a shadowing coefficient to account for reduced outgoing long-wave radiation from the road surface caused by vehicles. The treatment of traffic in this way is simplistic and could be greatly improved by consideration of daily traffic densities from sources such as Motorway Incident Detection and Automatic Signalling (MIDAS) loops, but

such data is not freely available in the UK, thus hindering the development of an accurate traffic coefficient. An alternative methodology could potentially involve the use of raw data from remote infrared temperature sensors which use traffic filtering algorithms to remove most of the noise associated with passing vehicles, and this would enable greater network coverage than MIDAS loops that are typically only installed on motorways and the most heavily congested A-roads.

2.2.2.2 Birmingham study route

Figure 2.3 displays a mixed urban and rural study route in Birmingham, UK, which was selected as a test bed for this research. The study route, which traverses through Birmingham city centre before passing through the south-west Birmingham suburbs and north Worcestershire countryside, was chosen for this study due to the large variation in geography around the route and also due to the large amount of thermal mapping data that exists for the route. Figure 2.4 (a) to (d) display elements of the *ENTICE* GPD for this study route plotted as a series of layers in a GIS to show the variation of geographical and road infrastructure parameters around the route. Altitude around the study route varies from between 120 m in the suburbs of Birmingham up to 250 m in the rural Clent Hills to the south-west of the route (Figure 2.4 (a)). Variations in land use and road type are clearly identifiable in Figure 2.4 (b) and (c), ranging from A-roads in the heavily urbanised city centre to more minor roads in the rural and semi-rural areas of the route. The variation in ψ_s around the route (Figure 2.4 (d)) is as expected, with ψ_s values generally lower in the city centre and higher in rural areas, although exceptions to this rule include some rural tree lined roads and locations underneath bridges and underpasses which have very low ψ_s values.

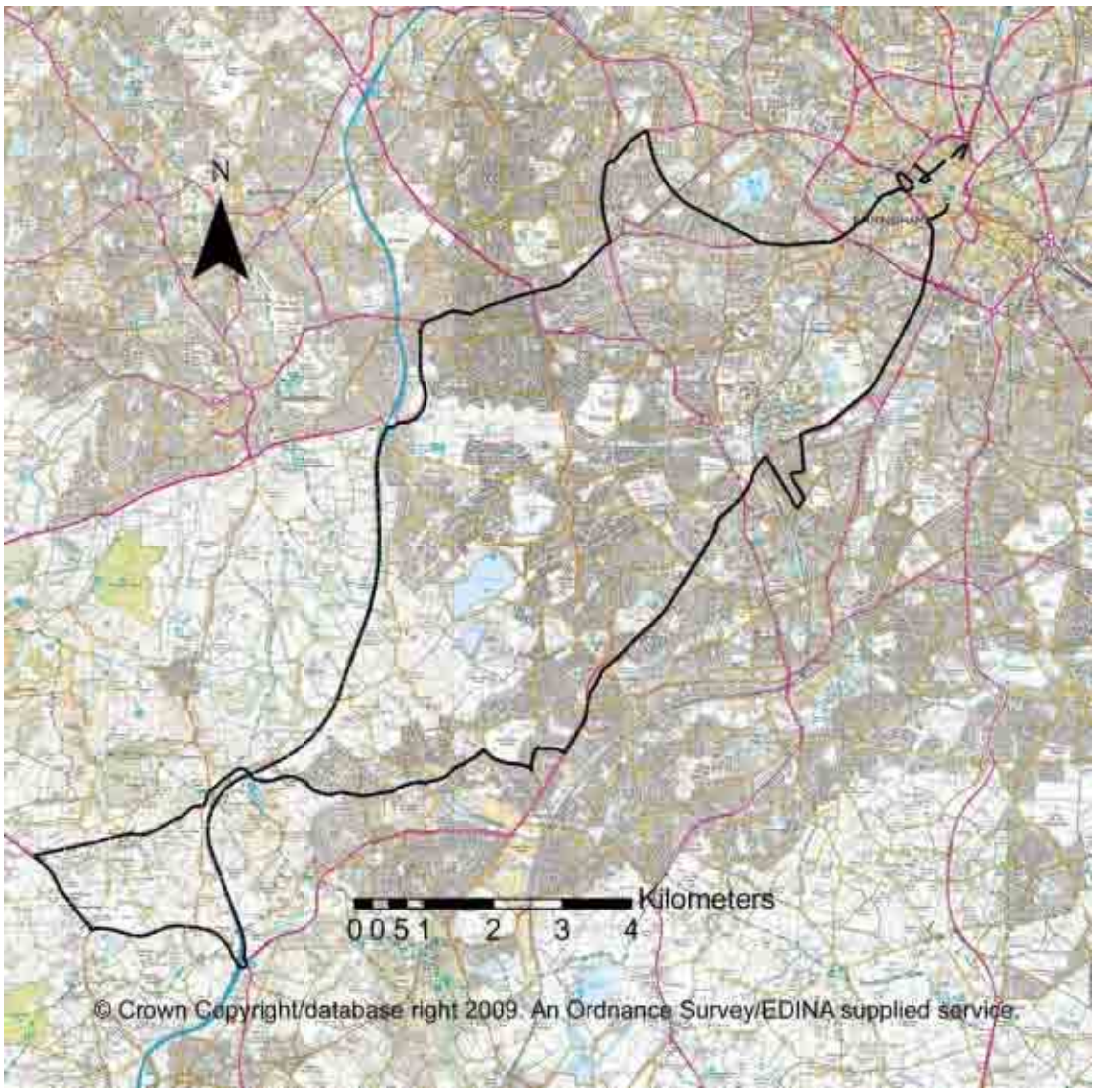

Figure 2.3 Map displaying the mixed urban and rural study route in Birmingham, UK, which was used as the test bed for the research in this thesis.

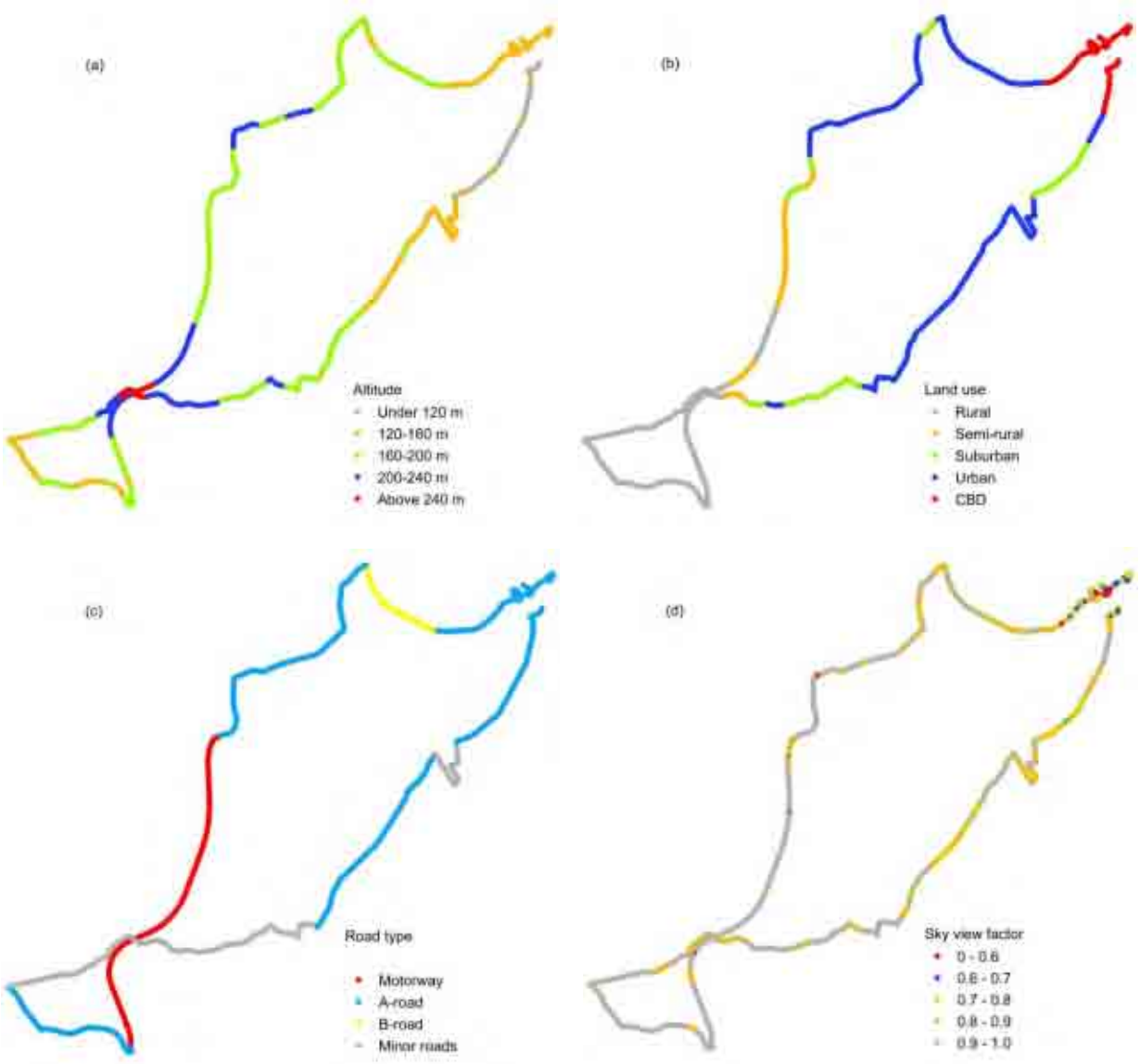

Figure 2.4 Geographical and infrastructure parameters from the *ENTICE* GPD plotted as layers in a GIS, showing variations in geographical and infrastructure parameters around the Birmingham study route for (a) altitude; (b) land use; (c) road type; (d) ψ_s.

2.2.2.3 Modifications to the *ENTICE* GPD

Modifications were required to some of the data within the GPD before data reduction could occur. For example, the ordinal nature of land use and road type data creates problems for clustering algorithms since the distance between two objects in an ordinal dataset may bear no relation to the similarity or dissimilarity between the objects, and could have a negative effect

on the clustering solution. To overcome this issue, average thermal conductivity values for the road surface at each forecast point were calculated based on the assumption of a five zone flexible pavement identical to that used by Chapman (2002), with variations in the materials and hence thermal properties of each zone according to the road type classification (see Chapter 3 for further details). Similarly, ordinal land use data was replaced with roughness length (Z_0) values similar to those used by Chapman (2002) which vary with respect to both the land use and road type classifications and are based on Z_0 values assimilated from scientific literature. Whilst these new variables still contain categorical data which it is recognised can reduce the objectivity of distance measures in clustering algorithms, numerous studies have shown that both land use and road construction can have a significant influence on RST (Shao et al. 1997; Gustavsson 1999; Chapman et al. 2001a a; Chapman 2002; Chapman & Thornes 2006), so the inclusion of these parameters in any data reduction exercise should be seen as a prerequisite. Finally, the sine and cosine trigonometric functions of the aspect data were calculated and used in place of the original aspect data since the feature space distance between 0° and 360° in a cluster analysis would be incorrectly large when in reality it should be zero since the values are exactly the same.

Table 2.3 (a) displays a correlation matrix and Table 2.3 (b) the resulting *p*-values matrix for the modified GPD. The correlation coefficients reveal relatively weak correlations ($-0.4 < r < 0.4$) between the various geographical and road infrastructure parameters. The only correlations of any note are ψ_s and Z_0 which are negatively correlated (-0.41) as can be expected due to the influence of urban street canyons on ψ_s values, which is well documented in the literature (Grimmond et al. 2001; Chapman & Thornes 2004; Chapman et al. 2007). The correlation between Z_0 and Sine Aspect (0.42) can partially be attributed to the fact that Birmingham city centre is located at the far eastern side of the study route and the most rural areas are located on the western side of the route. Likewise, the negative correlation between altitude and Z_0 (-0.38) is largely due to the topography of the route since the highest altitude

points are located on the more rural western side of the study route and some of the lowest lying points are found in the city centre. Almost all of the correlations between the parameters are statistically significant at the 5% level with the exception of those underlined in the *p*-values matrix in Table 2.3 (b).

Table 2.3 (a) Correlation matrix for the Birmingham GPD, showing the strength of correlations between the various geographical and infrastructure parameters, **(b)** *p*-values matrix for the Birmingham GPD indicating the significance of the correlations.

(a)	**SVF**	**Altitude**	**Slope**	**Sin Aspect**	**Cos Aspect**	Z_0	**Conductivity**
SVF	1.0000	0.3229	0.1539	-0.2088	0.0447	-0.4127	0.0799
Altitude	0.3229	1.0000	0.2820	-0.2199	-0.0366	-0.3808	-0.0268
Slope	0.1539	0.2820	1.0000	-0.2155	-0.0930	-0.2411	0.0451
Sin Aspect	-0.2088	-0.2199	-0.2155	1.0000	-0.0813	0.4236	0.0427
Cos Aspect	0.0447	-0.0366	-0.0930	-0.0813	1.0000	0.1173	-0.0469
Z	-0.4127	-0.3808	-0.2411	0.4236	0.1173	1.0000	0.0787
Conductivity	0.0799	-0.0268	0.0451	0.0427	-0.0469	0.0787	1.0000

(b)	**SVF**	**Altitude**	**Slope**	**Sin Aspect**	**Cos Aspect**	Z_0	**Conductivity**
SVF	1.0000	0.0000	0.0000	0.0000	0.0336	0.0000	0.0001
Altitude	0.0000	1.0000	0.0000	0.0000	0.0820	0.0000	0.2026
Slope	0.0000	0.0000	1.0000	0.0000	0.0000	0.0000	0.0320
Sin Aspect	0.0000	0.0000	0.0000	1.0000	0.0001	0.0000	0.0422
Cos Aspect	0.0336	0.0820	0.0000	0.0001	1.0000	0.0000	0.0257
Z	0.0000	0.0000	0.0000	0.0000	0.0000	1.0000	0.0002
Conductivity	0.0001	0.2026	0.0320	0.0422	0.0257	0.0002	1.0000

These weak correlations between the parameters help to justify the use of clustering techniques as a means of reducing a route-based forecast dataset rather than other common data reduction techniques such as PCA. For PCA to be of real benefit, a reasonable number of the variables in a dataset should be inter-correlated, otherwise it is likely that large proportions of the variance in the original dataset will be unaccounted for in the first few principal components. All of the variables within the *ENTICE* GPD have been shown to influence RST, so any variance in the GPD effectively represents thermal variations around the road network, a high proportion of which must be accounted for to be able to verify the forecast accurately. A large proportion of this thermal variance could be lost via PCA, but clustering techniques maintain the original data structure and simply organise a dataset into groups containing objects with a high degree of association and similarity. Hence, clustering maintains 100% of the variance within a dataset whilst providing a means for data reduction via the classification of objects into clusters. Any loss of variance resulting from the subsequent reduction of a clustered dataset can then be viewed as a function of the chosen sampling strategy.

2.3 Hierarchical and K-means Clustering of the *ENTICE* GPD

Data from the modified *ENTICE* GPD for all 2,261 forecast points along the study route was clustered using both hierarchical and K-means cluster analyses, the two most commonly used methods of clustering. To account for the range of measurement scales in the dataset which can distort proximity calculations in cluster analyses, all the values in the dataset were normalised to the same proportional z-score scale using the mean and standard deviation of the variables. Hierarchical clustering was performed in Matlab® using a bespoke cluster program (Appendix 1) designed to rapidly analyse geographical and infrastructure data from the *ENTICE* GPD. The process of hierarchical clustering firstly involved analysing the data to find the similarities between every pair of objects in the data set. Using the Euclidean metric

algorithm (Equation 2.2) a distance matrix was created where element *i*,*j* in the matrix corresponded to the distance between object *i* and object *j* in the original data set. Once the proximity between all objects in the data set was computed, the group average clustering algorithm (Equation 2.3) was used to link pairs of objects close together into binary clusters (clusters made up of two objects), and to link these newly formed clusters to each other and to other objects to create larger clusters until all the objects in the original data set were linked together in a hierarchical cluster tree.

For the Euclidean metric algorithm, given an *m*-by-*n* data matrix X, which is treated as *m* (1-by-*n*) row vectors $x_1, x_2, \ldots, x_m$, the distance between the vector x_r and x_s is defined as:

$$d_{rs} = \left\{\sum_{j=1}^{n} \left| x_{rj} - x_{sj} \right|^2 \right\}^{1/2} \tag{2.2}$$

If n_r is the number of objects in cluster *r* and n_s is the number of objects in cluster *s*, and x_{ri} is the *i*th object in cluster *r*, the group average clustering algorithm uses the average distance between all pairs of objects in cluster *r* and cluster *s*, i.e.

$$d(r,s) = \frac{1}{n_r n_s} \sum_{i-1}^{n_r} \sum_{j=1}^{n_s} dist\,(x_{ri}, x_{sj}) \tag{2.3}$$

Figure 2.5 shows the resulting dendrogram created by hierarchical clustering of the study route GPD using the Euclidean metric and group average clustering algorithms, which gave a cophenetic correlation coefficient of 0.74 indicating a good clustering solution for the data set. Partitioning of the data set into a set number of clusters was then required, but a major problem in any cluster analysis is the choice of *k*, the number of clusters. Given the exploratory nature of clustering it is virtually impossible to determine the 'optimum' number of clusters until analyses are run and the results examined. Examination of an expansive and often contradictory body of literature on cluster analysis reveals that there are no hard and fast

rules for defining the number of clusters, but simply a myriad of suggested methods and formulas, some of which receive greater support in the literature than others. It is generally recognised however that the number of clusters necessary to portray a dataset adequately is closely related to the number of objects within the dataset. An often quoted rule that determines the approximate number of clusters required (k) based on the number of objects (N) in the dataset uses the formula (Clark & Hosking 1986):

$$k = 1 + 3.3(\log_{10} N) \tag{2.4}$$

where $\log_{10} N$ is the logarithm to the base 10 of the total number of objects. For the Birmingham study route containing at total of 2261 forecast points, this gave a k value of 12.07 resulting in a horizontal slice across the dendrogram at a point where it intersects 12 links on the tree, thus dividing the data set into 12 clusters. Parsing the dendrogram in this way is less subjective, and the same method could potentially be used to determine the number of clusters for many different salting routes, hence adding an element of consistency to the clustering procedure. Visual analysis of the dendrogram in Figure 2.5 shows 12 clusters to be a reasonable solution for the study route since it parses a number of inconsistent links on the cluster tree which indicate the border of natural divisions in the data set. The top link on the dendrogram in Figure 2.5 indicates that approximately 10% of the data differs significantly from the remaining 90%, which would indicate possible outlying values at this point in the dataset rather than a true natural division, and further justifies the parsing of the dendrogram at a lower level.

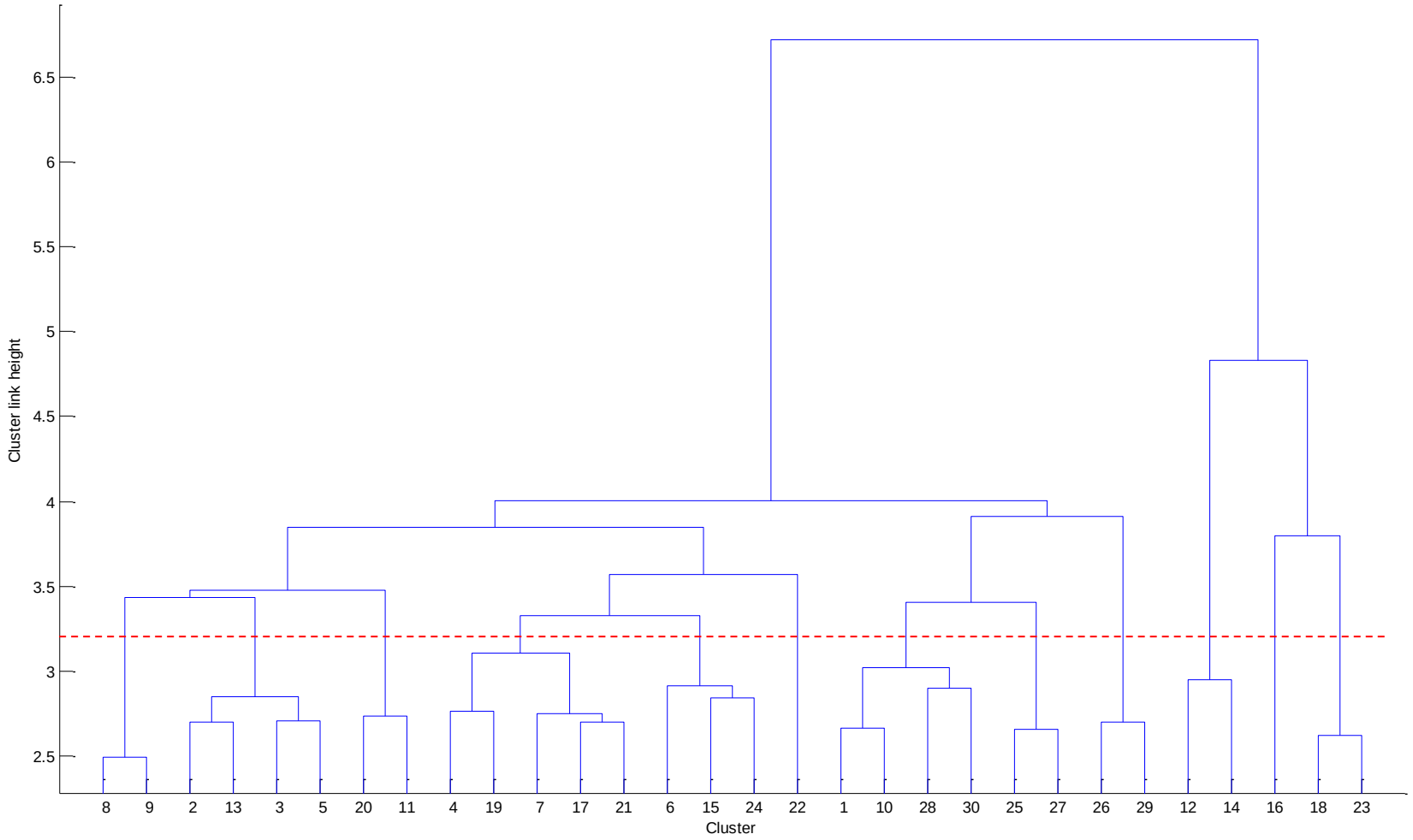

Figure 2.5 Top section of a dendrogram showing the hierarchical clustering solution for the Birmingham study route GPD generated using the Euclidean metric and group average clustering algorithms. The horizontal line across the dendrogram intersects 12 links on the cluster tree, demonstrating the partitioning of the dataset into 12 clusters.

K-means clustering was undertaken using the standard K-means clustering algorithm available within SPSS 16.0 for Windows®, with the dataset again partitioned into 12 clusters. Following the construction of initial cluster centres, all the objects in the dataset were assigned to clusters based on the squared Euclidean distance from the cluster centres. Objects were then individually reassigned to another cluster if doing so reduced the sum of distances from the cluster centre, with the cluster centres recalculated after each addition to the cluster based on the mean values of objects in the cluster. A benefit of the K-means procedure is it allows for a user-defined number of iterations, with a single iteration consisting of one pass through all the objects within the dataset. This enables K-means to converge to an optimum solution in which the reassignment of any single point to a different cluster would increase the total sum of distances. The K-Means algorithm updated the cluster centres iteratively and an optimum solution for 12 clusters was achieved after 16 iterations.

Figure 2.6 (a) and (b) display maps of the hierarchical and K-means clustering solutions respectively, together with summary GPDs showing the mean values within each cluster, and Table 2.4 (a) and (b) display the standard set of route-based forecast validation statistics calculated for each cluster based on data from 20 thermal assessments of the study route. Initial visual analysis of the maps and GPDs in Figure 2.6 (a) and (b) reveals that both the hierarchical and K-means solutions partition the dataset into reasonably distinct areas of road network with clear geographical and/or road infrastructure boundaries between the clusters. For example, the forecast points within cluster 8 of the hierarchical solution (Figure 2.6 (a)) are characterised by high altitude, high ψ_s and high road thermal conductivity values indicating forecast points located at a high altitude motorway section of the study route. In comparison, cluster 7 of the hierarchical solution represents forecast points at locations with a shallower road construction in a lower altitude, higher gradient rural area of the route, indicated by the lower average road thermal conductivity, altitude and Z_0 values and the higher average slope value. Despite this clear link between the clustering solution and the

physical geography and road infrastructure around the route, Figure 2.6 (a) and (b) reveal differences between the two clustering solutions. With the hierarchical solution it is evident that certain clusters are more dominant since they contain a greater number of forecast points than other clusters, with Table 2.4 (a) revealing that over 50% of the points along the study route were assigned to one cluster. In contrast, Figure 2.6 (b) reveals a lack of any single dominant cluster with the K-means clustering solution, possibly a result of the iterative nature of the clustering procedure which enables K-means to converge to an optimum solution.

Cluster	ψ_s	*Altitude*	*Slope*	*Sin Aspect*	*Cos Aspect*	Z_0	*Conductivity*
1	0.96	163	1.84	-0.32	0.16	31.02	0.0036
2	0.94	199	4.40	-0.64	0.06	55.75	0.0038
3	0.65	185	1.87	-0.54	0.84	50.00	0.0039
4	0.63	133	1.27	0.82	-0.27	99.80	0.0030
5	0.90	159	1.97	0.59	-0.01	78.49	0.0033
6	0.91	222	2.46	0.40	0.44	49.00	0.0022
7	0.93	193	3.06	-0.47	-0.73	32.16	0.0022
8	0.97	236	1.86	0.82	-0.13	50.00	0.0039
9	0.82	134	1.57	-0.33	0.67	86.44	0.0022
10	0.17	192	2.18	-0.77	0.48	50.00	0.0039
11	0.13	148	1.96	0.77	-0.48	100.00	0.0035
12	0.51	228	5.88	-0.87	-0.49	50.00	0.0039

(a)

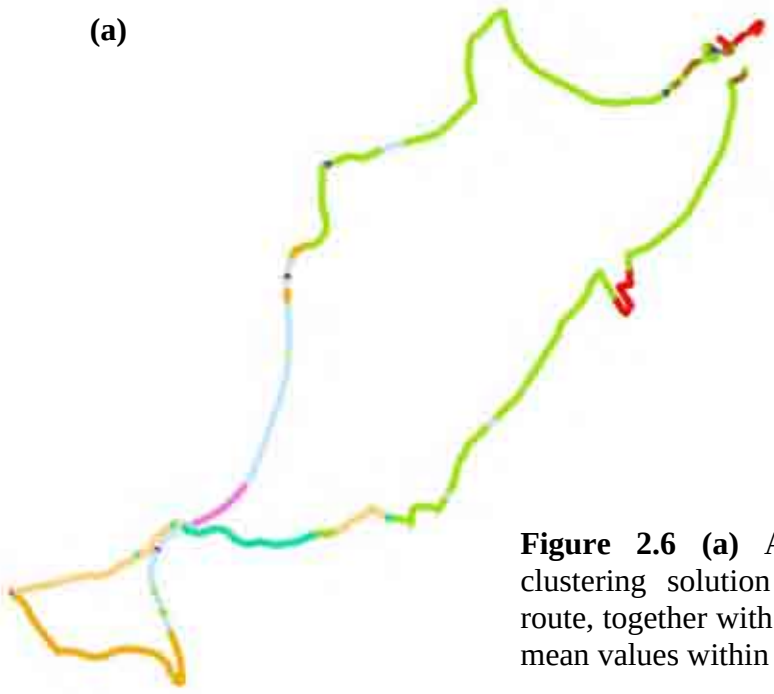

Figure 2.6 (a) A map of the hierarchical clustering solution for the Birmingham study route, together with a summary GPD showing the mean values within each hierarchical cluster.

Cluster	ψ_s	*Altitude*	*Slope*	*Sin Aspect*	*Cos Aspect*	Z_0	*Conductivity*
1	0.89	151	1.81	0.03	0.65	77.23	0.0023
2	0.90	215	4.59	0.11	-0.15	36.38	0.0022
3	0.13	148	1.96	0.77	-0.48	100.00	0.0035
4	0.89	159	1.42	0.49	0.68	85.47	0.0034
5	0.93	188	1.85	-0.48	-0.73	36.07	0.0022
6	0.85	124	2.40	0.74	-0.50	74.60	0.0035
7	0.17	192	2.18	-0.77	0.48	50.00	0.0039
8	0.91	177	1.95	0.19	-0.87	78.57	0.0034
9	0.63	132	1.31	0.76	-0.14	99.83	0.0028
10	0.96	164	1.67	-0.56	0.45	30.92	0.0035
11	0.94	200	4.57	-0.64	0.22	52.52	0.0038
12	0.94	191	2.20	0.89	-0.24	62.01	0.0032

(b)

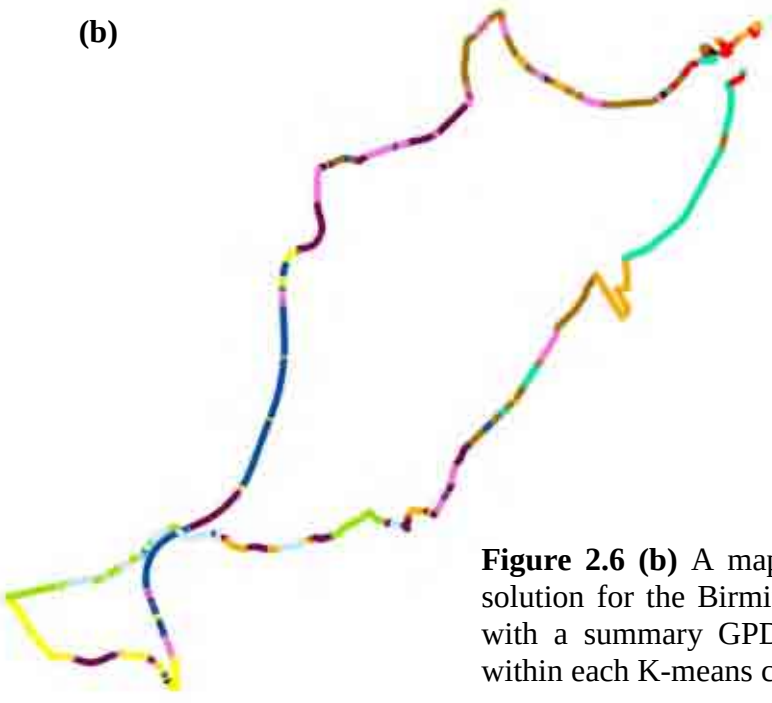

Figure 2.6 (b) A map of the K-means clustering solution for the Birmingham study route, together with a summary GPD showing the mean values within each K-means cluster.

The statistics in Table 2.4 (a) and (b) reveal how the performance of the forecast model can be better assessed by analysing the statistics at a cluster level. The statistics presented in this table are the standard forecast validation statistics used within the road weather industry for assessing road weather model performance. These statistical terms, which are defined in the mathematical description of *ENTICE* route-based forecast statistics at the start of the thesis, include the model bias (β), standard deviation of bias (σ_β), root mean square error (*RMSE*) of the forecast, and the percentage of modelled (*Pm*) and residual modelled (*Prm*) forecast points within ± 1℃ of the actual and residual actual values. Where entire route statistics are given, these are the average values based on all forecast points around the study route, and where cluster level statistics are given, these are average values based on all forecast points within that cluster. Unless otherwise stated, all the forecast validation statistics presented in this thesis are an average of 20 thermal mapping runs of the study route.

The model statistics shown in Table 2.4 (a) and (b) were obtained with the *ENTICE* model run in 'quasi-operational' mode, with all the parameters within the model set to their best values. A low σ_β is an indicator of similar thermal characteristics between forecast points, so a good clustering solution should aim to reduce the $\sigma_\beta$within as many clusters as possible to a value below that for the entire route, hence making the clusters more distinct. Of the twelve clusters shown in Table 2.4 (a) and (b), only three clusters in Table 2.4 (a) (clusters 1, 10 and 11) and two clusters in Table 2.4 (b) (clusters 7 and 10) have σ_β values greater than the overall route statistic, indicating that thermal variations around the road network are well represented by both clustering solutions. The significantly higher σ_β values in clusters 10 and 11 in Table 2.4 (a) and cluster 7 in Table 2.4 (b) can be explained by the fact that all of these clusters contain forecast points located under bridges or underpasses, locations which the model is known to be less accurate in forecasting for due to the lack of any advective component in the zero-dimensional heat balance model. The marginally higher σ_β values in

cluster 1 in Table 2.4 (a) and cluster 10 in Table 2.4 (b) are likely to be the result of varying ψ_s values within these clusters due to increased vegetation in rural locations where accuracy of the proxy method of ψ_s data collection is known to be more variable (Chapman & Thornes 2006). The accuracy of statistics regarding actual temperatures can sometimes be misleading since they are heavily dependent on the accuracy of the meteorological input data, so an analysis of the percentage of correct residuals (*Prm*) is useful for assessing a model's spatial forecasting performance (Chapman et al. 2001b). The residuals in Table 2.4 (a) for the hierarchical clustering solution reveal that in some clusters the model was 100% residually correct to within ±1°C, and in 9 of the 12 clusters which together account for 89% of the entire study route, the residual statistics are significantly better than the overall route statistic would otherwise indicate. Similarly, Table 2.4 (b) reveals that the residual statistics in 9 of the 12 clusters for the K-means solution are also significantly better that the overall route statistic would otherwise indicate, with these clusters accounting for 91% of the entire study route.

Table 2.4 (a) Route-based forecast validation statistics for the study route calculated for individual hierarchical clusters. Entire route statistics represent the validation statistics obtained using the existing methodology. **(b)** The same as (a), but for K-means clustering.

	β	σ_β	*RMSE*	*Pm*	*Prm*	No. Forecast Points
Entire Route	-1.06	0.86	1.48	46.94	79.56	2261
(a)						
Cluster 1	-0.77	0.87	1.32	46.97	78.45	216
Cluster 2	-0.29	0.55	0.83	77.30	94.38	200
Cluster 3	-0.78	0.00	0.99	55.00	100.00	1
Cluster 4	-2.32	0.73	2.45	9.53	85.00	128
Cluster 5	-1.12	0.70	1.45	44.80	87.01	1196
Cluster 6	-0.55	0.54	0.98	67.68	91.92	125
Cluster 7	-0.97	0.52	1.23	50.73	93.80	192
Cluster 8	-0.32	0.20	0.70	76.71	100.00	35
Cluster 9	-1.46	0.71	1.71	30.11	83.24	142
Cluster 10	-2.89	1.35	3.10	12.50	60.00	2
Cluster 11	-2.30	1.17	2.66	16.52	57.17	23
Cluster 12	-0.12	0.00	0.54	95.00	100.00	1
(b)						
Cluster 1	-0.89	0.66	1.48	41.80	87.43	269
Cluster 2	-0.76	0.58	1.12	58.92	91.01	134
Cluster 3	-2.30	0.00	2.66	16.52	57.17	23
Cluster 4	-1.17	0.69	1.47	45.28	87.20	394
Cluster 5	-1.02	0.51	1.25	49.85	94.35	131
Cluster 6	-1.62	0.66	1.85	20.64	86.58	250
Cluster 7	-2.89	1.35	3.10	12.50	60.00	2
Cluster 8	-0.88	0.64	1.21	56.85	90.16	252
Cluster 9	-2.29	0.70	2.41	9.41	85.62	145
Cluster 10	-0.73	0.92	1.33	47.37	75.44	169
Cluster 11	-0.30	0.58	0.85	76.40	93.06	186
Cluster 12	-0.75	0.00	1.09	58.86	93.14	306

2.4 Consistency of the Clustering Techniques

To quantify the consistency of the clustering techniques, Clustering Similarity Coefficients (CSC) were calculated for pairs of thermal mapping runs in the same weather category in order to measure the similarity of the spatial distribution of RST variation identified by the clustering solutions. CSC are calculated in a similar manner to Section Similarity Coefficients used in thermal mapping (Shao et al. 1996), but use clusters determined by the geography and road infrastructure around a route rather than sections determined by temperature variations around a route. For two independent thermal mapping runs in the same weather category, the mean temperature of a cluster is compared to the series mean and is assigned a positive sign if the cluster mean is greater than or equal to the series mean, or a negative sign if the cluster mean is less than the series mean. If the signs of the first clusters of both series are the same, $a = 1$. If the signs of the next clusters in both series are the same, $a = a+1$, otherwise $b = b+1$ if the signs are different. Once the values of a and b are calculated for each pair of series, CSC are calculated as follows:

$$CSC = \frac{a}{a+b} \tag{2.5}$$

The higher the value of CSC between two series, the greater the similarity of spatial temperature distribution between the series and the better the clustering solution is at capturing the physical relation between measured RST and the geographical and road infrastructure parameters used in the clustering solution. To assess the ability of both clustering techniques at capturing this physical relation, a CSC analysis was performed on pairs of thermal mapping runs for the study route. A total of 9 thermal mapping runs collected under various weather conditions (3 damped, 3 intermediate and 3 extreme) were analysed (Table 2.5). Results of the CSC analysis for both the hierarchical and K-means clustering solutions are shown in Table 2.6. It is seen from the table that the CSC vary from 0.75 to 1.00

with a mean of 0.87 over all weather categories for the hierarchical clustered data set, and from 0.67 to 1.00 with a mean of 0.91 for the K-means clustered data set. For individual weather categories, mean values ranged from 0.83 (Damped & Intermediate) to 0.95 (Extreme) for the hierarchical clustered data set, and from 0.78 (Damped) to 1.00 (Intermediate) for the K-means data set. This means that the clustering solutions successfully capture the physical relation between measured RST around the study route and the geographical and road infrastructure parameters used to cluster the data sets, with the spatial distribution of temperature around the study route repeatable for all three weather categories.

Table 2.5 Minimum, maximum, mean and $\boldsymbol{\sigma_\beta}$ of RST (°C) and category of thermal mapping (TM) fingerprint.

TM run	**Date**	**Min**	**Max**	**Mean**	$\boldsymbol{\sigma_\beta}$	**Category**
Damped (1)	13/01/00	-0.07	5.92	1.94	0.84	Damped
Damped (2)	29/02/00	2.68	7.01	4.21	0.57	Damped
Damped (3)	06/03/00	4.87	8.49	6.42	0.51	Damped
Intermediate (1)	10/12/99	3.04	9.36	5.16	1.00	Intermediate
Intermediate (2)	13/12/99	-0.95	7.14	1.69	1.12	Intermediate
Intermediate (3)	15/12/99	-2.47	4.32	-0.31	0.99	Intermediate
Extreme (1)	20/12/99	-7.01	3.63	-3.26	1.65	Extreme
Extreme (2)	14/02/00	-3.53	6.54	-0.29	1.42	Extreme
Extreme (3)	22/02/00	-4.01	4.81	-0.58	1.42	Extreme

Table 2.6 Clustering similarity coefficients (CSC) for independent pairs of thermal mapping runs in the same weather category, calculated using hierarchical clustered forecast points (a) and K-means clustered forecast points (b).

TM pairs	No. of records	No. of clusters	CSC (a)	CSC (b)
Damped (1,2)	2261	12	0.75	0.67
Damped (1,3)	2261	12	0.83	0.92
Damped (2,3)	2261	12	0.92	0.75
Intermediate (1,2)	2261	12	0.75	1.00
Intermediate (1,3)	2261	12	0.83	1.00
Intermediate (2,3)	2261	12	0.92	1.00
Extreme (1,2)	2261	12	0.92	0.92
Extreme (1,3)	2261	12	1.00	1.00
Extreme (2,3)	2261	12	0.92	0.92

2.5 Comparison of Hierarchical and K-means Clustering

To test the significance of any differences between the means of the hierarchical and K-means clustered datasets, an Independent Samples Students t-test was performed on the clustered GPD values in Figure 2.6 (a) and (b). Table 2.7 displays the results of the Independent Samples t-test, with group 1 representing hierarchical clustering and group 2 K-means clustering. The group statistics show that the two clustering techniques produced similar means over the 12 cluster solution ($t = 0.123$, $p = 0.902$), with the hierarchical values varying a little more around their mean than the K-means values. With a Levene significance value greater than 0.10 it can be assumed that the two clustering solutions have equal variances, and since the significance value of the t-test is greater than 0.05 it is safe to conclude (95% confidence level) that the clustering solutions obtained using the two techniques are extremely similar, and the differences which do exist are highly marginal and probably due to chance (P = 90.2%).

Table 2.7 SPSS output statistics for an Independent samples *t* test comparing clustered GPD values for the hierarchical and K-means clustering solutions.

Group Statistics

	Group	N	Mean	Std. Deviation	Std. Error Mean
Test	1.00	84	35.285231	65.9492132	7.1956491
	2.00	84	34.074735	61.6993518	6.7319512

Independent Samples Test

Equal variances assumed

	Levene's Test for Equality of Variances		t-test for Equality of Means						
								95% Confidence Interval of the Difference	
	F	Sig.	t	df	Sig. (2-tailed)	Mean Difference	Std. Error Difference	Lower	Upper
Test	.082	.775	.123	166	.902	1.2104964	9.8537573	-18.2443	20.66534

2.6 Implementing a Cluster Based Validation Strategy

The clustering of forecast points and the subsequent validation of a route-based forecast at the cluster level presents the opportunity for new sampling strategies that have the potential to reduce the number of points needing to be validated in order to verify a route-based forecast accurately. The current methodology requires every forecast point along a route to be thermally mapped in order to obtain a single set of validation statistics for the entire route. Validation using clustering techniques, however, has been shown here to provide a more representative measure of a model's spatial forecasting ability. By calculating clustering similarity coefficients the clustering techniques tested have been shown to repeatedly capture the spatial distribution of temperature around a salting route and hence the physical relation between measured RST and the geographical and road infrastructure parameters controlling the clustering. Since the majority of thermal variations around the route are identified within the clustering, and since the variance within most clusters is significantly lower than the entire route average, validation of the full spatial extent of a route-based forecast can potentially be achieved with fewer forecast points. Using the current methodology of thermal mapping, a route-based forecast dataset could potentially be reduced by randomly sampling a smaller

number of forecast points from within each cluster. It is likely, however, that such a methodology would still require large sections of a route to be driven in order to reach the required points, and whilst driving routes can be dynamically optimised (Handa et al. 2007) to reduce some of the associated wastage this would entail, such a methodology does not allow for validation at the full temporal resolution of the forecast.

A more robust sampling strategy could involve the installation of low cost remote infrared RST sensors at numerous forecast points covering all the clusters within a route. This research has shown that such a sampling strategy would capture the spatial distribution of temperature around the route whilst providing continuous data throughout the day and night to enable validation of the route-based forecast at the full temporal resolution. Whilst this scale of data reduction could be viewed with scepticism, it must not be forgotten that over the last two decades traditional road outstations have been strategically located based on a limited number of climatic zones within a region. The clustering of forecast points around a route is in effect combining the old paradigm with the new to create high resolution climatic zones where geographical and road infrastructure parameters have a greater influence on variations in RST than the meteorological parameters. Hence, it is perhaps more appropriate to refer to these high resolution climate zones as ‘geo-clusters’. Reducing validation to only a small number of points, however, potentially reduces the ability to identify and model small scale thermal singularities around the road network such as shallow bridge decks and katabatic frost hollows. On the other hand, recent research by the UK Met Office (Brown et al. 2008) suggests that thermal features such as these could soon be identified using downscaling techniques on high resolution numerical weather prediction (NWP) models. This would enable a cluster style validation strategy using remote infrared RST sensors to be implemented without fear of safety compromises, knowing that any areas identified as ‘cold spots’ through downscaling techniques would be well monitored and accounted for in the route-based forecast.

CHAPTER TWO SUMMARY

A new methodology for verifying route-based forecasts is described that uses clustering techniques to create clusters of forecast points with similar geographical and infrastructure characteristics. This facilitates the analysis of forecast statistics at the cluster level, which is found to improve statistical assessment of model performance since validation can be achieved at a much higher resolution than the current methodology allows. Furthermore, validation of the full spatial extent of a route-based forecast can be achieved with fewer forecast points since the majority of thermal variations around the road network are well represented by the clustering solutions. A new sampling strategy using remote infrared RST sensors is proposed that potentially enables validation at a vastly improved spatial and temporal resolution.

It is envisaged that the proposed validation technique could be used as a rapid integrity test for future measurement techniques designed to improve upon existing parameterisations within route-based forecast models. This will be put to the test in chapter 5 of this thesis by verifying the integrity of the new re-parameterised road construction and surface roughness measurements that are proposed in the following two chapters. Currently, both road construction and surface roughness are not measured at the spatial scale demanded by a route-based forecast. The following two chapters attempt to address this issue, starting with road construction.

3. SPATIAL RE-PARAMETERISATION OF THE *ENTICE* MODEL: PART 1 - ROAD CONSTRUCTION

3.1 Road Construction Modelling in Route-Based Forecasts

Variations in the thermal properties of materials used in road construction are a contributing factor to subtle variations in RST around a road network (Chapman et al. 2001b), with the thermal damping depth of a road dependent upon the materials of which it is composed. Thornes (1984) modelled the road heat flux beneath the surface based on a five zone flexible pavement that simulated the road construction at a motorway study site. However, to add a spatial component to the model, there was a need to develop similar profiles for other classes of road found in the UK. Chapman et al (2001b) proposed a modified simulation for non-motorway roads by making subtle changes to the materials and thermal properties of the model profile to represent the different road types accounted for in the *ENTICE* model (Table 3.1).

Table 3.1 The materials and thermal properties of the ordinal road construction profiles used in *ENTICE*. Note: thermal diffusivity of asphalt, concrete and soil is assumed to be $0.7x10^{-2}cm^2sec^{-1}$, $1.2x10^{-2}cm^2sec^{-1}$, and $0.1x10^{-2}cm^2sec^{-1}$ respectively (Chapman et al. 2001b).

Depth (cm)	Motorway (1)	A-Road (2)	B-Road (3)	C-Road (4)
	Materials			
0 - 4.5	Asphalt	Asphalt	Asphalt	Asphalt
4.5 – 9	Asphalt	Asphalt	Asphalt	Concrete
9 – 18	Asphalt	Asphalt	Concrete	Concrete
18 – 36	Concrete	Concrete	Concrete	Concrete
36 – 72	Concrete	80% Concrete 20% Subgrade/soil	50% Concrete 50% Subgrade/soil	Subgrade/soil
Over 72	Subgrade/soil	Subgrade/soil	Subgrade/soil	Subgrade/soil
	Average thermal conductivity			
	$3.9x10^{-3}$cal cm^{-1} sec^{-1} °C	$3.5x10^{-3}$cal cm^{-1} sec^{-1} °C	$2.9x10^{-3}$cal cm^{-1} sec^{-1} °C	$2.1x10^{-3}$cal cm^{-1} sec^{-1} °C

ENTICE assumes a flexible pavement with a constant damping depth of 72 cm split into five calculation zones. Variations in the construction of this 72 cm profile with respect to materials and thermal properties are parameterised in the model according to the ordinal road type

classification in the *ENTICE* GPD. These parameterisations are based on the assumption that a higher road classification (e.g. motorway) will have a profile with a greater proportion of asphalt and concrete at the expense of a soil sub-base (Table 3.1). In a sensitivity analysis on the *ENTICE* model, Chapman et al. (2001b) showed that variations in road construction were a significant factor controlling RST. By holding all geographical and infrastructure parameters within the model constant with the exception of road construction, Chapman et al. (2001b) found that *ENTICE* model predictions could explain up to 68% of the variation in RST around a study route (Figure 3.1). Furthermore, the impact of road construction on the prediction of RST was found to be most dominant at higher levels of atmospheric stability (Figure 3.1), during which road surfaces are more vulnerable to freezing in the winter months.

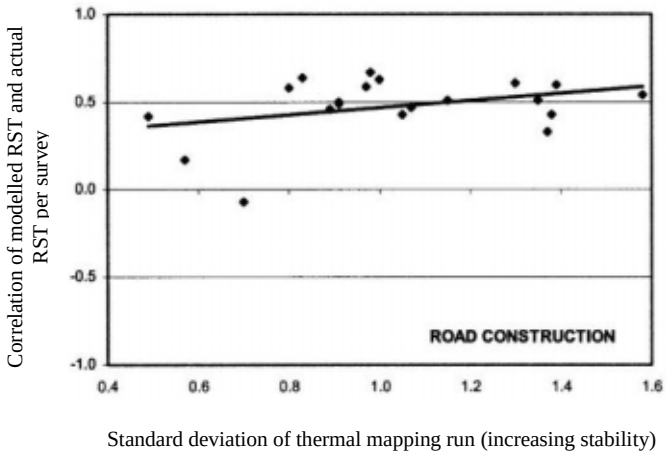

Figure 3.1 The influence of road construction on RST modelling at different levels of atmospheric stability, using actual RST data from 20 thermal mapping runs for comparison of model performance. The standard deviation of each thermal mapping run is used as a proxy to stability (Chapman et al. 2001b).

In general, however, approximations of road construction for different classes of road are difficult as no universal design procedure exists, and validation of profile parameterisations would require multiple road core samples. Not only are the costs associated with obtaining road cores for model validation too prohibitive, but the site specific nature of road coring makes it unsuitable for use over large areas as would be needed for route-based model

validation. The successful delivery of a route-based forecasting service relies on the accurate measurement of road construction at every forecast point around a route. The *ENTICE* model falls short in this respect since the parameterisation of road construction is based on an ordinal classification of road type which lacks the sophistication exhibited by other components of the model and fails to account for subtle variations in road construction around a route.

Bridge decks add further complexity to the issue, since the sudden change in construction from a standard road surface to a bridge deck of shallower construction can often result in a thermal singularity where the RST may be significantly lower. As a result, highway authorities often commission high resolution thermal mapping surveys of such areas to inform them of ice risk on bridges. The current methodology for parameterising road construction in *ENTICE*, however, fails to take into account the significant impact of bridge decks on RST. The original methodology used for locating bridges relies on manual identification from 1:50000 maps, and whilst there is some potential to use automated algorithms in GIS packages for this task, these are not widely implemented. Specific construction data is rarely available for all bridges, and hence, often the road type classification is simply lowered by a category to account for the shallower construction encountered on bridge decks. Whilst such a process may be a cost effective solution, it is clearly too simplistic since it fails to account for any variations in bridge construction. Furthermore, it fails to account for smaller bridges that may not appear on maps, are missed by human error, or conflict automatic GIS detection techniques.

3.2 Ground Penetrating Radar

Ground Penetrating Radar (GPR) is a non-invasive geophysical technique that can be used to detect electrical discontinuities in the shallow subsurface (< 50m) by generation, transmission, propagation, reflection and reception of discrete pulses of electromagnetic energy in the megahertz (MHz) frequency range (Neal 2004). The origins of GPR date back to the early 20th century when scientists were attempting to patent techniques to investigate the nature of various buried features (Reynolds, 1997), and following these initial developments GPR was primarily used in studies of glaciology (Plewes & Hubbard, 2001; cited in Neal, 2004) until the 1970s when civil engineering, archaeological and geological applications for GPR became more frequent (Reynolds, 1997; Conyers & Goodman, 1997). The advent of digital data collection in the 1980s led to the first commercially available GPR systems, and since the mid-1990s the technique has increasingly been used by the geology and sedimentology research communities as a cost effective method of investigating the shallow subsurface for purposes such as the reconstruction of past depositional environments or for groundwater reservoir characterisation (Neal 2004).

Beyond the geological applications of GPR, the technology is widely used in a variety of other fields including the highway industry where it is regularly used to assess the performance and structure of roadways (Al-Qadi & Lahouar 2005). GPR technology was first used on roads in the mid-1970s when tests were performed by the US FHWA on the feasibility of using radars in tunnel applications (Morey 1998). In 1985 the first vehicle mounted GPR system for highways was developed under a FHWA contract, and this led to a rapid expansion in the use of GPR technology for evaluating subsurface conditions for transportation facilities. From the mid-1990s onwards GPR has primarily been used for road layer thickness estimation and the identification of moisture accumulation within road layers. Accurate predictions of road layer thicknesses provide important data for roadway management systems since they are needed for overlay design, quality control and for

structural capacity estimation of existing roads to predict their remaining serviceable life (Al-Qadi & Lahouar 2005).

3.2.1 Calculating layer depth

In road applications, the GPR technique is based on the principle of sending a short electromagnetic pulse through an antenna to the road surface and then recording the reflected pulses from the surface and any subsurface layer interfaces bearing discontinuities in electrical properties. The time difference measured between the reflected pulses, known as the two-way travel time, can be used together with the dielectric properties of the surveyed layer to determine layer thickness using Equation 3.1 (Wimsatt et al. 1998):

$$d_i = \frac{ct_i}{2\sqrt{\varepsilon_{r,i}}} \tag{3.1}$$

where d_i is the thickness of the ith layer, t_i is the electromagnetic pulse two-way travel time through the ith layer, c is the speed of light in free space (c = 3 x 10^8 m/s) and $\varepsilon_{r,i}$ is the dielectric constant of the ith layer.

The main difficulty in interpreting GPR data for measuring the thickness of road layers is illustrated by Equation 3.1. Specifically, if it is assumed that the two-way travel time t_i can be accurately measured from the GPR signal, the dielectric constant of the material within the layer being measured remains unknown. Road layers are typically composed of various construction materials such as asphalt binder, aggregate, air-voids and water, all of which combine to make physically inhomogeneous layers. Since the bulk dielectric properties of an inhomogeneous material are typically a combination of the dielectric properties and volume proportions of the individual components, the dielectric properties of road layers will vary both between layers and within layers depending on the mixtures used. Furthermore, the dielectric properties of road layers are greatly affected by rain and the resulting moisture accumulation within road layers, and consequently their values are usually unknown and are

difficult to predict. This problem has resulted in a wealth of research over the past decade focused towards the development of data analysis algorithms for better estimation of the dielectric constant of different road layers (Al-Qadi & Lahouar 2005; Lahouar & Al-Qadi 2008). Such algorithms however are only necessary in applications requiring high levels of accuracy, such as structural capacity estimation, and are beyond the scope of a pilot study such as this.

3.2.2 GPR traces and radargrams

Data collected during a GPR survey is typically displayed as a trace (Figure 3.2), showing the travel time of the electromagnetic pulse at a set location. Each inflexion in the trace represents a discontinuity where there is potentially a change in the subsurface construction and hence a change in thermal properties. Over the course of a survey, traces are obtained at a fixed spatial resolution allowing a radargram to gradually be built up (Figure 3.3). These show cross-sectional views of the subsurface, where the magnitude of reflected pulses from the surface and any subsurface layer interfaces are plotted against their two-way travel time to reveal a cross-sectional view of discontinuities / layers in the subsurface.

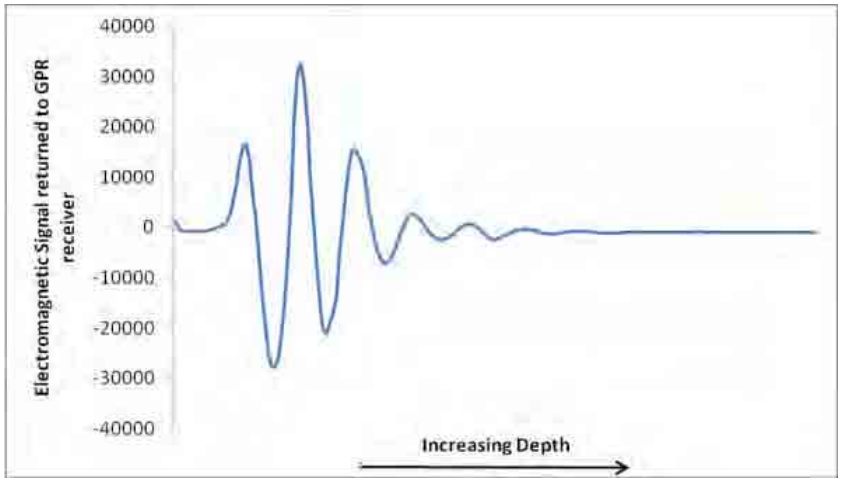

Figure 3.2 A sample GPR trace, showing the varying amplitude of the electromagnetic pulse as it penetrates the subsurface.

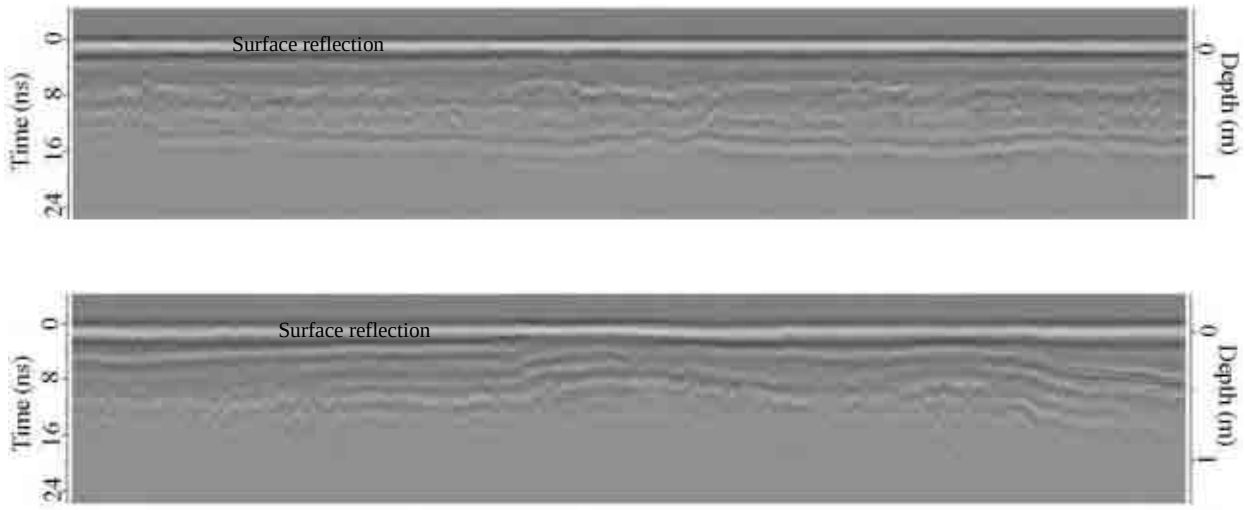

Figure 3.3 (a) Radargram collected on a motorway showing a deep and uniform road construction and (b) radargram collected on a minor c-road showing a less uniform, shallower construction.

3.3 Application of GPR Data within the *ENTICE* Model

3.3.1 Data collection

To investigate the potential use of GPR data for modelling road construction in the *ENTICE* route-based forecast model, a GPR survey of the Birmingham study route (Figure 2.3) was undertaken using a Malå RoadCart GPR unit (Figure 3.4). The equipment setup included a shielded 500 MHz low frequency antenna, designed for high speed GPR measurements on roads, attached to a custom made trailer which also housed a differential GPS receiver capable of sub-metre accuracy. Data from the GPR antenna was fed into a Malå CUII GPR control unit with high frequency module and stored on a data logger. The RoadCart trailer was attached by towbar to a Land Rover Freelander vehicle which was used to drive the study route, and during the survey the GPR data could be viewed as a real-time radargram (Figure 3.3) on a Malå XV11 monitor positioned in the vehicle.

Figure 3.4 Equipment setup showing the Malå RoadCart in action.

In order to collect and store GPR data, the electromagnetic waveform has to be digitised into samples. Each sample represents the digital amplitude value of the waveform at a specific time, and the travel time at each sample is a function of the total number of samples in the trace and the total trace length in time. The number of samples per GPR trace was pre-set to 512 samples over a time window of 72 ns, thus giving a travel time of 0.140625 ns per sample.

3.3.2 Identification of bridge decks from radargrams

As a bridge deck represents (in most cases) a dramatic change in construction, the first goal was to investigate if GPR had the capability to detect the three known bridge decks on the study route. The radargrams associated with these bridges are shown in Figure 3.5. Figure 3.5 (a) shows a relatively small bridge deck located on the M5 motorway. Thermal mapping data has previously shown that this bridge typically produces a thermal singularity under stable conditions of about -0.3°C when compared to the adjoining carriageway. Changes in the reflected GPR signal are clearly visible over the bridge section (Figure 3.5 (a)). The signal received is a consequence of the air void under bridges which causes multiple direct air waves to be returned rather than the normal reflections from subsurface discontinuities. Similar GPR signals can be identified in Figure 3.5 (b) and (c) which show larger bridges crossing the M5 motorway. Of particular interest in Figure 3.5 (c) is the clear visibility of the pillars (P1 – P4) at both sides of (and in-between) the two carriageways of the motorway. Instead of having a lower RST common to most bridges, thermal mapping data has shown that the thermal singularity on this bridge is typically +0.3°C warmer than the adjoining road sections under stable atmospheric conditions. This can easily be explained, however, by the presence of frequent standing traffic on the bridge caused by traffic lights at the motorway exit (Figure 3.6).

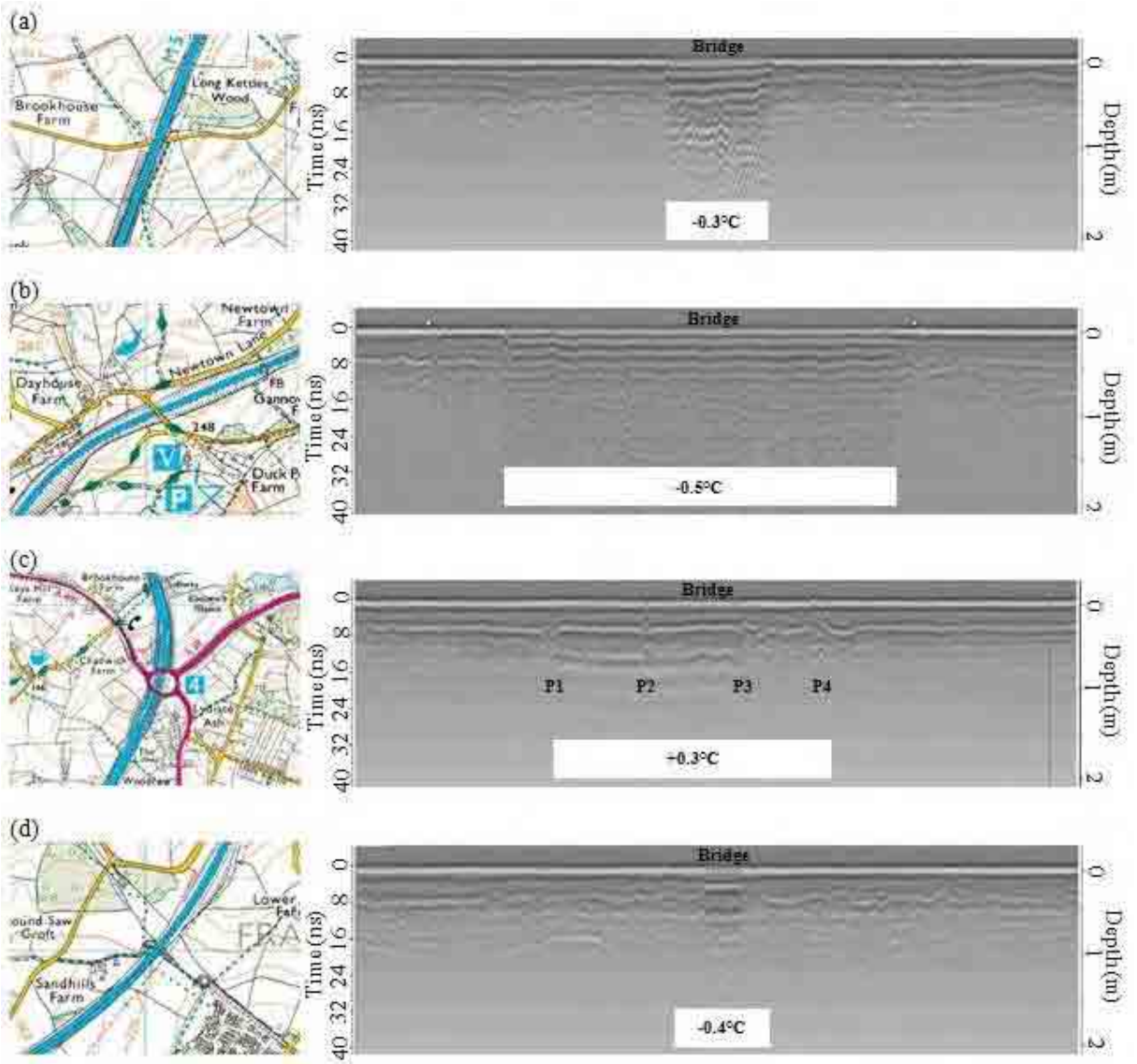

Figure 3.5 Location, radargrams and typical magnitude of the known thermal singularities (under stable conditions) of four bridge decks on the study route. Thermal singularities were previously identified from thermal mapping surveys. Location maps ©Crown Copyright/database right 2009. An Ordnance Survey/Digimap supplied service.

Figure 3.5 (d) shows a small bridge that was originally missed when the bridges were manually identified from a 1:50000 map. Again, a bridge signature can clearly be inferred from the radargram and upon inspection of the thermal data, a thermal singularity in the order of -0.4°C is present under stable atmospheric conditions. Thermal mapping data reveals that the overall variation in RST on the motorway section of the study route is relatively small, so known thermal singularities such as bridge decks can be problematic and therefore require proper identification. These results immediately show that there is some potential to GPR as a

tool for locating even the smallest of bridges along routes from the analysis of radargrams. It is clear that with minimal processing, bridge decks can be identified in a more objective manner than manual identification from a map.

Figure 3.6 Aerial photograph of the motorway bridge identified in Figure 3.5(c), showing the location of traffic lights on the bridge which often leads to standing traffic causing the warm thermal singularity of +0.3°C observed at this location.

3.3.3 Subsurface layer depths

Based on the original ordinal road type classification and the associated road profiles (Table 3.1) initiated by Chapman et al. (2001b), we would expect to see variations in road construction profiles around the study route as the road type varies. The two radargrams shown in Figure 3.3 were collected from a motorway (Figure 3.3 (a)) and a minor C-road (Figure 3.3 (b)) along the study route, and reveal differences in the road construction profile between the two road types. The main differences are in the uniformity of the profiles, with the motorway section appearing to have a deeper and more uniform construction than the minor C-road. However, despite the more uniform nature of the motorway profile, subtle fluctuations in the subsurface horizons are still evident, and the ordinal road profiles currently used in the *ENTICE* model (Table 3.1) are too simplistic to enable such fluctuations to be quantified and accounted for in the parameterisation of subsurface temperatures.

In an attempt to re-parameterise the road construction profile in the *ENTICE* model for each forecast point along the study route, an inflexion point detection algorithm (Appendix 2) capable of analysing the digitised electromagnetic waveform of each GPR trace for evidence of subsurface horizons/discontinuities was developed. Firstly, an Exponentially Weighted Moving Average (EWMA) was applied to the raw GPR data over an average of 5 GPR traces, corresponding to 5 metres of road length. Applying an EWMA to a dataset helps to reduce noise in the dataset whilst keeping the lag associated with moving averages to a minimum. Typical noise for GPR data from roads could include erroneous measurements from objects such as drainage covers or underground utility pipes which distort the GPR signal. Next, the EWMA modified GPR dataset was spatially joined to the *ENTICE* GPD for the study route using the spatial join feature available in ESRI ArcMap. The modified GPD, which now included the digitised electromagnetic waveform of the GPR trace for each forecast point, was then loaded into Matlab ready to be analysed by the inflexion point detection algorithm (Appendix 2).

The inflexion algorithm maintains the existing *ENTICE* parameterisation of a five zone flexible pavement whose layer materials vary according to road type (Table 3.1). Hence, the algorithm attempts to identify 5 subsurface layer interfaces/discontinuities by searching for significant inflexions in the electromagnetic waveforms forming the GPR traces measured at each point along the study route. Once an inflexion is identified, the travel time associated with this inflexion is calculated and assigned to this point in the GPR trace, and the algorithm then continues to search for further inflexions within the same GPR trace. Once no more inflexions can be found within a trace, the algorithm moves onto the next trace (next point along the route) and the same process is repeated until the GPR trace at every point along the study route has been examined for subsurface layer interfaces.

The algorithm then calculates the depths of all identified layers in each trace using Equation 3.1, assigning dielectric constant values to each layer based on the materials assigned to each layer in the existing *ENTICE* road type parameterisation (Table 3.1). Hence, for a point located on a motorway, the top three layers in the road profile are assigned a dielectric value of 6 in Equation 3.1 to represent asphalt, whilst the bottom two layers are assigned a dielectric value of 10 corresponding to concrete. In contrast, where points are located on a minor C-road only the top layer is assigned a dielectric value of 6 (asphalt), with the middle three layers assigned a dielectric value of 10 (concrete) and the bottom layer a value of 25 to represent a soil layer. The dielectric constants used are approximate values taken from the Malå GroundVision software manual and represent typical values for these materials based on an unsaturated media. In reality, for the reasons highlighted in section 3.2.1 the differences in the dielectric values between layers will vary considerably along the study route, but without road core data to verify the subsurface materials at each point, such approximations are necessary for modelling purposes.

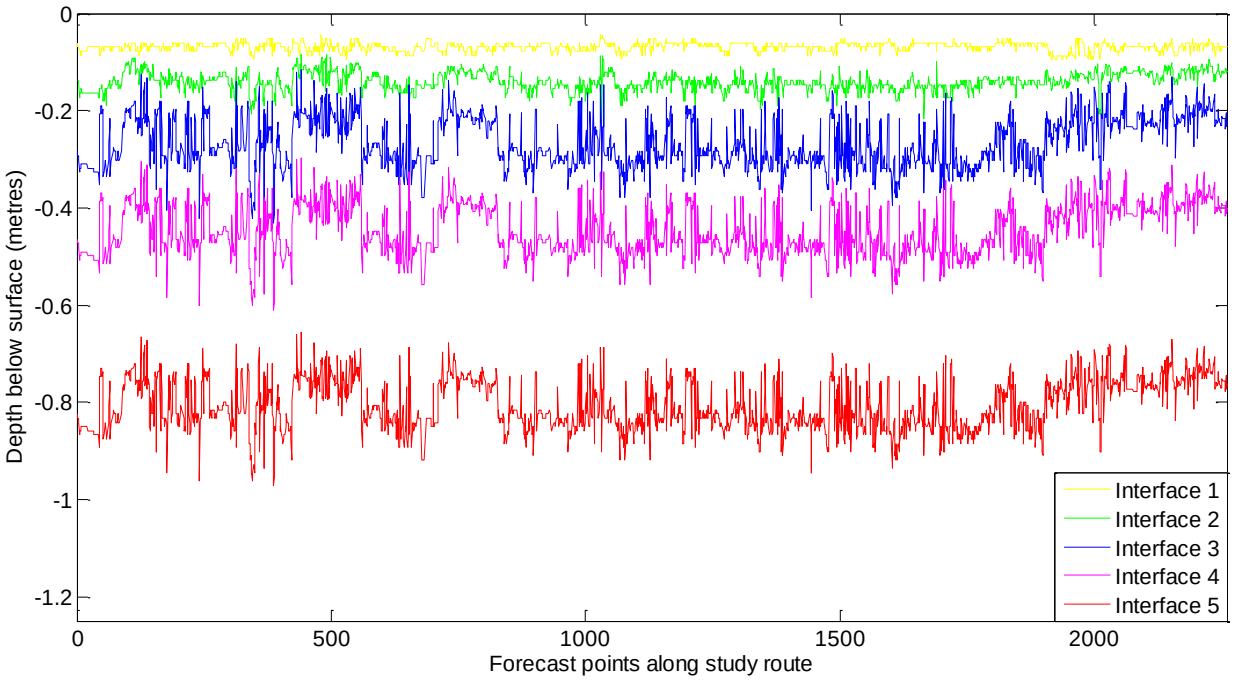

Figure 3.7 Calculated depths of subsurface interfaces at each forecast point along the study route, assuming a five zone flexible pavement with material composition matching that of the existing *ENTICE* road construction parameterisation shown in Table 3.1.

Initial analysis of the calculated depths from the inflexion algorithm revealed difficulties in identifying the lower two subsurface interfaces over the majority of the study route, most likely due to poorer than expected penetration depth with the 500 MHz antenna. Whilst it was expected that a 500 MHz antenna would provide a good balance between resolution and signal penetration depth, in hindsight a lower frequency antenna, perhaps 250 MHz, would have given a better balance and provided greater depth penetration. To overcome this problem and enable the modelling of a five zone flexible pavement to continue, the depths (thickness) of the fourth and fifth layer interfaces were pre-set to the existing *ENTICE* values of 18 cm and 36 cm respectively, with the total depth of these layers from the surface dependent on the thickness of the upper three layers which varied based on the GPR measurements. Figure 3.7 reveals the depths of the five subsurface interfaces at each forecast point calculated by the

inflexion algorithm, and Table 3.2 summarises the average depths of each layer and the total average profile depth for each of the road type classifications in the *ENTICE* model.

Table 3.2 Average depths for each layer of the re-parameterised five zone flexible pavement in the *ENTICE* model, based on analysis of the digitised electromagnetic waveform data from a GPR survey using an algorithm (Appendix 2) designed to identify subsurface interfaces from significant inflexions in the waveform of individual GPR traces.

	Motorway (1)	A-Road (2)	B-Road (3)	C-Road (4)
Layer 1	Asphalt	Asphalt	Asphalt	Asphalt
Av. Depth (cm)	6.5	6.8	6.8	7.1
Layer 2	Asphalt	Asphalt	Asphalt	Concrete
Av. Depth (cm)	8.8	7.9	7.7	5.1
Layer 3	Asphalt	Asphalt	Concrete	Concrete
Av. Depth (cm)	14.4	14.2	14.1	9.1
Layer 4	Concrete	Concrete	Concrete	Concrete
Av. Depth (cm)	18	18	18	18
Layer 5	Concrete	80% Concrete 20% Subgrade/soil	50% Concrete 50% Subgrade/soil	Subgrade/soil
Av. Depth (cm)	36	36	36	36
Total Depth (cm)	83.7	83	82.5	75.3
	Average thermal conductivity			
	4.09×10^{-3}cal cm^{-1} sec^{-1} °C	3.86×10^{-3}cal cm^{-1} sec^{-1} °C	4.07×10^{-3}cal cm^{-1} sec^{-1} °C	3.59×10^{-3}cal cm^{-1} sec^{-1} °C

In the original *ENTICE* road type parameterisation (Table 3.1) the depth of each layer in the five zone flexible pavement is assumed to be constant with no variation between road type. The new parameterisation (Table 3.2) derived from GPR measurements attempts to improve upon this by identifying real changes in the depth of the upper three layers of the five zone profile at each forecast point. With the incorporation of GPR measurements, the total average depth of the five zone profile varies between the different road types in the *ENTICE* model, with motorways on average having a slightly deeper construction than A and B roads, and C-roads displaying the shallowest construction as we would expect for minor lower trafficked roads (Table 3.2). The GPR measurements reveal that the average depth of the uppermost asphalt layer is greatest on the minor C-roads (7.1 cm) and most shallow on the motorway sections of the study route (6.5 cm), possibly the result of greater wear on the motorway

surface due to the higher volume of traffic on these roads. However, the increased strength and stability of the motorway roads compared to the minor C-roads is evident in the second and third subsurface layers, whose combined average depth is some 9 cm greater at motorway locations due to the more stringent design procedures for motorways that are designed to withstand much higher traffic loads.

Average thermal conductivity values calculated for the four road profiles in Table 3.2 are derived from thermal conductivity values for asphalt, concrete and soil that have been altered from the original *ENTICE* values due to numerous inconsistencies in the literature. In the original Thornes (1984) model, thermal conductivity values of 0.0048 and 0.0031 cal cm^{-1} sec^{-1} °C were used for concrete and asphalt respectively, and the thermal conductivity of soil was assumed to be the same as that of concrete. Chapman et al. (2001b) used these values to calculate an average thermal conductivity for each road type in the *ENTICE* model based on the materials and depths of each zone of the five zone flexible pavement (Table 3.1). However, the thermal conductivity of asphalt and concrete varies considerably depending upon the exact composition of the materials used to produce the end product, and likewise the ability of different soils to conduct heat will vary based on factors such as the density and chemical composition of the soil. To bring an element of consistency to road weather models, it was decided that *ENTICE* would use the same thermal conductivity values that are implemented in the METRo model, which is probably the most widely used heat balance model in road weather forecasting as a result of the MDSS project in the US (Chapter 1). Hence, thermal conductivity values for concrete, asphalt and soil in the *ENTICE* model were altered to 0.0053, 0.0019 and 0.0024 cal cm^{-1} sec^{-1} °C respectively (Crevier & Delage 2001), giving average values for the original *ENTICE* 72 cm pavement parameterisation of 0.00438, 0.00410, 0.00409 and 0.00359 cal cm^{-1} sec^{-1} °C for motorways, A-roads, B-roads and minor C-roads respectively:

for all forecast points **do**
    set depth of road construction to 72 cm
    if road type = 3000 (motorway)
        set thermal conductivity to 0.00438 cal cm^{-1} sec^{-1} °C
    else if road type = 3001 (A-road)
        set thermal conductivity to 0.00410 cal cm^{-1} sec^{-1} °C
    else if road type = 3002 (B-road)
        set thermal conductivity to 0.00409 cal cm^{-1} sec^{-1} °C
    else if road type = 3004 (C-road)
        set thermal conductivity to 0.00359 cal cm^{-1} sec^{-1} °C
    else
        set thermal conductivity to default value (motorway)
    end if
end for

To assess the impact of these altered thermal conductivity values on the spatial forecasting performance of *ENTICE*, statistical analysis was conducted on 20 nights thermal mapping data for the study route. During these tests all of the geographical parameters in the model, with the exception of road type, were fixed spatially to default values, rather than running the model in 'quasi-operational' mode. By fixing all other geographical parameters spatially, it ensures any changes identified in the model forecast are solely due to the change in thermal conductivity. If the model were run in 'quasi-operational' mode in this instance, then changes to road type in the model would also lead to changes in Z_0 since Z_0 varies in the model with respect to the ordinal land use and road type classification (Chapter 4), making it impossible to quantify the effect of road type changes alone on model performance. By fixing all other geographical parameters spatially, the resultant forecast statistics are not providing a true measure of model performance, but instead are a reflection of model bias caused by the spatial fixing of the geographical parameters. However, by running the model twice, first using the original thermal conductivity (road type) values (Table 3.1) and again using the newly calculated averages based on the thermal conductivity values used in the METRo model, changes in the model results between the two model runs enables us to quantify the

impact of thermal conductivity changes on model performance. Forecast statistics for both model runs are summarised in Table 3.3.

Table 3.3 Forecast statistics from a statistical analysis on average thermal conductivity profiles in *ENTICE*, where all geographical variables in the model were held constant with the exception of road type.

	Analysis 1 – Using original *ENTICE* thermal conductivity values						**Analysis 2 – Using METRo based thermal conductivity values**					
Night	β	σ_β	*RMSE*	*Pm*	*Prm*	R^2	β	σ_β	*RMSE*	*Pm*	*Prm*	R^2
1	-0.58	0.96	1.12	69.79	72.98	0.23	-0.48	0.98	1.09	70.32	72.00	0.24
2	0.09	1.10	1.10	67.76	69.48	0.08	0.22	1.11	1.13	64.35	69.70	0.08
3	-1.44	1.30	1.94	40.78	59.71	0.14	-1.26	1.32	1.83	43.61	58.43	0.14
4	-0.6	0.96	1.13	67.01	71.61	0.18	-0.52	0.97	1.10	67.45	70.15	0.19
5	-1.45	1.43	2.04	48.70	55.11	0.10	-1.21	1.46	1.89	54.18	55.51	0.10
6	-1.13	1.44	1.83	55.86	52.28	0.05	-0.89	1.45	1.70	60.11	52.19	0.05
7	-1.51	1.57	2.18	36.22	52.10	0.13	-1.24	1.60	2.02	41.13	51.53	0.13
8	-0.10	0.77	0.77	83.37	82.57	0.19	0.16	0.79	0.81	78.77	80.19	0.19
9	-2.19	0.90	2.37	6.10	77.00	0.11	-1.98	0.92	2.19	12.43	74.88	0.07
10	-0.71	1.11	1.31	66.74	74.13	0.06	-0.28	1.10	1.14	72.89	71.07	0.07
11	-0.76	0.77	1.08	67.58	84.52	0.13	-0.65	0.78	1.01	71.21	83.19	0.14
12	0.54	1.38	1.48	46.57	65.72	0.06	0.98	1.38	1.69	32.77	64.31	0.08
13	-0.22	0.89	0.92	79.39	81.16	0.08	0.08	0.90	0.90	76.82	78.55	0.10
14	0.28	0.71	0.76	79.30	87.93	0.19	0.34	0.72	0.79	75.54	86.73	0.20
15	0.15	1.33	1.34	58.43	61.88	0.12	0.70	1.34	1.51	43.92	61.34	0.14
16	-0.01	0.56	0.56	93.68	93.72	0.05	0.04	0.57	0.57	93.41	93.59	0.05
17	-0.50	1.16	1.26	67.71	66.34	0.10	-0.13	1.16	1.17	65.68	65.28	0.12
18	-1.40	0.96	1.70	37.51	78.24	0.17	-0.94	0.97	1.35	59.22	75.90	0.18
19	-1.08	0.48	1.18	50.60	95.40	0.15	-0.83	0.47	0.95	70.28	96.28	0.16
20	-1.62	0.90	1.85	25.48	78.51	0.10	-1.30	0.90	1.59	36.36	77.27	0.11
Average	**-0.71**	**1.03**	**1.40**	**57.43**	**73.02**	**0.12**	**-0.46**	**1.04**	**1.32**	**59.52**	**71.90**	**0.13**

The statistics in Table 3.3 reveal an improvement in the *RMSE* of the route-based forecast, indicating that the magnitude of any errors in the forecasts has been reduced by using the new thermal conductivity values, which is reflected by a reduction in the negative bias of the forecast of 0.25°C, with only a marginal increase in σ_β. The overall percentage of modelled forecast values within ±1°C of the actual values (*Pm*) has increased by 2.09%, whilst the percentage of residual modelled forecast values within ±1°C of the residual actual values (*Prm*) decreases by a smaller margin (1.12%). Whilst such statistics are a good indicator of the spatial forecasting ability of a model, they are nonetheless limited to a resolution of ±1°C, and can potentially ignore finer scale improvements to a model. Analysis of the coefficient of determination (R^2) for modelled versus actual RST is a further method of analysing the spatial forecasting performance of *ENTICE* which, unlike the *Pm* and *Prm* values, is not limited by temperature resolution. Analysis of the R^2 values for modelled versus actual RST reveals a small increase (1%) in the variability of RST accounted for by *ENTICE* with the new thermal conductivity values. Hence, using the new average thermal conductivity profiles with the original *ENTICE* five zone fixed depth pavement parameterisation, a small improvement is observed in the overall spatial forecasting performance of the *ENTICE* model when run in a non 'quasi-operational' mode.

Despite the observed improvement in forecasting performance with the new thermal conductivity profiles, these are still based on the existing road type parameterisation in *ENTICE* (Table 3.1) which is clearly too simplistic since it fails to account for the clear differences in subsurface layer depths between road types identified in the GPR measurements. Such variations in road profiles are important and should be included in the forecast model since they have a direct effect on the surface heat flux controlling the thermal memory of the road surface.

3.3.4 Surface heat flux

Thermal memory is a term used to describe the length of time which a surface stores heat from daytime solar radiation (Thornes 1991). The thermal damping depth in a road obviously depends upon the materials of which it is composed, and the changes in construction depth along the study route identified from the GPR survey (Figure 3.7 & Table 3.2) will have an impact on the thermal damping depth around the study route. Outcalt (1972) assumed that the temperature at the damping depth of the ground equalled the temperature at the damping depth in the atmosphere, with no attempts made to measure temperatures at depth in the ground. Thornes (1984) used temperature measurements at 36 cm and 18 cm below the surface, with the temperature at 36 cm taken to be the temperature half way between the surface and a damping depth of 72 cm. A damping depth of 72 cm was seen by Thornes (1984) as being reasonable since it lies between the damping depths for asphalt and concrete.

Thermal memory is accounted for in *ENTICE* through calculation of the surface heat flux at each forecast point. Assuming a constant damping depth of 72 cm, *ENTICE* calculates the soil temperature change at each layer of the five zone flexible pavement, starting with the soil temperature change midway between the surface and the damping depth, i.e. 36 cm, and then halving the distance to the surface at each computation level. The soil heat flux is then calculated between the surface and a depth one-sixteenth the depth of thermal damping (Outcalt 1972), which currently equates to a constant depth of 4.5 cm at every forecast point in the model. The heat flow in *ENTICE* is described by a one-dimensional conduction equation described by Thornes (1984) such that at depth ZU:

$$\frac{\partial TU}{\partial t} = RD\ (T_0 - (2\ TU + TX)/ZU^2) \qquad (3.2)$$

where *RD* is the thermal diffusivity and *TX* the temperature at depth (2 x *ZU*). The heat flux is calculated as follows:

$$S = (RK \cdot ZU)(TU - T_0) \quad (3.3)$$

where *RK* is the thermal conductivity, *ZU* is the depth 4.5 cm, and *TU* is the temperature at depth *ZU*.

To incorporate the changes in layer depth identified through the GPR measurements (Figure 3.7), the *ENTICE* model code was modified to include the newly calculated depths for the upper three subsurface layers within the calculation of average thermal conductivity profiles at each forecast point. Firstly, the total depth (`$ZG[$M]`) at each forecast point was calculated by summing the thicknesses of the upper three layers calculated via the GPR inflexion point algorithm (Appendix 2), and adding these to the depth of the bottom two layers which was pre-set to the existing *ENTICE* value of 54 cm as described in section 3.3.3. Next, an average thermal conductivity value (`$RKA[$M]`) was calculated at each forecast point by calculating the total depth of asphalt, concrete and soil within the profile and multiplying each of these by their respective thermal conductivity values, and then summing these values and diving by the total depth of the profile. The material assigned to each of the five layers was dependent on the road type classification at each forecast point (Table 3.2).

for all forecast points **do**
  calculate the total depth of road construction by adding the depths of the top three layers together (calculated from GPR data), and adding an additional 54cm (to account for pre-set depth of bottom two layers)
  if road type = 3000 (motorway)
    calculate average thermal conductivity by multiplying the depth of each subsurface material (asphalt, concrete & soil) by the conductivity value for that material, then summing these values and dividing by the total depth of road construction
  repeat for all road types
  end if
end for

In the *ENTICE* model, the total depth (`$ZG[$M]`) at each forecast point was used as the new damping depth for each subsurface profile, and the soil temperature change was then calculated at each layer starting with the temperature change at the interface of the fourth and fifth subsurface layers (`$ZT`), followed by each of the other subsurface layer interfaces in turn (`$ZZ, $ZX and $ZU`) (see Appendix 5). As with the original *ENTICE* model, the soil heat flux (`$S[$I]`) is then calculated between the surface and the first subsurface layer interface (`$ZU`), but unlike the original model the depth of this layer interface now varies at each forecast point based on the calculated depths from the GPR measurements, rather than remaining a constant 4.5 cm along the entire route.

3.4 Statistical Analysis of New Subsurface Parameterisation

To test whether the re-parameterised subsurface profiles at each forecast point improve the spatial forecasting performance of *ENTICE*, further statistical analyses were conducted on the same 20 nights thermal mapping data used throughout this study. Again, during this analysis the geographical parameters in the model, with the exception of road type and traffic, were fixed spatially to default values, instead of running the model in 'quasi-operational' mode, to enable just the impact of thermal conductivity changes to be quantified. Traffic is also included in the analysis to give an indication of the influence that the general traffic algorithm used in *ENTICE* (Chapter 6) has on model performance. Again, the analysis was run twice, first using the original *ENTICE* road construction parameterisation containing fixed layer depths (Table 3.1), and again using the re-coded model which included the new average thermal conductivity values and variable layer depths at each forecast point calculated from the GPR measurements. The inclusion of traffic is acceptable since its impact remains the same over both analyses, thus enabling us to quantify the impact of thermal conductivity

changes alone on model performance. Forecast statistics for both analyses are summarised in Table 3.4.

Table 3.4 Forecast statistics from a statistical analysis on road construction parameterisation in the *ENTICE* model. Statistics in Analysis 1 relate to modelled vs. actual RST using the original *ENTICE* road construction parameterisation proposed by Chapman et al. (2001b), and statistics in Analysis 2 relate to modelled vs. actual RST using the new re-parameterised subsurface road construction measurements derived from GPR data.

	Analysis 1 – Using METRo based thermal conductivity values, with traffic on						**Analysis 2 – Using new thermal conductivity values calculated from new depth profiles**					
Night	β	σ_β	*RMSE*	*Pm*	*Prm*	R^2	β	σ_β	*RMSE*	*Pm*	*Prm*	R^2
1	-1.60	0.86	1.82	22.60	84.03	0.26	-1.48	0.87	1.72	31.93	83.72	0.26
2	-0.88	1.06	1.38	63.78	71.83	0.14	-0.78	1.05	1.31	66.74	71.65	0.14
3	-2.38	1.19	2.66	5.44	68.20	0.23	-2.20	1.19	2.50	9.20	68.24	0.23
4	-1.59	0.89	1.82	25.65	75.94	0.22	-1.46	0.89	1.71	34.14	76.07	0.22
5	-2.38	1.43	2.78	13.45	58.65	0.10	-2.18	1.44	2.61	16.14	57.94	0.09
6	-2.08	1.49	2.55	19.55	58.03	0.06	-1.83	1.50	2.37	25.21	57.81	0.05
7	-2.38	1.49	2.80	13.93	49.49	0.18	-2.09	1.49	2.57	26.05	48.92	0.18
8	-1.12	0.79	1.37	46.70	82.18	0.26	-0.90	0.77	1.19	58.91	83.10	0.25
9	-3.12	0.95	3.26	0.93	74.35	0.16	-2.68	0.99	2.85	5.04	74.04	0.17
10	-1.60	1.21	2.01	30.87	65.72	0.10	-1.21	1.20	1.70	42.72	65.33	0.09
11	-1.74	0.76	1.90	14.55	83.28	0.21	-1.64	0.75	1.80	17.43	84.17	0.21
12	-0.27	1.37	1.39	70.10	65.02	0.15	0.29	1.39	1.42	54.22	62.80	0.14
13	-1.15	1.01	1.53	44.54	72.40	0.12	-0.82	1.01	1.30	58.03	72.93	0.10
14	-0.78	0.69	1.04	65.33	84.87	0.20	-0.63	0.71	0.94	70.28	84.12	0.21
15	-0.63	1.33	1.47	62.72	60.50	0.20	0.02	1.33	1.33	60.68	61.48	0.21
16	-1.07	0.71	1.28	38.92	84.56	0.05	-0.87	0.77	1.16	50.60	81.20	0.05
17	-1.39	1.17	1.82	41.00	66.92	0.16	-0.93	1.19	1.51	55.29	66.96	0.16
18	-2.29	1.00	2.50	4.95	75.06	0.26	-1.66	1.02	1.95	24.81	75.45	0.25
19	-2.07	0.74	2.20	11.37	80.76	0.14	-1.50	0.84	1.72	21.49	77.62	0.15
20	-2.51	0.97	2.69	6.02	74.35	0.15	-2.16	0.99	2.37	11.59	74.35	0.15
Average	**-1.65**	**1.06**	**2.01**	**30.12**	**71.81**	**0.17**	**-1.34**	**1.07**	**1.80**	**37.03**	**71.40**	**0.17**

Comparing the statistics in Table 3.4 with those in Table 3.3 which do not take into account the *ENTICE* traffic algorithm, it can be seen that the inclusion of traffic has increased the negative bias of the forecast and the magnitude of any errors (Table 3.4), but the overall variability of RST which is accounted for by the model has increased by 5% as shown by the overall increase in the R^2 value. From Table 3.4 it is clear that the magnitude of any errors in the forecast is significantly reduced when the original fixed-depth subsurface parameterisation is replaced by the new variable subsurface road profiles calculated from GPR measurements, with the negative bias of the route-based forecast falling by 0.31°C and the *RMSE* by 0.21°C. Another indicator of improved forecasting ability with the new variable subsurface measurements is an increase of almost 7% in the overall *Pm* values (Table 3.4 & Figure 3.8), with negligible change (-0.41%) in the *Prm* values. Analysis of the coefficient of determination for modelled versus actual RST (Table 3.4 & Figure 3.9) reveals little change in the overall variability of RST which is accounted for by the model.

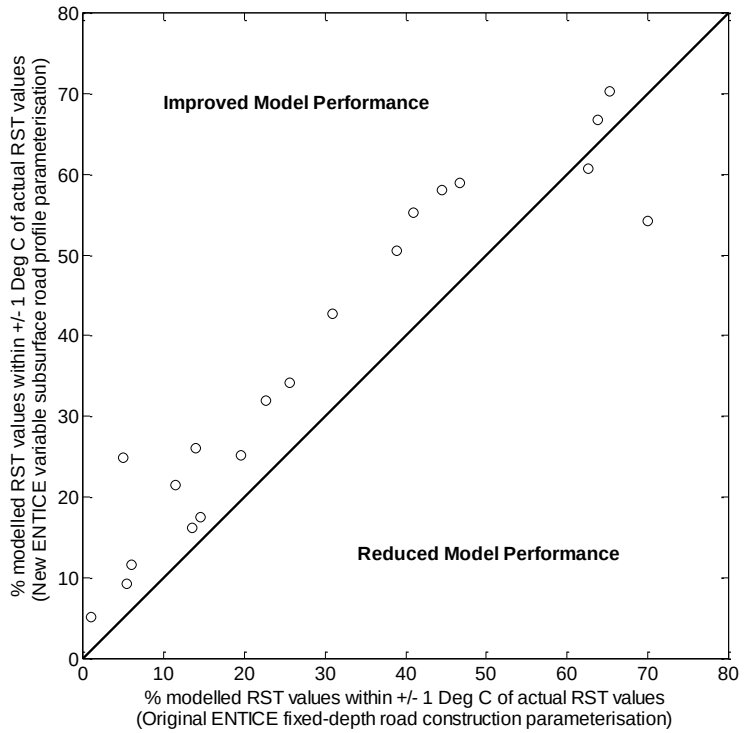

Figure 3.8 Comparison of *ENTICE* model accuracy in predicting RST to within ± 1°C of actual values. X-axis values relate to model runs using the original *ENTICE* road construction parameterisation, and y-axis values relate to model runs using the new variable subsurface measurements derived from GPR data.

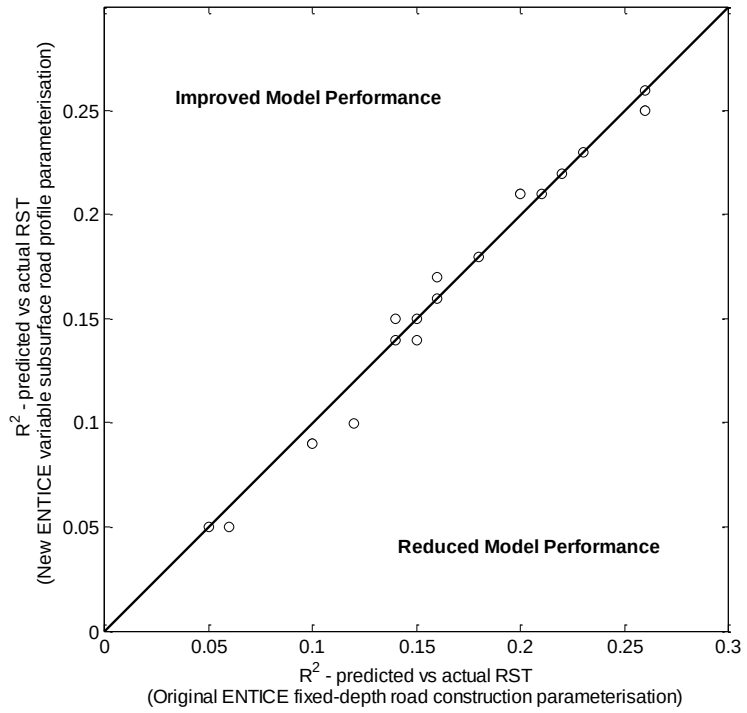

Figure 3.9 R^2 values for *ENTICE* predicted RST vs. actual RST collected from thermal mapping runs. X-axis values relate to model runs using the original *ENTICE* road construction parameterisation, and y-axis values relate to model runs using the new variable subsurface measurements derived from GPR data.

Hence, with the new variable subsurface measurements the overall accuracy of the *ENTICE* model has improved significantly (Figure 3.8) with the *Pm* values increasing on 90% of the study nights, and by up to 20% on individual nights. This suggests that the variable depth profiles calculated from GPR measurements provide a more realistic representation of the subsurface road construction around the study route than was attainable with the original parameterisation proposed by Chapman et al. (2001b), enabling *ENTICE* to more accurately model the thermal memory of the road surface at each forecast point. The new subsurface measurements alone, however, appear to provide insufficient spatial data to increase the overall amount of RST variability which is accounted for by the model.

Whilst the focus of this study is on the *ENTICE* model, it is important to emphasise that the methodologies used in parameterising subsurface layer depths from GPR measurements would be compatible with other surface energy balance models, and it is envisaged that such a methodology could be used to integrate a spatial component into the existing heat conduction module of the METRo model (Crevier & Delage 2001). In its current format METRo uses standard XML code for all data input (Figure 3.10), enabling the subsurface layer depths calculated from the inflexion point algorithm to easily be integrated into the model.

```
<?xml version="1.0"?>
<station>
  <header>
      <filetype>rwis-configuration</filetype>
      <version>1.0</version>
      <road-station>oaa</road-station>
      <time-zone>EST5EDT</time-zone>
      <production-date>2003-09-26T15:34Z</production-date>
      <coordinate>
          <latitude>45.10</latitude>
          <longitude>-76.02</longitude>
      </coordinate>
      <station-type>road</station-type>
  </header>
  <roadlayer-list>
      <roadlayer>
          <position>1</position>
          <type>asphalt</type>
          <thickness>0.1905</thickness>
      </roadlayer>
      <roadlayer>
      ...
  </roadlayer-list>
</station>
```

Figure 3.10 Sample METRo model code displaying the existing road layer parameterisation, into which the new subsurface layers depths derived from GPR data could easily be added. Source – METRo repository http://gna.org/projects/metro/

CHAPTER THREE SUMMARY

A study route was surveyed using GPR in an attempt to ascertain high resolution subsurface road profile measurements to improve road construction parameterisation in the ENTICE model. GPR has been shown to have considerable skill in objectively locating both major and minor bridge decks around a route, all of which produce thermal singularities that have implications for winter maintenance. The depths of subsurface layer interfaces around the study route have been estimated via an inflexion point algorithm designed to identify significant inflexions in the electromagnetic waveform of raw GPR trace data. Calculated depths are then used to estimate subsurface temperatures and the subsurface heat flux at each forecast point. A statistical analysis on road construction parameterisation has revealed an increase of almost 7% in the overall percentage of modelled forecast values within ± 1°C of the actual values, indicating a significant improvement in the spatial forecasting ability of the ENTICE model as a result of the new re-parameterised road construction measurements.

4. SPATIAL RE-PARAMETERISATION OF THE *ENTICE* MODEL: PART 2 – SURFACE ROUGHNESS

4.1 Surface Roughness

The roughness length parameter Z_0 is a theoretical measure of the aerodynamic roughness of a surface affecting the height at which the neutral wind profile near to the ground extrapolates to zero (Oke 1992). Z_0 is not a real, tangible quantity that can be measured, but is an artefact of an equation structure. In practice, Z_0 is determined from the least-square fitting of the logarithmic velocity profile law (Equation 4.1) using wind profile data, or by graphically plotting z versus U and extrapolating down to the level where $U = 0$, with its intercept on the ordinate axis being $ln\ Z_0$ (Arya 1988).

$$\frac{U}{u_*} = \left(\frac{1}{k}\right) ln\left(\frac{z}{z_0}\right) \tag{4.1}$$

Estimation of Z_0 at site specific locations within regions of inhomogeneity can be difficult. At any site specific location, Z_0 is related to the height of the surface elements and is a function of the shape and density of the elements at that location and within the upwind "effective fetch" or source area. However, the detailed resolution of individual patches comprising an inhomogeneous surface (e.g., buildings, trees, agricultural patchwork, etc.) means that the spatial resolution of turbulent exchanges of heat, mass and momentum is generally not known at all or only vaguely guessed at (Schmid 1994). As a result, practical estimation of Z_0 at a specific locality is often based on published values for roughness of similar terrain elsewhere (Wieringa et al. 2001). These values, which are usually ordered according to terrain type, typically vary over five orders of magnitude from 10^{-5} m for smooth water surfaces to several meters for forests and urban areas. A detailed review of roughness data derived from boundary layer experiments conducted in the 1970s and 1980s was undertaken by Wieringa

(1993), who found that the Davenport (1960) classification of effective terrain roughness most reliably described the effective roughness of realistic landscape types. This original classification has since been updated at both ends of the roughness scale (Wieringa 1992; Wieringa et al. 2001), providing one of the most thorough field-validated roughness classifications to date (Table 4.1).

Table 4.1 Updated Davenport classification of terrain roughness (Wieringa et al. 2001)

Z_0 (m)	Landscape Description
1. 0.0002 "*Sea*"	Open sea or lake (irrespective of wave size), tidal flat, snow-covered flat plain, featureless desert, tarmac and concrete, with a free fetch of several kilometres.
2. 0.005 "*Smooth*"	Featureless land surface without any noticeable obstacles and with negligible vegetation; e.g. beaches, pack ice without large ridges, marsh and snow-covered or fallow open country.
3. 0.03 "*Open*"	Level country with low vegetation (e.g. grass) and isolated obstacles with separations of at least 50 obstacle heights; e.g. grazing land without wind breaks, heather, moor and tundra, runway area of airports. Ice with ridges across-wind.
4. 0.10 "*Roughly Open*"	Cultivated or natural area with low crops or plant covers, or moderately open country with occasional obstacles (e.g. low hedges, isolated low buildings or trees) at relative horizontal distances of at least 20 obstacle heights.
5. 0.25 "*Rough*"	Cultivated or natural area with high crops or crops of varying height, and scattered obstacles at relative distances of 12 to 15 obstacle heights for porous objects (e.g. shelterbelts) or 8 to 12 obstacle heights for low solid objects (e.g. buildings).
6. 0.5 "*Very Rough*"	Intensively cultivated landscape with many rather large obstacle groups (large farms, clumps of forest) separated by open spaces of about 8 obstacle heights. Low densely-planted major vegetation like bushland, orchards, young forest. Also, area moderately covered by low buildings with interspaces of 3 to 7 building heights and no high trees.
7. 1.0 "*Skimming*"	Landscape regularly covered with similar-size large obstacles, with open spaces of the same order of magnitude as obstacle heights; e.g. mature regular forests, densely built-up area without much building height variation.
8. ≥ 2.0 "*Chaotic*"	City centres with mixture of low-rise and high-rise buildings, or large forests of irregular height with many clearings.

4.2 Existing Z_0 Parameterisation in *ENTICE*

It has been observed empirically that the wind speed over a surface increases logarithmically with height under neutral stability. Some air molecules close the surface collide and stick to the surface, whilst others bounce off in the direction from which they came and collide with other air molecules moving in the direction of the wind, causing what is commonly known as turbulent shear. The layer in which this turbulent shear has an effect is referred to as the boundary layer, and the height of this layer depends upon the wind speed and Z_0. In the *ENTICE* model, Z_0 is used both to influence the height of the boundary layer through the calculation of an atmospheric damping depth, and also to calculate the exchange of heat between the surface and the air (i.e. sensible heat flux (H)) through the use of a stability correction factor that relies on a logarithmic form of the Richardson number.

In view of the fact that the height at the top of the boundary layer is likely to vary day by day, Outcalt (1972) introduced the idea of an atmospheric damping depth (Z_2) that corresponds to the height at which the thermal diffusivity (Equation 4.2), which increases with height, becomes greater than the bulk adiabatic diffusivity (Equation 4.3) which decreases with height. The solution occurs at the depth where the declining bulk diffusivity is smaller than the thermal diffusivity and is estimated through an iterative solution where the damping depth is increased in 1 cm increments starting at Z_0, i.e.

$$d = {Z_2}^2/12t \tag{4.2}$$

$$d' = k^2 U_Z / \ln(\frac{Z_2}{Z_0}) \tag{4.3}$$

Solution at: $d > d'$

where Z_2 is the atmospheric damping depth (i.e. height at which $d > d'$), k is von Karman's constant, U_z is the wind speed at height Z, t is a time increment (a step function for the

estimation of the penetration depth of a 12-hour thermal disturbance) and Z_0 is the roughness length.

The exchange of heat between the surface and the air (H), as given in Equation (1.4), can be expanded to give the following expression for H which includes a stability correction factor R:

$$H = \frac{(k^2 U_z \rho)}{ln\frac{Z_2}{Z_0}} R\ Cp\ (T_2 - \Gamma Z_2 - T_0) \tag{4.4}$$

where k is von Karman's constant, U_z is the wind speed at the boundary layer top (Z_2), ρ is air density, Z_0 is the roughness length, Cp is the specific heat of air at constant pressure, T_2 is the air temperature at Z_2, Γ is the dry adiabatic lapse rate, T_0 is the surface temperature, and R is a stability correction factor $(1 - aRi)^{1/2}$, where Ri is Richardson's number and a is the adiabatic exchange coefficient for atmospheric stability.

In the *ENTICE* model, Z_0 influences the sensible heat flux to air (H) by altering a logarithmic form of the Richardson number (Equation 4.5) given by Outcalt (1972) which is used to adjust the adiabatic exchange coefficient (a) for atmospheric stability. The exchange coefficient used at each iteration of *ENTICE* is the product of the adiabatic coefficient and the stability correction factor R, i.e.

$$\text{correction factor } R = |1 - aRi|^{\frac{1}{2}}$$

$$Ri = \frac{\frac{g}{\bar{T}}[(T_z - T_0)/ln(Z_2/Z_0)]}{[U_z/ln(Z_2/Z_0)]^2} \tag{4.5}$$

where g is acceleration due to gravity, U_z is the wind speed at height Z, T bar is the mean temperature gradient between the surface and the upper measurement level (Z_2), T_z is the temperature at height Z, T_0 is the surface temperature and Z_0 is the roughness length.

The *ENTICE* model uses the stability correction factor R such that if Ri is negative (i.e. unstable conditions), the correction factor R is greater than unity and H is increased.

Conversely, if *Ri* is positive (i.e. stable conditions), *R* is less than unity and *H* is reduced. From the equation structure of *H*, the greater the value of Z_0 used in the *ENTICE* model, the greater the value of *H* calculated.

Z_0 is varied in *ENTICE* with respect to the ordinal land use and road type classifications in the model. In the original site specific forecast model, Thornes (1984) made the estimate that Z_0 would be approximately 15 cm due to the effect of moving traffic. Previous estimates of Z_0 for roads were smaller than this and ranged from 0.5 cm (Nysten, 1980; cited in Thornes (1984)) to 6 cm (Greene, 1980; cited in Thornes (1984)), but these estimates were based on the assumption of no traffic. Indeed, if the wind is blowing parallel with a traffic free road then Z_0 values less than 1 cm could be feasible. However, with a continuous presence of traffic assumed, Thornes (1984) suggested a Z_0 value more appropriate to an urban environment should be used, and selected a value of 15 cm which lies towards the lower end of the urban roughness scale. This estimate related to a single site specific location (rural motorway), unlike *ENTICE* which requires estimates of Z_0 at any location. To overcome this problem, Chapman (2002) created a look-up table of Z_0 values assimilated from the scientific literature (Table 4.2), providing typical estimates of how Z_0 varies with respect to the ordinal land use and road type classifications.

Table 4.2 Z_0 values (cm) currently used in the *ENTICE* model in relation to the ordinal land use and road type classification (modified from Chapman (2002) to account for an additional 'semi-rural' land use class).

	Motorway	A-Road	B-Road	C-Road
City Centre	200	200	200	200
Urban	100	100	100	100
Suburban	75	75	75	75
Semi-rural	50	50	50	50
Rural	50	25	25	25

The use of an ordinal Z_0 dataset based on land use and road type classifications is a major oversimplification. Such values fail to account for variations in static surface elements (buildings, trees, etc.) within land use classes, and they take no account of wind direction and the associated surface elements within the upwind fetch of a specific forecast point. Hence, the existing method of Z_0 parameterisation in *ENTICE* requires further improvement.

4.3 New Methodology for Z_0 Estimation in *ENTICE*

4.3.1 Roughness length estimation

The roughest surfaces are typically found in urban areas, creating complex flow patterns that characterise the atmospheric surface layer. The roughness of a surface has major implications for surface drag, aerodynamic conductance for momentum transport, the depths of the roughness layer and Ekman layer, wind speed and the shape of the wind profile, and the flow type found in the urban canopy layer (Grimmond & Oke 1999). Knowledge of the aerodynamic characteristics in urban areas is essential for describing, modelling and forecasting the behaviour or urban flow patterns, but detailed field observations are seldom available, thus requiring model simulations that in the majority of cases are not based directly on observed measurements at the locality of interest (Tieleman 2003).

The roughness length parameter Z_0, used as a theoretical measure of the aerodynamic roughness of a surface, is commonly estimated using one of two approaches defined by Grimmond & Oke (1999). The first of these is *morphometric* methods that utilise algorithms relating aerodynamic parameters to measures of surface morphometry, whilst the second is *micrometeorological* methods that use field observations of wind or turbulence to solve for aerodynamic parameters included in theoretical relations derived from the logarithmic wind profile (Grimmond & Oke 1999). Aside from the expense and difficulty involved in obtaining and operating a field site, a major disadvantage of micrometeorological methods is that even

with the best available instrumentation, appropriate wind conditions for all directions are rarely found during a field experiment and the natural heterogeneity of urban sites combined with the sensitivity of analyses to small errors can result in unreliable measurements (Schaudt 1998). Morphometric methods on the other hand have the advantage that estimates of surface roughness can be obtained without the need for expensive on-site instrumentation, but most morphometric methods are based on empirical relations derived from wind tunnel work where the simulation of flow rarely mimics the true conditions found in real world situations, where wind direction is ever changing and the shape and density of roughness elements are not regular.

As a prerequisite any method of Z_0 estimation for use in road weather modelling should be practically simple and cost effective to implement given the budgetary constraints that the road weather industry is rapidly becoming accustomed with. Given the extensive geographical areas over which road weather forecasting is required, the use of micrometeorological methods requiring expensive on-site instrumentation can be ruled out in favour of a morphometric method. Grimmond & Oke (1999) provide a detailed critical review of several morphometric methods which the authors split into three main categories, a simple height based approach, methods that use height and plan areal fraction, and methods that consider height and frontal area index. Estimates of Z_0 using these methods were compared with values obtained from analysis of wind and turbulence observations based on a survey of approximately 60 field studies and 14 laboratory studies of real and scale model cities. Over the range of morphometric conditions found, the results provided no objective bias for selecting one morphometric method over another, but when considering factors such as ease of implementation, applicability across the full range of typical urban morphometries, and conformity with suggested curves and envelopes of reasonableness, morphometric methods that consider height and frontal area index were most favoured by the authors (Grimmond & Oke 1999). In particular, the height and frontal area index model presented by Bottema (1997)

was found to generate estimates of Z_0 that best conformed to observed measurements, but this method required the most demanding set of input requirements of all the morphometric methods. On the other hand, the simple height based approach is very simple to implement within a GIS environment and was found to work well in the mean, but because its formulation includes no recognition of density it fails to respond to the effects of packing and increasingly overestimates roughness at very high and low densities (Grimmond & Oke 1999).

Hence, there are clearly benefits and drawbacks to each method, and given the lack of any objective bias for selecting one morphometric method over another, one can argue that this choice should relate to the specific requirements of the application, which is this instance is road weather forecasting. As described in section 4.2, current estimation of Z_0 in road weather models is based on a fixed ordinal dataset of roughness values which has a number of limitations already discussed. The main objective for re-parameterising Z_0 in the *ENTICE* model is to remove the reliance of the model on this ordinal classification in favour of a continuous dataset of roughness values derived from some form of ground observation. As a proof of concept, the use of a simple height based morphometric approach which will be simple to implement within even the most basic of GIS environments provides a suitable starting point.

4.3.2 Height based rule of thumb

Chapman (2002) attempted to approximate Z_0 at hundreds of site specific locations around a route from fish-eye images using the assumption that Z_0 can be approximated by the ratio 1/10 of the height of the surface elements (Oke 1992). However, this direct calculation method was eventually abandoned due to difficulties in measuring the horizontal distance from lens to object required in order to calculate the height of intrusion from the object (e.g. buildings, trees, etc.) angle. The 1/10 ratio is based on a well-known simple rule of thumb for

estimating Z_0 (Equation 4.6) whereby, to a first order, Z_0 is related to the height of the surface elements (Z_H) by the empirical coefficient f_0 derived from observation, i.e.

$$Z_0 = f_0 \overline{Z_H} \tag{4.6}$$

Both Garratt (1992) and Hanna & Chang (1992) estimate the value of f_0 to be ~ 0.1, which is a commonly quoted value for surfaces in general, and across the range of roughness values it has been shown to yield reasonable values of Z_0 (Grimmond & Oke 1999). Hence, this height-based rule of thumb is used as the basis for testing a new Z_0 estimation in *ENTICE* designed to eliminate the current dependence of the model on the aforementioned ordinal based Z_0 values and their associated limitations.

4.3.3 Local Z_0 estimation from LIDAR data

The height-based rule of thumb (Equation 4.6) was applied to a Light Detection And Ranging (LIDAR) height dataset of the West Midlands, UK, to provide local estimations of Z_0 around the Birmingham study route described in Chapter 2. The LIDAR dataset, obtained via the Landmap Service (http://www.landmap.ac.uk/), included a 2 m horizontal resolution Digital Terrain Model (DTM), providing elevation measurements of the natural terrain features, and a 2 m horizontal resolution Digital Surface Model (DSM), which together with the natural terrain features included additional features such as buildings, vegetation and roads. Hence, subtracting the DTM from the DSM produced a dataset containing height measurements at 2 m horizontal resolution of all surface objects, from which local Z_0 estimations for each 2 m grid cell were calculated by applying the simple height-based rule of thumb (Equation 4.6).

4.3.4 Calculating effective Z_0

To account for the effect of upstream surface elements on the local Z_0 values at each point along the route, and the influence of the prevailing wind direction on the magnitude of this effect, an effective roughness length (Z_0^{eff}) similar to that used by Vihma & Savijärvi (1991) was calculated for each 2 m grid cell from the areal average (denoted $\langle\ \rangle$) of all local Z_0 estimations within set geometric areas spanning away from each grid cell to a specified distance of upwind fetch, i.e.

$$Z_0{}^{eff} = \langle Z_0 \rangle \tag{4.7}$$

The distance of upwind fetch used to calculate surface roughness at a point source will relate to the source area or 'footprint' within which the shape and density of the surface elements has an influence on the localised flow at the point source where surface roughness is to be estimated. In a study by Heilman et al (1989), several Bowen-ratio systems deployed at a range of fetch to height ratios downwind of a change in surface roughness found that under small Bowen ratio measurements (e.g. night-time), ratios of fetch to measurement height as small as 20:1 can provide acceptable accuracy. This is considerably lower than the commonly recommended ratio of 100:1 (Gash 1986; cited in Horst 1999), or even 250:1 as suggested by Bottema (1997), and serves to show the uncertainty that exists in accurately determining an 'optimum' distance of upwind fetch to include in surface roughness estimation. Horst & Weil (1994) used model estimates of the flux footprint to examine the fetch requirements for accurate micrometeorological measurement of surface fluxes of passive, conservative scalars within the surface flux layer, and found fetch to be a strong function of atmospheric stability. Stable conditions were found to require a much greater fetch than unstable conditions, and the fetch required even under moderately stable conditions was found in many cases to be considerably greater than the commonly used rule of thumb of an upwind fetch equal to 100 times the measurement height (Businger 1986).

Table 4.3 shows values for minimum fetch computed using Equation 4.8 (ASCE, 1996), which is derived from the early work of Brutsaert (1982) in providing theoretical considerations of boundary layer development for use in estimating minimum fetch requirements as a function of surface roughness. Equation 4.8 estimates x_f for near neutral conditions, requiring the exponent (0.14) to be increased for situations of increasing stability and decreased for situations of increasing instability (ASCE, 1996).

$$x_f = \left(\frac{30(z-d)}{Z_{0m}{}^{0.125}}\right)^{1.14} \tag{4.8}$$

where x_f is the minimum fetch distance required for complete boundary layer development (m), z is the maximum sensor height above the ground (m), d is the zero plane displacement (m), and Z_{0m} is the momentum roughness height of the surface (m).

Table 4.3 Minimum recommended upwind fetch distances (m) for various types of surface cover, derived from Equation 4.8 (ASCE, 1996).

Height and type of surface cover	$z = 1$	$z = 2$	$z = 3$	$z = 12$
0-0.0001m Water	180	400	630	3000
0.12m Grass	80	190	300	1500
0.5m Alfalfa	45	130	220	1200
1.5m Cattails	n/a	60	140	950
10m Dense Trees	n/a	n/a	n/a	320

The values for minimum fetch shown in Table 4.3 indicate that Equation 4.8 follows the 100:1 rule for a relatively wide range of vegetation and heights. However, since stable conditions are shown in the literature to require much greater fetch than unstable conditions, and since stable conditions are the most important conditions from a road weather modelling perspective in relation to the potential for ice formation, an upwind fetch in the order of

1:250, which Bottema (1997) suggests is required for reasonable roughness estimates, is used in the following analysis.

Based on the local Z_0 values calculated for each forecast point along the Birmingham study route using Equation 4.6, an upwind fetch ratio of 1:250 would require a fetch of 500 m to ensure inclusion of the upper fetch threshold within the analysis. To determine whether a 500 m fetch would provide representative Z_0^{eff} values, Kruskal-Wallis rank order tests (Dytham 1999) and Wilcoxon rank-sum tests were used to compare five LIDAR based Z_0^{eff} datasets, calculated for five distances of upwind fetch (100, 150, 200, 250 and 500 m), against an urban land use classification (OWEN) derived by Owen et al (2006) for the UK West Midlands metropolitan area (Figure 4.1). Each of the five roughness datasets were calculated assuming a prevailing westerly wind direction (247.5 - 292.5°) typical of the study locality (Figure 4.2). The OWEN land use dataset consists of eight land use classes at 1 km^2 resolution (*villages/farms, suburban, light suburban, dense suburban, urban/transport, urban, light urban/open water* and *woodland/open land*) derived from dimensionality reduction of 25 spatial land-cover attributes using principal components analysis. Using the assumption that surface roughness will vary significantly between each of the OWEN land use classes, the most representative Z_0^{eff} values for the study route will be those that vary the most, and hence show the most significant differences, between land use classes.

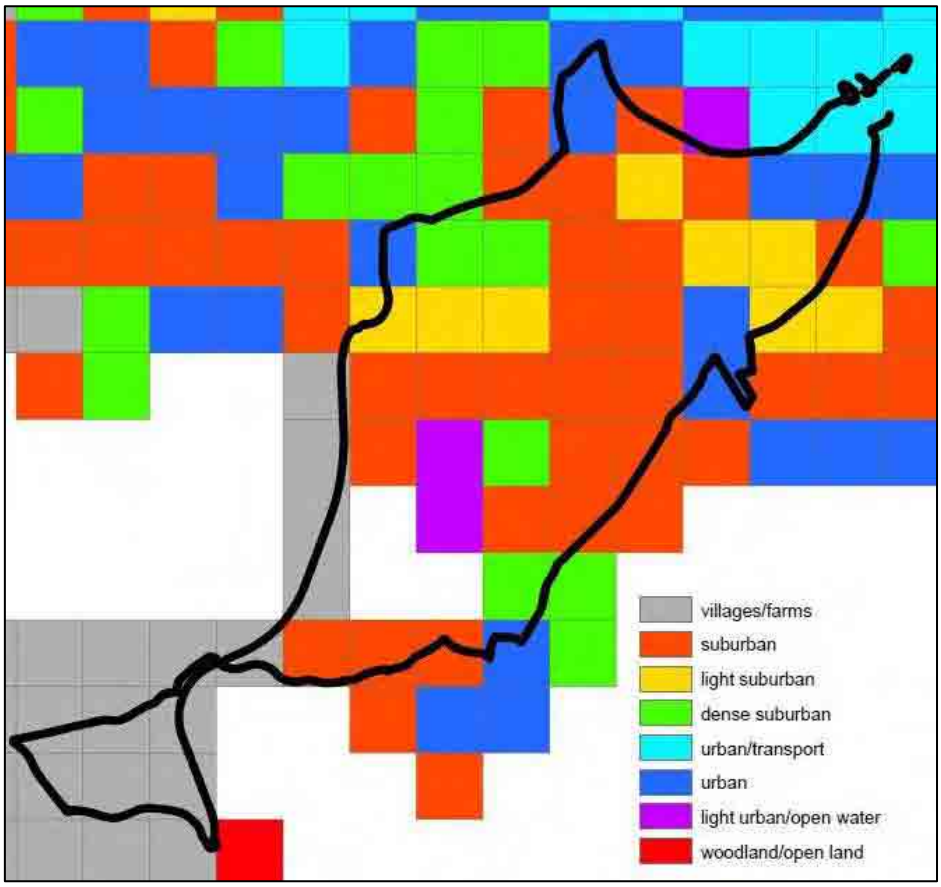

Figure 4.1 Eight land use classes around the study route as defined by the OWEN land use classification (Owen et al. 2006).

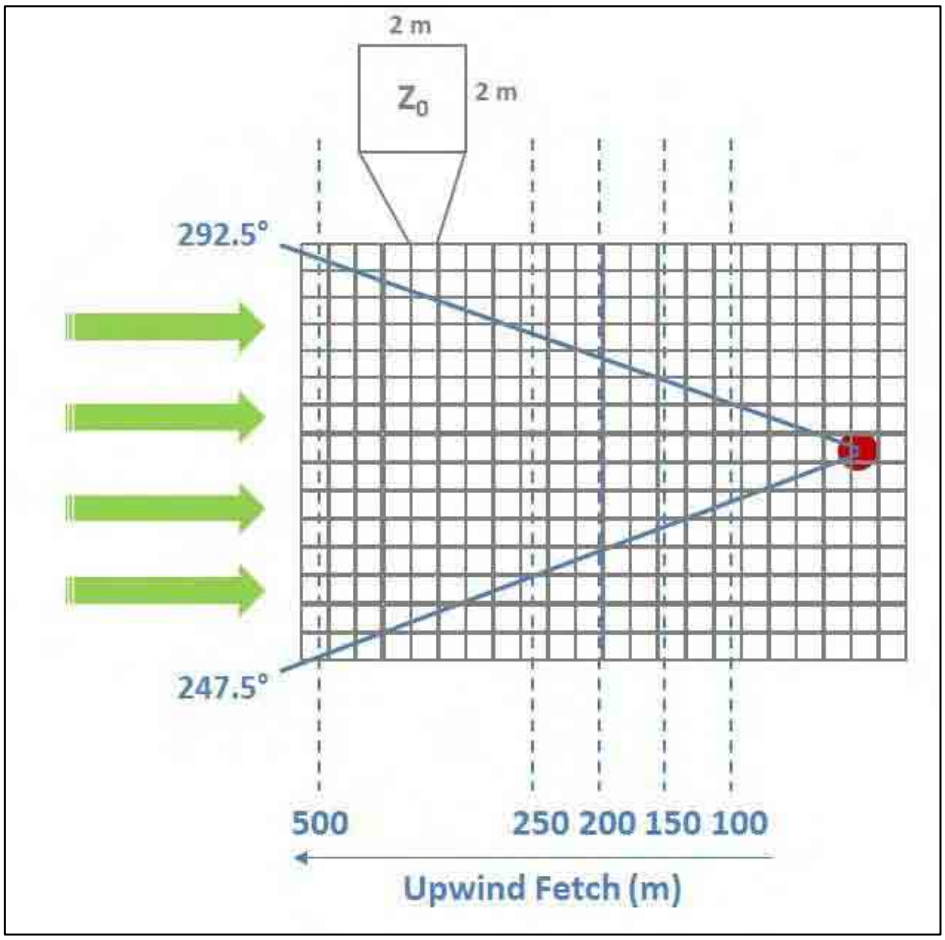

Figure 4.2 Illustration of effective roughness length (Z_0^{eff}) calculation for each 2 m LIDAR grid cell over distances of upwind fetch ranging from 100 m up to 500 m, assuming a westerly prevailing wind.

Kruskal-Wallis is the non-parametric equivalent of a one-way analysis of variance (ANOVA) and is used when a dataset violates the ANOVA assumptions about normality and homogeneity of variance. Levene's test for homogeneity of variance produced highly significant values (p-value < 0.001) for all five roughness datasets, indicating that significant differences exist in the variances of the Z_0^{eff} values between the land use groups. Thus, Levene's null hypothesis of equal group variances was rejected and the Kruskal-Wallis test, which makes no assumptions about homogeneity of variance or normal distributions, was selected for analysis. The Kruskal-Wallis test is employed with rank-order data whereby the raw data is converted to a rank in the overall dataset (Sheskin 2007), with the lowest value obtaining a rank of 1. Hence, for each of the five roughness datasets the lowest Z_0^{eff} value is

assigned a rank of 1, the next lowest value a rank of 2, and so on until every value in the dataset is assigned a rank. The ranked samples are then returned to their original land use groupings and a mean rank calculated for each group. If the result of the Kruskal-Wallis test is significant, it indicates there is a significant difference between at least two of the land use group mean ranks, and hence a significant difference in the Z_0^{eff} values between these land use classes.

The results from the Kruskal-Wallis analyses were highly significant ($p < 0.001$) over all five distances of fetch (Table 4.4). This indicates that significant differences exist in the Z_0^{eff} values between at least two of the land use classes for all five distances of fetch, but Kruskal-Wallis tests do not reveal where these differences occur. Hence, for all five roughness datasets post-hoc Wilcoxon rank-sum tests (Table 4.5) were performed on the Z_0^{eff} values within each independent land use class, comparing each class against each other to reveal where the significant differences occur.

Table 4.4 Kruskal-Wallis results for Z_0^{eff} comparisons between OWEN land use classes

Fetch (m)		100		150		200		250		500	
		N	Mean Rank	N	Mean Rank	N	Mean Rank	N	Mean Rank	N	Mean Rank
OWEN	**1. Villages/farms**	463	668.32	461	645.84	460	606.58	458	586.3	447	580.73
Land use	**2. Suburban**	534	1035.19	534	1088.43	534	1107.03	534	1125.84	534	1102.76
	3. Light suburban	125	1079.15	125	995.38	125	1010.3	125	1018.55	125	1103.52
	4. Dense suburban	123	848.68	123	775.21	123	775.56	123	779.85	123	644.34
	5. Urban/transport	341	1755.18	341	1808.78	341	1837.63	341	1851.92	341	1851.89
	6. Urban	489	1008.56	489	949.89	489	934.92	489	915.41	489	927.37
	7. Light urban/open water	42	1351.67	42	1567.95	42	1643.5	42	1637.5	42	1614.83
	8. Woodland/open land	5	504.8	5	479	5	288.8	5	204.4	5	43
	Total	2122		2120		2119					
Chi-Square (Z0)		660.867		799.676		900.591		954.626		988.674	
df (Z0)		7		7		7		7		7	
Sig. (Z0)		0.000		0.000		0.000		0.000		0.000	

Table 4.5 Wilcoxon *P*-values matrices comparing Z_0^{eff} values between each OWEN land use class over five distances of upwind fetch

OWEN 100m Fetch									OWEN 150m Fetch								OWEN 200m Fetch							
Land Use	**1**	**2**	**3**	**4**	**5**	**6**	**7**	**8**	**1**	**2**	**3**	**4**	**5**	**6**	**7**	**8**	**1**	**2**	**3**	**4**	**5**	**6**	**7**	**8**
1		0.000	0.000	0.000	0.000	0.000	0.000	***0.751***		0.000	0.000	0.000	0.000	0.000	0.000	***0.468***		0.000	0.000	0.000	0.000	0.000	0.000	***0.730***
2	0.000		***0.212***	0.000	0.000	***0.261***	0.000	***0.019***	0.000		***0.102***	0.000	0.000	0.000	0.000	***0.008***	0.000		***0.052***	0.000	0.000	0.000	0.000	0.001
3	0.000	***0.212***		0.001	0.000	***0.048***	***0.032***	***0.049***	0.000	***0.102***		0.000	0.000	***0.162***	0.000	***0.023***	0.000	***0.052***		0.000	0.000	***0.017***	0.000	***0.005***
4	0.000	0.000	0.001		0.000	0.000	0.000	***0.017***	0.000	0.000	0.000		0.000	0.000	0.000	***0.027***	0.000	0.000	0.000		0.000	0.000	0.000	0.001
5	0.000	0.000	0.000	0.000		0.000	0.000	0.000	0.000	0.000	0.000	0.000		0.000	0.000	0.000	0.000	0.000	0.000	0.000		0.000	0.000	0.000
6	0.000	***0.261***	***0.048***	0.000	0.000		0.000	***0.008***	0.000	0.000	***0.162***	0.000	0.000		0.000	***0.004***	0.000	0.000	***0.017***	0.000	0.000		0.000	0.001
7	0.000	0.000	***0.032***	0.000	0.000	0.000		0.002	0.000	0.000	0.000	0.000	0.000	0.000		0.000	0.000	0.000	0.000	0.000	0.000	0.000		0.000
8	***0.751***	***0.019***	***0.049***	***0.017***	0.000	***0.008***	0.002		***0.468***	***0.008***	***0.023***	***0.027***	0.000	***0.004***	0.000		***0.730***	0.001	***0.005***	0.001	0.000	0.001	0.000	

OWEN 250m Fetch									OWEN 500m Fetch							
Land Use	**1**	**2**	**3**	**4**	**5**	**6**	**7**	**8**	**1**	**2**	**3**	**4**	**5**	**6**	**7**	**8**
1		0.000	0.000	0.000	0.000	0.000	0.000	***0.290***		0.000	0.000	0.000	0.000	0.000	0.000	0.002
2	0.000		***0.016***	0.000	0.000	0.000	0.000	0.000	0.000		***0.902***	0.000	0.000	0.000	0.000	0.000
3	0.000	***0.016***		0.000	0.000	0.002	0.000	0.001	0.000	***0.902***		0.000	0.000	0.000	0.000	0.000
4	0.000	0.000	0.000		0.000	0.000	0.000	0.000	0.000	0.000	0.000		0.000	0.000	0.000	0.000
5	0.000	0.000	0.000	0.000		0.000	0.000	0.000	0.000	0.000	0.000	0.000		0.000	0.000	0.000
6	0.000	0.000	0.002	0.000	0.000		0.000	0.000	0.000	0.000	0.000	0.000	0.000		0.000	0.000
7	0.000	0.000	0.000	0.000	0.000	0.000		0.000	0.000	0.000	0.000	0.000	0.000	0.000		0.000
8	***0.290***	0.000	0.001	0.000	0.000	0.000	0.000		0.002	0.000	0.000	0.000	0.000	0.000	0.000	

Land Use Classification

1: villages/farms
2: suburban
3: light suburban
4: dense suburban
5: urban/transport
6: urban
7: light urban/open water
8: woodland/open land

To account for the problem of inflated error rates when conducting multiple Wilcoxon tests, the Bonferroni Correction factor was applied to the standard 95% significance level, giving a new independent test level of 99.8% (0.002). Without this correction factor, the probability of rejecting the null hypothesis when it is actually true (Type 1 error) for at least one comparison increases from 5% to 76% (based on a total of 28 comparisons) when comparing all the land use classes. The Wilcoxon *p*-values (Table 4.5) reveal that with a fetch of just 100 m, only 68% of the roughness comparisons between all the land use classes are statistically significant, increasing to 75%, 86% and 93% for distances of 150, 200 and 250 m respectively. With a fetch of 500 m, however, 96% of the roughness comparisons between the land use groups are statistically significant. Hence, using the assumption that surface roughness is significantly different between each of the land use classes, then an upwind fetch of 500 m produces Z_0^{eff} values that most accurately reflect these conditions.

It is accepted that the use of a pre-defined distance is a major oversimplification, since most recommendations in the literature suggest the fetch requirement to be a function of obstacle height. However, whilst a variable approach is feasible for *ENTICE*, a pre-defined distance enabled the use of inbuilt neighbourhood functions within ArcMap and allowed a buffer equal to the fetch distance to be created and used as an analysis mask around each forecast point, significantly reducing the processing requirements on the LIDAR dataset. Therefore, using a pre-defined fetch of 500 m, Z_0^{eff} values at each forecast point were calculated for eight prevailing wind directions categorised into 45° approach angles (Figure 4.3) using a focal mean wedge neighbourhood function in ArcMap. The resulting Z_0^{eff} dataset contained eight possible Z_0^{eff} values for each forecast point along the study route (1 for each wind direction), the maximum values of which for each wind category are shown in Figure 4.3. The selection of 45° approach angles corresponding to the eight wind directions shown in Figure 4.3 was made partly to simplify analysis for a proof of concept study such as this, but largely because reliable wind direction data for the entire study route was not available, with the data used

taken from an automatic weather station located some distance from the study route (see section 4.4.2). It is acknowledged however that in a real forecasting situation much smaller approach angles should ideally be used, together with higher resolution reliable wind direction data which was not available for this study.

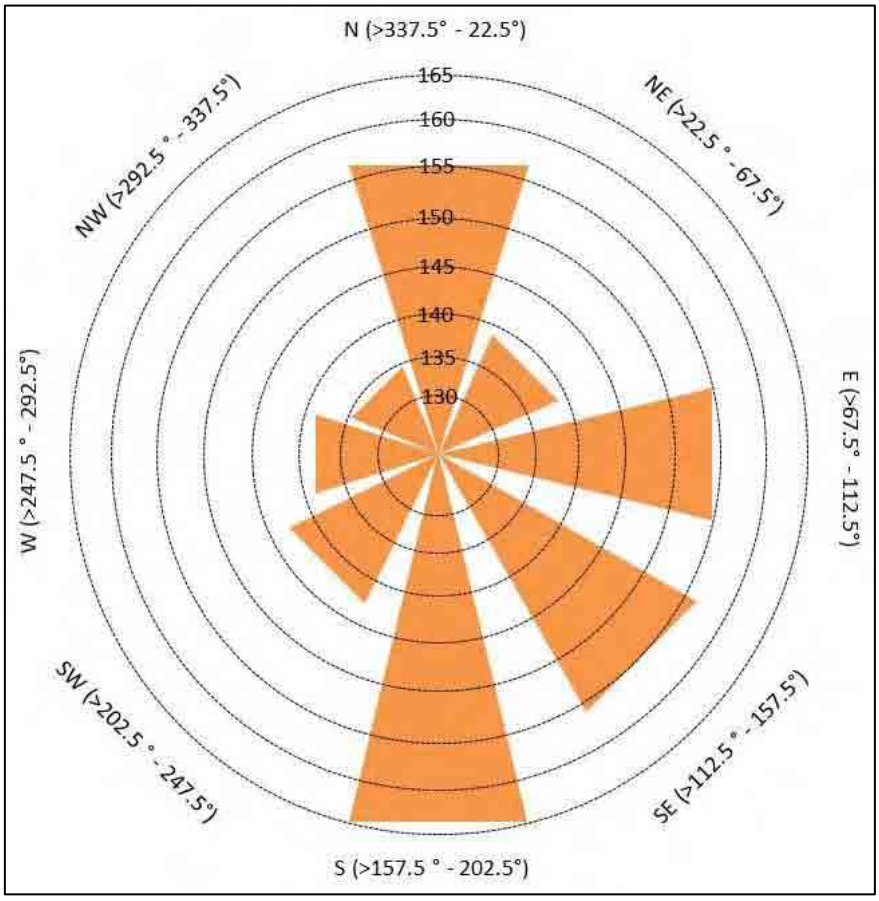

Figure 4.3 Variation in maximum Z_0^{eff} values (cm) around the study route with approaching wind direction.

The minimum range of the Z_0^{eff} values in each wind category was manually forced to 15 cm. Whilst some of the calculated Z_0^{eff} values were significantly below this threshold, the proposed technique fails to account for the increased turbulence and mixing caused by moving traffic which would imply a boundary layer deeper than for an untrafficked road. Hence, a lower threshold of 15 cm was set for the Z_0^{eff} values in each wind category to account for moving traffic, the same value used by Thornes (1984) to simulate the effect of moving traffic on a rural motorway. The Z_0^{eff} values obtained for the study route using this

new methodology are typical of the range of values we could expect from a look-up table of roughness values such as the Davenport classification of terrain roughness (Table 4.1) given the land use classes that the study route encompasses (Figure 4.1).

The σ_β of Z_0^{eff} values around the route for the eight directions of upwind fetch (Figure 4.4 (a)) reveals large variations with wind direction in the urbanised city centre (> 40 SD) as one might expect given the variety in the shape and density of surface elements in city centres. Similar variations in surface roughness are also evident in the largely rural south-westerly section of the route (Figure 4.4 (b)), where a forested area adjacent to the route appears to act as a natural screen against any approaching winds from a predominantly northerly to westerly direction. In contrast, other sections of the route show little variation in surface roughness with wind direction, including some suburban and urban areas where the surface elements are less dense and more uniform in height than in the city centre. Hence, the need to account for various directions of upwind fetch in the estimation of surface roughness at each forecast point for *ENTICE* has been demonstrated. To implement this in *ENTICE*, changes are required to the Geographical Parameter Database used to drive the model, along with changes to the meteorological input files and the coding of the model in order to provide a variable roughness parameter for each forecast point based on the forecast wind direction at each time-step in the model.

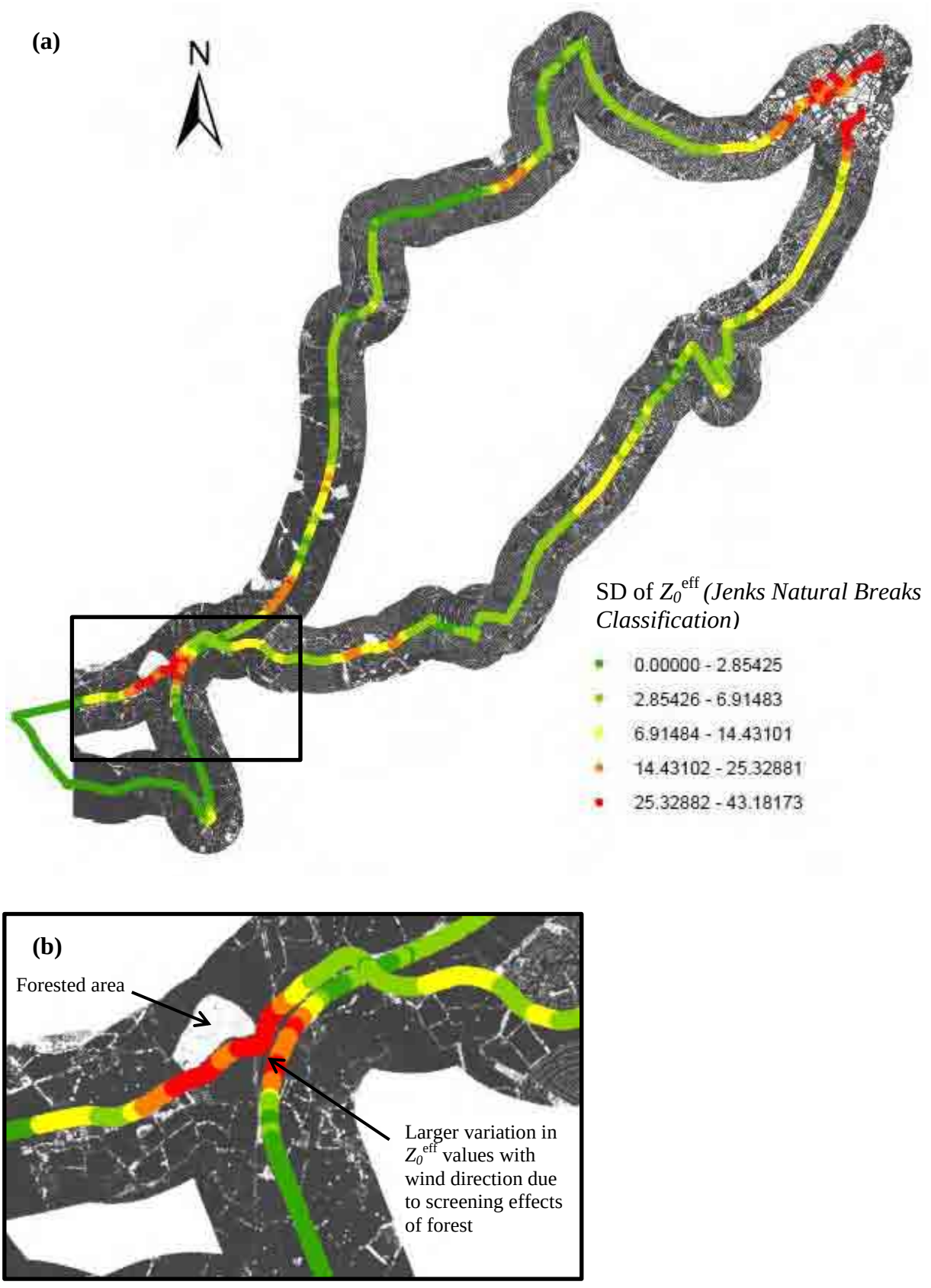

Figure 4.4(a) Standard deviation of Z_0^{eff} values at each forecast point around the study route over the eight wind directions shown in Figure 4.3 and **(b)** enlarged view of a rural section of the study route, revealing a forested area acting as a natural screen to approaching northerly to westerly winds. LIDAR data courtesy of the Landmap Service.

4.4 Changes to *ENTICE* to Enable Inclusion of Z_0^{eff}

4.4.1 Z_0^{eff} values

The new LIDAR based Z_0^{eff} values were appended to the existing *ENTICE* GPD for the study route, consisting of a database file containing the geographical and road infrastructure data for every forecast point around the study route (Figure 4.5). Eight columns of Z_0^{eff} values were appended to the GPD file, corresponding to the eight different upwind approach angles from which the Z_0^{eff} values at each forecast point were calculated. The GPD file was then fed into the *ENTICE* model (Appendix 5) as a GPD array via a spatial iterative loop, with all eight sets of Z_0^{eff} values assigned to individual variables within the GPD array ready for automatic selection based on the wind direction:

EASTING	NORTHING	LATITUDE	SVF	ALTITUDE	SLOPE	ASPECT	LANDUSE	FC	ZONORTH	ZONEAST	ZOEAST	ZOSEAST	ZOSOUTH	ZOSWEST	ZOWEST	ZONWEST
398915.27	283025.83	52.45	0.89	186	3.20	259.70	2	3000	0.17	0.28	0.20	0.22	0.28	0.10	0.28	0.07
398916.34	281939.08	52.44	0.89	190	4.70	289.54	2	3000	0.16	0.15	0.20	0.22	0.10	0.10	0.12	0.14
398917.59	281521.96	52.43	0.96	195	3.14	300.07	2	3000	0.08	0.22	0.22	0.14	0.17	0.06	0.03	0.12
398917.70	281916.84	52.44	0.94	190	4.70	289.54	2	3000	0.15	0.15	0.19	0.22	0.11	0.09	0.11	0.14
398918.37	281893.48	52.44	0.97	189	4.74	264.81	2	3000	0.14	0.15	0.19	0.23	0.11	0.08	0.11	0.12
398919.04	281847.87	52.43	0.96	188	4.97	251.57	2	3000	0.12	0.16	0.19	0.23	0.12	0.08	0.13	0.08
398919.64	281546.43	52.43	0.97	195	3.14	300.07	2	3000	0.08	0.23	0.21	0.15	0.17	0.06	0.03	0.12
398920.04	283046.96	52.45	0.89	186	3.20	259.70	2	3000	0.17	0.27	0.19	0.23	0.28	0.10	0.26	0.08
398921.01	281569.79	52.43	0.96	193	3.34	329.04	2	3000	0.07	0.22	0.21	0.16	0.15	0.05	0.03	0.12

Figure 4.5 Excerpt from the *ENTICE* GPD database file, showing the new LIDAR based Z_0^{eff} values appended to the end of the database.

4.4.2 Wind direction

The existing *ENTICE* model does not include wind direction within its meteorological input parameters. Hourly wind direction data for the appropriate nights was obtained from the Coleshill automatic weather station run by the UK Meteorological Office and accessed through the BADC website (http://badc.nerc.ac.uk/home/index.html). The raw meteorological input files for *ENTICE* are simple comma separated files, to which the hourly wind direction data was added as an extra comma separated value at the end of each line:

```
LOCATION,DATE,TIME,T,Td,WIND,Wx,CLOUD-COVER(OCTAS),CLOUD-BASE(FT),WDIR
BHAM1,'09/12/1999, 12:00:00',7,6.8,6.4,NONE,3,2500,200
BHAM1,'09/12/1999, 13:00:00',6.5,6,6,NONE,4,2500,210
BHAM1,'09/12/1999, 14:00:00',6,5.7,5.6,NONE,5,2500,210
BHAM1,'09/12/1999, 15:00:00',5.6,5.4,5.3,RA,6,2500,220
BHAM1,'09/12/1999, 16:00:00',5.6,5.3,5,RA,6,2500,220
BHAM1,'09/12/1999, 17:00:00',5.6,5.1,4,RA,7,2500,220
```

Figure 4.6 Excerpt from an *ENTICE* comma separated raw meteorological input data file, showing the wind direction appended to the end of each row.

Wind direction data was then fed into the model along with the other meteorological parameters as an additional array and the values were averaged linearly for the 20 minute intervals between actual input values. With each iteration of the spatial loop, a temporal iterative loop was run to enable the correct column of Z_0^{eff} values to be selected based on the wind direction at each iteration. Each iteration of the temporal loop corresponded to the next 20 minute wind direction data, whilst each iteration of the spatial loop corresponded to the next forecast point along the route.

for all forecast points **do**

  for each 20 minute interval **do**

    if wind direction >= 337.5 or < 22.5

      select the northerly Z_0^{eff} database

    else if wind direction >= 22.5 and < 67.5

      select the north-easterly Z_0^{eff} database

    else if wind direction >= 67.5 and < 112.5

      select the easterly Z_0^{eff} database

    else if wind direction >= 112.5 and < 157.5

      select the south-easterly Z_0^{eff} database

    else if wind direction >= 157.5 and < 202.5

      select the southerly Z_0^{eff} database

    else if wind direction >= 202.5 and < 247.5

      select the south-westerly Z_0^{eff} database

    else if wind direction >= 247.5 and < 292.5

select the westerly Z_0^{eff} database

else if wind direction >= 292.5 and < 337.5

select the north-westerly Z_0^{eff} database

else select the westerly Z_0^{eff} database

end if

end for

end for

4.5 Statistical Analysis of New Z_0^{eff} Values

To test whether the newly calculated Z_0^{eff} values improve the spatial forecasting performance of *ENTICE*, a statistical analysis was conducted on 20 nights thermal mapping data for the study route. During the analysis, all of the geographical parameters in the model, with the exception of roughness length, were fixed spatially to default values, rather than running the model in 'quasi-operational' mode. As with the analyses undertaken in Chapter 3, fixing all other geographical parameters spatially ensures any changes identified in the model forecast are solely due to the change in surface roughness, allowing us to quantify the effect of surface roughness changes alone on model performance. Again, the resultant forecast statistics (Table 4.6) are not providing a true measure of model performance but a reflection of model bias caused by the spatial fixing of the geographical parameters. However, like with the road construction analyses in Chapter 3, by running the model twice, first using the original ordinal Z_0 values (Table 4.2) and then using the re-coded model with the new Z_0^{eff} values calculated from the LIDAR data, changes in the model results between the two model runs can be identified, enabling us to quantify the impact of surface roughness changes on model performance. Forecast statistics for both model runs are summarised in Table 4.6.

Table 4.6 Forecast statistics from a statistical analysis on surface roughness in *ENTICE*, where all geographical variables in the model were held constant with the exception of surface roughness

	Analysis 1 – Existing ordinal Z_0 values						**Analysis 2 – New Z_0^{eff} values**					
Night	β	σ_β	*RMSE*	*Pm*	*Prm*	R^2	β	σ_β	*RMSE*	*Pm*	*Prm*	R^2
1	-0.24	0.98	1.01	71.92	72.89	0.14	-0.39	0.96	1.03	70.99	71.34	0.27
2	0.61	1.06	1.22	54.22	69.75	0.32	0.38	1.03	1.09	65.19	71.65	0.50
3	-0.79	1.28	1.50	52.94	57.54	0.29	-1.08	1.26	1.66	45.47	58.20	0.30
4	-0.11	0.92	0.93	74.48	72.36	0.28	-0.36	0.92	0.98	69.17	73.86	0.29
5	-0.97	1.45	1.74	58.20	56.66	0.31	-1.10	1.44	1.81	53.6	56.57	0.38
6	-0.73	1.45	1.63	60.77	54.22	0.31	-0.81	1.44	1.66	58.65	54.49	0.40
7	-0.75	1.57	1.74	49.45	51.84	0.30	-1.03	1.54	1.85	40.91	53.34	0.37
8	-0.06	0.87	0.88	76.25	75.90	0.18	0.09	0.89	0.90	74.97	76.12	0.24
9	-1.88	0.90	2.09	15.52	74.57	0.34	-1.92	0.93	2.14	15.52	72.93	0.17
10	-0.23	1.13	1.15	68.69	67.76	0.23	-0.24	1.13	1.16	68.60	67.58	0.42
11	-0.28	0.76	0.81	82.57	85.01	0.23	-0.48	0.74	0.88	78.06	85.23	0.30
12	1.14	1.39	1.8	30.74	59.40	0.23	1.04	1.39	1.73	32.95	59.40	0.37
13	-0.09	0.96	0.96	72.18	70.54	0.19	0.02	0.98	0.98	70.01	70.41	0.35
14	0.42	0.72	0.83	71.47	86.60	0.14	0.36	0.72	0.80	74.83	86.33	0.24
15	0.69	1.41	1.57	44.80	57.76	0.28	0.71	1.43	1.59	44.94	57.59	0.04
16	0.09	0.56	0.57	93.98	94.47	0.16	0.05	0.56	0.57	94.60	94.12	0.16
17	-0.21	1.22	1.24	61.26	59.93	0.08	-0.15	1.25	1.25	60.19	58.60	0.27
18	-1.22	1.09	1.63	40.78	67.58	0.18	-1.04	1.12	1.53	51.44	67.32	0.28
19	-1.19	0.55	1.31	33.92	91.91	0.17	-0.96	0.61	1.14	57.23	90.40	0.29
20	-1.13	0.91	1.45	44.67	75.19	0.35	-1.23	0.91	1.53	38.57	74.26	0.35
Average	**-0.35**	**1.06**	**1.30**	**57.94**	**70.09**	**0.24**	**-0.41**	**1.06**	**1.31**	**58.29**	**69.99**	**0.30**

These statistics reveal that replacing the original ordinal Z_0 values with the new Z_0^{eff} values has little impact on the overall *RMSE* of the route-based forecast. Hence, the magnitude of any errors in the forecasts remains similar, even though the new Z_0^{eff} values increase the overall negative bias in the forecast. In terms of model accuracy, the overall *Pm* value increases slightly (+ 0.35%) using the new Z_0^{eff} values (Table 4.6 & Figure 4.7) with a range over the 20 nights of -8.5% to +23%. Negligible change is observed (-0.1%) in the *Prm* values.

Whilst such statistics are a good indicator of the spatial forecasting ability of a model, they are nonetheless limited to a resolution of ±1°C, and can potentially ignore finer scale improvements to a model. In the previous chapter an analysis of R^2 values for modelled versus predicted RST, which unlike the *Prm* values is not limited by temperature resolution, revealed no overall change in the variability of RST accounted for by *ENTICE* when the new re-parameterised GPR based subsurface road construction measurements were incorporated into the model. The same analysis here based on changes made to the surface roughness estimation in the model reveals a 6% increase in the variability of RST accounted for by *ENTICE* with the new Z_0^{eff} values (Table 4.6 & Figure 4.8). Hence, with the new LIDAR based Z_0^{eff} values the overall spatial forecasting performance of the *ENTICE* model is improved, suggesting that the new Z_0^{eff} values used in *ENTICE* provide a more realistic representation of the turbulent heat transfer in the boundary layer close to the road surface than was possible with the original ordinal Z_0 values. Accordingly, with the new Z_0^{eff} values *ENTICE* is able to better predict thermal temperature variations around a route.

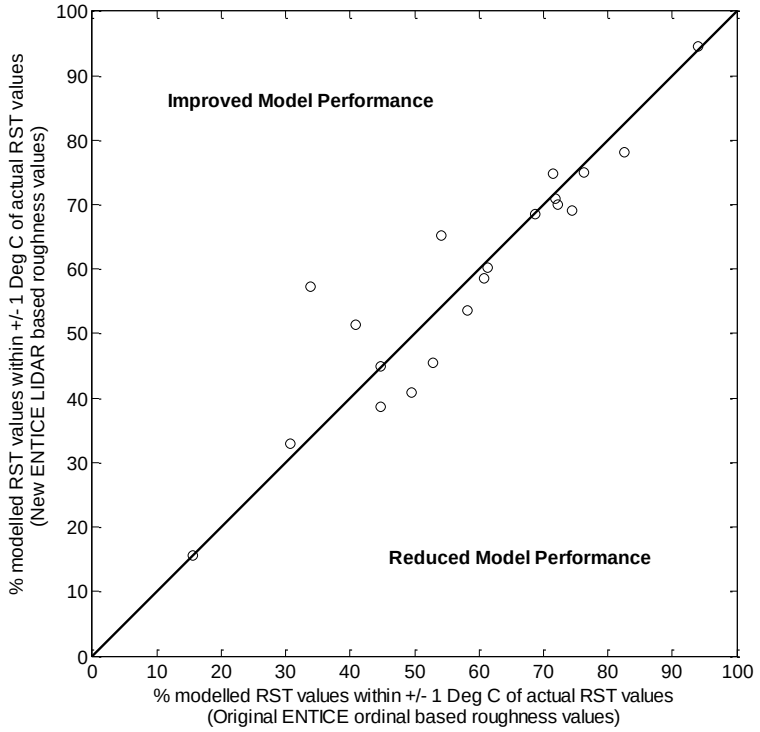

Figure 4.7 Comparison of *ENTICE* model accuracy in predicting RST to within ± 1°C of actual values. X-axis values relate to model runs using the original *ENTICE* ordinal based Z_0 values, and y-axis values relate to model runs using the new LIDAR based Z_0^{eff} values.

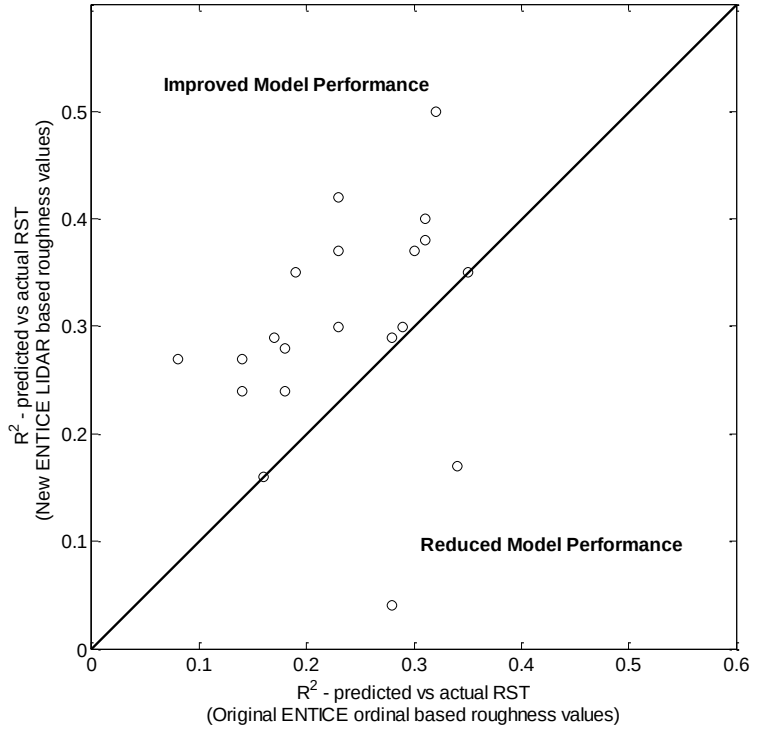

Figure 4.8 R^2 values for *ENTICE* predicted road surface temperature vs. actual road surface temperature collected from thermal mapping runs. X-axis values relate to model runs using the original *ENTICE* ordinal based Z_0 values, and y-axis values relate to model runs using the new LIDAR based Z_0^{eff} values.

CHAPTER FOUR SUMMARY

A new method for de-parameterising surface roughness in route-based forecast models using high resolution LIDAR data coupled with spatial processing techniques has been described. The technique calculates an effective roughness length at each forecast point from the areal average of all height based local Z_0 estimations within defined areas spanning away from each forecast point. The roughness values obtained have been implemented in the ENTICE model, and a statistical analysis on surface roughness has revealed a 6% increase in the variability of RST accounted for by ENTICE with the new re-parameterised surface roughness measurements, despite there being negligible change in the overall Pm values using this new technique. In the following chapter the integrity of the new re-parameterised surface roughness and road construction measurements proposed in this thesis will be fully tested through spatial validation of the ENTICE route-based forecast model using the new cluster based validation strategy proposed in Chapter 2.

5. SPATIAL VALIDATION OF THE *ENTICE* ROUTE-BASED FORECAST MODEL

When developing the validation technique outlined in Chapter 2 of this thesis, it was envisaged that the technique could be used as a rapid integrity test for any future measurement techniques that are designed to improve upon existing parameterisations within route-based forecast models. This chapter aims to test this by verifying the integrity of the re-parameterisations to surface roughness and road construction proposed in Chapters 3 and 4 using the new cluster based validation strategy proposed in Chapter 2. The new LIDAR based Z_0^{eff} values and subsurface road construction profiles provide the opportunity to replace the existing categorical land use and road type parameterisations used in the original clustering solutions with a much higher resolution continuous dataset derived from LIDAR and GPR measurements.

5.1 Summary of Overall Model Performance

Prior to undertaking the cluster based validation strategy, an analysis of the entire route statistics is required in order to prove the benefits of a cluster level analysis. With the *ENTICE* model returned to a 'quasi-operational' (hence, true model performance) mode with all the parameters within the model set to their best values, the model was re-run for all 20 nights taking into account the new surface roughness and road construction parameterisations identified in Chapters 3 and 4. These results were then compared to the original model runs (Table 2.4) before any changes had been made to the model. Figure 5.1 displays the average *RMSE* values for the modelled RST over the 20 nights, and shows a clear reduction in the magnitude of any model errors when the re-parameterised surface roughness and road construction measurements are introduced into the model. On 85% of the study nights the *RMSE* of the forecast is reduced when model changes are introduced, with the overall average

for the 20 nights falling by 0.28°C from 1.48°C to 1.20°C. The overall spatial forecasting ability of the model, as represented by the *Pm* values, has also improved significantly (Figure 5.2), increasing on 85% of the study nights when the model changes are introduced, with the overall average for the 20 nights increasing from 46.94% (Table 2.4) to 60.93%. The three nights where the spatial forecasting performance of the model appears to decrease were all damped nights where thermal mapping is generally more susceptible to errors due to factors such as increasing variability in surface emissivity. Emissivity in the *ENTICE* model is held at a constant 0.95 which can introduce considerable error during a survey (Gustavsson 1999), and such errors are often greatest on damped nights where road surface conditions are more changeable. To overcome such errors, continued research is required into improving the accuracy of the thermal mapping technique. The overall variability of RST accounted for by *ENTICE* increases on 60% of the study nights when model changes are introduced (Figure 5.3), with an overall increase of 3% over the 20 nights. Those nights where the largest decreases were found in the variability of RST accounted for by *ENTICE* were again damped nights.

Analysis of model performance using entire route statistics has therefore shown that the overall spatial forecasting ability of the *ENTICE* model has improved as a result of the re-parameterisation of surface roughness and road construction within the model. As shown in Chapter 2, however, the performance of a route-based forecast model can be better assessed by analysing model statistics at a cluster level, since an entire route analysis can often mask deficiencies (and improvements) in the spatial forecasting ability of the model. Cluster level analyses also enable the consistency of new clustering solutions, and hence new measurement techniques, to be tested via the calculation of clustering similarity coefficients. Such analyses indicate the ability of clusters in capturing the physical relation between RST around a route and the geographical and road infrastructure parameters used to create the cluster, and thus

provide a good integrity test for any new measurement techniques which alter a clustering solution.

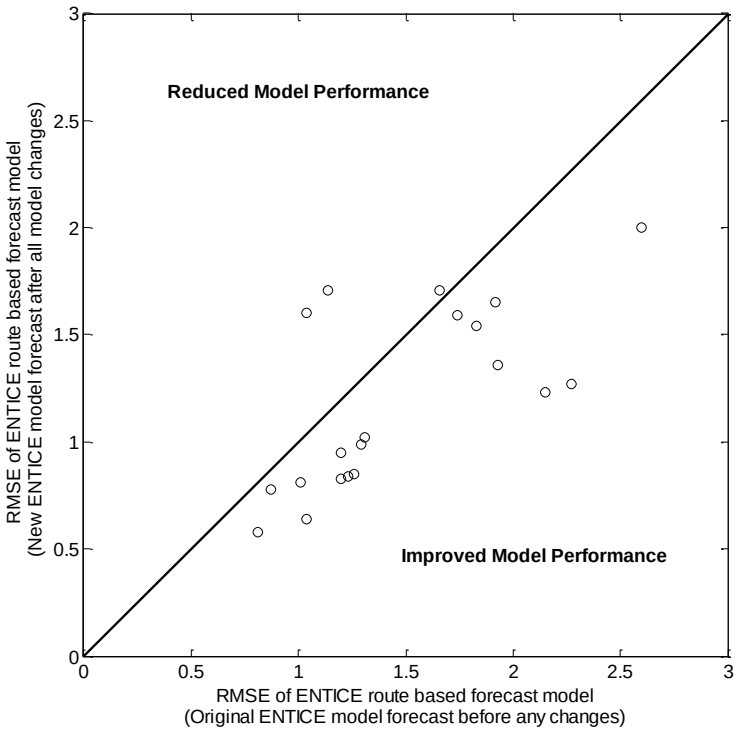

Figure 5.1 Average *RMSE* values for *ENTICE* predicted RST over the Birmingham study route (20 nights). X-axis values relate to model runs before any changes were made to the *ENTICE* model, and y-axis values relate to model runs which incorporate the re-parameterised surface roughness and road construction measurements.

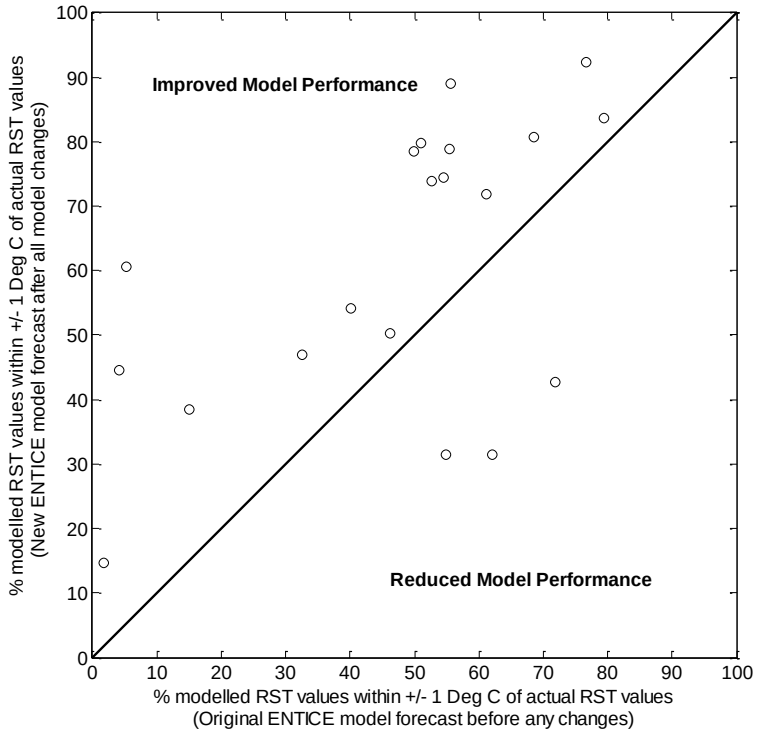

Figure 5.2 Comparison of *ENTICE* model accuracy in predicting RST to within ± 1°C of actual values. X-axis values relate to model runs before any changes were made to the *ENTICE* model, and y-axis values relate to model runs which incorporate the re-parameterised surface roughness and road construction measurements.

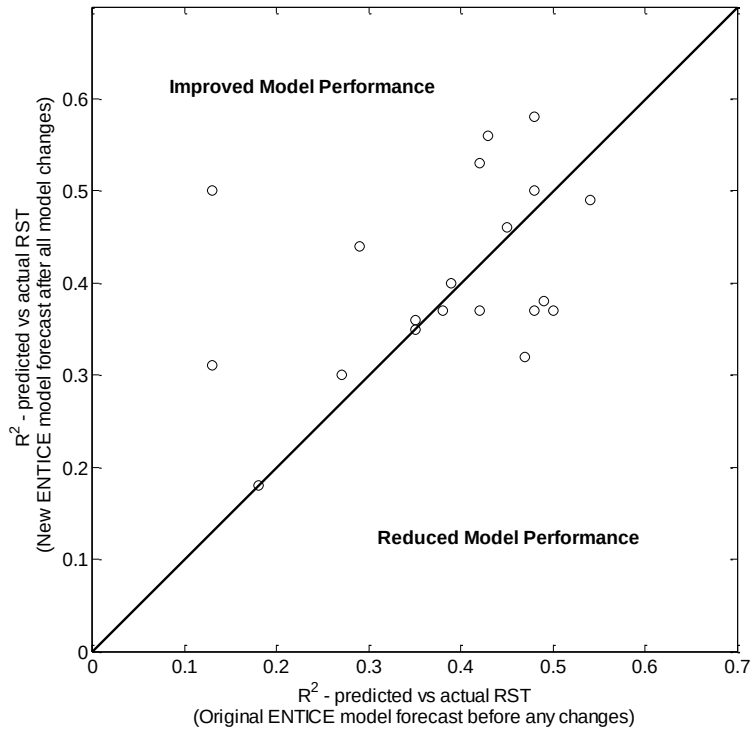

Figure 5.3 R^2 values for *ENTICE* predicted RST vs. actual RST collected from thermal mapping runs. X-axis values relate to model runs before any changes were made to the *ENTICE* model, and y-axis values relate to model runs which incorporate the re-parameterised surface roughness and road construction measurements.

5.2 K-means Clustering of the New *ENTICE* GPD

Statistical comparison of the hierarchical and K-means clustering solutions in Chapter 2 revealed that the two clustering solutions obtained for the Birmingham study route were statistically very similar, but preference can be given to the K-means clustering solution due to the iterative nature of K-means clustering which allows the convergence to an optimum clustering solution. In contrast, hierarchical clustering is more prone to errors since the grouping of objects within a dendrogram is irreversible, meaning any weak groupings which K-means would automatically reclassify during the iterative process will propagate through the dendrogram and always be present within the hierarchical clustering solution. Hence, to test the integrity of the new re-parameterised surface roughness and road construction measurements, validation of the *ENTICE* route-based forecast over the same 20 thermal assessments used throughout this study was undertaken using the K-means clustering

technique described in Chapter 2. As with the original analysis in Chapter 2, the *ENTICE* model was run in 'quasi-operational' mode with all the parameters within the model set to their best values, and the standard K-means clustering algorithm available within SPSS 16.0 for Windows® was used with the dataset again partitioned into 12 clusters based on Equation 2.4. Given that the Z_0^{eff} values at each forecast point vary temporally based on the forecast wind direction, the Z_0^{eff} values associated with a westerly wind direction, which was the most dominant wind direction over the 20 nights, were used in the clustering analysis to enable comparison with the original K-means clustering solution.

Figure 5.4 displays a map of the new K-means clustering solution for the Birmingham study route, together with a summary GPD showing the mean values of the geographical and road infrastructure parameters within each cluster. Comparison of this new clustering solution with the original K-means solution in Chapter 2 (Figure 2.6 (b)) reveals similarities within some of the clusters. For example, clusters 5 and 6 in the new clustering solution (Figure 5.4) are representative of forecast points located under bridges or underpasses, as indicated by the low ψ_s values within these clusters, and they account for exactly the same forecast points as clusters 3 and 7 in the original K-means clustering solution (Figure 2.6 (b)). Within these clusters ψ_s is the most dominant parameter, so we would expect to see similarities in these clusters given that the ψ_s measurement is the same in both clustering solutions. As with the original K-means clustering solution (Figure 2.4 (b)) there is a lack of any single dominant cluster, but the re-parameterisation of surface roughness and road construction within the *ENTICE* model appears to have created subtle differences between the original and the new K-means clustering solutions.

Cluster	ψ_s	*Altitude*	*Slope*	*Sin Aspect*	*Cos Aspect*	Z_0^{eff}	*Conductivity*
1	0.92	155	1.69	-0.23	0.72	21.79	0.00362
2	0.68	130	1.65	0.53	-0.13	87.49	0.00365
3	0.91	211	4.81	0.12	-0.08	20.38	0.00355
4	0.51	228	5.88	-0.87	-0.49	80.00	0.00400
5	0.13	148	1.96	0.77	-0.48	63.48	0.00380
6	0.17	192	2.18	-0.77	0.48	17.50	0.00349
7	0.87	129	1.81	0.81	-0.30	36.77	0.00378
8	0.94	192	2.14	0.86	-0.25	22.92	0.00374
9	0.94	192	4.45	-0.57	0.22	20.31	0.00402
10	0.90	164	1.48	0.34	0.76	25.57	0.00394
11	0.92	177	1.97	-0.19	-0.85	20.16	0.00376
12	0.93	217	3.03	-0.84	-0.28	88.00	0.00375

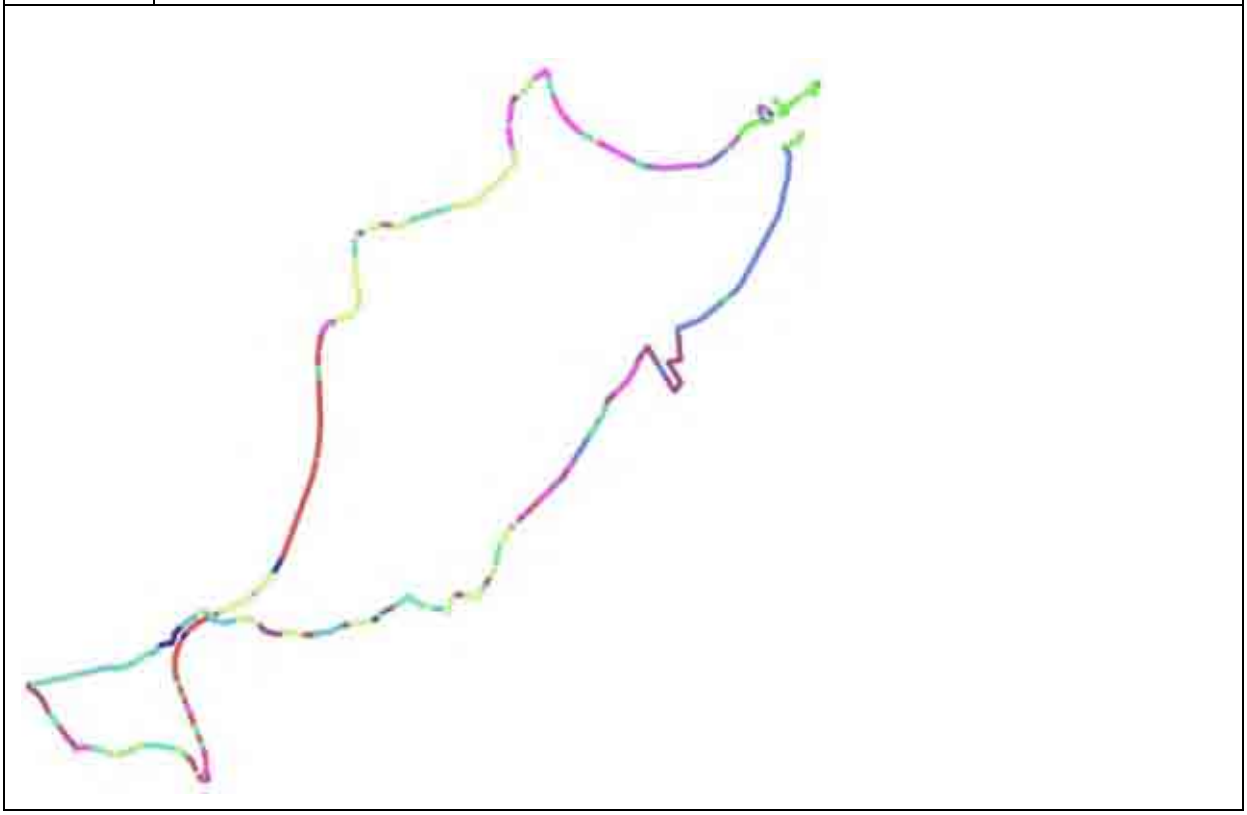

Figure 5.4 A map of the new K-means clustering solution for the Birmingham study route, together with a summary GPD showing the mean values within each cluster.

A comparison of cluster 3 in the new K-means solution (Figure 5.4) with cluster 2 in the original K-means clustering (Figure 2.6 (b)) reveals how both of these clusters represent forecast points located at higher altitude, higher gradient rural parts of the study route where the road construction appears to be shallower. This is indicated by the lower average road thermal conductivity and Z_0^{eff} values and the higher altitude and slope values within these clusters. In both cases these clusters account for only a small proportion of the overall study route. However, a reduction from 6% in the original clustering solution to 5.3% in the new K-means solution provides an indication of the fine-tuning of clusters, which is evidenced by a substantial increase in optimisation iterations during clustering, increasing from 16 iterations in the original K-means clustering to 26 iterations in the new clustering solution in order to reach the optimum solution. Hence, having replaced the existing ordinal road type and land use data in *ENTICE* with new higher resolution continuous datasets derived from LIDAR and GPR data, clusters of forecast points have been refined to account for greater variations in surface roughness and road construction which are now accounted for in the *ENTICE* GPD.

Table 5.1 displays the standard set of route-based forecast validation statistics calculated for each of the new K-means clusters, based on the same 20 thermal assessments of the study route used throughout this study. Analysis of the overall entire route statistics has already revealed a significant improvement in the overall forecasting ability of the *ENTICE* model as a result of the new re-parameterised surface roughness and road construction measurements within the model (Figure 5.1 to Figure 5.3). However, analysing the statistics in Table 5.1 at the cluster level reveals further information regarding model performance.

Table 5.1 *ENTICE* route-based forecast validation statistics for the Birmingham study route calculated for individual K-means clusters.

	β	σ_β	*RMSE*	*Pm*	*Prm*	Forecast Points
Entire Route	-0.49	0.89	1.20	60.93	79.35	2261
Original	***-1.06***	***0.86***	***1.48***	***46.94***	***79.56***	***2261***
Cluster 1	-0.34	0.57	0.93	70.18	92.52	305
Cluster 2	-1.63	0.77	1.84	27.54	84.03	211
Cluster 3	-0.53	0.85	1.19	61.46	87.54	120
Cluster 4	-0.11	0.00	0.57	95.00	100.00	1
Cluster 5	-0.95	1.60	1.99	33.70	48.48	23
Cluster 6	-2.70	1.42	2.96	20.00	55.00	2
Cluster 7	-0.86	0.69	1.30	52.00	86.61	310
Cluster 8	-0.31	0.62	0.95	68.51	92.19	404
Cluster 9	0.31	0.56	0.88	72.81	91.86	196
Cluster 10	-0.29	0.94	1.19	61.96	77.79	332
Cluster 11	-0.37	0.65	0.97	66.32	87.82	307
Cluster 12	-0.55	0.56	0.99	65.30	92.60	50

In 75% of the clusters in Table 5.1, the SD values are lower than the overall route statistic, indicating that thermal variations are well represented by the new clustering solution. Eight clusters in the new K-means clustering solution have *RMSE* values lower than the overall route statistic, which together account for 75.9% of the entire study route. This compares to seven clusters and 69.5% of the study route in the original K-means clustering solution, indicating that the overall magnitude of errors around the study route has decreased as a result of the new re-parameterised surface roughness and road construction measurements in the *ENTICE* model. The clusters also reveal a large improvement in the overall spatial forecasting ability of the model, with 75.9% of the entire study route (8 clusters) having a higher *Pm* value than the overall route statistic of 60.93%. This represents an increase of 23.8% from the

original K-means clustering solution where a little over half of the study route (52.1%) showed better spatial forecasting performance than the overall route statistic would otherwise indicate. Analysis of the overall *Prm* values reveals little change from the original K-means clustering solution, with the residual statistics in 9 out of the 12 clusters, which accounts for 84.2% of entire study route, significantly better than the entire route statistic of 79.35%.

The statistics in Table 5.1 also reveal areas where model performance needs to be improved. The poorest performing clusters are clusters 2, 5 and 6. As previously mentioned, clusters 5 and 6 are representative of forecast points located under bridges or underpasses, locations which the *ENTICE* model is known to be less accurate in forecasting for due to the lack of any advective component in the zero-dimensional heat balance model which *ENTICE* uses. From Figure 5.4 it can be seen that cluster 2 is representative of forecast points located mainly in the city centre where ψ_s values are much lower, mainly due to the presence of tall buildings in the city centre, and Z_0^{eff} values are higher due to the increased drag imposed on the airflow by the rough terrain in the city centre. This is comparable to cluster 9 in the original K-means clustering solution (Table 2.4 (b) & Figure 2.6 (b)), where on average less than 10% of modelled RST values were within ± 1°C of the actual values. With the new clustering solution this has improved to over 27%, but it is still well below the entire route average. The large negative bias of -1.63°C within this cluster suggests that the *ENTICE* model is failing to fully account for the typical 'urban heat island' effect which is common to city centres. Canyon geometry in city centres typically results in increased shading from solar radiation during the day but increased heat retention throughout the night by blocking the escape of long wave radiation from the surface and storing heat within the fabric of buildings. Also, levels of traffic are generally higher in city centres and provide a major source of anthropogenic heat (Smith et al. 2009) which further adds to this retention of heat in city centres. Whilst the *ENTICE* model attempts to account for such factors the cluster statistics in Table 5.1 reveal that further work is required with this aspect of model. Hence, validation of the *ENTICE*

route-based forecast model using clustering techniques has again been shown to provide a much more representative measure of the model's spatial forecasting ability. Without validation at the cluster level, a simple analysis of the entire route statistics would have failed to reveal these deficiencies in the model. Accordingly, validation at the cluster level should be seen as the new minimum standard with which to verify route-based forecast models.

5.3 Consistency of the New K-means Clustering Solution

To further test the integrity of the new re-parameterised surface roughness and road construction measurements in *ENTICE*, calculation of a new CSC dataset can be undertaken using the new forecast data obtained from the re-runs of the *ENTICE* model which incorporated the new Z_0^{eff} values and subsurface thermal profiles. An improvement in the CSC dataset for the same pairs of thermal mapping runs would indicate that the re-parameterised surface roughness and road construction measurements help the clusters to better capture the physical relation between measured RST around the study route and the geographical and road infrastructure parameters used to cluster the data. The CSC analysis was performed on the same pairs of thermal mapping runs as used in the original CSC analysis in Chapter 2 (Table 2.5), giving a total of 9 comparisons (3 damped, 3 intermediate and 3 extreme), the results of which are shown in Table 5.2.

Table 5.2 Clustering similarity coefficients (CSC) for independent pairs of thermal mapping runs in the same weather category, calculated using the new K-means clustered forecast points.

TM pairs	**No. of records**	**No. of clusters**	**CSC**
Damped (1,2)	2261	12	0.58
Damped (1,3)	2261	12	0.83
Damped (2,3)	2261	12	0.75
Intermediate (1,2)	2261	12	1.00
Intermediate (1,3)	2261	12	1.00
Intermediate (2,3)	2261	12	1.00
Extreme (1,2)	2261	12	1.00
Extreme (1,3)	2261	12	1.00
Extreme (2,3)	2261	12	1.00

Results of the new CSC analysis reveal that the coefficients vary from 0.58 to 1.00 with a mean over all weather categories of 0.91, which is the same as the mean coefficient value in the previous CSC analysis (Table 2.6 (b)). For individual weather categories, a decrease in the coefficient values under damped conditions occurs with the new clustering solution, but under highly stable atmospheric conditions (extreme) when the accuracy of road weather forecasts is most crucial, the coefficient values increase to a mean of 1.00 for the new K-means clustering solution compared to an original mean of 0.95 for the extreme comparisons with the original K-means clustering solution (Table 2.6 (b)). Hence, whilst the overall ability of the clusters in capturing the physical relation between RST around the study route and the geographical and road infrastructure parameters used to cluster the data has remained the same, on the extreme nights when road weather forecasts need to be most accurate and factors such as road construction and surface roughness have a greater influence on RST (Chapman et al. 2001b), the refined clusters have been shown to better capture this relationship.

CHAPTER FIVE SUMMARY

Spatial validation of the ENTICE model has been undertaken using the new cluster based validation technique proposed in Chapter 2. Statistical analysis of model performance using entire route statistics has revealed an overall reduction in model error and a significant increase in the overall spatial forecasting ability of the model. Integration of the new re-parameterised road construction and surface roughness measurements into the ENTICE model has led to subtle changes in the clustering solution for the study route and an increase in optimisation iterations for the K-means clustering solution, which is symptomatic of cluster refinement. On extreme nights when the accuracy of road weather forecasts is most crucial, the refined clustering solution is shown to better capture the physical relation between RST and the geographical and infrastructure parameters around the study route.

The new re-parameterised road construction and surface roughness measurements proposed in this thesis have therefore passed the integrity test, but the cluster level statistics presented in this chapter reveal further scope for improvement with the ENTICE model, particularly in city centre locations where anthropogenic heat emissions are most prevalent. Vehicle emissions provide a major source of anthropogenic heat in urban areas, but the ability to parameterise the effects of traffic on the spatial variation of RST has continually proven to be problematic in route-based forecasts. This will be considered in the following chapter where a critique of the analysis techniques used in this thesis is provided along with suggestions for future research within this field.

6. CRITIQUE AND SUGGESTED IMPROVEMENTS

This thesis has started to address some of the issues relating to the validation and parameterisation of route-based forecast models, using the *ENTICE* route-based forecast model as a case study. The spatial component of route-based forecast models such as *ENTICE* has significantly increased the resolution of RST forecasts to the microclimatic level, but such fine scale modelling of some of the geographical and road infrastructure parameters used to drive the *ENTICE* model (Table 2.2) can be challenging. The work presented in Chapters 3 and 4 of this thesis has shown that progress is being made on this front, with basic ordinal land use and road type parameterisations in the *ENTICE* GPD being replaced by much higher resolution surface roughness and road construction measurements derived from LIDAR and GPR data respectively. Whilst the validation statistics presented in this thesis have shown significant improvements in model performance with the new re-parameterised surface roughness and road construction measurements, they have also revealed that the *ENTICE* model is by no means perfect, and that further improvements can be made. At each stage of the research problems have been highlighted, and this chapter presents a summary of how this project could be improved and makes recommendations for future research within this field.

6.1 Critique of Techniques

6.1.1 GPR road construction data

The integrity of the new re-parameterised road construction measurements presented in this thesis ultimately depends upon the quality of the GPR data. In hindsight the use of a 250 MHz antenna would have provided greater depth penetration than was achieved with a 500 MHz antenna, and may have prevented the need to manually parameterise the bottom two layers of the subsurface profile. The true quality of GPR data can only be fully assessed through road core samples, but such an exercise is impractical at this scale so an alternative methodology is

required. As a starting point, a comparison of the same route using several radars from different manufacturers would provide a good indication of data quality, but a shortage of financial resources proved to be the main obstacle preventing such an analysis from being undertaken. Indeed, the costs associated with obtaining GPR surveys are still relatively high, but it is envisaged that these costs will come down over time and GPR data will become more widely available.

Whilst the integration of GPR data into route-based forecasts provides an opportunity to revolutionise the modelling of road construction in surface energy balance models, the whole methodology of having to drive a route in order to obtain a subsurface GPR dataset could be seen as a backwards step for route-based forecasting. Current advancements in shading and sky view estimation using a fully GIS-based approach (Gal et al. 2007; Gal et al. 2009; Brown et al. 2008a) suggest that route-based forecasting is rapidly moving towards a complete desktop surveying solution, where forecast providers would no longer have to rely on mobile surveying techniques to obtain the geographical and infrastructure data required for the spatial component of a route-based model. An ideal scenario would see local authorities become responsible by law for maintaining an up to date GPR database for their road network, with this data made freely accessible to forecasting agencies as and when needed for parameterising road construction in route-based forecast models. Indeed, some local authorities (e.g. Neath Port Talbot) already hold GPR datasets for parts of their road network (B Williams 2009, pers. comm., 3 Feb), which suggests that local authorities would be more able to absorb the costs associated with this than a forecasting agency, and the data provided would be useful for other applications beyond road weather forecasting such as structural capacity estimation of roads and bridges to identify the remaining serviceable life of these structures. Many roads nowadays can go for up to 10 years between resurfacing cycles, so it is envisaged that a 5 year maximum update cycle for GPR surveys would be sufficient to ensure

most changes are documented within a reasonable time frame. Of course, the more frequent this update cycle, the more accurate a GPR database will ultimately be.

The inflexion point algorithm used in this thesis (Appendix 2) to detect subsurface layer interfaces in the electromagnetic waveform of the raw GPR traces relies on the basic assumption that any inflexion in the waveform above a predefined amplitude is a subsurface layer interface. Whilst for the majority of GPR traces this is the case, the algorithm fails to account for potential anomalies in the electromagnetic waveform which can be caused by objects such as utility pipes or drainage covers. By calculating an EWMA for the GPR dataset, the effects of any such anomalies are minimised to some extent, but further research aimed at improving the existing algorithm (or developing an new algorithm) to enable such anomalies to be rapidly identified would be a valuable addition to this research.

6.1.2 LIDAR based Z_0^{eff} values

The calculation of Z_0^{eff} values using the methodology outlined in Chapter 4 has been shown to increase the overall variability of RST accounted for in the *ENTICE* model by 6%, but the methodology presented has a number of limitations. Whilst the inclusion of wind direction in the estimation of Z_0^{eff} values is a major step forward for the *ENTICE* model, the technique fails to take into account wind speed. Ultimately this is a result of the real-time nature of the forecast, which relies on the model having a pre-defined look-up table of Z_0^{eff} values for each forecast point. A potential improvement could involve the weighting of all LIDAR grid cells for each forecast point, based on the distance of the cell from a given forecast point and the forecast wind speed. Indeed, this highlights a further limitation of the proposed height based technique, since in its current guise the technique assumes that every LIDAR grid cell within the upwind fetch of a forecast point is an equal contributor to the surface roughness at the forecast point. Equally, the technique only accounts for a constant direction of flow which is normal to the face of the forecast point, whereas in reality wind direction (and speed) is ever

changing and, even if a street pattern is relatively regular, the size and shape of individual roughness elements such as buildings and trees are not regular (Grimmond & Oke 1999). Ultimately it is envisaged that the proposed technique could be further developed to allow for a variable distance of upwind fetch at every forecast point, based not only on obstacle height and wind speed but also on the active surface area presented to the oncoming flow such as the frontal area index (Grimmond & Oke 1999) of the surface elements within the upwind fetch, which could be approximated from LIDAR data.

The cost of LIDAR data has fallen recently to the extent that high resolution height data is available to the academic community for as little as £1 per square kilometre through commercial enterprises such as Bluesky International Limited (http://www.bluesky-world.com/), although the costs to commercial companies are usually considerably higher. Whether this proves to be an obstacle to the widespread use of LIDAR data in road weather modelling remains to be seen, but recent work undertaken in Denmark to estimate shadowing effects on RST using a high resolution LIDAR dataset known as the Danish Height Model (Pedersen et al. 2010) is encouraging.

6.2 Traffic Parameterisation

Whilst this thesis has so far concentrated on improving the parameterisation of surface roughness and road construction in the *ENTICE* model, traffic is a further parameter which is currently not fully accounted for in the model. The re-parameterisation of road construction and surface roughness in the *ENTICE* model means that the original road type and land use parameterisations are no longer a requirement, and since the existing *ENTICE* traffic parameterisation relies on these ordinal classifications (see section 6.2.2 for further details), a new methodology for parameterising traffic is required. Modelling the effects of traffic on the spatial variation of RST, however, has proven to be problematic in route-based forecasts, largely due to the lack of detailed information regarding the spatial variation of traffic density with time. Traffic information has traditionally been collected using inductive-loop detectors embedded in the road or with video cameras. These fixed installations fail to provide any traffic information beyond their installed locations, and their coverage is usually confined to congestion-sensitive motorways and a limited number of tunnels, bridges and intersections (Kristiansen et al. 2003).

6.2.1 Impacts of traffic on RST

Various studies have been undertaken over the past 25 years to assess the impact of traffic on RST, and this impact is now reasonably well quantified and understood. Prusa et al. (2002) identified several ways in which vehicles can modify RST, and these can be generally grouped into three main categories; Heating, Shading and Motion. Heat can be added to the road surface from the engine and exhaust via sensible heat and moisture fluxes (Figure 6.1 (a)) as well as frictional heat dissipation from the tyres (Figure 6.1 (b)) and braking. Vehicles also have a dominant shading effect, blocking long-wave radiation exchange and preventing incoming short-wave radiation from reaching the road surface during the daytime. The motion of vehicles also generates eddies that cause mixing of the air above the road surface, leading

to increased turbulent flow above the surface instead of the normal ambient airflow. As previous studies have shown (Parmenter & Thornes 1986; Shao 1990; Gustavsson et al. 2001; Chapman & Thornes 2005; Chapman & Thornes 2008), the general cumulative effect of these impacts is to promote increased RST in the order of 1-2°C in more heavily trafficked areas.

Figure 6.1 (a) Differential drying on the E4 highway north of Gävle, Sweden (approximately 60.5°N), showing how heat fluxes from traffic dry the road surface on the heavily trafficked inside lane, and (b) thermal image of the southbound M5 carriageway where frictional heat dissipation from tyre tracks is clearly evident (Chapman & Thornes 2008).

6.2.2 Existing traffic parameterisation in the *ENTICE* model

Whilst the impact of traffic on RST is well quantified, the ability to model this impact in a route-based forecast model remains problematic. Traffic parameterisation in the *ENTICE* model currently consists of a basic traffic algorithm that considers atmospheric stability along with the road type and land use classifications. The algorithm operates in an ordinal fashion whereby the effects of traffic on RST are replicated at every forecast point which satisfies a particular set of ordinal criteria, much like the original *ENTICE* land use and road type parameterisations. Specifically, to account for differential heating of the road surface caused by the input of anthropogenic heat emissions from vehicles, *ENTICE* applies a slight bias to the forecast RST which is dependent on the ordinal land use and road type classifications in the model. This bias assumes that city centres and motorways are the most heavily trafficked sections of road, after which there is an exponential decrease in bias through urban, suburban

and rural areas. To further account for the shadowing effect of vehicles which reduces long-wave radiation loss from a road surface, *ENTICE* incorporates a shadow coefficient for outgoing radiation into the model radiation budget which is dependent on the land use classification. Finally, *ENTICE* attempts to account for the increased turbulence caused by vehicles by simply increasing wind speed in the energy balance by 2 ms^{-1}.

6.2.3 Potential alternative modelling techniques

Whilst the existing *ENTICE* traffic parameterisation makes a basic attempt to model the effects of traffic on the spatial variation of RST, it ultimately lacks the sophistication shown by other aspects of the model. Traffic parameterisation could potentially be improved by disaggregating Annual Average Daily Traffic (AADT) count data to assign traffic flows for a range of vehicle classes to individual roads, and then calculating vehicular heat emissions using the method proposed by Smith et al. (2009) to calculate the quantity of waste heat from vehicles (Q_{FV}):

$$Q_{FV} = \frac{\sum(n_{mri}(t)L_{ri})EF_{mr}}{A_i}(Wm^{-2}) \quad (6.1)$$

where n_{mri} is equal to the number of vehicles of type m on road r in area i, t is the hour of day, L_{ri} is the length of road r in area i, EF_{mr} is a speed-dependent fuel consumption emission factor and A_i is the source area. To determine the temporal and spatial patterns of anthropogenic heat fluxes in UK urban areas, Smith et al. (2009) modelled the major sources of waste heat in the urban environment, namely buildings, vehicular and human metabolic heat emissions, and found that road traffic accounted for around 32% of the total anthropogenic heat emissions across a city. The study also found that the diurnal patterns of anthropogenic heat flux matched the movement of people, with heat emissions highest in residential areas during the early morning, then becoming more concentrated in the city centre by midday and more homogenous during the evening as people return to residential areas.

Such an analysis could potentially enable more accurate location specific bias weightings to be applied to forecast surface temperatures in *ENTICE* to better quantify the differential heating of the road surface caused by vehicular emissions. As Equation 6.1 reveals, however, a range of data are required in order to calculate heat emissions from traffic using this methodology, some of which are not freely available outside of the academic community. Equally, the availability of some of this data for certain areas will be limited, such as traffic flow data for minor roads which Smith et al. (2009) were required to estimate.

Clearly one of the biggest issues concerning traffic parameterisation in route-based forecasts is the availability of traffic density data over an entire route. Traffic count data at the full spatial resolution of the *ENTICE* model simply does not exist, and whilst data could be extrapolated from the sparse network of inductive-loop detectors, acquiring this data is often a complex and prohibitively expensive task. An alternative approach could be to create a spatiotemporal network model of traffic flow in *ENTICE* from the spatial characteristics and the topology of the road network, using a similar method to that proposed by Demiryurek et al. (2009). In a recent study in Los Angeles, California, Demiryurek et al. (2009) introduced a framework for realistic and accurate modelling of traffic flows around a road network based on the grouping of similar traffic flows into respective spatial characteristics. Firstly, a time-dependent travel time is computed for each road network segment using historical time-series sensor data, after which semantic information is attached to the road network by labelling regions of the network based on its geographical and topological characteristics. Finally, a hierarchical clustering algorithm (Figure 6.2) is used to group similar types of traffic flow into respective spatial characteristics, the idea being to find the most representative traffic flows in and between the network regions based on their spatial characteristics (Demiryurek et al. 2009).

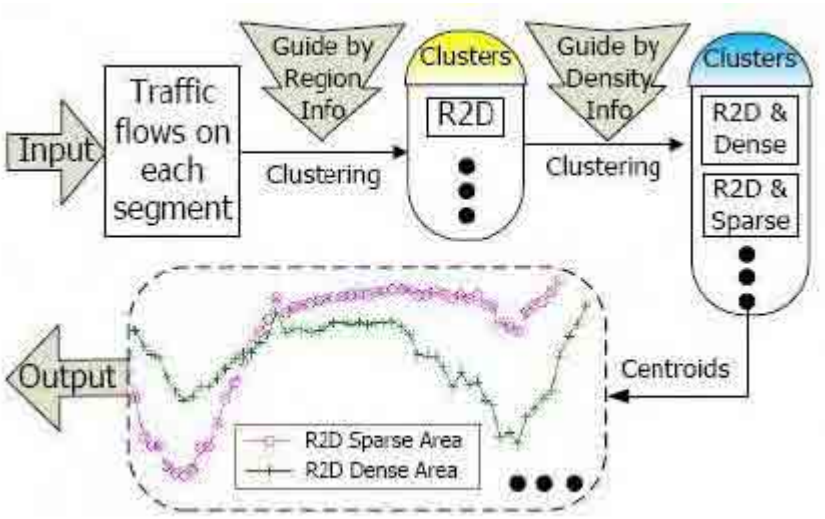

Figure 6.2 Hierarchical semantic clustering flowchart for the two spatial characteristics of region and density (Demiryurek et al. 2009).

Figure 6.2 depicts an example of the hierarchical clustering method for the two spatial characteristics of region and density, although other spatial characteristics, such as segment length, could easily be added to the system. The clustering method guides the clusters in multiple levels by considering a single type of characteristic at each level. Firstly, regional information is used to compute the initial traffic flow clusters, then density information is used to further define the traffic clusters, creating a traffic flow output corresponding to each spatial characteristic. Assuming that the traffic pattern obtained from the study site is typical and generic, such a framework can then be used to generate traffic flow information for any given road network that has no temporal traffic data but has similar spatial characteristics (Demiryurek et al. 2009). It is envisaged that this type of traffic flow modelling could be incorporated into a route-based forecast model such as *ENTICE*, using the existing geographical parameters stored for each forecast point in order to spatially characterise traffic flow data around the route. However, such a methodology requires some initial traffic data from various locations around a route in order to determine the time-dependent travel-time along different segments of the route. Loop detectors provide a possible source of data, but as

previously mentioned the coverage of such devices is usually confined to motorways or major A-roads, with little if any coverage of more minor roads.

6.2.4 Pilot study – traffic counting with infrared RST sensor

Whilst it is clear that traffic count data at the same spatial resolution as the *ENTICE* model is both unfeasible and unnecessary, greater information on the spatial variation of traffic density around a route is still a necessity in order to improve traffic parameterisations in route-based forecast models. One potential source of additional traffic count data is low cost infrared RST sensors that are increasingly being installed around the road network to fill in the gaps between existing road outstations. Remote infrared RST sensors such as the IRIS sensor (Figure 2.1) manufactured by Campbell Scientific contain traffic filtering algorithms designed to smooth data and remove erroneous measurements from passing vehicles, but their use as a traffic counting device has yet to be studied. Hence, a small pilot study has been undertaken to investigate the effectiveness of IRIS sensors as a source of traffic count data.

Figure 6.3 IRIS sensor monitoring traffic flow at the site of an active loop detector as part of a pilot study into traffic parameterisation in route-based forecast models.

The pilot study involved installing an IRIS unit at the same location as an active loop detector (Figure 6.3), leaving both sensors running for a period of 2 months, and then collecting and statistically analysing the data from both sensors to determine the correlation between measurements. The site selected for the study was the A4067 near Pontardawe in South Wales, a typical single lane A-road for which free access to loop detector data was available through Network Management at Neath Port Talbot County Borough Council. The IRIS system was programmed to automatically send data to Campbell Scientific's central data bureau at 20 minute intervals using remote GPRS communications. The standard IRIS datalogger program was modified in LoggerNet using CRBasic, with additional lines of code added to create incremental traffic count variables which recorded 10 minute traffic count values based on the number of times the thermal infrared signal exceeded pre-defined threshold values (Appendix 3).

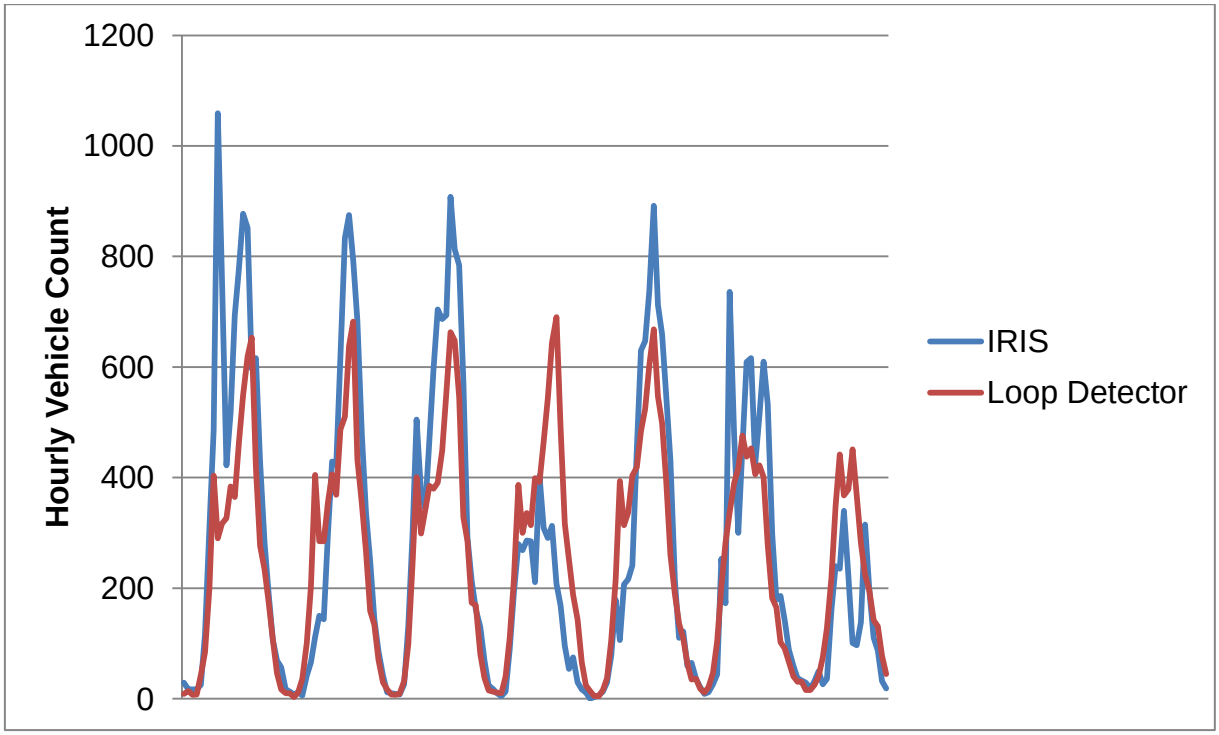

Figure 6.4 Hourly vehicle count data over 7 days (Mon 28/06/10 – Sun 04/07/10) from an IRIS infrared RST sensor (blue line) compared against data collected from a loop detector at the same location (red line).

Vehicle count data for the 2 month period can be found in Appendix 4, and Figure 6.4 displays a plot of the data for the first week of the trial. 10 minute traffic count values from the IRIS system were totalled into hourly values to match the loop detector data, and the Pearson product-moment correlation coefficient between the two data sets was calculated, giving an overall R-value of 0.73 over the entire 2 month dataset. Visual analysis of the hourly vehicle counts reveals that the IRIS unit has a general tendency to over-estimate the vehicle count during periods of heavier traffic, most likely due to the sensor also seeing some influence from traffic in the opposite lane. Occasions where the IRIS unit considerably under-estimated the vehicle count, such as the fourth and seventh days in Figure 6.4, cannot be explained at present, but the data from this trail has been forwarded to Campbell Scientific where further analysis, modification and trials of the traffic counting algorithm are being undertaken.

To assess the consistency of the IRIS unit in estimating traffic flow during a 24 hour period, a basic traffic flow classification scale was devised whereby a vehicle count of 0-100 vehicles/hour represented a very low traffic flow, 101-250 represented low traffic flow, 251-500 vehicles represented moderate traffic flow, and anything above 501 vehicles represented heavy traffic flow. It is acknowledged that such a classification of traffic flow is very subjective, but for the purposes of this small pilot study such a classification will suffice. Five days traffic data was then selected at random and the traffic count value estimated by the IRIS unit for each hourly period was compared against the equivalent hourly value in the loop detector data, and a score of 1 was assigned to each hourly period where both values fell within the same traffic flow classification band (i.e. very low, low, moderate or heavy), otherwise a score of 0 was assigned. This methodology was repeated for all hourly values over the 5 days, and each day was then split into four 6-hourly periods (00:00-05:00, 06:00-11:00, 12:00-17:00, 18:00-23:00). The hourly scores within each 6 hour period were then compared against the equivalent hourly scores of the other days in pairs, and where the hourly

scores between two days matched, a = 1. If the next hourly scores in the 6 hour period also matched, $a = a + 1$, otherwise $b = b + 1$ if the hourly scores were different. Once the values of a and b were calculated for each 6-hourly period for every pair of days, traffic similarity coefficients (TSC) were calculated as follows:

$$TSC = \frac{a}{a+b} \tag{6.2}$$

The higher the value of TSC for a 6-hourly period between two days, the more consistent the IRIS unit is at estimating traffic flow (based on the traffic flow classification scale) during that 6 hour time period. Results of the TSC analysis for each of the 6-hourly periods are shown in Table 6.1. It can be seen from the table that during the early hours of the day (00:00-05:00) when the volume of traffic is generally very low, traffic count data from the IRIS sensor consistently falls within the same traffic flow classification scale as the data from the loop detector, with TSC values of 1.00 over all pairs during this 6 hour time period (Table 6.1). However, over the next 12 hour period (06:00-11:00 and 12:00-17:00) large variability is evident between the IRIS and the loop detector traffic flow classification, with TSC values over this period ranging from 0 (no similarity at all) to 0.67, with mean TSC over both 6-hourly periods of 0.47. Such values were not unexpected given the data in Figure 6.4, and are largely a result of the IRIS sensor over-estimating traffic flow during periods of heavier traffic. During the last 6 hours of the day (18:00-23:00) the IRIS sensor shows mixed performance, with TSC values ranging from 0.33 to 0.83 with an overall average of 0.60.

Table 6.1 Traffic similarity coefficients (TSC) for pairs of traffic count data in the same 6-hourly time period, calculated using traffic count data from a loop detector and estimates of traffic count from an IRIS sensor postioned at the same location as the loop detector.

Day pairs	**00:00-05:00**	**06:00-11:00**	**12:00-17:00**	**18:00-23:00**
(1,2)	1.00	0.67	0.67	0.50
(1,3)	1.00	0.67	0.67	0.83
(1,4)	1.00	0.83	0.67	0.50
(1,5)	1.00	0.17	0.33	0.83
(2,3)	1.00	0.33	0.67	0.67
(2,4)	1.00	0.50	0.33	0.67
(2,5)	1.00	0.17	0.33	0.33
(3,4)	1.00	0.50	0.33	0.67
(3,5)	1.00	0.50	0	0.67
(4,5)	1.00	0.33	0.67	0.33

This small pilot study has therefore revealed mixed performance for the IRIS sensor as a traffic counting device. The sensor is clearly not accurate enough to be used as a replacement for loop detectors to provide precise traffic count data, but the sensor was never designed for such a purpose. Data from the TSC analysis, however, has revealed that with further development and testing, there may be potential for such a device to provide a basic traffic flow classification parameter at various locations around a route.

6.2.5 Other potential sources of traffic density data

The transportation community is quickly moving toward the development of wireless vehicle capabilities whereby vehicles are able to communicate with other vehicles and the road infrastructure to improve safety and mobility (Drobot et al. 2010). The US Department of Transportation's IntelliDrive^{SM} program is a pioneering Vehicle Integrated Infrastructure (VII) initiative focussed on advancing connectivity among vehicles and roadway infrastructure in order to significantly improve the safety and mobility of the US transportation system. As part of the VII initiative, transportation agencies will have access to data needed to better manage traffic operations, support planning, and more efficiently manage maintenance services. The system architecture will allow real-time traffic information for the entire network, which could provide useful real-time traffic data for road weather forecast models, but whether such a system will ever be fully realised will depend on numerous technical issues being overcome. A major issue is the costs associated with installing the technology in vehicles and providing the necessary infrastructure at every road intersection. Furthermore, such a system would undoubtedly require updates and maintenance, and location data from the vehicles would need to the uploaded to weather forecasting agencies running the road weather models, the logistics of which still need to be overcome.

Recent IntelliDrive^{SM} funded research carried out by the National Centre for Atmospheric Research developed a prototype Vehicle Data Translator (VDT) for extracting, filtering, quality checking and then combining vehicle probed data into derived observations that are valid for a given length of roadway over a given time period (Drobot et al. 2010). The final function of the VDT is to disseminate the quality-checked and statistically processed data to organisations that collect, process and generate weather and transportation products. It is feasible that such a system could provide a means of disseminating real-time traffic density data to forecast providers alongside other vehicle probe data for ingesting into route-based

road weather models, where the spatial resolution of the data would be determined by the number of data polling stations along a route. In an ideal world these would be installed at every road intersection to provide true high resolution real-time traffic density data. All of the probed weather data from vehicles, however, would need to undergo complex and computationally intensive quality checking procedures, which along with the standard sensor and climatological range tests would require some form of model surface analysis to compare observed vehicular values to a range of grid values along a road segment or against a predetermined threshold of the grid value closest to the vehicle location (Drobot et al. 2010). Since the current resolution of atmospheric numerical models is in the region of several kilometres at best, the installation of data polling stations at a resolution any greater than this would be unnecessary from a quality control perspective. Hence, VII initiatives such as the IntelliDrive^{SM} program have the potential to provide accurate traffic density data to weather forecast organisations, but the resolution is unlikely to be any greater than what could be achieved with low cost thermal infrared sensors.

Satellite-based systems offer a potential alternative to terrestrial means for obtaining high resolution traffic density data for use in route-based road weather models. As well as providing coverage over large areas, including locations not covered by mobile communications (e.g. GMS, GPRS) which terrestrial systems are reliant upon, the use of a satellite-based system could be more economical provided the system design is optimised for the specific nature of the vehicular data (Kristiansen et al. 2003). To date satellite-based studies for road traffic monitoring have focused on a 'floating-car' system design, whereby a small percentage of the vehicle population generates real-time traffic information which is communicated to a central server for processing. Such a system was tested by the European Space Agency (ESA) in 2002 (Kristiansen et al. 2003) where in-car systems installed in the 'floater' vehicles read the vehicle's position every second using the GPS network. A map matching algorithm then uses the position data together with a digital road map to determine

the vehicle's speed and identify its road location, and based on knowledge of the expected speed on that road under non-congested conditions, any traffic congestion is automatically detected for each road segment and a message sent to the central server. On the server side, an application called the 'Communication Manager' interfaces with the satellite system and is able to remotely configure the in-car units, broadcast requests for tracer vehicles and receive traffic data from the vehicle fleet (Kristiansen et al. 2003). The system architecture used in the ESA trial is shown in Figure 6.5.

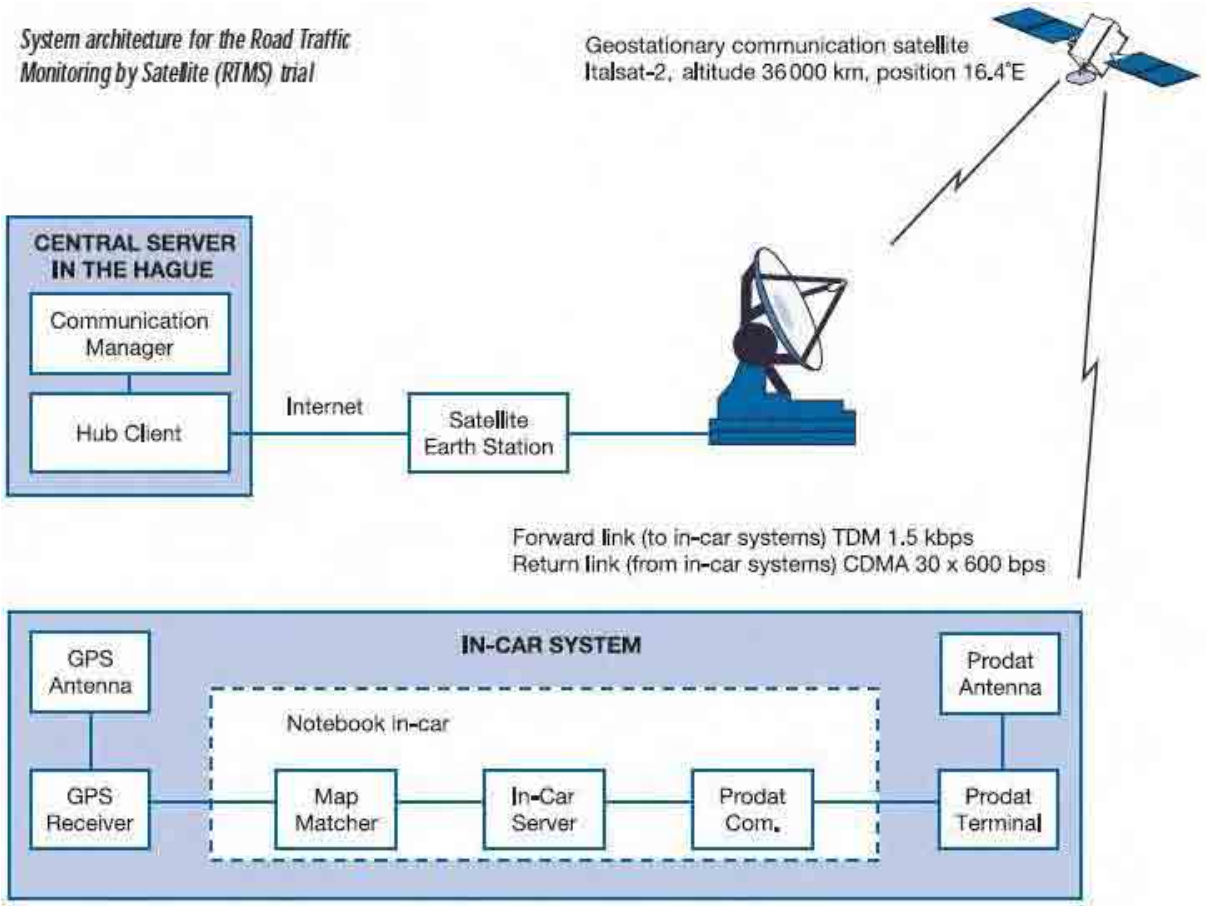

Figure 6.5 System architecture for the ESA Road Traffic Monitoring by Satellite (RTMS) trial (Kristiansen et al. 2003).

Such systems allow for the collection of traffic data across the wider road network, including both urban and rural roads, but true real-time traffic density data would require every vehicle on the road to act as a 'floating-car'. With the rapid increase in on-board satellite navigation units over the past few years, it is conceivable that the system architecture shown in Figure 6.5 could be modified to accept GPS data from these navigation units so that the in-car system is effectively removed altogether, with the GPS antenna and receiver built into the existing on-board navigation unit and all data processing undertaken on the server side. Further research would be required to investigate the feasibility of such a system. However, with every vehicle (or the vast majority at least) in the next decade likely to have some form of onboard GPS technology, either for satellite navigation, road pricing (Department for Transport 2004), or potentially to satisfy legislation related to initiatives such as the European Commissions in-vehicle emergency call (eCall) project (McClure & Graham 2006; Ostafe 2009), a satellite-based system perhaps offers greater potential than terrestrial means for providing true high resolution real-time traffic density data to help to parameterise the spatial variation in traffic for use in route-based road weather models.

The realisation of a satellite-based traffic monitoring system would undoubtedly provide useful data for any surface energy balance model used in road weather forecasting, not just *ENTICE*. The METRo model, for example, contains a mechanism to compensate for the increased turbulence caused by vehicles by setting a minimum value for the wind speed at different times of the day (Figure 6.6), but a lack of reliable traffic data often results in the minimum wind value being set to zero (Crevier & Delage 2001). However, the availability of high resolution traffic density data from a satellite-based monitoring system would enable the effects of anthropogenic contributions from vehicles on the spatial variation of RST to be modelled in much greater detail.

```
*     Subroutine   VENMIN: Impose the minimum winds specified by the WW
*                          variable. WW(1) is minimum wind for the day
*                          WW(2) is minimum wind for the night.
*                          FT is Forecast Time
*                          VA is wind speed (Vitesse Air)
*                          Default is currently 0.
*
*     Auteur / Author: Louis-Philippe Crevier
*     Date: Decembre 1999 / December 1999
***
      SUBROUTINE VENMIN ( WW, FT, VA )
      IMPLICIT NONE
***                  ***
*     DEFINITIONS     *
***                  ***
***
*     Input
*     -------
*     WW : Minimum winds for the day and the night (m/s)
*     FT : Forecast time
*     VA : Wind speed (m/s)
***
      DOUBLE PRECISION WW(2), FT
***
*     Input/Output
*     ---------------
***
      DOUBLE PRECISION VA
***
*
*     Procedure
*     =========
*     Specification of a minimum wind based on the time of the day
*     WARNING: UTC time. Based on East timezone
*     ------------------------------------------------
      if ( FT .gt. 12.5 .and. FT .lt. 25.5 .or.
     *     FT .gt. 36.5 .and. FT .lt. 50.0 ) then
         VA = max( WW(1), VA )
      else if ( FT .ge. 11.5 .and. FT .le. 12.5 ) then
         VA = max( WW(2)+(FT-11.5)*(WW(1)-WW(2)), VA )
      else if ( FT .ge. 25.5 .and. FT .le. 26.5 ) then
         VA = max( WW(1)+(FT-25.5)*(WW(2)-WW(1)), VA )
      else if ( FT .ge. 35.5 .and. FT .le. 36.5 ) then
         VA = max( WW(2)+(FT-35.5)*(WW(1)-WW(2)), VA )
      else
         VA = max( WW(2), VA )
      end if

      return
      end
```

Figure 6.6 Sample METRo model code for imposing a minimum wind speed at difference times of the day to account for increased turbulence caused by vehicles. Source – METRo repository http://gna.org/projects/metro/

6.3 A Blueprint for the Next Generation of Route-Based Forecasts

The origins of route-based forecasting can be traced back to a blueprint for 21st century road ice prediction proposed by Chapman (2002). This blueprint envisaged the synergy of GIS and GPS technologies accompanied by ψ_s analyses in developing a fully automated ice prediction system that would bring to an end the projection of RST by thermal maps. When the first generation of route-based road weather forecasts such as *ENTICE* were first introduced, they were the first real change in ice prediction systems in more than a decade and were long overdue. Slowly but surely over the past decade, local authorities have started to integrate route-based forecasting into their winter maintenance strategies, and as we enter the second decade of the 21st century route-based forecasting appears to have replaced traditional site specific forecasting as the norm for road weather forecasting in the UK. During this gradual period of acceptance for route-based forecasting, however, research within the road weather community had already shifted towards the next generation of route-based forecasts, and this thesis sits firmly within this wider body of research.

Whist the *ENTICE* route-based forecast model revolutionised the road weather industry by significantly increasing the spatial resolution of road weather forecasts to approximately 50 m, other forecast providers such as the UK Met Office have adopted a different approach where essentially forecasts are provided for a greater number of smaller routes, typically a kilometre or so in length (Figure 6.7), in what is commonly referred to as a stretch-wise route-based forecast (Brown et al. 2008a). These smaller routes could potentially be optimised and grouped with other routes according to different weather situations and geographical parameters around the road network, enabling validation of a stretch-wise route-based forecast along the lines of the cluster level validation proposed in this thesis for the *ENTICE* model.

Figure 6.7 UK Met Office route-based forecasting graphical user interface.

The high spatial resolution provided by the *ENTICE* model is in many ways excessive given that the resolution (grid-spacings) of the newest generation of high resolution NWP models used in road weather forecasting is still in the order of a few kilometres (Brown et al. 2008b), and also since some of the geographical and infrastructure parameters used in route-based models have not, up until now, been measured at the resolution demanded by *ENTICE*. Equally, there has for some time been a lingering question mark over how to verify such a high resolution route-based forecast. This thesis has attempted to address these issues, and in doing so the research has revealed that although the resolution of key geographical and infrastructure parameters has been aligned with the model forecast resolution and improved the overall spatial forecasting ability of the model as a result, validation of the model could ultimately be achieved at a lower resolution by sampling fewer forecast points from within each of the defined clusters. The danger in reducing forecast resolution to a few points in every cluster or to a stretch-wise approach, however, is that small scale thermal singularities

such as katabatic frost hollows and minor bridge decks could potentially be omitted from forecasts. Since the highway engineer has a duty of care to protect the motorist, it is essential that these small scale variations are accounted for in road weather models, leading some to suggest that 'worst case scenario' pessimistic forecasts may be a sensible approach for future route-based forecasts (Chapman & Thornes 2008). However, the integration of thermal mapping with a stretch-wise forecasting approach should help to identify such 'cold spots' around a road network, which could then be treated separately within the model. In the future it is anticipated that many of these thermal features will be identified using downscaling techniques on high resolution NWP models to obtain high resolution meteorological data along small stretches of a route (Brown et al. 2008a; Brown et al. 2008b). Combine this with a mobile infrared sensor such as IRIS positioned within each stretch-wise segment (or a cluster of road stretches should they be further optimised), and full spatial validation of the route-based forecast would be achievable without any need for thermal mapping surveys.

With the current advancements in shading and sky view estimation using a fully GIS-based approach (Gal et al. 2007; Brown et al. 2008a), route-based forecasting is rapidly moving towards a complete desktop surveying solution. However, local authorities are often not the most flexible of organisations, and the safety of the public must always remain the top priority even during the present challenging economic climate, so until these new desktop surveying technologies have been thoroughly tested and proven to bring financial savings without compromising safety, mobile surveying techniques will continue to be used in route-based forecasting.

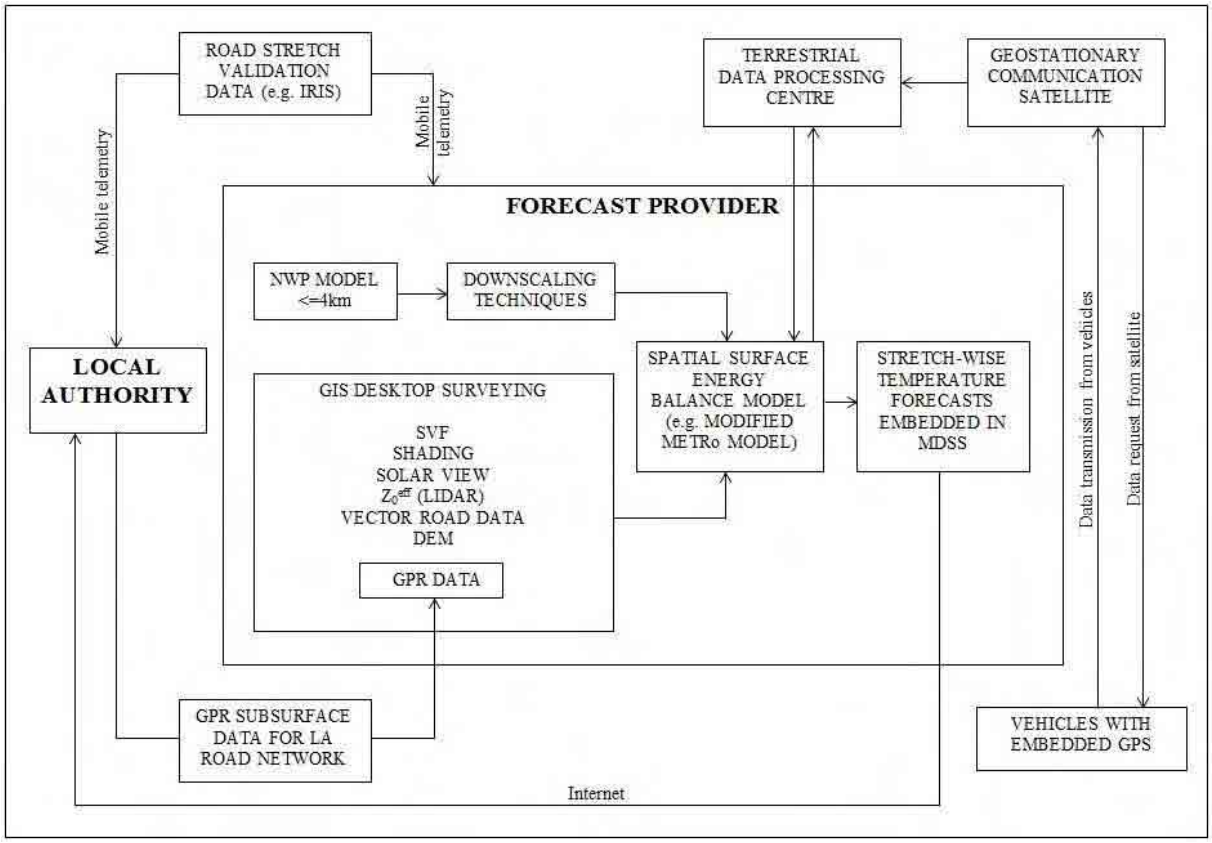

Figure 6.8 Schematic of the proposed next generation route-based forecasting system.

Figure 6.8 shows the synergy of the individual components discussed in this thesis in providing the next generation of route-based road weather forecasts. Forecast providers are likely to use high resolution NWP models with grid spacings of a few kilometres or less which will be downscaled using a variety of new modelling techniques such as high resolution valley parameterisation and lapse rate height based corrections (Brown et al. 2008a). These will allow more accurate prediction of topographic effects such as cold air pooling and fog formation in valleys and enable better prediction of showers and convective storms, and increased vertical resolution will improve the prediction of thin stratocumulus clouds which in turn should lead to better near-surface temperature predictions (Brown et al. 2008b). Hence, downscaling techniques will create a high resolution meteorological dataset for each individual stretch-wise segment of a route (typically 1 km in length), which will be used to drive a surface energy balance model to predict RST and road state using a stretch-

wise approach. The spatial aspect of the route-based forecast is likely to be fully derived from GIS-based desktop surveying techniques, with the addition of GPR subsurface data obtained from local authority managed GPR databases. Satellite tracking of vehicle locations could provide real-time traffic density data which forecast providers would be able to call upon in order to more accurately parameterise the effects of traffic on the spatial variation of RST around routes. Finally, strategic placing of a number of remote infrared RST sensors based on the grouping of similar stretch-wise segments of roads using clustering techniques would enable validation of the route-based forecast at a vastly improved spatial and temporal resolution, eliminating the need for thermal mapping surveys.

Whilst numerous energy balance models are in existence, there has been a recent trend towards the use of the METRo model which is now used throughout North America and is becoming increasingly prevalent around Europe. The embedding of a route-based METRo model into the MDSS framework (Chapter 1) would in many ways be the ideal solution in the wider research context, given the popularity and widespread use of the METRo model which has resulted in an abundance of knowledge and resources available to further test and develop the model. Indeed, it is hoped that the findings of this research will provide the foundations from which to start the development of a high resolution spatial component for the METRo model.

In summary, the entire methodology of route-based forecasting is gradually changing as new technologies emerge, and the transition towards a complete desktop surveying solution has begun. Whilst the *ENTICE* model has been used as a case study, this model is no longer in wide-scale commercial use, and the findings of this research will be of most benefit to the development of a spatial component in the METRo model, which it is envisaged will become the standard surface energy balance model for road weather forecasting over the next 10 years. The synergy of the various components shown in Figure 6.8 would need to be fully tested before being phased in, as safety is of paramount importance in road weather

forecasting. Hence, the days of mobile surveying are not over just yet, but with further time and effort the next generation of route-based road weather forecasts should soon emerge.

CHAPTER SIX SUMMARY

A number of refinements to the new re-parameterised road construction and surface roughness measurement techniques have been discussed which it is suggested could further improve the overall spatial forecasting ability of the ENTICE route-based forecast model. An evaluation of the current technology available for parameterising traffic in route-based forecast models has indicated that a satellite-based system perhaps offers the greatest potential for providing high resolution traffic density data, but further work is required before such a system can be realised. Particular attention has been drawn to the spatial resolution of route-based forecasts given the current limitations of NWP models at resolutions higher than 4 km. However, advancements in model downscaling techniques suggest that a resolution in the order of 1 km, which equates to a stretch-wise forecasting approach, will provide an appropriate balance between the spatial accuracy demands of winter maintenance operations and the capabilities of NWP models in providing high resolution meteorological data for individual stretches of road. The synergy of all these components is presented as a blueprint for the future of route-based road weather forecasts.

7. CONCLUSIONS

When route-based forecasting was first introduced nearly a decade ago, it was in some ways ahead of its time since some of the geographical and infrastructure parameters used to drive the spatial component of a route-based model had never been measured at the spatial scale demanded by a route-based forecast. Similarly, the increased spatial resolution provided by route-based forecasts has resulted in validation techniques which for many years served as a benchmark for road weather models suddenly becoming wholly inadequate tools for model validation. This thesis has aimed to address these issues by developing the foundations for a new validation strategy for route-based forecasts that enables validation at a much higher spatial and temporal resolution than is currently possible, and by de-parameterising key geographical and infrastructure parameters within the *ENTICE* model to the spatial scale demanded by a route-based forecast. This has been achieved by fulfilling the following objectives outlined in Chapter 1.

1. To critically review existing road weather validation techniques as tools for verifying route-based road weather forecasts.

The increased resolution of route-based road weather forecasts requires validation at a whole new spatial scale in order to fully account for the variations in geographical and road infrastructure parameters which influence thermal variations around a route. A review of existing validation techniques has shown that, due to the vast number of forecast points that need to be validated, no single technique was capable of achieving validation at anywhere near the full spatial and temporal resolution of a route-based forecast. Hence, this highlighted the need for a new validation methodology which could be used to provide a rapid appraisal of model performance. Due to the large quantity of data involved data reduction techniques provided a suitable starting point.

2. From the outcome of (1), devise a new methodology to facilitate validation of the ENTICE model at a spatial scale previously unseen with route-based forecasts.

This objective was the key milestone of this research. It was essential to develop a technique that allowed validation at a much higher spatial and temporal resolution than current methodologies allow. The proposed clustering technique has been shown to provide a more representative measure of the model's spatial forecasting ability by segregating the validation of routes into what are essentially high resolution climate zones, within which the geographical and road infrastructure parameters have a greater influence on RST than the meteorological parameters. The technique has been proven to repeatedly capture the spatial distribution of temperature around a salting route, and hence the physical relation between measured RST and the geographical and road infrastructure parameters controlling the clustering. The methodology proposed could equally be used to optimise and verify stretch-wise route-based forecasts, and has the potential to vastly improve the spatial and temporal validation of route-based forecasts when used in conjunction with low cost infrared RST sensors or similar measurement systems. Indeed, it is recommended that a low cost infrared sensor be installed within each defined 'geo-cluster' as a starting point for improving the spatial and temporal validation of route-based forecasts.

3. Investigate new techniques to remove geographical and infrastructure parameterisations in the ENTICE model, namely:

i. Road construction re-parameterisation through the use of Ground Penetrating Radar technology.

By surveying the subsurface road construction around a route using GPR technology, variable depth profiles have been created in the *ENTICE* model that have been shown to provide a more realistic representation of the true subsurface road construction around a route than was attainable with the original parameterisation proposed by Chapman et al. (2001b). The depths of subsurface layer interfaces have been estimated from GPR trace data via an inflexion point

algorithm designed to identify significant inflexions in the electromagnetic waveform of a GPR trace. Calculated depths are then used to estimate subsurface temperatures and the surface heat flux at each forecast point around the route. An increase of almost 7% in the overall *Pm* values was observed in a statistical analysis on *ENTICE* road construction parameterisation, indicating a significant improvement in the spatial forecasting ability of the *ENTICE* model as a result of the new re-parameterised road construction measurements. The methodologies used in parameterising subsurface layer depths from GPR measurements could be used for subsurface layer depth parameterisation in other surface energy balance models, particularly the METRo model where it is hoped the findings of this research will encourage the development of a spatial component within the existing METRo heat conduction module.

ii. Surface roughness (land use) re-parameterisation using airborne LIDAR data.

Turbulent heat transfer in the boundary layer close to the road surface is represented in *ENTICE* using a theoretical roughness length parameter. Existing parameterisation of Z_0 fails to account for the effect of upstream surface elements on local Z_0 values at each forecast point and the influence of the prevailing wind direction on local turbulence. A methodology has been proposed that uses high resolution LIDAR data coupled with spatial processing techniques to calculate an effective roughness length at each forecast point in a route-based forecast from the distribution of local Z_0 estimations within the upwind fetch of each forecast point. A statistical analysis comparing RST forecast values obtained using the existing Z_0 parameterisation with values obtained using the new Z_0^{eff} measurements has revealed a 6% increase in the variability of RST accounted for by *ENTICE* with the new re-parameterised Z_0^{eff} measurements. The methodologies proposed compliment other current research relating to geographical parameterisations in route-based models, most notably the on-going Danish Height Model research to estimate shadowing effects on RST using high resolution LIDAR data (Pedersen et al. 2010).

4. To use the validation strategy devised in (2) as a new methodology for testing whether the changes to geographical and infrastructure parameterisation improve the overall spatial forecasting performance of the ENTICE model.

Changes to road construction and surface roughness parameterisation in the *ENTICE* model have led to refinement of the clustering solution for the study route, and the spatial forecasting ability of the model has been proven to increase through an analysis of forecast statistics at the cluster level. On extreme nights during winter when atmospheric conditions are most stable and RST is most likely to fall below zero, the refined clustering solution has been shown, via CSC analysis, to better capture the physical relationship between RST and the geographical and infrastructure parameters around the study route. Cluster level statistics reveal poor model performance in city centre locations, believed to be linked to the inadequate parameterisation of traffic in the *ENTICE* model, for which recommendations are made in Chapter 6.

5. Make recommendations for the future of route-based forecasting.

The entire methodology of route-based forecasting is starting to change as new technologies emerge, and with further time and effort these technologies will be utilised to their full capabilities, enabling the next generation of route-based forecasts proposed in the blueprint in Figure 6.8 to be realised. The spatial resolution of route-based forecasts is likely to be dictated by the capabilities of high resolution NWP models over the coming years, and there is sufficient evidence to suggest that geographical surveying techniques, whether mobile or desktop based, will at some point in the future become surplus to requirements, with NWP models themselves providing the geographical parameterisations required to drive the spatial component of route-based forecast models. However, public safety must always remain the top priority, so until these new technologies have been thoroughly tested and proven, mobile and desktop surveying techniques will continue to be used in route-based forecasting.

To conclude, the specific aims and objectives of this thesis have been fulfilled. The findings of this research should give winter maintenance engineers further confidence in route-based forecasting, with a validation technique now in place which not only provides a better representation of a models spatial forecasting ability, but also enables identification of those areas within a route where model performance is not as accurate and where extra caution should be exercised when making treatment decisions. Such locations are ideal sites for the new generation of low cost infrared sensors now readily available, and such information will be vital in helping local authorities progress towards selective salting strategies, where the greatest financial savings in road weather forecasting will ultimately be found.

REFERENCES

Al-Qadi, I. & Lahouar, S., 2005. Measuring layer thickness with GPR - Theory to practice. *Construction and Building Materials*, 19, 763-772.

American Society of Civil Engineers (ASCE)., 1996. *Hydrology Handbook Second Edition*. ASCE Manuals and Reports on Engineering Practice No. 28, Washington, USA.

Astbury, A., 1996. Use of a high resolution mesoscale model to prepare site specific road temperature. In *Proceedings of the 8th International Road Weather Conference*. SIRWEC. Birmingham, pp. 122-128.

Arya, S., 1988. *Introduction to micrometeorology*, London: Academic Press.

Baik, J. & Kim, J., 1999. A numerical study of flow and pollutant dispersion characteristics in urban street canyons. *Journal of Applied Meteorology*, 38, 1576-1589.

Bergendahl, S., 1998. A study of surface temperature variations with the use of IR-technique. In *Earth Sciences Centre: B143*. Univeristy of Göteborg.

Best, M., 2005. Representing urban areas within operational numerical weather prediction models. *Boundary-Layer Meteorology*, 114, 91-109.

Bogren, J. & Gustavsson, T., 1991. Nocturnal air and road surface temperature variations in complex terrain. *International Journal of Climatology*, 11, 443-455.

Bogren, J., Gustavsson, T., Karlsson, M. & Postgård, U., 2000. The impact of screening on road surface temperature. *Meteorological Applications*, 7, 97-104.

Bogren, J., Gustavsson, T. & Lindqvist, S., 1992. A description of a local climatological model used to predict temperature variations along stretches of road. *Meteorological Magazine*, 121, 157-164.

Bogren, J., Gustavsson, T. & Postgård, U., 2000. Temperature differences in relation to weather parameters. *International Journal of Climatology*, 20, 151-170.

Bottema, M., 1997. Urban roughness modelling in relation to pollutant dispersion. *Atmospheric Environment*, 31, 3059-3075.

Brown, A., Jackson, S., Murkin, P., Sheridan, P., Skea, A., Smith, S., Veal, A. & Vosper, S., 2008a. New techniques for route-based forecasting. In *Proceedings of the 14th Standing International Road Weather Conference*. SIRWEC. Prague, Czech Republic, ID17.

Brown, A., Jackson, S., Murkin, P., Skea, A., Smith, S. & Veal, A., 2008b. Weather prediction for the road industry. In *Proceedings of the 14th Standing International Road Weather Conference*. SIRWEC. Prague, Czech Republic, ID16.

Businger, J.A., 1986. Evaluation of the accuracy with which dry deposition can be measured with current micrometeorological techniques. *Journal of Climate and Applied Meteorology*, 25, 1100-1124.

Chapman, L., 2002. *A Blueprint for 21st Century Road Ice Prediction*. Birmingham: University of Birmingham.

Chapman, L. & Thornes, J.E., 2004. Real-time sky-view factor calculation and approximation. *Journal of Atmospheric and Oceanic Technology*, 21, 730-741.

Chapman, L. & Thornes, J.E., 2005. The influence of traffic on road surface temperatures: implications for thermal mapping studies. *Meteorological Applications*, 12, 371-380.

Chapman, L. & Thornes, J.E., 2006. A geomatics-based road surface temperature prediction model. *Science of the Total Environment*, 360, 68-80.

Chapman, L. & Thornes, J.E., 2008. Small-scale road surface temperature and condition variations across a road profile. In *Proceedings of the 14th Standing International Road Weather Conference*. SIRWEC. Prague, Czech Republic.

Chapman, L., Thornes, J.E. & Bradley, A., 2001a. Modelling of road surface temperature from a geographical parameter database. Part 1: Statistical. *Meteorological Applications*, 8, 409-419.

Chapman, L., Thornes, J.E. & Bradley, A., 2001b. Modelling of road surface temperature from a geographical parameter database. Part 2: Numerical. *Meteorological Applications*, 8, 421-436.

Chapman, L., Thornes, J.E., Muller, J.P. & McMuldroch, S., 2007. Potential applications of thermal fisheye imagery in urban environments. *IEEE Geoscience and Remote Sensing Letters*, 4(1), 56-59.

Christen, A. & Vogt, R., 2004. Energy and radiation balance of a central European city. *International Journal of Climatology*, 24, 1394-1421.

Clark, W. & Hosking, P., 1986. *Statistical methods for geographers*, Chichester: Wiley.

Cleugh, H. & Oke, T., 1986. Suburban-rural energy balance comparisons in summer for Vancouver, B.C. *Boundary-Layer Meteorology*, 36(4), 351-369.

Cornford, D. & Thornes, J., 1996. A comparison between spatial winter indices and expenditure on winter road maintenance in Scotland. *International Journal of Climatology*, 16, 339-357.

Crevier, L. & Delage, Y., 2001. METRo: A new model for road-condition forecasting in Canada. *Journal of Applied Meteorology*, 40, 2026-2037.

Davenport, A.G., 1960. Rationale for determining design wind velocities. *Journal of Structural Division, American Society of Civil Engineers*, 86, 39-68.

Demiryurek, U., Pan, B., Banaei-Kashani, F. & Shahabi, C., 2009. Towards the modelling of traffic data on road networks. In *2nd International Workshop on Computational Transportation Science*. IWCTS 2009 Workshop Report. Seattle, Washington.

Department of Transport, 1984. Winter maintenance of motorways and trunk roads: statement of service and code of practice.

Department for Transport, 2004. *Feasibility study of road pricing in the UK - A report to the Secretary of State*, Department for Transport.

Drobot, S., Chapman, M., Schuler, E., Wiener, G., Mahoney, W.P., Pisano, P.A. & McKeever, B., 2010. Overview of the vehicle data translator. In *Proceedings of the 15th Standing International Road Weather Conference*. SIRWEC. Québec City, Canada.

Dytham, C., 1999. *Choosing and using statistics: A biologist's guide*, Malden, MA: Blackwell Science.

Edwards, S., Lavagno, L., Lee, E.A. & Sangiovanni-Vincentelli, A., 2002. Design of Embedded Systems: Formal Models, Validation and Synthesis. In De Micheli, G., Ernst, R. & Wolf, W., (eds). *Readings in hardware/software co-design*. San Francisco, Academic Press.

Gal, T., Rzepa, M., Gromek, B. & Unger, J., 2007. Comparison between sky view factor values computed by two different methods in an urban environment. *Acta Climatologica et Chorologica*, (40-41), 17-26.

Gal, T., Lindberg, F. & Unger, J., 2009. Computing continuous sky view factors using 3D urban raster and vector databases: comparison and application to urban climate. *Theoretical and Applied Climatology*, 95, 111-123.

Garratt, J., 1992. *The atmospheric boundary layer*, Cambridge: Cambridge University Press.

Grimmond, C.S.B., 1992. Suburban energy balance, Vancouver. *International Journal of Climatology*, 12(5), 481-497.

Grimmond, C.S.B. & Oke, T.R., 1995. Comparison of heat fluxes from summertime observations in the suburbs of four North American cities. *Journal of Applied Meteorology*, 34, 873-889.

Grimmond, C.S.B. & Oke, T.R., 1999a. Heat storage in urban areas: local-scale observations and evaluation of a simple model. *Journal of Applied Meteorology*, 38, 922-940.

Grimmond, C.S.B. & Oke, T.R., 1999b. Aerodynamic properties of urban areas derived from analysis of surface form. *Journal of Applied Meteorology*, 38, 1262-1292.

Grimmond, C.S.B., Salmond, J.A., Oke, T.R., Offerle, B. & Lemonsu, A., 2004. Flux and turbulence measurements at a dense urban site in Marseille: heat, mass (water, carbon dioxide) and momentum. *Journal of Geophysical Research, Atmospheres*, 109, 1-19.

Grimmond, C.S.B., Potter, S.K., Zutter, H.N. & Souch, C., 2001. Rapid methods to estimate sky-view factors applied to urban areas. *International Journal of Climatology*, 21, 903-913.

Gustavsson, T., 1999. Thermal mapping - a technique for road climatological studies. *Meteorological Applications*, 6, 385-394.

Gustavsson, T. & Bogren, J., 1993. Evaluation of a local climatological model - test carried out in the county of Halland, Sweden. *Meteorological Magazine*, 122, 257-266.

Gustavsson, T., Bogren, J. & Green, C., 2001. Road climate in cities: A study of the Stockholm area, south-east Sweden. *Meteorological Applications*, 8, 481-489.

Gustavsson, T., Karlsson, M., Bogren, J. & Lindqvist, S., 1998. Development of temperature patterns during clear nights. *Journal of Applied Meteorology*, 559-571.

Handa, H., Chapman, L. & Yao, X., 2007. Robust salting route optimization using evolutionary algorithms. *Studies in Computational Intelligence*, 51, 497-517.

Hanna, S. & Chang, J., 1992. Boundary layer parameterisations for applied dispersion modelling over urban areas. *Boundary Layer Meteorology*, 58, 229-259.

Harman, I., Best, M. & Belcher, S., 2004. Radiative exchange in an urban street canyon. *Boundary-Layer Meteorology*, 110, 301-316.

Hartigan, J., 1975. *Clustering Algorithms*, New York: Wiley.

Heilman, J.L., Brittin, C.L. & Neale, C.M.U., 1989. Fetch requirements for bowen ratio measurements of latent and sensible heat fluxes. *Agricultural and Forest Meteorology*, 44, 262-273.

Horst, T.W., 1999. The footprint for estimation of atmosphere-surface exchange fluxes by profile techniques. *Boundary-Layer Meteorology*, 90, 171-188.

Horst, T.W. & Weil, J.C., 1994. How far is far enough? The fetch requirements for micrometeorological measurement of surface fluxes. *Journal of Atmospheric and Oceanic Technology*, 11, 1018-1025.

Kim, J. & Baik, J., 2001. Urban street-canyon flows with bottom heating. *Atmospheric Environment*, 35, 3395-3404.

Kondo, A., Ueno, M., Kaga, A. & Yamaguchi, K., 2001. The influence of urban canopy configuration on urban albedo. *Boundary-Layer Meteorology*, 100, 225-242.

Kristiansen, K., Loisy, C. & Bosch, W., 2003. Road traffic monitoring by satellite. *ESA Bulletin*, 52-57.

Lagourade, J., Kerr, Y. & Brunet, Y., 1995. An experimental study of angular effects on surface temperature for various plant canopies and bare soils. *Agricultural and Forest Meteorology*, 77, 167-190.

Lahouar, S. & Al-Qadi, I., 2008. Automatic detection of multiple pavement layers from GPR data. *NDT & E International*, 41(2), 69-81.

Linden, S. & Drobot, S., 2010. The evolution of METRo in a roadway DSS. In *Proceedings of the 15th International Road Weather Conference*. SIRWEC. Québec City, Canada.

Liou, K., 2002. *An Introduction to Atmospheric Radiation* Second Edition., London: Academic Press.

Mahoney, W., Bernstein, B., Wolff, J., Linden, S., Myres, W.L., Hallowell, R.G., Cowie, J., Stern, A.D., Koenig, G., Phetteplace, G., Schultz, P., Pisano, P.A. & Burkheimer, D., 2005. FHWA's Maintenance Decision Support System Project: Results and Recommendations. *Transportation Research Board: Journal of the Transportation Research Board*, 1911, 133-142.

Maisey, P., Hopwood, W. & Pearman, I., 2000. Impact of high resolution site specific modelling on road surface temperature forecasts. In *Proceedings of the 10th International Road Weather Conference*. SIRWEC. Davos, Switzerland, pp. 41-45.

Masson, V., 2000. A physically-based scheme for the urban energy balance in atmospheric models. *Boundary-Layer Meteorology*, 94, 357-397.

McClure, D. & Graham, A., 2006. *eCall - The Case for Deployment in the UK*, Department for Transport.

Moore, D., 1975. *The friction of pneumatic tyres*, Oxford: Elsevier Scientific.

Morey, R., 1998. Ground Penetrating Radar for evaluating subsurface conditions for transportation facilities. *National Cooperative Highway Research Program Synthesis 255*.

Mylne, K.R., 1999. The use of forecast value calculations for optimising decision making using probability forecasts. In *Proceedings of the 17th Conference on Weather Analysis and Forecasting*. Denver, Colorado, USA.

Myrup, L., 1969. A numerical model of the urban heat island. *Journal of Applied Meteorology*, 8, 908-919.

Neal, A., 2004. Ground-penetrating radar and its use in sedimentology: principles, problems and progress. *Earth-Science Reviews*, 66, 261-330.

Nunez, M. & Oke, T., 1977. The energy balance of an urban canopy. *Journal of Applied Meteorology*, 16, 11-19.

Offerle, B., Grimmond, C.S.B., Fortuniak, K., Klysik, K. & Oke, T.R., 2006. Temporal variations in heat fluxes over a central European city centre. *Theoretical and Applied Climatology*, 84, 103-116.

Offerle, B., Eliasson, I., Grimmond, C.S.B. & Holmer, B., 2007. Surface heating in relation to air temperature, wind and turbulence in an urban street canyon. *Boundary-Layer Meteorology*, 122, 273-292.

Oke, T.R., 1992. *Boundary Layer Climates* Second Edition., London: Routledge.

Oke, T.R., Sproken-Smith, R.A., Jáuregui, E. & Grimmond, C.S.B., 1999. The energy balance of central Mexico City during the dry season. *Atmospheric Environment*, 33, 3919-3930.

Ostafe, M., 2009. eCall Toolbox. *eSafetySupport.org*. Available at: http://www.esafety support.org/en/ecall_toolbox/ [Accessed April 13, 2010].

Outcalt, S., 1971. A numerical surface climate simulator. *Geographical Analysis*, 3, 379-393.

Outcalt, S., 1972. The development and application of a simple digital surface-climate simulator. *Journal of Applied Meteorology*, 11, 629-636.

Owen, S.M., MacKenzie, A.R., Bunce, R.G.H., Stewart, H.E., Donovan, R.G., Stark, G. & Hewitt, C.N., 2006. Urban land classification and its uncertainties using principal component and cluster analyses: A case study for the UK West Midlands. *Landscape and Urban Planning*, 78, 311-321.

Parmenter, B. & Thornes, J., 1986. The use of a computer model to predict the formation of ice on road surfaces. *Transport and Road Research Laboratory Research Report*, 71, 1-19.

Pedersen, T.S., Petersen, C., Sattler, K. & Mahura, A., 2010. Physiographic data for road stretch forecasting. In *Proceedings of the 15th Standing International Road Weather Conference*. SIRWEC. Québec City, Canada.

Petty, K. & Mahoney, W., 2008. The U.S. Federal Highway Administration Winter Road Maintenance Decision Support System (MDSS): Recent Enhancements and Refinements. In *Proceedings of the 14th Standing International Road Weather Conference*. Prague, Czech Republic.

Preisendorfer, R., 1988. *Principal components analysis in meteorology and oceanography.*, New York: Elsevier.

Prusa, J.M., Segal, M., Temeyer, B.R., Gallus, W.A. & Takle, E.S., 2002. Conceptual and scaling evaluation of vehicle traffic thermal effects on snow/ice covered roads. *Journal of Applied Meteorology*, 41, 1225-1240.

Quarmby, D., Smith, B. & Green, C., 2010. *The resilience of England's transport system in winter. An independent review - interim report*, London: Department for Transport.

Rayer, P., 1987. The Meteorological Office forecast road surface temperature model. *Meteorological Magazine*, 116, 180-191.

Salmond, J.A., Oke, T.R., Grimmond, C.S.B., Roberts, S. & Offerle, B., 2005. Venting of heat and carbon dioxide from urban canyons at night. *Journal of Applied Meteorology*, 44, 1180-1194.

Schaudt, K.J., 1998. A new method for estimating roughness parameters and evaluating the quality of observations. *Journal of Applied Meteorology*, 37, 470-476.

Schmid, H., 1994. Source areas for scalars and scalar fluxes. *Boundary-Layer Meteorology*, 67, 293-318.

Schultz, P., 2005. An ensemble of WRF and MM5 configurations for winter weather forecasting. In *Joint WRF/MM5 Users Workshop*. Boulder, Colorado, p. 4.

Scott, J., 1986. Incorporation of angular emissivity effects in long wave infrared image models. *SPIE*, 687, 44-53.

Seber, G., 2004. *Multivariate observations.*, Chichester: Wiley.

Shao, J., 1990. *A winter road surface temperature model with comparison to others. Unpublished PhD thesis*. UK: University of Birmingham.

Shao, J., 1998. Improving nowcasts of road surface temperature by a backpropagation neural network. *Weather and Forecasting*, 13, 164-171.

Shao, J. & Lister, P., 1995. The prediction of road surface state and simulation of the shading effect. *Boundary-Layer Meteorology*, 73(4), 411-419.

Shao, J. & Lister, P., 1996. An automated nowcasting model of road surface temperature and State for winter road maintenance. *Journal of Applied Meteorology*, 35, 1352-1361.

Shao, J., Lister, P.J., Hart, G.D. & Pearson, H.B., 1996. Thermal mapping: reliability and repeatability. In *Proceedings of the 8th International Road Weather Conference*. SIRWEC. Birmingham, pp. 235-242.

Shao, J., Swanson, J.C., Patterson, R., Lister, P.J. & McDonald, A.N., 1997. Variation of winter road surface temperature due to topography and application of thermal mapping. *Meteorological Applications*, 4(2), 131-137.

Sheskin, D., 2007. *Handbook of Parametric and Nonparametric Statistical Procedures* Fourth Edition., London: Chapman & Hall//CRC.

Sini, J., Anquetin, S. & Mestayer, P., 1996. Pollutant dispersion and thermal effects in urban street canyons. *Atmospheric Environment*, 30, 2659-2677.

Smith, C., Lindley, S. & Levermore, G., 2009. Estimating spatial and temporal patterns of urban anthropogenic heat fluxes for UK cities: the case of Manchester. *Theoretical and Applied Climatology*, 98, 19-35.

Sneath, P. & Sokal, R., 1973. *Numerical taxonomy - the principles and practice of numerical classification.*, San Francisco: W.H.Freeman.

Stephenson, D.B., 2000. Use of the 'odds ratio' for diagnosing forecast skill. *Weather and Forecasting*, 15, 221-232.

Sugrue, G., 1983. Infrared thermometry - advantages and disadvantages. In Atmosphere-Road Surface Interaction Group Working Paper 7.

Tieleman, H.W., 2003. Roughness estimation for wind-load simulation experiments. *Journal of Wind Engineering and Industrial Aerodynamics*, 91, 1163-1173.

Thompson, N., 1988. The Meteorological Office road surface temperature prediction model. In *Proceedings of the 4th International Road Weather Conference*. Florence, Italy.

Thornes, J.E., 1984. *The prediction of ice formation on motorways in Britain*. London: University of London.

Thornes, J.E., 1985. The prediction of ice formation on roads. *Journal of the Institution of Highways and Transportation*, 32, 3-12.

Thornes, J.E., 1991. Thermal mapping and road-weather information systems for highway engineers. In *Highway Meteorology*. London: E & FN Spon, pp. 39-67.

Thornes, J.E., 1994. Salt of the Earth. *The Surveyor*. 8 December, 16-18.

Thornes, J.E., 1995. A comparative real-time trial between the Met Office and Oceanroutes to predict road surface temperatures. *Meteorological Applications*, 2, 113-119.

Thornes, J.E., 1996. The cost benefit of winter road maintenance in the United Kingdom. In *Proceedings of the 8th International Road Weather Commission*. SIRWEC. Birmingham, pp. 1-10.

Thornes, J.E. & Shao, J., 1992. Objective method for improving the operational performance of a road ice prediction model using interpolated mesoscale output and a template for correcting systematic error. *Meteorological Magazine*, 121, 197-204.

Thornes, J.E. & Proctor, E.A.J., 1999. Persisting with persistence: the verification of Radio 4 weather forecasts. *Weather*, 54, 311-321.

Thornes, J.E. & Stephenson, D.B., 2001. How to judge the quality and value of weather forecast products. *Meteorological Applications*, 8, 307-314.

Vihma, T. & Savijärvi, H., 1991. On the effective roughness length for heterogeneous terrain. *Quarterly Journal of the Royal Meteorological Society*, 117, 399-407.

White, S., 2007. The route treatment. *Surveyor Magazine*, 12-14.

Wieringa, J., 1992. Updating the Davenport roughness classification. *Journal of Wind Engineering and Industrial Aerodynamics*, 41, 357-368.

Wieringa, J., 1993. Representative roughness parameters for homogeneous terrain. *Boundary Layer Meteorology*, 63, 323-363.

Wieringa, J., Davenport, A.G., Grimmond, C.S.B. & Oke, T.R., 2001. New revision of Davenport roughness classification. In *Proceedings of the 3rd European & African Conference on Wind Engineering*. Eindoven, Netherlands, p. 8.

Wimsatt, A. et al., 1998. Use of ground penetrating radar data in pavement rehabilitation strategy selection and pavement condition assessment. In *Proceedings of SPIE Volume 3400*. Structural Materials Technology III: An NDT Conference. San Antonio, TX, USA, pp. 372-383.

Yoshida, A., Tominaga, K. & Watatani, S., 1991. Field measurements on energy balance of an urban canyon in the summer season. *Energy and Buildings*, 15, 417-423.

WEBSITE ADDRESSES CITED IN TEXT

http://www.safecote.com/

http://meteogroup.co.uk/

http://landmap.ac.uk/

http://badc.nerc.ac.uk/home/index.html/

http://www.bluesky-world.com/

http://gna.org/projects/metro/

APPENDIX 1

MATLAB HIERARCHICAL CLUSTER PROGRAM

```
%RWIS Cluster Program Optional Settings
%
% Optional distance algorithms:
%
% 'euclidean' - Euclidean distance
% 'seuclidean' - Standardized Euclidean distance. Each coordinate in the
sum of squares is inverse weighted by the sample variance of that
%coordinate
% 'cityblock' - City Block metric
% 'minkowski' - Minkowski metric
% 'cosine' - One minus the cosine of the included angle between points
(treated as vectors)
% 'correlation' - One minus the sample correlation between points (treated
as sequences of values).
% 'spearman' - One minus the sample Spearman's rank correlation between
observations,
%    treated as sequences of values
%
% Optional linkage algorthims:
%
% 'single' - Shortest distance
% 'complete' - Furthest distance
% 'average' - Unweighted average distance (UPGMA) (also known as group
average)
% 'weighted' - Weighted average distance (WPGMA)
% 'centroid' - Centroid distance (UPGMC)
% 'median' - Weighted center of mass distance (WPGMC)
% 'ward' - Inner squared distance (minimum variance algorithm)

clc;
input ('RWIS Cluster Program. Press Enter to start: ');
filename = input ('Enter survey filename within single quotes, e.g.
''Test'': ');
file_name = input ('Enter output filename within single quotes, e.g.
''Cluster_PhDleices'': ');
%rst_data = input ('Enter filename containing RST data, e.g.
''Test_20080217.xls'': ');
disp('Importing Excel survey file')
[data, headings, raw] = xlsread(filename,'A:P');
D = data(:,6:12); %select data columns required for analysis
X = zscore(D); %normalize the data
Y1 = pdist(X,'euclidean'); %calculate distance between all object pairs -
various methods of distance methods can be specified - euclidean is default
Z1 = linkage(Y1,'average'); %use linkage function to determine how objects
in the data set should be grouped into clusters linkage method can be
specified - single is default
dendrogram(Z1); %plot hierarchical binary cluster tree information as a
graph
hold on;
xlabel('Cluster');
ylabel('Cluster link height');
c1 = cophenet(Z1,Y1); %calculate cophenetic correlation coefficient -
closer to 1 this value is, the more accurately the clustering solution
reflects data
%rst = xlsread(rst_data,'Join_Output','CM2:CN2146');
```

```
title = {'ICOEFF' 'CLUSTER' 'CLUSTER_STD' '' 'FORECAST_RST' 'ACTUAL_RST'
'ACTUAL_RST_STD' 'ERROR' 'MOD_ERROR' 'MOD_LOGIC' 'SQ_ERROR' 'BIAS'
'SD_of_BIAS' 'RMSE' '%FORECAST_WITHIN_1DEG_ACTUAL' 'RESID_FORECAST'
'RESID_ACTUAL' 'RESID_ERROR' 'MOD_RESID_ERROR' 'MOD_RESID_LOGIC'
'%RESID_FORECAST_WITHIN_1DEG_RESID_ACTUAL' 'STDEV_STABILITY'};
code1 = {'=standardize(V3,average(V$3:V$2263),stdev(V$3:V$2263))' '=U3-V3'
'=if(X3<0,X3*-1,X3)' '=if(Y3<=1,1,0)' '=X3^2'};
code2 = {'=average(X3:X2263)' '=stdev(X3:X2263)' '=average(AA3:AA2263)^0.5'
'=sum(Z3:Z2263)/2263*100'};
code3 = {'=U3-average(U$3:U$2263)' '=V3-average(V$3:V$2263)' '=AF3-AG3'
'=if(AH3<0,AH3*-1,AH3)' '=if(AI3<=1,1,0)'};
code4 = {'=sum(AJ3:AJ2263)/2263*100' '=stdev(V3:V2263)'};

for i = 10:2:12;
    str = num2str(i);
    str2 = ['Analysing data and organising into ' str ' clusters'];
    disp(' ')
    disp(str2)
    warning off MATLAB:xlswrite:AddSheet
    clust = cluster(Z1,'maxclust',i);
    clust_std = zscore(clust);
    xlswrite(file_name,headings,str,'A1');
    xlswrite(file_name,title,str,'Q1');
    xlswrite(file_name,clust,str,'R3');
    xlswrite(file_name,clust_std,str,'S3');
    %xlswrite(file_name,rst,str,'P3');
    xlswrite(file_name,data,str,'A3');
    xlswrite(file_name,c1,str,'Q3');
    xlswrite(file_name,code1,str,'W3:AA2263');
    xlswrite(file_name,code2,str,'AB3:AE3');
    xlswrite(file_name,code3,str,'AF3:AJ2263');
    xlswrite(file_name,code4,str,'AK3:AL3');
    str3 = ['Clustering complete for ' str ' clusters'];
    disp(str3)
end;

disp('Hierarchical Clustering Complete!)
```

APPENDIX 2

GPR TRACE INFLEXION POINT FLOWCHART

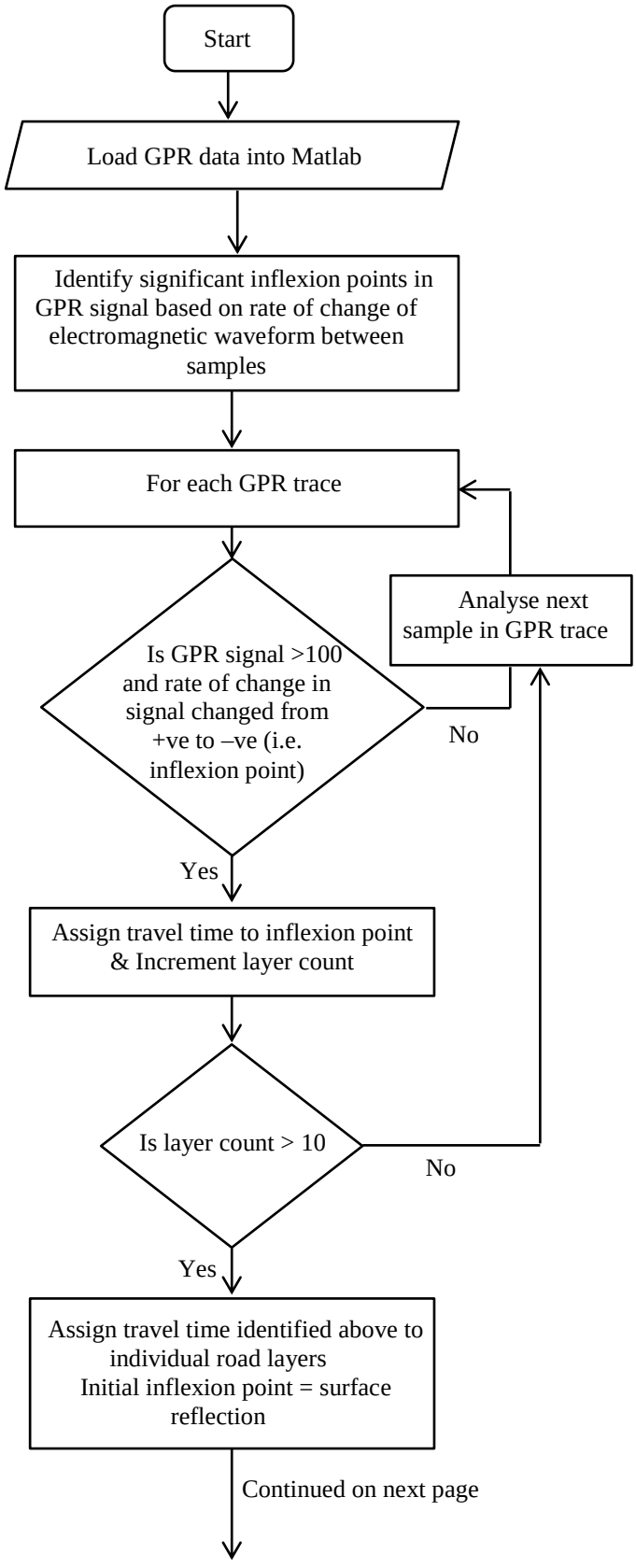

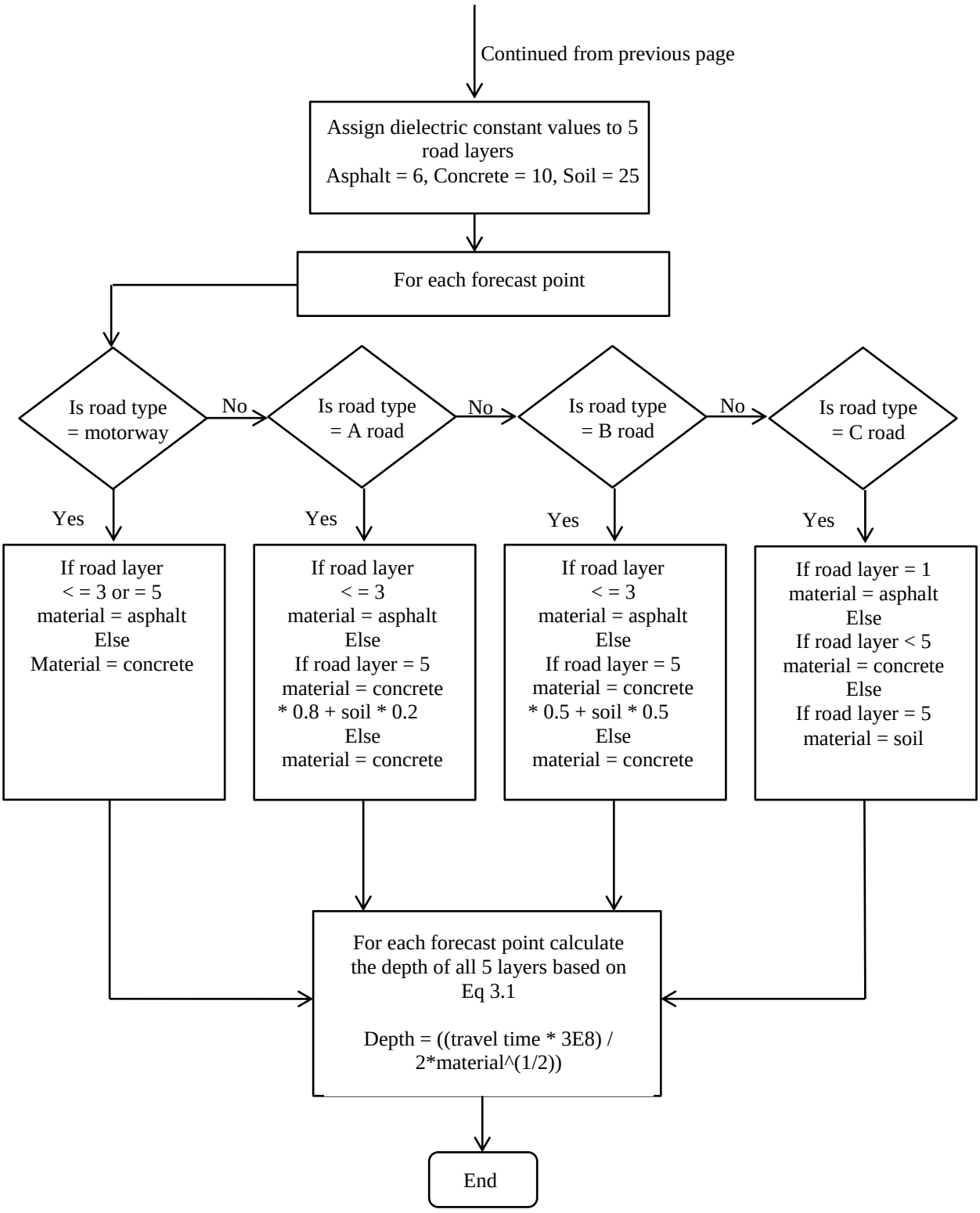
Continued from previous page
Assign dielectric constant values to 5 road layers
Asphalt = 6, Concrete = 10, Soil = 25
For each forecast point
Is road type = motorway
No
Is road type = A road
No
Is road type = B road
No
Is road type = C road
Yes
Yes
Yes
Yes
If road layer < = 3 or = 5 material = asphalt Else Material = concrete
If road layer < = 3 material = asphalt Else If road layer = 5 material = concrete * 0.8 + soil * 0.2 Else material = concrete
If road layer < = 3 material = asphalt Else If road layer = 5 material = concrete * 0.5 + soil * 0.5 Else material = concrete
If road layer = 1 material = asphalt Else If road layer < 5 material = concrete Else If road layer = 5 material = soil
For each forecast point calculate the depth of all 5 layers based on Eq 3.1
Depth = ((travel time * 3E8) / 2*material^(1/2))
End

APPENDIX 3

IRIS DATALOGGER PROGRAM

```
''-------------------------------------------------------------------------------------------------
----------------------------
'' Program.....................: IRIS Road Weather Station
''-------------------------------------------------------------------------------------------------
----------------------------
'' Copyright...................: Copyright (C) 2006-2008 Campbell Scientific Ltd. All Rights
Reserved.
''-------------------------------------------------------------------------------------------------
----------------------------
'' Author(s)...................: David Hammond, Simon Massey, Andrew Sandford
'' Company.....................: Campbell Scientific Ltd
''-------------------------------------------------------------------------------------------------
----------------------------
'' Version.....................: 1.10.15 RELEASE
'' Last Revised................: 06/05/2010
''-------------------------------------------------------------------------------------------------
----------------------------
'' Notes.......................: v1.10.15 originally modified by David Hammond, further
modified to utilise the full
'' ............................: 10 minute median due to timing changes.
'' ............................: - also includes updated modem configuration routine (SRM)
'' ............................:
''-------------------------------------------------------------------------------------------------
----------------------------
'' Required Operating System(s).: CR800.Std.06.07 (BETA - Contains the 15 second connection
timeout fix from this version)
''-------------------------------------------------------------------------------------------------
----------------------------
SequentialMode

PreserveVariables
AngleDegrees

'Debug Mode Control.
Const DebugMode = True 'When true enables all debug information within the IRIS program
(Default is False).
'Event Logging Control.
Const EventLogging = True 'When true enables event logging capability (Default is True).

'These defaults are used when no settings exist and should reflect the
'coefficients produced for the IR100 Sensor
Const DefaultIR100SerialNumber = ""
Const Default_Coeff_A = 9.434170E-04
Const Default_Coeff_B = 2.198455E-04
Const Default_Coeff_C = 1.388907E-07
Const Default_Coeff_X = 1.503168E-05
Const Default_Coeff_Y = 3.421465E-01
Const Default_Coeff_Z = -1.638007E-01

'This is the default Sky View Factor.
Const Default_SVF = 0.9

'Version Information
#If DebugMode Then
Const IRISProgVer = "IRIS.CR800.1.10.15.DIAG"
#Else
Const IRISProgVer = "IRIS.CR800.1.10.15"
#EndIf
'The name of the file that contains the IRIS settings.
Const IRISSettingsFilename = "USR:IRISCONFIG.INI"
'Comms Settings
Const ModemPort = ComME
Const CR = CHR(13)

'O2 Specific Configruation
Const PPPUsername="bypass"
Const PPPPassword="password"
'Modem set to numeric at 9600 baud (CSL default)
Const PPPdialresponse="21"
```

```
Const ModemNetwork = "mobile.O2.co.uk"
Const ModemConfig1 = CR & "AT+CGDCONT=1,""IP"","""" & ModemNetwork & """" & CR
Const ModemConfig2 = "AT+WIND=255" & CR
Const ModemConfig3 = "AT&W" & CR
Const DefaultTCPPort = 5794
Const DefaultPrimaryIPAddress = "81.110.79.59"
Const DefaultBackupIPAddress = "82.70.75.213"
Const MinimumBatteryThresholdForComms = 11 'Specified in Volts.
Const PPPTimeOut = 300 '60 'Maximum Time to Wait for a PPP connection in Seconds (back to 60)
Const PPPBlank = "0.0.0.0"
Const IPPortBlank = 0
Const IPTimeOut = 15 '120 'Maximum Time to Wait for an IP connection in Seconds.
Const COMMSTimeOut = 300 'The maximum time in seconds that the data connection will stay live.
Const ExtendedOnlineStartTime = 480 'Time in Minutes that extended online time starts. 480 =
8am.
Const ExtendedOnlineEndTime = 1080 'Time in Minutes that extended online time ends. 1080 =
6pm.
Const OneDayInMinutes = 1440 '24 Hours specified in minutes.
'Settings.
Const MaxNumberOfSettings = 8 'Maximum Number of Numeric Settings
Const MaxNumberOfStringSettings = 4 'Maximum Number of String Settings
Const STRINGSETTING_PrimaryIPAddress = 1
Const STRINGSETTING_BackupIPAddress = 2
Const STRINGSETTING_TCPPort = 3
Const STRINGSETTING_IR100SerialNumber = 4
Const SETTING_Emissivity = 1
Const SETTING_SVF = 2
Const SETTING_Coeff_A = 3
Const SETTING_Coeff_B = 4
Const SETTING_Coeff_C = 5
Const SETTING_Coeff_X = 6
Const SETTING_Coeff_Y = 7
Const SETTING_Coeff_Z = 8

'Film
Const Film = 0.79
'Surface Types
Const Asphalt = 0.956
Const Concrete = 0.966
Const Brick = 0.88
Const Ice = 0.97
Const Snow = 0.99
Const Ocean = 0.98
'On / Off
Const On = True
Const Off = False
'Traffic
Public Previous_TSurface
Public Traffic_Count1, Traffic_Count2, Traffic_Count3, Traffic_Count4
Public Traffic_Count11, Traffic_Count22, Traffic_Count33, Traffic_Count44
Public Difference_TSurface

'Controls Event Logging Capability.
#If EventLogging Then
'IRIS Event Logging Constants.
Const IRISEventLogMaximumSize = 20
Const IRISEventDescriptionMaximumLength = 32
Const IRISEventLogSize = 50 'The maximum size the event log can grow to.
Const IRISEventCode_Undefined = 0 'Indicates an event where no specific error code exists.
Const IRISEventCode_ProgramStarted = 1 'Indicates program started.
Const IRISEventCode_ProgramStopped = 2 'Indicates program stopped.
Const IRISEventCode_SettingsLoaded = 3 'Indicates IRIS settings file has been loaded from the
USR Drive
Const IRISEventCode_SettingsSaved = 4 'Indicates IRIS settings file has been saved to the USR
Drive
Const IRISEventCode_SettingsDefaulted = 5 'Indicates that default settings were stored.
Const IRISEventCode_CS215Error = 6 'Indicates an error with the CS215.
Const IRISEventCode_CommsStarting = 7 'Used to indicate that comms are beginning (DEBUG)
Const IRISEventCode_PPPStartFailed = 8  'Indicates PPP startup has failed.
Const IRISEventCode_PPPCloseFailed = 9  'Indicates PPP closing has failed.
Const IRISEventCode_IPConnectFailed = 10 'Indicates IP open with primary and backup has
failed.
Const IRISEventCode_ModemStartFailed = 11  'Indicates that the modem has failed to initialise.
Const IRISEventCode_BatteryTooLowForComms = 12 'Indicates that the battery has too little
power for comms to run.
'IRIS Event Logging Variables.
Dim IRISEventCode As Long 'Stores the event code to be sampled.
Dim IRISEventDescription As String * IRISEventDescriptionMaximumLength 'Stores an event
description to be sampled.
Dim IRISEventLog(IRISEventLogMaximumSize,2) As String * IRISEventDescriptionMaximumLength
```

```
Dim IRISEventLogCurrentPosition As Long
Dim SavingEventLog As Boolean
#EndIf

'Debuggable Variable Declarations (note dependent on debug mode)
#If DebugMode Then
Public IRISProgramVersion As String * 50 'Holds the current version of the program for
sampling
'Menu and Settings Control.
Public MENUStringSettings(MaxNumberOfStringSettings) As String * 20
Public StringSettings(MaxNumberOfStringSettings) As String * 20
Public MENUSettings(MaxNumberOfSettings) 'Stores the settings as modified through the menu.
Public Settings(MaxNumberOfSettings) 'Stores the settings currently being used by the program.
Public SettingsChanged As Boolean 'This flag will be set if the settings are changed in the
menus.
Public SettingsLoading As Boolean 'This flag is set if the settings are currently being
reloaded.
Public ReloadSettings As Boolean 'If this flag is set to true then the settings will be
reloaded at the top of the next minute.
'Working Variables.
Public PTemp, Batt_Volt, FirstRun As Boolean
Public CS215(2)
Public CosBeta_A, CosBeta_B, CosBeta_C, CosBeta_D
Public SVF, SVP, VP
Public Dew_Point, SkyTemp
Public Cal_Can, IRSensor_Resis, IRSensorCan_Temp, IRSensor_Volt, IRSensor_E, IRSensor_T4,
IRSensor_T, IRTemp, IRSensor_Volt_TC
Public TSurface, TFilm
Public IRSpreadIndex
'Communications Variables
Public OpenPPP As String * 30
Public ConnectDelay As Boolean
Public COMMSTimer 'Uses Timer 0
Public PPPAddress As String * 20
Public ModemStarted As Boolean 'This flag is set to true if the modem is started successfully.
Public IPPort As Long, CommsTCPPort As Long, SendResult, Scratch
Public ModemConfigured As Boolean
#Else
Dim IRISProgramVersion As String * 50 'Holds the current version of the program for sampling
'Menu and Settings Control.
Dim MENUStringSettings(MaxNumberOfStringSettings) As String * 20
Dim StringSettings(MaxNumberOfStringSettings) As String * 20
Dim MENUSettings(MaxNumberOfSettings) 'Stores the settings as modified through the menu.
Dim Settings(MaxNumberOfSettings) 'Stores the settings currently being used by the program.
Dim SettingsChanged As Boolean 'This flag will be set if the settings are changed in the
menus.
Dim SettingsLoading As Boolean 'This flag is set if the settings are currently being reloaded.
Public ReloadSettings As Boolean 'If this flag is set to true then the settings will be
reloaded at the top of the next minute.
'Working Variables.
Dim PTemp, Batt_Volt, FirstRun As Boolean
Dim CS215(2)
Dim CosBeta_A, CosBeta_B, CosBeta_C, CosBeta_D
Dim SVF, SVP, VP
Dim Dew_Point, SkyTemp
Dim Cal_Can, IRSensor_Resis, IRSensorCan_Temp, IRSensor_Volt, IRSensor_E, IRSensor_T4,
IRSensor_T, IRTemp, IRSensor_Volt_TC
Dim TSurface, TFilm
Dim IRSpreadIndex
'Communications Variables
Dim OpenPPP As String * 30
Dim ConnectDelay As Boolean
Dim COMMSTimer 'Uses Timer 0
Dim PPPAddress As String * 20
Dim ModemStarted As Boolean 'This flag is set to true if the modem is started successfully.
Dim IPPort As Long, CommsTCPPort As Long, SendResult, Scratch
Dim ModemConfigured As Boolean
#EndIf

'These public variables are used purely to provide live data during setup.
Public Live_RoadTemp, Live_AirTemp, Live_RH, Live_DewPoint, Live_PanelTemp, Live_Battery,
Live_BodyTemp
Public Live_SerialNumber As String * 10

'When true indicates that coefficients are available.
Public CoeffsAvailable As Boolean

'This variable is always public and ocntains a running status for GPRS comms.
Public CommsStep As String * 32
'When this flag is set the logger tmeperature will be used as a substitute for
```

```
'AirTemp and Dew_Point.  This option is available to allow for data to be
'generated even if the CS215 should be unavailable.
Public UseLoggerTemperature As Boolean '(Default is False)

Alias CS215(1) = AirTemp
Alias CS215(2) = RH

'*****************************************************************************
'Table Name ..: IrisData
'Frequency....: 10 Minutes
'History......: Automatic
'Purpose......: The main data source for the IRIS Bureau
'*****************************************************************************
DataTable(IrisData,True,-1)
  DataInterval(0,10,Min,10)
  'Logger Stats.
  Minimum(1,Batt_Volt,FP2,0,False) : FieldNames("Battery_Voltage")
  Sample(1,PTemp,FP2) : FieldNames("Panel_Temp")
  'IRIS Return Values.
  Median(1,TSurface,120,FP2,False) : FieldNames("IRTemp")
  Average(1,AirTemp,FP2,False) : FieldNames("Air_Temp")
  Average(1,RH,FP2,False) : FieldNames("RH")
  Average(1,Dew_Point,FP2,False) : FieldNames("Dew_Point")
  'Status Flags
  Sample(1,UseLoggerTemperature,Boolean) : FieldNames("UsingLoggerTemperature")
EndTable

'*****************************************************************************
'Table Name ..: Traffic
'Frequency....: 10 Minutes
'History......: Automatic
'Purpose......: Stores total traffic count information
'*****************************************************************************
DataTable(Traffic,True,-1)
  DataInterval(0,10,Min,10)
  Totalize(1,Traffic_Count1,FP2,False)
  Totalize(1,Traffic_Count2,FP2,False)
  Totalize(1,Traffic_Count3,FP2,False)
  Totalize(1,Traffic_Count4,FP2,False)
  Totalize(1,Traffic_Count11,FP2,False)
  Totalize(1,Traffic_Count22,FP2,False)
  Totalize(1,Traffic_Count33,FP2,False)
  Totalize(1,Traffic_Count44,FP2,False)
EndTable

#If EventLogging Then
'*****************************************************************************
'Table Name ..: IRISEventLog
'Frequency....: as required, no fixed interval
'History......: as defined by IRISEventLogSize constant
'Purpose......: Stores IRIS Events for logging purposes,
'.............: records are added by calling the LogEvent procedure.
'*****************************************************************************
DataTable(IRISEventLog,True,IRISEventLogSize)
  Sample(1,IRISEventCode,Long) : FieldNames("EventCode")
  Sample(1,IRISEventDescription,String) : FieldNames("EventDescription")
EndTable

'This procedure takes an event code and and event description and stores them to the IRIS
Event Log.
Sub LogEvent(LogEvent_EventCode As Long, LogEvent_EventDescription As String *
IRISEventDescriptionMaximumLength)
  'Transfer the event details ready for sampling later
  If NOT SavingEventLog Then
    If IRISEventLogCurrentPosition <= IRISEventLogMaximumSize Then
      IRISEventLog(IRISEventLogCurrentPosition,1) = LogEvent_EventCode
      IRISEventLog(IRISEventLogCurrentPosition,2) = LogEvent_EventDescription
      IRISEventLogCurrentPosition = IRISEventLogCurrentPosition + 1
    EndIf
  EndIf
EndSub

'This procedure copies all the currently stored events to the table.
Dim SaveEventLogIndex As Long
Sub SaveEventLog
  SavingEventLog = True
  If IRISEventLogCurrentPosition > 1 Then
    For SaveEventLogIndex = 1 To (IRISEventLogCurrentPosition - 1)
      IRISEventCode = IRISEventLog(SaveEventLogIndex,1)
      IRISEventDescription = IRISEventLog(SaveEventLogIndex,2)
```

```
      'Store the event in the event log.
      CallTable IRISEventLog
    Next SaveEventLogIndex
  EndIf
  IRISEventLogCurrentPosition = 1
  SavingEventLog = False
EndSub
#EndIf

Dim ConfigureModemSucceeded As Boolean
Sub ConfigureModem(ConfigureModemSuccess As Boolean)
  ConfigureModemSucceeded = True
  SW12(On)
  Delay(1,10,Sec)
  SerialOpen(ModemPort,9600,0,20000,1000)
  If SerialOut(ModemPort,"ATV0" & CHR(13),"0",1,150) = 0 Then ConfigureModemSucceeded = False
  If SerialOut(ModemPort,"ATE1" & CHR(13),"0",1,150) = 0 Then ConfigureModemSucceeded = False
  If SerialOut(ModemPort,ModemConfig1,"0",1,150) = 0 Then ConfigureModemSucceeded = False
  If SerialOut(ModemPort,ModemConfig2,"0",1,150) = 0 Then ConfigureModemSucceeded = False
  If SerialOut(ModemPort,ModemConfig3,"0",1,150) = 0 Then ConfigureModemSucceeded = False
  SerialClose(ModemPort)
  SW12(Off)
  ConfigureModemSuccess = ConfigureModemSucceeded
EndSub


'This procedure generates menus for changing settings.
Sub GenerateSettingsMenu
  DisplayMenu("IRIS Main Menu",-1)
    SubMenu("Live Values")
      DisplayValue("Road Temp",Live_RoadTemp)
      DisplayValue("Air Temp",Live_AirTemp)
      DisplayValue("RH",Live_RH)
      DisplayValue("Dew Point",Live_DewPoint)
      DisplayValue("Panel Temp",Live_PanelTemp)
      DisplayValue("Battery",Live_Battery)
    EndSubMenu
    SubMenu("Communications")
      MenuItem("TCP Port",MENUStringSettings(STRINGSETTING_TCPPort))
      MenuItem("IP Address",MENUStringSettings(STRINGSETTING_PrimaryIPAddress))
      MenuItem("Backup IP",MENUStringSettings(STRINGSETTING_BackupIPAddress))
    EndSubMenu
    SubMenu("IR100 Settings")
      MenuItem("Serial #",MENUStringSettings(STRINGSETTING_IR100SerialNumber))
      MenuItem("Coeff A",MENUSettings(SETTING_Coeff_A))
      MenuItem("Coeff B",MENUSettings(SETTING_Coeff_B))
      MenuItem("Coeff C",MENUSettings(SETTING_Coeff_C))
      MenuItem("Coeff X",MENUSettings(SETTING_Coeff_X))
      MenuItem("Coeff Y",MENUSettings(SETTING_Coeff_Y))
      MenuItem("Coeff Z",MENUSettings(SETTING_Coeff_Z))
    EndSubMenu
    SubMenu("Emissivity")
      MenuItem("Surface",MENUSettings(SETTING_Emissivity))
      MenuPick(Asphalt,Concrete,Brick,Ice,Snow,Ocean)'Pick list for Emissivity
    EndSubMenu
    SubMenu("Sky View Factor")
      MenuItem("SVF Value",MENUSettings(SETTING_SVF))
    EndSubMenu
  EndMenu
EndSub

'This procedure saves the current menu settings to file and transfers them into actual
locations.
Dim SaveSettings_FileHandle As Long
Dim SaveSettings_OutputString As String * 400
Dim SaveSettings_Index As Long
Sub SaveSettings
  SettingsChanged = False
  SaveSettings_FileHandle = FileOpen(IRISSettingsFilename,"w",0)
  If SaveSettings_FileHandle <> 0 Then
    'Generate an output string from the current menu settings.
    SaveSettings_OutputString = ""
    'Numeric
    For SaveSettings_Index = 1 To MaxNumberOfSettings
      SaveSettings_OutputString = SaveSettings_OutputString & MENUSettings(SaveSettings_Index)
& ","
    Next SaveSettings_Index
    'Strings
    For SaveSettings_Index = 1 To MaxNumberOfStringSettings
```

```
      SaveSettings_OutputString = SaveSettings_OutputString &
MENUStringSettings(SaveSettings_Index) & ","
    Next SaveSettings_Index
    'Save new settings to file.
    FileWrite(SaveSettings_FileHandle,SaveSettings_OutputString,0)
    'Transfer new settings to actual locations.
    'Numeric
    For SaveSettings_Index = 1 To MaxNumberOfSettings
      Settings(SaveSettings_Index) = MENUSettings(SaveSettings_Index)
    Next SaveSettings_Index
    'Strings
    For SaveSettings_Index = 1 To MaxNumberOfStringSettings
      StringSettings(SaveSettings_Index) = MENUStringSettings(SaveSettings_Index)
    Next LoadSettings_Index
    'Copy Values where necessary.
    SVF = Settings(SETTING_SVF)
    Live_SerialNumber = StringSettings(STRINGSETTING_IR100SerialNumber)
  EndIf
  FileClose(SaveSettings_FileHandle)
  #If EventLogging Then
  'Log a startup event and include version.
  LogEvent(IRISEventCode_SettingsSaved,IRISSettingsFilename)
  #EndIf
EndSub

'This procedure loads the settings from the settings file,
'if no file exists then it loads defaults and create a new settings file.
Dim LoadSettings_FileHandle As Long
Dim SettingsFileLine As String * 400
Dim SettingsStringResult(MaxNumberOfSettings + MaxNumberOfStringSettings) As String
Dim LoadSettings_Index As Long
Sub LoadSettings
  SettingsLoading = True
  ReloadSettings = False
  LoadSettings_FileHandle = FileOpen(IRISSettingsFilename,"r",0)
  If LoadSettings_FileHandle = 0 Then
    'Unable to find or open the file, so default all values.
    'Strings
    MENUStringSettings(STRINGSETTING_PrimaryIPAddress) = DefaultPrimaryIPAddress
    MENUStringSettings(STRINGSETTING_BackupIPAddress) = DefaultBackupIPAddress
    MENUStringSettings(STRINGSETTING_TCPPort) = DefaultTCPPort
    MENUStringSettings(STRINGSETTING_IR100SerialNumber) = DefaultIR100SerialNumber
    'Numeric
    MENUSettings(SETTING_Emissivity) = Asphalt
    MENUSettings(SETTING_SVF) = Default_SVF
    MENUSettings(SETTING_Coeff_A) = Default_Coeff_A
    MENUSettings(SETTING_Coeff_B) = Default_Coeff_B
    MENUSettings(SETTING_Coeff_C) = Default_Coeff_C
    MENUSettings(SETTING_Coeff_X) = Default_Coeff_X
    MENUSettings(SETTING_Coeff_Y) = Default_Coeff_Y
    MENUSettings(SETTING_Coeff_Z) = Default_Coeff_Z
    #If EventLogging Then
    'Log a startup event and include version.
    LogEvent(IRISEventCode_SettingsDefaulted,IRISSettingsFilename)
    #EndIf
    'Now store the values as they didn't exist.
    SaveSettings
  Else
    'Load the settings from the file.
    FileReadLine(LoadSettings_FileHandle,SettingsFileLine,200)
    'Split the values up.
    SplitStr(SettingsStringResult(),SettingsFileLine,",",MaxNumberOfSettings +
MaxNumberOfStringSettings,5)
    'Transfer the values into respective locations.
    'Strings
    MENUStringSettings(STRINGSETTING_PrimaryIPAddress) = SettingsStringResult(9)
    MENUStringSettings(STRINGSETTING_BackupIPAddress) = SettingsStringResult(10)
    MENUStringSettings(STRINGSETTING_TCPPort) = SettingsStringResult(11)
    MENUStringSettings(STRINGSETTING_IR100SerialNumber) = SettingsStringResult(12)
    'Numeric
    MENUSettings(SETTING_Emissivity) = SettingsStringResult(1)
    MENUSettings(SETTING_SVF) = SettingsStringResult(2)
    MENUSettings(SETTING_Coeff_A) = SettingsStringResult(3)
    MENUSettings(SETTING_Coeff_B) =  SettingsStringResult(4)
    MENUSettings(SETTING_Coeff_C) = SettingsStringResult(5)
    MENUSettings(SETTING_Coeff_X) = SettingsStringResult(6)
    MENUSettings(SETTING_Coeff_Y) = SettingsStringResult(7)
    MENUSettings(SETTING_Coeff_Z) = SettingsStringResult(8)
  EndIf
  'Copy into actual locations.
```

```
  'Numeric
  For LoadSettings_Index = 1 To MaxNumberOfSettings
    Settings(LoadSettings_Index) = MENUSettings(LoadSettings_Index)
  Next LoadSettings_Index
  'Strings
  For LoadSettings_Index = 1 To MaxNumberOfStringSettings
    StringSettings(LoadSettings_Index) = MENUStringSettings(LoadSettings_Index)
  Next LoadSettings_Index
  'Close the file.
  FileClose(LoadSettings_FileHandle)
  'Copy Values where necessary.
  SVF = Settings(SETTING_SVF)
  Live_SerialNumber = StringSettings(STRINGSETTING_IR100SerialNumber)
  'Finished Loading.
  SettingsLoading = False
  #If EventLogging Then
  'Log a startup event and include version.
  LogEvent(IRISEventCode_SettingsLoaded,IRISSettingsFilename)
  #EndIf
EndSub

'This procedure checks to see if any changes have been made to the settings through the menu.
Sub CheckForChanges
  SettingsChanged = False
  'Numeric
  If MENUSettings(SETTING_Emissivity) <> Settings(SETTING_Emissivity) Then SettingsChanged =
True
  If MENUSettings(SETTING_Coeff_A) <> Settings(SETTING_Coeff_A) Then SettingsChanged = True
  If MENUSettings(SETTING_Coeff_B) <> Settings(SETTING_Coeff_B) Then SettingsChanged = True
  If MENUSettings(SETTING_Coeff_C) <> Settings(SETTING_Coeff_C) Then SettingsChanged = True
  If MENUSettings(SETTING_Coeff_X) <> Settings(SETTING_Coeff_X) Then SettingsChanged = True
  If MENUSettings(SETTING_Coeff_Y) <> Settings(SETTING_Coeff_Y) Then SettingsChanged = True
  If MENUSettings(SETTING_Coeff_Z) <> Settings(SETTING_Coeff_Z) Then SettingsChanged = True
  If MENUSettings(SETTING_SVF) <> Settings(SETTING_SVF) Then SettingsChanged = True
  'Strings
  If MENUStringSettings(STRINGSETTING_PrimaryIPAddress) <>
StringSettings(STRINGSETTING_PrimaryIPAddress) Then SettingsChanged = True
  If MENUStringSettings(STRINGSETTING_BackupIPAddress) <>
StringSettings(STRINGSETTING_BackupIPAddress) Then SettingsChanged = True
  If MENUStringSettings(STRINGSETTING_TCPPort) <> StringSettings(STRINGSETTING_TCPPort) Then
SettingsChanged = True
  If MENUStringSettings(STRINGSETTING_IR100SerialNumber) <>
StringSettings(STRINGSETTING_IR100SerialNumber) Then SettingsChanged = True
  If SettingsChanged Then SaveSettings
EndSub

'This procedure updates live values which can be used during setup or for quick reference.
Sub UpdateLiveValues
  Live_RoadTemp = TSurface
  Live_AirTemp = AirTemp
  Live_RH = RH
  Live_DewPoint = Dew_Point
  Live_PanelTemp = PTemp
  Live_Battery = Batt_Volt
  Live_BodyTemp = IRSensorCan_Temp
EndSub

'Main Porgram
BeginProg
  'Version Control - Transfer from conditional constant.
  IRISProgramVersion = IRISProgVer
  #If EventLogging Then
  SavingEventLog = False
  IRISEventLogCurrentPosition = 1
  'Log a startup event and include version.
  LogEvent(IRISEventCode_ProgramStarted,IRISProgramVersion)
  #EndIf
  'Configure the logger.
  SetStatus("USRDriveSize",8192) 'Create a USR drive for the site parameters file.
  'Initialise.
  CoeffsAvailable = False
  UseLoggerTemperature = False 'Default the use of the logger temperature in calcs to off.
  FirstRun = True 'Indicates that this is the first run and allows some initialisation.
  SettingsChanged = False
  SettingsLoading = False
  ReloadSettings = False
  ConnectDelay = True 'Default the connection delay to On.
  Live_RoadTemp = NaN
  Live_AirTemp = NaN
  Live_RH = NaN
```

```
  Live_DewPoint = NaN
  Live_PanelTemp = NaN
  Live_Battery = NaN
  'Load the settings from file on startup if it exists, if it is not there it will be created
with defaults.
  LoadSettings
  'Generate the menu structure.
  GenerateSettingsMenu
  'Ensure the modem is configured correctly.
  PPPClose
  CommsStep = "Configuring Modem for GPRS..."
  ModemConfigured = False
  ConfigureModem(ModemConfigured)
  If ModemConfigured Then
    CommsStep = "Modem Configured."
  Else
    CommsStep = "Unable to Configure Modem."
  EndIf

  'Setup the PPP settings in the logger to match the correct provider configuration
  SetStatus("pppinterface",ModemPort)
  SetStatus("pppUsername",PPPUsername)
  SetStatus("ppppassword",PPPPassword)
  SetStatus("pppDial","*99***1#") 'Fixed
  SetStatus("pppDialresponse",PPPdialresponse) 'Fixed if modem set to numeric response
  PPPClose 'Again as setting the above may retrigger autoconnection

  '*********************************************************************************
  'Scan Type....: Main Scan
  'Frequency....: 500 mSeconds
  'Purpose......: Use IR signal to calculate traffic count
  '*********************************************************************************
  Scan (500,mSec,0,0)
    '*** IR100 Measurements and Calculations - Start
    'IR100 Body Temperature Measurement
    BrHalf(Cal_Can,1,mV2500,3,Vx1,1,-2500,False,20000,_50Hz,1,0)
    IRSensor_Resis = 77020 * (Cal_Can / (1 - Cal_Can))
    IRSensorCan_Temp = 1 / (Settings(SETTING_Coeff_A) + Settings(SETTING_Coeff_B) *
LN(IRSensor_Resis) + Settings(SETTING_Coeff_C) * (LN(IRSensor_Resis))^3) - 273.15
    'IR100 Infrared Temperature Measurement - Temperature Compensated
    ExciteV(Vx1,2500,0)
    Delay(0,75,mSec)
    BrFull(IRSensor_Volt,1,mV2500,1,Vx1,1,2500,False,False,0,_50Hz,2.5,0)
    IRSensor_Volt_TC =  IRSensor_Volt * 1.0004 ^(IRSensorCan_Temp - 25) 'Temperature
compensated
    IRSensor_E = Settings(SETTING_Coeff_X) * IRSensor_Volt_TC^2 + Settings(SETTING_Coeff_Y) *
IRSensor_Volt_TC + Settings(SETTING_Coeff_Z)
    IRSensor_T4 = (IRSensor_E / 5.67E-8) + ((IRSensorCan_Temp + 273.15)^4)
    Previous_TSurface = TSurface
    IRSensor_T = (IRSensor_T4^0.25) - 273.15
    'Define the source for Sky Temperature.
    SkyTemp = Dew_Point
    'Correction for IRIS high infrared transmission film
    TFilm = ((IRSensor_T4 - ((AirTemp + 273.15)^4 * (1 - Film))) / Film)
    'Correction for Emissivity and Sky View Factor
    TSurface = ((TFilm - (((SkyTemp + 273.15)^4 * SVF + ((AirTemp + 273.15)^4 * (1 - SVF))) *
(1 - Settings(SETTING_Emissivity)))) / Settings(SETTING_Emissivity))^0.25 - 273.15
    '*** IR100 Measurements and Calculations - End

    'Additional Traffic Routine - Added 06/05/2010
    If TimeIntoInterval(0,10,Min) Then
      CallTable Traffic
      Traffic_Count1 = 0
      Traffic_Count2 = 0
      Traffic_Count3 = 0
      Traffic_Count4 = 0
      Traffic_Count11 = 0
      Traffic_Count22 = 0
      Traffic_Count33 = 0
      Traffic_Count44 = 0
    EndIf
    'Calculate change in signal
    Difference_TSurface = TSurface - Previous_TSurface
    'Calculate traffic count based only on +ve change in IR signal
    If Difference_TSurface >= 0.25 Then
      Traffic_Count1 = Traffic_Count1 + 1
    EndIf
    If Difference_TSurface >= 0.5 Then
      Traffic_Count2 = Traffic_Count2 + 1
    EndIf
```

```
    If Difference_TSurface >= 0.75 Then
      Traffic_Count3 = Traffic_Count3 + 1
    EndIf
    If Difference_TSurface >= 1 Then
      Traffic_Count4 = Traffic_Count4 + 1
    EndIf
    'Calculate traffic count based on +ve and -ve changes in IR signal
    If Difference_TSurface >= 0.25 OR Difference_TSurface <= -0.25 Then
      Traffic_Count11 = Traffic_Count11 + 1
    EndIf
    If Difference_TSurface >= 0.5 OR Difference_TSurface <= -0.5 Then
      Traffic_Count22 = Traffic_Count22 + 1
    EndIf
    If Difference_TSurface >= 0.75 OR Difference_TSurface <= -0.75 Then
      Traffic_Count33 = Traffic_Count33 + 1
    EndIf
    If Difference_TSurface >= 1 OR Difference_TSurface <= -1 Then
      Traffic_Count44 = Traffic_Count44 + 1
    EndIf
  NextScan

  '*********************************************************************************
  'Scan Type....: Slow Sequence - One
  'Frequency....: 5 Seconds
  'Purpose......: CS215 Measurement
  '*********************************************************************************
  SlowSequence
  Scan (5,Sec,10,0)
    'Store the Panel Temperature and Battery Voltage
    PanelTemp(PTemp,250)
    Battery(Batt_Volt)
    'Compile Coefficients Flag
    CoeffsAvailable = (Settings(SETTING_Coeff_A) <> NaN) AND (Settings(SETTING_Coeff_B) <>
NaN) AND (Settings(SETTING_Coeff_C) <> NaN) AND (Settings(SETTING_Coeff_X) <> NaN) AND
(Settings(SETTING_Coeff_Y) <> NaN) AND (Settings(SETTING_Coeff_Z) <> NaN)
    'Every 2 Minutes measure the Air Temperature and RH and calculate a Dew Point.
    If TimeIntoInterval(0,2,Min) OR FirstRun Then
      'If the UseLoggerTemperature flag is set then substitue the logger temperature for the
CS215.
      If UseLoggerTemperature Then
        AirTemp = PTemp
        Dew_Point = AirTemp
      Else
        'Use the CS215
        SDI12Recorder(CS215(),1,0,"M!",1,0) 'CS215 Air Temp & RH measurement
        #If EventLogging Then
        If (AirTemp = NaN) AND (RH = NaN) Then
          LogEvent(IRISEventCode_CS215Error,"CS215 No Air Temp or RH")
        ElseIf (AirTemp = NaN) Then
          LogEvent(IRISEventCode_CS215Error,"CS215 No Air Temp")
        ElseIf (RH = NaN) Then
          LogEvent(IRISEventCode_CS215Error,"CS215 No RH")
        EndIf
        #EndIf
        'Calculate Dew Point using Teten's equation.
        SatVP(SVP,AirTemp)
        VP = RH*(SVP/100)
        Dew_Point = (241.88 * LN(VP/0.61078)) / (17.558 - LN(VP/0.61078))
      EndIf
    EndIf
    'Store Data.
    CallTable IrisData
    'Update the live values.
    UpdateLiveValues
    'Turn off first run.
    If FirstRun Then FirstRun = False
  NextScan

  SlowSequence
  '*********************************************************************************
  'Scan Type....: Slow Sequence - Two
  'Frequency....: 1 Minute
  'Purpose......: Monitoring of setting changes and reloading of settings
  '*********************************************************************************
  Scan (1,Min,0,0)
    'Check for changes to the settings or for a forced reload.
    If NOT SettingsLoading Then CheckForChanges
    If ReloadSettings Then LoadSettings
    #If EventLogging Then
    SaveEventLog
```

```
    #EndIf
  NextScan

  SlowSequence
  '*********************************************************************************
  'Scan Type....: Slow Sequence - Three
  'Frequency....: 20 Minutes
  'Purpose......: Callback communications for the IRIS Bureau Service.
  '*********************************************************************************
  Scan (20,Min,0,0)
    CommsStep = "Comms Initialising..."
    '***** COMMS START *****
    If Batt_Volt > MinimumBatteryThresholdForComms Then
      #If DebugMode AND EventLogging Then
      'Log a stop event and include version.
      LogEvent(IRISEventCode_CommsStarting,"Callback Comms Starting")
      #EndIf
      'Power on and start the modem.
      CommsStep = "Powering Modem"
      SW12(On) 'Power on the Modem.
      CommsStep = "Checking Modem"
      SerialOpen(ModemPort,9600,0,20000,1000) 'Open a serial connection to the modem.
      ModemStarted = (SerialOut(ModemPort,CR,"+WIND: 4",1,5000) <> 0)
      If NOT ModemStarted Then ModemStarted = (SerialOut(ModemPort,"AT+CFUN=1" & CR,"+WIND:
4",1,5000) <> 0) 'Try again after resetting the modem
      SerialClose(ModemPort) 'Release the serial port connection.
      'Open ports.
      If NOT ModemStarted Then
        'Modem failed to start suitably so flag an error.
        #If EventLogging Then
        'Log a failure event and include version.
        LogEvent(IRISEventCode_ModemStartFailed,"Modem Failed to Start")
        #EndIf
      EndIf
      'The program will attempt to create a PPP connection regardless of the modem startup,
      'this allows for testing or configurations with a permanently powered modem, an event
will
      'already have been logged anyway.
      CommsStep = "Opening PPP Connection"
      'Modem started so attempt to open a PPP Connection.
      PPPAddress = PPPBlank 'Set the PPPAddress to a known blank value.
      Timer(0,uSec,2)
      Do
        PPPAddress = PPPOpen
        COMMSTimer = Timer(0,uSec,4)/1000000
      Loop Until (PPPAddress <> PPPBlank) OR (COMMSTimer >= PPPTimeOut)
      Timer(0,uSec,1)
      If PPPAddress <> PPPBlank Then
        'PPP Connection successful so attempt to open an IP Port using the primary IP address.
        CommsStep = "Opening Primary IP - " & StringSettings(STRINGSETTING_PrimaryIPAddress) &
" - " & StringSettings(STRINGSETTING_TCPPort)
        IPPort = IPPortBlank 'Set to Default IP Port
        Timer(0,uSec,2)
        Do
          CommsTCPPort = StringSettings(STRINGSETTING_TCPPort)
          IPPort = TCPOpen(StringSettings(STRINGSETTING_PrimaryIPAddress),CommsTCPPort,0)
          COMMSTimer = Timer(0,uSec,4)/1000000
        Loop Until (IPPort <> IPPortBlank) OR (COMMSTimer >= IPTimeOut)
        Timer(0,uSec,1)
        'Try opening an IP Port using the alternative IP address if the primary address has
failed.
        If IPPort = IPPortBlank Then
          CommsStep = "Opening Backup IP - " & StringSettings(STRINGSETTING_BackupIPAddress) &
" - " & StringSettings(STRINGSETTING_TCPPort)
          Timer(0,uSec,2)
          Do
            CommsTCPPort = StringSettings(STRINGSETTING_TCPPort)
            IPPort = TCPOpen(StringSettings(STRINGSETTING_BackupIPAddress),CommsTCPPort,0)
            COMMSTimer = Timer(0,uSec,4)/1000000
          Loop Until (IPPort <> IPPortBlank) OR (COMMSTimer >= IPTimeOut)
          Timer(0,uSec,1)
        EndIf
        'Check IP success.
        If IPPort <> IPPortBlank Then
          CommsStep = "Initiating Callback"
          'We have an open IP port so continue and initiate callback to LoggerNet
          SendVariables(SendResult,IPPort,4091,4091,0,1000,"Public","Callback",Scratch,1)
          'Check if we need to stay online longer at the moment, this allows us to grab the
connection should it be necessary.
```

```
          If TimeIntoInterval(ExtendedOnlineStartTime,OneDayInMinutes,Min) Then ConnectDelay =
True 'At 8am enable connection delaying.
          If TimeIntoInterval(ExtendedOnlineEndTime,OneDayInMinutes,Min) Then ConnectDelay =
False 'At 6pm disable connection delaying.
          If ConnectDelay Then Delay(1,5,Sec)
          'Time the remainder to limit time online.
          Timer(0,uSec,2)
          Do
            COMMSTimer = Timer(0,uSec,4)/1000000
          Loop Until (ComPortIsActive(IPPort) = 0) OR (COMMSTimer >= COMMSTimeOut)
          Timer(0,uSec,1)
          'Close the PPP Connection.
          If NOT PPPClose Then
            'Failed to close PPP port properly so flag error.
            #If EventLogging Then
            'Log a stop event and include version.
            LogEvent(IRISEventCode_PPPCloseFailed,"PPP Connection Close Failed")
            #EndIf
          EndIf
        Else
          'We failed to open an IP port on either the primary or secondary port so flag an
error.
          #If EventLogging Then
          'Log a stop event and include version.
          LogEvent(IRISEventCode_IPConnectFailed,"IP Connection Open Failed")
          #EndIf
        EndIf
      Else
        'PPP Connection Failed.
        PPPClose
        #If EventLogging Then
        'Log a stop event and include version.
        LogEvent(IRISEventCode_PPPStartFailed,"PPP Connection Open Failed")
        #EndIf
      EndIf
      'Force PPP close.
      PPPClose
      'Shut down the modem
      CommsStep = "Powering Off Modem"
      SerialOpen(ModemPort,9600,0,20000,1000) 'Open a serial connection to the modem.
      Delay(1,1,sec) 'Delay needed for the Wavecom to let it respond to further commands
      SerialOut(ModemPort,"AT+CFUN=0" & CR,"+WIND: 8",1,1000)
      SerialClose(ModemPort) 'Release the serial port connection.
      SW12(Off) 'Power on the Modem.
    Else
      'Battery too low for comms.
      #If EventLogging Then
      'Log a stop event and include version.
      LogEvent(IRISEventCode_BatteryTooLowForComms,"Battery Voltage = " & Batt_Volt)
      #EndIf
    EndIf
    '***** COMMS END *****
    CommsStep = "Comms Idle"
  NextScan

EndProg
```

APPENDIX 4

TRAFFIC DATA

DATE & TIME	IRIS TR	Loop D SB
28/06/2010 01:00	29	9
28/06/2010 02:00	17	14
28/06/2010 03:00	17	7
28/06/2010 04:00	17	8
28/06/2010 05:00	25	43
28/06/2010 06:00	117	84
28/06/2010 07:00	312	202
28/06/2010 08:00	485	404
28/06/2010 09:00	1059	290
28/06/2010 10:00	760	317
28/06/2010 11:00	422	327
28/06/2010 12:00	518	384
28/06/2010 13:00	694	365
28/06/2010 14:00	778	464
28/06/2010 15:00	877	549
28/06/2010 16:00	852	619
28/06/2010 17:00	597	653
28/06/2010 18:00	616	418
28/06/2010 19:00	429	277
28/06/2010 20:00	283	234
28/06/2010 21:00	189	174
28/06/2010 22:00	106	107
28/06/2010 23:00	69	46
29/06/2010 00:00	57	17
29/06/2010 01:00	17	10
29/06/2010 02:00	13	10
29/06/2010 03:00	8	3
29/06/2010 04:00	12	12
29/06/2010 05:00	6	36
29/06/2010 06:00	42	101
29/06/2010 07:00	66	204
29/06/2010 08:00	112	405
29/06/2010 09:00	150	285
29/06/2010 10:00	144	285
29/06/2010 11:00	298	355
29/06/2010 12:00	429	406
29/06/2010 13:00	423	369
29/06/2010 14:00	618	487
29/06/2010 15:00	833	510
29/06/2010 16:00	875	638
29/06/2010 17:00	793	682
29/06/2010 18:00	684	433
29/06/2010 19:00	478	353
29/06/2010 20:00	336	266
29/06/2010 21:00	249	159
29/06/2010 22:00	144	134
29/06/2010 23:00	86	70
30/06/2010 00:00	42	30
30/06/2010 01:00	12	17
30/06/2010 02:00	10	8
30/06/2010 03:00	9	7
30/06/2010 04:00	8	9
30/06/2010 05:00	26	32
30/06/2010 06:00	131	98
30/06/2010 07:00	293	240
30/06/2010 08:00	505	401
30/06/2010 09:00	371	299
30/06/2010 10:00	344	341
30/06/2010 11:00	468	385
30/06/2010 12:00	597	380
30/06/2010 13:00	704	391
30/06/2010 14:00	687	449
30/06/2010 15:00	694	553
30/06/2010 16:00	908	663
30/06/2010 17:00	813	648
30/06/2010 18:00	784	546
30/06/2010 19:00	576	329
30/06/2010 20:00	291	285
30/06/2010 21:00	214	174
30/06/2010 22:00	162	169
30/06/2010 23:00	130	81
01/07/2010 00:00	69	38
01/07/2010 01:00	24	15
01/07/2010 02:00	18	13
01/07/2010 03:00	10	11
01/07/2010 04:00	5	10
01/07/2010 05:00	13	40
01/07/2010 06:00	90	111
01/07/2010 07:00	192	216
01/07/2010 08:00	280	387
01/07/2010 09:00	269	300
01/07/2010 10:00	286	336
01/07/2010 11:00	285	314

01/07/2010 12:00	211	399
01/07/2010 13:00	404	392
01/07/2010 14:00	309	465
01/07/2010 15:00	291	544
01/07/2010 16:00	313	644
01/07/2010 17:00	208	690
01/07/2010 18:00	168	488
01/07/2010 19:00	96	317
01/07/2010 20:00	54	252
01/07/2010 21:00	75	188
01/07/2010 22:00	30	143
01/07/2010 23:00	17	66
02/07/2010 00:00	11	24
02/07/2010 01:00	0	14
02/07/2010 02:00	3	5
02/07/2010 03:00	6	5
02/07/2010 04:00	13	16
02/07/2010 05:00	30	37
02/07/2010 06:00	78	105
02/07/2010 07:00	179	216
02/07/2010 08:00	106	394
02/07/2010 09:00	207	314
02/07/2010 10:00	216	337
02/07/2010 11:00	241	404
02/07/2010 12:00	451	419
02/07/2010 13:00	630	484
02/07/2010 14:00	647	524
02/07/2010 15:00	737	603
02/07/2010 16:00	892	668
02/07/2010 17:00	712	547
02/07/2010 18:00	659	498
02/07/2010 19:00	547	392
02/07/2010 20:00	431	260
02/07/2010 21:00	214	189
02/07/2010 22:00	110	136
02/07/2010 23:00	122	109
03/07/2010 00:00	59	64
03/07/2010 01:00	65	35
03/07/2010 02:00	36	36
03/07/2010 03:00	21	18
03/07/2010 04:00	9	11
03/07/2010 05:00	12	21
03/07/2010 06:00	26	47
03/07/2010 07:00	44	104
03/07/2010 08:00	253	201
03/07/2010 09:00	173	282
03/07/2010 10:00	736	337
03/07/2010 11:00	478	390
03/07/2010 12:00	300	417
03/07/2010 13:00	456	476
03/07/2010 14:00	609	438
03/07/2010 15:00	616	453
03/07/2010 16:00	426	406
03/07/2010 17:00	512	422
03/07/2010 18:00	610	401
03/07/2010 19:00	533	278
03/07/2010 20:00	298	182
03/07/2010 21:00	179	165
03/07/2010 22:00	186	102
03/07/2010 23:00	142	91
04/07/2010 00:00	89	67
04/07/2010 01:00	60	41
04/07/2010 02:00	37	31
04/07/2010 03:00	33	31
04/07/2010 04:00	29	16
04/07/2010 05:00	18	16
04/07/2010 06:00	32	25
04/07/2010 07:00	50	41
04/07/2010 08:00	26	75
04/07/2010 09:00	36	128
04/07/2010 10:00	161	219
04/07/2010 11:00	240	349
04/07/2010 12:00	235	442
04/07/2010 13:00	340	368
04/07/2010 14:00	222	379
04/07/2010 15:00	101	451
04/07/2010 16:00	97	368
04/07/2010 17:00	138	282
04/07/2010 18:00	315	225
04/07/2010 19:00	192	194
04/07/2010 20:00	110	142
04/07/2010 21:00	87	131
04/07/2010 22:00	32	78
04/07/2010 23:00	19	45
06/07/2010 00:00	32	28
06/07/2010 01:00	6	8
06/07/2010 02:00	10	6
06/07/2010 03:00	6	3
06/07/2010 04:00	9	10
06/07/2010 05:00	12	41
06/07/2010 06:00	127	124
06/07/2010 07:00	294	189
06/07/2010 08:00	277	425
06/07/2010 09:00	1082	326
06/07/2010 10:00	965	313
06/07/2010 11:00	452	368

06/07/2010 12:00	482	365
06/07/2010 13:00	524	346
06/07/2010 14:00	708	466
06/07/2010 15:00	899	530
06/07/2010 16:00	1002	672
06/07/2010 17:00	803	669
06/07/2010 18:00	608	443
06/07/2010 19:00	563	337
06/07/2010 20:00	354	242
06/07/2010 21:00	186	143
06/07/2010 22:00	144	119
06/07/2010 23:00	82	74
07/07/2010 00:00	59	26
07/07/2010 01:00	16	10
07/07/2010 02:00	11	4
07/07/2010 03:00	8	4
07/07/2010 04:00	0	8
07/07/2010 05:00	4	30
07/07/2010 06:00	22	112
07/07/2010 07:00	55	227
07/07/2010 08:00	178	409
07/07/2010 09:00	174	309
07/07/2010 10:00	200	332
07/07/2010 11:00	265	355
07/07/2010 12:00	202	402
07/07/2010 13:00	180	408
07/07/2010 14:00	115	467
07/07/2010 15:00	273	540
07/07/2010 16:00	139	642
07/07/2010 17:00	228	643
07/07/2010 18:00	107	477
07/07/2010 19:00	71	302
07/07/2010 20:00	77	241
07/07/2010 21:00	55	172
07/07/2010 22:00	36	130
07/07/2010 23:00	25	59
08/07/2010 00:00	7	23
08/07/2010 01:00	5	16
08/07/2010 02:00	2	10
08/07/2010 03:00	3	8
08/07/2010 04:00	9	12
08/07/2010 05:00	2	38
08/07/2010 06:00	38	121
08/07/2010 07:00	60	196
08/07/2010 08:00	188	408
08/07/2010 09:00	936	335
08/07/2010 10:00	989	284
08/07/2010 11:00	559	356
08/07/2010 12:00	319	405
08/07/2010 13:00	408	383
08/07/2010 14:00	596	456
08/07/2010 15:00	612	545
08/07/2010 16:00	605	623
08/07/2010 17:00	605	666
08/07/2010 18:00	648	478
08/07/2010 19:00	431	339
08/07/2010 20:00	274	288
08/07/2010 21:00	179	201
08/07/2010 22:00	121	170
08/07/2010 23:00	95	62
09/07/2010 00:00	54	35
09/07/2010 01:00	32	13
09/07/2010 02:00	6	9
09/07/2010 03:00	1	5
09/07/2010 04:00	13	7
09/07/2010 05:00	20	35
09/07/2010 06:00	85	105
09/07/2010 07:00	232	199
09/07/2010 08:00	374	390
09/07/2010 09:00	220	310
09/07/2010 10:00	193	354
09/07/2010 11:00	292	322
09/07/2010 12:00	305	448
09/07/2010 13:00	312	493
09/07/2010 14:00	383	501
09/07/2010 15:00	216	616
09/07/2010 16:00	349	631
09/07/2010 17:00	341	601
09/07/2010 18:00	472	458
09/07/2010 19:00	325	321
09/07/2010 20:00	229	291
09/07/2010 21:00	103	193
09/07/2010 22:00	55	135
09/07/2010 23:00	16	100
10/07/2010 00:00	13	62
10/07/2010 01:00	17	47
10/07/2010 02:00	15	21
10/07/2010 03:00	4	11
10/07/2010 04:00	3	18
10/07/2010 05:00	6	21
10/07/2010 06:00	5	58
10/07/2010 07:00	15	91
10/07/2010 08:00	15	166
10/07/2010 09:00	30	219
10/07/2010 10:00	50	276
10/07/2010 11:00	129	394

10/07/2010 12:00	186	489
10/07/2010 13:00	342	424
10/07/2010 14:00	346	463
10/07/2010 15:00	275	430
10/07/2010 16:00	435	490
10/07/2010 17:00	276	437
10/07/2010 18:00	383	397
10/07/2010 19:00	348	286
10/07/2010 20:00	215	180
10/07/2010 21:00	118	138
10/07/2010 22:00	80	124
10/07/2010 23:00	36	87
11/07/2010 00:00	61	74
11/07/2010 01:00	31	36
11/07/2010 02:00	8	38
11/07/2010 03:00	2	30
11/07/2010 04:00	4	15
11/07/2010 05:00	12	11
11/07/2010 06:00	23	29
11/07/2010 07:00	35	49
11/07/2010 08:00	106	86
11/07/2010 09:00	209	153
11/07/2010 10:00	545	257
11/07/2010 11:00	624	371
11/07/2010 12:00	391	465
11/07/2010 13:00	668	380
11/07/2010 14:00	702	432
11/07/2010 15:00	645	444
11/07/2010 16:00	552	384
11/07/2010 17:00	463	292
11/07/2010 18:00	392	262
11/07/2010 19:00	298	205
11/07/2010 20:00	188	120
11/07/2010 21:00	112	102
11/07/2010 22:00	79	70
11/07/2010 23:00	69	52
12/07/2010 00:00	32	21
12/07/2010 01:00	9	8
12/07/2010 02:00	8	5
12/07/2010 03:00	8	14
12/07/2010 04:00	14	11
12/07/2010 05:00	28	35
12/07/2010 06:00	90	108
12/07/2010 07:00	208	204
12/07/2010 08:00	152	380
12/07/2010 09:00	160	298
12/07/2010 10:00	343	276
12/07/2010 11:00	404	350
12/07/2010 12:00	530	358
12/07/2010 13:00	736	361
12/07/2010 14:00	534	448
12/07/2010 15:00	895	551
12/07/2010 16:00	675	660
12/07/2010 17:00	641	644
12/07/2010 18:00	521	448
12/07/2010 19:00	273	310
12/07/2010 20:00	209	262
12/07/2010 21:00	164	174
12/07/2010 22:00	99	120
12/07/2010 23:00	46	52
13/07/2010 00:00	42	23
13/07/2010 01:00	5	15
13/07/2010 02:00	7	4
13/07/2010 03:00	11	8
13/07/2010 04:00	9	10
13/07/2010 05:00	12	37
13/07/2010 06:00	84	115
13/07/2010 07:00	197	223
13/07/2010 08:00	342	407
13/07/2010 09:00	423	317
13/07/2010 10:00	442	287
13/07/2010 11:00	162	299
13/07/2010 12:00	141	360
13/07/2010 13:00	373	365
13/07/2010 14:00	375	464
13/07/2010 15:00	345	551
13/07/2010 16:00	161	624
13/07/2010 17:00	171	697
13/07/2010 18:00	174	477
13/07/2010 19:00	102	297
13/07/2010 20:00	31	253
13/07/2010 21:00	10	151
13/07/2010 22:00	8	118
13/07/2010 23:00	22	52
14/07/2010 00:00	6	22
14/07/2010 01:00	5	15
14/07/2010 02:00	6	12
14/07/2010 03:00	1	4
14/07/2010 04:00	1	8
14/07/2010 05:00	2	45
14/07/2010 06:00	15	98
14/07/2010 07:00	42	199
14/07/2010 08:00	159	383
14/07/2010 09:00	378	276
14/07/2010 10:00	622	298
14/07/2010 11:00	365	387

14/07/2010 12:00	265	386
14/07/2010 13:00	340	387
14/07/2010 14:00	285	455
14/07/2010 15:00	402	543
14/07/2010 16:00	501	654
14/07/2010 17:00	490	659
14/07/2010 18:00	510	484
14/07/2010 19:00	232	298
14/07/2010 20:00	133	256
14/07/2010 21:00	95	187
14/07/2010 22:00	51	145
14/07/2010 23:00	9	81
15/07/2010 00:00	6	30
15/07/2010 01:00	1	19
15/07/2010 02:00	2	5
15/07/2010 03:00	0	14
15/07/2010 04:00	3	11
15/07/2010 05:00	2	39
15/07/2010 06:00	19	104
15/07/2010 07:00	32	200
15/07/2010 08:00	88	376
15/07/2010 09:00	134	336
15/07/2010 10:00	205	308
15/07/2010 11:00	223	397
15/07/2010 12:00	197	417
15/07/2010 13:00	269	382
15/07/2010 14:00	301	459
15/07/2010 15:00	326	564
15/07/2010 16:00	191	663
15/07/2010 17:00	473	641
15/07/2010 18:00	391	478
15/07/2010 19:00	186	314
15/07/2010 20:00	43	253
15/07/2010 21:00	12	184
15/07/2010 22:00	8	131
15/07/2010 23:00	1	62
16/07/2010 00:00	3	35
16/07/2010 01:00	4	22
16/07/2010 02:00	8	11
16/07/2010 03:00	2	7
16/07/2010 04:00	4	7
16/07/2010 05:00	0	38
16/07/2010 06:00	25	116
16/07/2010 07:00	29	179
16/07/2010 08:00	62	420
16/07/2010 09:00	96	281
16/07/2010 10:00	107	335
16/07/2010 11:00	221	404
16/07/2010 12:00	169	428
16/07/2010 13:00	300	434
16/07/2010 14:00	314	486
16/07/2010 15:00	377	586
16/07/2010 16:00	683	657
16/07/2010 17:00	656	640
16/07/2010 18:00	697	439
16/07/2010 19:00	482	390
16/07/2010 20:00	256	266
27/07/2010 00:00	15	27
27/07/2010 01:00	5	14
27/07/2010 02:00	9	3
27/07/2010 03:00	6	9
27/07/2010 04:00	6	9
27/07/2010 05:00	6	39
27/07/2010 06:00	79	83
27/07/2010 07:00	95	166
27/07/2010 08:00	188	265
27/07/2010 09:00	257	261
27/07/2010 10:00	171	312
27/07/2010 11:00	342	371
27/07/2010 12:00	459	389
27/07/2010 13:00	610	413
27/07/2010 14:00	581	444
27/07/2010 15:00	626	575
27/07/2010 16:00	630	614
27/07/2010 17:00	604	670
27/07/2010 18:00	536	451
27/07/2010 19:00	440	332
27/07/2010 20:00	334	252
27/07/2010 21:00	198	175
27/07/2010 22:00	90	119
27/07/2010 23:00	76	55
28/07/2010 00:00	40	36
28/07/2010 01:00	23	24
28/07/2010 02:00	10	6
28/07/2010 03:00	7	9
28/07/2010 04:00	18	7
28/07/2010 05:00	23	40
28/07/2010 06:00	73	85
28/07/2010 07:00	168	184
28/07/2010 08:00	669	275
28/07/2010 09:00	917	256
28/07/2010 10:00	490	320
28/07/2010 11:00	248	393
28/07/2010 12:00	403	388
28/07/2010 13:00	290	375
28/07/2010 14:00	541	433

28/07/2010 15:00	515	505	30/07/2010 15:00	386	565
28/07/2010 16:00	414	570	30/07/2010 16:00	177	644
28/07/2010 17:00	580	633	30/07/2010 17:00	80	586
28/07/2010 18:00	514	489	30/07/2010 18:00	116	443
28/07/2010 19:00	312	343	30/07/2010 19:00	62	341
28/07/2010 20:00	231	286	30/07/2010 20:00	43	269
28/07/2010 21:00	153	190	30/07/2010 21:00	9	200
28/07/2010 22:00	125	138	30/07/2010 22:00	4	131
28/07/2010 23:00	102	76	30/07/2010 23:00	4	97
29/07/2010 00:00	31	34	31/07/2010 00:00	2	56
29/07/2010 01:00	16	22	31/07/2010 01:00	3	26
29/07/2010 02:00	11	10	31/07/2010 02:00	0	16
29/07/2010 03:00	8	9	31/07/2010 03:00	2	15
29/07/2010 04:00	17	13	31/07/2010 04:00	2	15
29/07/2010 05:00	9	33	31/07/2010 05:00	8	15
29/07/2010 06:00	40	83	31/07/2010 06:00	25	42
29/07/2010 07:00	106	153	31/07/2010 07:00	46	96
29/07/2010 08:00	211	292	31/07/2010 08:00	46	139
29/07/2010 09:00	180	299	31/07/2010 09:00	63	199
29/07/2010 10:00	195	320	31/07/2010 10:00	101	362
29/07/2010 11:00	345	348	31/07/2010 11:00	174	421
29/07/2010 12:00	426	408	31/07/2010 12:00	262	458
29/07/2010 13:00	431	413	31/07/2010 13:00	392	483
29/07/2010 14:00	620	458	31/07/2010 14:00	457	454
29/07/2010 15:00	610	539	31/07/2010 15:00	465	490
29/07/2010 16:00	633	666	31/07/2010 16:00	484	460
29/07/2010 17:00	730	647	31/07/2010 17:00	522	435
29/07/2010 18:00	614	473	31/07/2010 18:00	455	393
29/07/2010 19:00	450	341	31/07/2010 19:00	382	295
29/07/2010 20:00	293	301	31/07/2010 20:00	251	193
29/07/2010 21:00	216	211	31/07/2010 21:00	125	178
29/07/2010 22:00	159	130	31/07/2010 22:00	54	115
29/07/2010 23:00	78	67	31/07/2010 23:00	34	79
30/07/2010 00:00	54	36	01/08/2010 00:00	18	65
30/07/2010 01:00	29	21	01/08/2010 01:00	21	50
30/07/2010 02:00	12	10	01/08/2010 02:00	13	36
30/07/2010 03:00	14	8	01/08/2010 03:00	19	29
30/07/2010 04:00	14	7	01/08/2010 04:00	10	18
30/07/2010 05:00	10	40	01/08/2010 05:00	9	19
30/07/2010 06:00	93	90	01/08/2010 06:00	23	32
30/07/2010 07:00	177	175	01/08/2010 07:00	21	61
30/07/2010 08:00	215	265	01/08/2010 08:00	20	72
30/07/2010 09:00	184	287	01/08/2010 09:00	22	115
30/07/2010 10:00	195	323	01/08/2010 10:00	34	247
30/07/2010 11:00	333	396	01/08/2010 11:00	108	336
30/07/2010 12:00	576	452	01/08/2010 12:00	265	406
30/07/2010 13:00	472	460	01/08/2010 13:00	438	420
30/07/2010 14:00	436	519	01/08/2010 14:00	475	409

01/08/2010 15:00	423	433
01/08/2010 16:00	475	383
01/08/2010 17:00	393	247
01/08/2010 18:00	387	209
01/08/2010 19:00	307	178
01/08/2010 20:00	144	185
01/08/2010 21:00	141	109
01/08/2010 22:00	139	100
01/08/2010 23:00	70	48
02/08/2010 00:00	33	38
02/08/2010 01:00	19	8
02/08/2010 02:00	7	9
02/08/2010 03:00	14	7
02/08/2010 04:00	14	13
02/08/2010 05:00	31	28
02/08/2010 06:00	80	85
02/08/2010 07:00	144	144
02/08/2010 08:00	381	263
02/08/2010 09:00	662	273
02/08/2010 10:00	465	321
02/08/2010 11:00	663	342
02/08/2010 12:00	565	336
02/08/2010 14:00	836	441
02/08/2010 15:00	899	481
02/08/2010 16:00	810	609
02/08/2010 17:00	701	625
02/08/2010 18:00	566	443
02/08/2010 19:00	362	292
02/08/2010 20:00	226	244
02/08/2010 21:00	170	171
02/08/2010 22:00	160	135
02/08/2010 23:00	89	40
03/08/2010 00:00	31	20
03/08/2010 01:00	14	15
03/08/2010 02:00	6	9
03/08/2010 03:00	21	6
03/08/2010 04:00	5	4
03/08/2010 05:00	14	29
03/08/2010 06:00	95	99
03/08/2010 07:00	168	145
03/08/2010 08:00	143	259
03/08/2010 09:00	243	268
03/08/2010 10:00	198	275
03/08/2010 11:00	255	401
03/08/2010 12:00	267	395
03/08/2010 13:00	274	408
03/08/2010 14:00	414	429
03/08/2010 15:00	506	476
03/08/2010 16:00	515	614
03/08/2010 17:00	552	655
03/08/2010 18:00	620	496
03/08/2010 19:00	364	296
03/08/2010 20:00	278	242
03/08/2010 21:00	140	168
03/08/2010 22:00	108	103
03/08/2010 23:00	62	62
04/08/2010 00:00	33	19
04/08/2010 01:00	6	10
04/08/2010 02:00	3	6
04/08/2010 03:00	1	8
04/08/2010 04:00	8	10
04/08/2010 05:00	18	32
04/08/2010 06:00	83	84
04/08/2010 07:00	144	156
04/08/2010 08:00	149	295
04/08/2010 09:00	86	261
04/08/2010 10:00	291	349
04/08/2010 11:00	498	411
04/08/2010 12:00	418	398
04/08/2010 13:00	419	423
04/08/2010 14:00	474	452
04/08/2010 15:00	590	498
04/08/2010 16:00	762	628
04/08/2010 17:00	748	728
04/08/2010 18:00	584	463
04/08/2010 19:00	382	336
04/08/2010 20:00	265	244
04/08/2010 21:00	205	205
04/08/2010 22:00	205	124
04/08/2010 23:00	103	79
05/08/2010 00:00	52	33
05/08/2010 01:00	23	13
05/08/2010 02:00	17	16
05/08/2010 03:00	14	11
05/08/2010 04:00	13	12
05/08/2010 05:00	19	31
05/08/2010 06:00	52	80
05/08/2010 07:00	113	156
05/08/2010 08:00	486	269
05/08/2010 09:00	441	295
05/08/2010 10:00	344	340
05/08/2010 11:00	429	394
05/08/2010 12:00	398	397
05/08/2010 13:00	541	434
05/08/2010 14:00	820	471
05/08/2010 15:00	957	544

05/08/2010 16:00	854	601
05/08/2010 17:00	667	627
05/08/2010 18:00	587	502
05/08/2010 19:00	477	311
05/08/2010 20:00	316	298
05/08/2010 21:00	190	181
05/08/2010 22:00	151	159
05/08/2010 23:00	100	52
06/08/2010 00:00	43	34
06/08/2010 01:00	13	10
06/08/2010 02:00	4	10
06/08/2010 03:00	12	9
06/08/2010 04:00	11	7
06/08/2010 05:00	12	33
06/08/2010 06:00	72	82
06/08/2010 07:00	165	156
06/08/2010 08:00	180	286
06/08/2010 09:00	111	272
06/08/2010 10:00	84	321
06/08/2010 11:00	78	429
06/08/2010 12:00	147	447
06/08/2010 13:00	357	462
06/08/2010 14:00	186	528
06/08/2010 15:00	216	551
06/08/2010 16:00	187	609
06/08/2010 17:00	314	610
06/08/2010 18:00	167	478
06/08/2010 19:00	122	338
06/08/2010 20:00	70	261
06/08/2010 21:00	21	201
06/08/2010 22:00	23	140
06/08/2010 23:00	35	100
07/08/2010 00:00	8	76
07/08/2010 01:00	18	25
07/08/2010 02:00	7	20
07/08/2010 03:00	4	12
07/08/2010 04:00	2	12
07/08/2010 05:00	2	25
07/08/2010 06:00	15	47
07/08/2010 07:00	29	85
07/08/2010 08:00	31	135
07/08/2010 09:00	50	184
07/08/2010 10:00	61	326
07/08/2010 11:00	337	440
07/08/2010 12:00	411	430
07/08/2010 13:00	439	470
07/08/2010 14:00	491	425
07/08/2010 15:00	505	445
07/08/2010 16:00	713	454
07/08/2010 17:00	542	443
07/08/2010 18:00	463	372
07/08/2010 19:00	348	308
07/08/2010 20:00	265	210
07/08/2010 21:00	179	150
07/08/2010 22:00	81	117
07/08/2010 23:00	84	88
08/08/2010 00:00	49	62
08/08/2010 01:00	34	49
08/08/2010 02:00	42	41
08/08/2010 03:00	25	31
08/08/2010 04:00	16	19
08/08/2010 05:00	16	16
08/08/2010 06:00	28	20
08/08/2010 07:00	35	44
08/08/2010 08:00	46	77
08/08/2010 09:00	183	150
08/08/2010 10:00	349	276
08/08/2010 11:00	206	380
08/08/2010 12:00	271	429
08/08/2010 13:00	491	425
08/08/2010 14:00	486	415
08/08/2010 15:00	490	409
08/08/2010 16:00	442	356
08/08/2010 17:00	453	296
08/08/2010 18:00	426	236
08/08/2010 19:00	291	183
08/08/2010 20:00	208	185
08/08/2010 21:00	160	144
08/08/2010 22:00	123	67
08/08/2010 23:00	83	47
09/08/2010 00:00	39	17
09/08/2010 01:00	21	18
09/08/2010 02:00	9	9
09/08/2010 03:00	13	7
09/08/2010 04:00	10	12
09/08/2010 05:00	21	36
09/08/2010 06:00	78	80
09/08/2010 07:00	177	159
09/08/2010 08:00	274	282
09/08/2010 09:00	177	283
09/08/2010 10:00	129	276
09/08/2010 11:00	254	345
09/08/2010 12:00	228	403
09/08/2010 13:00	141	435
09/08/2010 14:00	130	416
09/08/2010 15:00	79	572

09/08/2010 16:00	242	713
09/08/2010 17:00	249	739
09/08/2010 18:00	157	465
09/08/2010 19:00	99	303
09/08/2010 20:00	21	210
09/08/2010 21:00	4	150
09/08/2010 22:00	9	113
09/08/2010 23:00	1	41
10/08/2010 00:00	0	28
10/08/2010 01:00	14	9
10/08/2010 02:00	3	7
10/08/2010 03:00	6	4
10/08/2010 04:00	4	7
10/08/2010 05:00	4	28
10/08/2010 06:00	24	87
10/08/2010 07:00	51	164
10/08/2010 08:00	173	302
10/08/2010 09:00	231	292
10/08/2010 10:00	305	244
10/08/2010 11:00	361	383
10/08/2010 12:00	411	362
10/08/2010 13:00	339	359
10/08/2010 14:00	288	488
10/08/2010 15:00	194	499
10/08/2010 16:00	397	603
10/08/2010 17:00	558	672
10/08/2010 18:00	538	459
10/08/2010 19:00	683	298
10/08/2010 20:00	386	271
10/08/2010 21:00	262	182
10/08/2010 22:00	105	187
10/08/2010 23:00	85	54
11/08/2010 00:00	25	30
11/08/2010 01:00	14	15
11/08/2010 02:00	10	3
11/08/2010 03:00	15	5
11/08/2010 04:00	10	8
11/08/2010 05:00	7	35
11/08/2010 06:00	56	75
11/08/2010 07:00	147	162
11/08/2010 08:00	258	280
11/08/2010 09:00	252	295
11/08/2010 10:00	679	372
11/08/2010 11:00	1008	397
11/08/2010 12:00	709	402
11/08/2010 13:00	352	375
11/08/2010 14:00	442	444
11/08/2010 15:00	532	517
11/08/2010 16:00	643	645
11/08/2010 17:00	665	696
11/08/2010 18:00	530	456
11/08/2010 19:00	446	347
11/08/2010 20:00	277	264
11/08/2010 21:00	152	207
11/08/2010 22:00	122	146
11/08/2010 23:00	101	80
12/08/2010 00:00	31	36
12/08/2010 01:00	17	15
12/08/2010 02:00	7	10
12/08/2010 03:00	9	6
12/08/2010 04:00	7	9
12/08/2010 05:00	22	40
12/08/2010 06:00	65	98
12/08/2010 07:00	143	178
12/08/2010 08:00	708	286
12/08/2010 09:00	656	285
12/08/2010 10:00	440	345
12/08/2010 11:00	450	385
12/08/2010 12:00	212	396
12/08/2010 13:00	284	432
12/08/2010 14:00	559	469
12/08/2010 15:00	460	555
12/08/2010 16:00	436	609
12/08/2010 17:00	471	663
12/08/2010 18:00	356	501
12/08/2010 19:00	343	329
12/08/2010 20:00	226	286
12/08/2010 21:00	130	207
12/08/2010 22:00	98	151
12/08/2010 23:00	88	73
13/08/2010 00:00	33	30
13/08/2010 01:00	22	13
13/08/2010 02:00	10	15
13/08/2010 03:00	11	4
13/08/2010 04:00	4	6
13/08/2010 05:00	20	40
13/08/2010 06:00	116	95
13/08/2010 07:00	193	172
13/08/2010 08:00	444	261
13/08/2010 09:00	772	254
13/08/2010 10:00	924	348
13/08/2010 11:00	769	391
13/08/2010 12:00	620	432
13/08/2010 13:00	564	451
13/08/2010 14:00	274	488
13/08/2010 15:00	254	607

13/08/2010 16:00	274	640
13/08/2010 17:00	512	610
13/08/2010 18:00	645	459
13/08/2010 19:00	372	358
13/08/2010 20:00	274	251
13/08/2010 21:00	54	226
13/08/2010 22:00	92	138
13/08/2010 23:00	86	74
14/08/2010 00:00	29	59
14/08/2010 01:00	28	34
14/08/2010 02:00	7	19
14/08/2010 03:00	9	19
14/08/2010 04:00	8	9
14/08/2010 05:00	14	25
14/08/2010 06:00	54	40
14/08/2010 07:00	59	113
14/08/2010 08:00	71	130
14/08/2010 09:00	74	194
14/08/2010 10:00	124	312
14/08/2010 11:00	629	417
14/08/2010 12:00	604	455
14/08/2010 13:00	355	449
14/08/2010 14:00	482	451
14/08/2010 15:00	404	458
14/08/2010 16:00	479	470
14/08/2010 17:00	444	484
14/08/2010 18:00	325	440
14/08/2010 19:00	361	248
14/08/2010 20:00	226	203
14/08/2010 21:00	133	148
14/08/2010 22:00	91	124
14/08/2010 23:00	55	76
15/08/2010 00:00	42	74
15/08/2010 01:00	42	48
15/08/2010 02:00	28	36
15/08/2010 03:00	58	36
15/08/2010 04:00	41	15
15/08/2010 05:00	18	19
15/08/2010 06:00	34	32
15/08/2010 07:00	72	48
15/08/2010 08:00	152	99
15/08/2010 09:00	313	129
15/08/2010 10:00	503	280
15/08/2010 11:00	864	400
15/08/2010 12:00	631	435
15/08/2010 13:00	404	381
15/08/2010 14:00	353	374
15/08/2010 15:00	340	424
15/08/2010 16:00	399	383
15/08/2010 17:00	330	290
15/08/2010 18:00	295	281
15/08/2010 19:00	248	207
15/08/2010 20:00	144	162
15/08/2010 21:00	115	155
15/08/2010 22:00	139	74
15/08/2010 23:00	72	39
16/08/2010 00:00	30	23
16/08/2010 01:00	19	13
16/08/2010 02:00	11	8
16/08/2010 03:00	14	9
16/08/2010 04:00	14	5
16/08/2010 05:00	18	39
16/08/2010 06:00	42	94
16/08/2010 07:00	157	172
16/08/2010 08:00	568	268
16/08/2010 09:00	920	287
16/08/2010 10:00	1042	333
16/08/2010 11:00	1233	378
16/08/2010 12:00	875	350
16/08/2010 13:00	452	359
16/08/2010 14:00	485	425
16/08/2010 15:00	588	518
16/08/2010 16:00	548	639
16/08/2010 17:00	564	654
16/08/2010 18:00	438	443
16/08/2010 19:00	282	293
16/08/2010 20:00	201	254
16/08/2010 21:00	137	173
16/08/2010 22:00	84	105
16/08/2010 23:00	53	47
17/08/2010 00:00	27	11
17/08/2010 01:00	7	11
17/08/2010 02:00	4	10
17/08/2010 03:00	14	6
17/08/2010 04:00	0	6
17/08/2010 05:00	18	44
17/08/2010 06:00	91	98
17/08/2010 07:00	147	158
17/08/2010 08:00	114	277
17/08/2010 09:00	70	256
17/08/2010 10:00	74	301
17/08/2010 11:00	125	392
17/08/2010 12:00	411	355
17/08/2010 13:00	440	377
17/08/2010 14:00	433	439
17/08/2010 15:00	634	518

17/08/2010 16:00	554	649
17/08/2010 17:00	617	682
17/08/2010 18:00	515	505
17/08/2010 19:00	319	278
17/08/2010 20:00	219	284
17/08/2010 21:00	167	182
17/08/2010 22:00	163	118
17/08/2010 23:00	54	42
18/08/2010 00:00	36	21
18/08/2010 01:00	13	12
18/08/2010 02:00	11	5
18/08/2010 03:00	10	9
18/08/2010 04:00	4	7
18/08/2010 05:00	16	38
18/08/2010 06:00	95	107
18/08/2010 07:00	143	170
18/08/2010 08:00	281	273
18/08/2010 09:00	736	291
18/08/2010 10:00	303	364
18/08/2010 11:00	338	414
18/08/2010 12:00	458	379
18/08/2010 13:00	483	374
18/08/2010 14:00	367	441
18/08/2010 15:00	268	533
18/08/2010 16:00	531	621
18/08/2010 17:00	780	741
18/08/2010 18:00	607	465
18/08/2010 19:00	294	318
18/08/2010 20:00	192	262
18/08/2010 21:00	190	200
18/08/2010 22:00	184	130
18/08/2010 23:00	67	60
19/08/2010 00:00	26	30
19/08/2010 01:00	14	20
19/08/2010 02:00	7	18
19/08/2010 03:00	7	7
19/08/2010 04:00	5	11
19/08/2010 05:00	20	29
19/08/2010 06:00	67	98
19/08/2010 07:00	79	161
19/08/2010 08:00	130	306
19/08/2010 09:00	127	293
19/08/2010 10:00	116	328
19/08/2010 11:00	346	386
19/08/2010 12:00	429	398
19/08/2010 13:00	295	412
19/08/2010 14:00	411	439
19/08/2010 15:00	480	535
19/08/2010 16:00	435	600
19/08/2010 17:00	276	661
19/08/2010 18:00	142	507
19/08/2010 19:00	37	295
19/08/2010 20:00	4	229
19/08/2010 21:00	6	166
19/08/2010 22:00	3	136
19/08/2010 23:00	5	59
20/08/2010 00:00	3	45
20/08/2010 01:00	6	19
20/08/2010 02:00	3	25
20/08/2010 03:00	5	14
20/08/2010 04:00	10	8
22/08/2010 09:00	96	153
22/08/2010 10:00	167	253
22/08/2010 11:00	270	341
22/08/2010 12:00	288	406
22/08/2010 13:00	317	380
22/08/2010 14:00	480	401
22/08/2010 15:00	470	419
22/08/2010 16:00	391	398
22/08/2010 17:00	440	336
22/08/2010 18:00	347	248
22/08/2010 19:00	305	168
22/08/2010 20:00	226	179
22/08/2010 21:00	153	115
22/08/2010 22:00	91	81
22/08/2010 23:00	43	41
23/08/2010 00:00	23	32
23/08/2010 01:00	13	14
23/08/2010 02:00	14	5
23/08/2010 03:00	6	10
23/08/2010 04:00	14	12
23/08/2010 05:00	10	27
23/08/2010 06:00	32	111
23/08/2010 07:00	93	171
23/08/2010 08:00	123	274
23/08/2010 09:00	440	246
23/08/2010 10:00	162	286
23/08/2010 11:00	98	371
23/08/2010 12:00	154	408
23/08/2010 13:00	246	421
23/08/2010 14:00	304	438
23/08/2010 15:00	438	496
23/08/2010 16:00	665	642
23/08/2010 17:00	693	647
23/08/2010 18:00	492	455
23/08/2010 19:00	284	271

23/08/2010 20:00	218	231
23/08/2010 21:00	214	181
23/08/2010 22:00	155	124
23/08/2010 23:00	62	55
24/08/2010 00:00	38	21
24/08/2010 01:00	10	11
24/08/2010 02:00	8	10
24/08/2010 03:00	4	8
24/08/2010 04:00	10	8
24/08/2010 05:00	13	33
24/08/2010 06:00	72	98
24/08/2010 07:00	214	164
24/08/2010 08:00	544	317
24/08/2010 09:00	391	349
24/08/2010 10:00	841	360
24/08/2010 11:00	1064	385
24/08/2010 12:00	682	396
24/08/2010 13:00	427	374
24/08/2010 14:00	557	484
24/08/2010 15:00	715	484
24/08/2010 16:00	657	666
24/08/2010 17:00	724	723
24/08/2010 18:00	585	497
24/08/2010 19:00	353	317
24/08/2010 20:00	236	235
24/08/2010 21:00	166	167
24/08/2010 22:00	79	128
24/08/2010 23:00	91	67
25/08/2010 00:00	28	39
25/08/2010 01:00	22	12
25/08/2010 02:00	4	12
25/08/2010 03:00	12	8
25/08/2010 04:00	15	12
25/08/2010 05:00	12	34
25/08/2010 06:00	60	87
25/08/2010 07:00	101	176
25/08/2010 08:00	150	258
25/08/2010 09:00	187	277
25/08/2010 10:00	184	319
25/08/2010 11:00	118	406
25/08/2010 12:00	121	401
25/08/2010 13:00	236	420
25/08/2010 14:00	293	446
25/08/2010 15:00	285	516
25/08/2010 16:00	279	609
25/08/2010 17:00	103	598
25/08/2010 18:00	78	479
25/08/2010 19:00	37	324
25/08/2010 20:00	12	233
25/08/2010 21:00	15	173
25/08/2010 22:00	7	130
25/08/2010 23:00	12	69
26/08/2010 00:00	5	34
26/08/2010 01:00	0	17
26/08/2010 02:00	3	9
26/08/2010 03:00	2	11
26/08/2010 04:00	3	10
26/08/2010 05:00	0	27
26/08/2010 06:00	17	102
26/08/2010 07:00	27	160
26/08/2010 08:00	76	275
26/08/2010 09:00	97	291
26/08/2010 10:00	149	312
26/08/2010 11:00	232	404
26/08/2010 12:00	298	393
26/08/2010 13:00	167	440
26/08/2010 14:00	186	459
26/08/2010 15:00	220	578
26/08/2010 16:00	258	685
26/08/2010 17:00	378	707
26/08/2010 18:00	233	519
26/08/2010 19:00	109	335
26/08/2010 20:00	80	284
26/08/2010 21:00	39	194
26/08/2010 22:00	33	141
26/08/2010 23:00	22	58
27/08/2010 00:00	11	31
27/08/2010 01:00	4	20
27/08/2010 02:00	6	6
27/08/2010 03:00	5	10
27/08/2010 04:00	6	7
27/08/2010 05:00	9	35
27/08/2010 06:00	26	106
27/08/2010 07:00	228	156
27/08/2010 08:00	671	265
27/08/2010 09:00	1000	319
27/08/2010 10:00	1103	374
27/08/2010 11:00	1189	426
27/08/2010 12:00	1046	453
27/08/2010 13:00	386	464
27/08/2010 14:00	507	519
27/08/2010 15:00	633	636
27/08/2010 16:00	671	635
27/08/2010 17:00	670	614
27/08/2010 18:00	493	497
27/08/2010 19:00	379	356

27/08/2010 20:00	375	290
27/08/2010 21:00	242	203
27/08/2010 22:00	160	144
27/08/2010 23:00	90	88
28/08/2010 00:00	61	48
28/08/2010 01:00	36	38
28/08/2010 02:00	24	21
28/08/2010 03:00	15	16
28/08/2010 04:00	15	17
28/08/2010 05:00	14	22
28/08/2010 06:00	35	41
28/08/2010 07:00	63	82
28/08/2010 08:00	76	163
28/08/2010 09:00	434	206
28/08/2010 10:00	796	345
28/08/2010 11:00	1074	436
28/08/2010 12:00	918	461
28/08/2010 13:00	465	455
28/08/2010 14:00	604	442
28/08/2010 15:00	509	395
28/08/2010 16:00	525	444
28/08/2010 17:00	529	479
28/08/2010 18:00	317	458
28/08/2010 19:00	286	261
28/08/2010 20:00	237	167
28/08/2010 21:00	152	163
28/08/2010 22:00	116	120
28/08/2010 23:00	69	72
29/08/2010 00:00	40	48
29/08/2010 01:00	53	31
29/08/2010 02:00	20	25
29/08/2010 03:00	23	29
29/08/2010 04:00	16	9
29/08/2010 05:00	5	13
29/08/2010 06:00	10	18
29/08/2010 07:00	6	53
29/08/2010 08:00	10	56
29/08/2010 09:00	10	127
29/08/2010 10:00	52	237
29/08/2010 11:00	40	378
29/08/2010 12:00	123	403
29/08/2010 13:00	241	365
29/08/2010 14:00	119	408
29/08/2010 15:00	296	400
29/08/2010 16:00	295	408
29/08/2010 17:00	518	271
29/08/2010 18:00	600	244
29/08/2010 19:00	463	199
29/08/2010 20:00	231	166
29/08/2010 21:00	160	143
29/08/2010 22:00	135	68
29/08/2010 23:00	49	56
30/08/2010 00:00	42	57
30/08/2010 01:00	32	42
30/08/2010 02:00	30	37
30/08/2010 03:00	24	31
30/08/2010 04:00	13	20
30/08/2010 05:00	12	15
30/08/2010 06:00	16	39
30/08/2010 07:00	44	56
30/08/2010 08:00	70	75
30/08/2010 09:00	179	154
30/08/2010 10:00	519	322
30/08/2010 11:00	1087	485
30/08/2010 12:00	1319	480
30/08/2010 13:00	694	465
30/08/2010 14:00	485	479
30/08/2010 15:00	635	489
30/08/2010 16:00	671	467
30/08/2010 17:00	643	361
30/08/2010 18:00	571	319
30/08/2010 19:00	421	247
30/08/2010 20:00	277	196
30/08/2010 21:00	221	155
30/08/2010 22:00	147	65
30/08/2010 23:00	42	47
31/08/2010 00:00	49	18
31/08/2010 01:00	10	5
31/08/2010 02:00	9	9
31/08/2010 03:00	15	4
31/08/2010 04:00	9	6
31/08/2010 05:00	9	24
31/08/2010 06:00	31	104
31/08/2010 07:00	125	148
31/08/2010 08:00	335	273
31/08/2010 09:00	862	272
31/08/2010 10:00	1025	344
31/08/2010 11:00	1321	420
31/08/2010 12:00	1228	391
31/08/2010 13:00	915	425
31/08/2010 14:00	751	478
31/08/2010 15:00	710	533
31/08/2010 16:00	565	622
31/08/2010 17:00	761	680
31/08/2010 18:00	1120	519
31/08/2010 19:00	785	343

31/08/2010 20:00	332	267
31/08/2010 21:00	231	190
31/08/2010 22:00	144	127
31/08/2010 23:00	64	65
01/09/2010 00:00	32	25
01/09/2010 01:00	19	11
01/09/2010 02:00	13	6
01/09/2010 03:00	8	13
01/09/2010 04:00	14	5
01/09/2010 05:00	7	33
01/09/2010 06:00	56	110
01/09/2010 07:00	150	208
01/09/2010 08:00	417	403
01/09/2010 09:00	854	291
01/09/2010 10:00	925	316
01/09/2010 11:00	1233	359
01/09/2010 12:00	1124	412
01/09/2010 13:00	647	426
01/09/2010 14:00	433	453
01/09/2010 15:00	627	563
01/09/2010 16:00	618	674
01/09/2010 17:00	856	674
01/09/2010 18:00	950	489
01/09/2010 19:00	661	365
01/09/2010 20:00	356	261
01/09/2010 21:00	259	185
01/09/2010 22:00	128	126
01/09/2010 23:00	86	67
02/09/2010 00:00	44	28
02/09/2010 01:00	13	10
02/09/2010 02:00	8	13
02/09/2010 03:00	13	14
02/09/2010 04:00	10	11
02/09/2010 05:00	12	40
02/09/2010 06:00	33	117
02/09/2010 07:00	151	191
02/09/2010 08:00	369	402
02/09/2010 09:00	1102	306
02/09/2010 10:00	1148	338
02/09/2010 11:00	1290	358
02/09/2010 12:00	1127	399
02/09/2010 13:00	779	396
02/09/2010 14:00	448	488
02/09/2010 15:00	455	561
02/09/2010 16:00	704	669
02/09/2010 17:00	902	667
02/09/2010 18:00	1020	514
02/09/2010 19:00	611	344
02/09/2010 20:00	302	285
02/09/2010 21:00	203	197
02/09/2010 22:00	155	113
02/09/2010 23:00	82	45
03/09/2010 00:00	34	27
03/09/2010 01:00	19	12
03/09/2010 02:00	11	10
03/09/2010 03:00	9	7
03/09/2010 04:00	6	12
03/09/2010 05:00	19	32
03/09/2010 06:00	80	100
03/09/2010 07:00	177	191
03/09/2010 08:00	470	423
03/09/2010 09:00	1069	307
03/09/2010 10:00	1136	323
03/09/2010 11:00	1050	430
03/09/2010 12:00	965	423
03/09/2010 13:00	521	460
03/09/2010 14:00	486	513
03/09/2010 15:00	586	655
03/09/2010 16:00	785	659
03/09/2010 17:00	765	592
03/09/2010 18:00	684	470
03/09/2010 19:00	517	351
03/09/2010 20:00	326	274
03/09/2010 21:00	192	162
03/09/2010 22:00	140	159
03/09/2010 23:00	86	91
04/09/2010 00:00	49	62
04/09/2010 01:00	50	26
04/09/2010 02:00	8	27
04/09/2010 03:00	10	17
04/09/2010 04:00	12	12
04/09/2010 05:00	11	23
04/09/2010 06:00	14	55
04/09/2010 07:00	62	96
04/09/2010 08:00	126	172
04/09/2010 09:00	433	274
04/09/2010 10:00	875	315
04/09/2010 11:00	1061	433
04/09/2010 12:00	740	501
04/09/2010 13:00	353	555
04/09/2010 14:00	238	462
04/09/2010 15:00	150	409
04/09/2010 16:00	461	497
04/09/2010 17:00	511	450
04/09/2010 18:00	571	411
04/09/2010 19:00	559	228

04/09/2010 20:00	174	175
04/09/2010 21:00	100	138
04/09/2010 22:00	71	120
04/09/2010 23:00	93	61
05/09/2010 00:00	55	61
05/09/2010 01:00	49	52
05/09/2010 02:00	56	24
05/09/2010 03:00	25	19
05/09/2010 04:00	5	9
05/09/2010 05:00	16	13
05/09/2010 06:00	15	26
05/09/2010 07:00	16	30
05/09/2010 08:00	8	69
05/09/2010 09:00	13	111
05/09/2010 10:00	67	228
05/09/2010 11:00	273	356
05/09/2010 12:00	112	431
05/09/2010 13:00	243	424
05/09/2010 14:00	145	452
05/09/2010 15:00	124	386
05/09/2010 16:00	131	401
05/09/2010 17:00	213	294
05/09/2010 18:00	138	227
05/09/2010 19:00	70	187
05/09/2010 20:00	140	148
05/09/2010 21:00	141	115
05/09/2010 22:00	137	73
05/09/2010 23:00	70	46
06/09/2010 00:00	52	15
06/09/2010 01:00	36	9
06/09/2010 02:00	25	7
06/09/2010 03:00	18	9
06/09/2010 04:00	20	13
06/09/2010 05:00	55	42
06/09/2010 06:00	151	94
06/09/2010 07:00	410	188
06/09/2010 08:00	549	374
06/09/2010 09:00	472	289
06/09/2010 10:00	91	266
06/09/2010 11:00	92	325
06/09/2010 12:00	118	398
06/09/2010 13:00	77	376
06/09/2010 14:00	64	404
06/09/2010 15:00	128	501
06/09/2010 16:00	162	617
06/09/2010 17:00	104	637
06/09/2010 18:00	32	437
06/09/2010 19:00	21	225
06/09/2010 20:00	18	227
06/09/2010 21:00	14	152
06/09/2010 22:00	6	95
06/09/2010 23:00	6	50
07/09/2010 00:00	10	22
07/09/2010 01:00	7	9
07/09/2010 02:00	2	5
07/09/2010 03:00	1	11
07/09/2010 04:00	11	10
07/09/2010 05:00	7	34
07/09/2010 06:00	54	119
07/09/2010 07:00	134	199
07/09/2010 08:00	139	421
07/09/2010 09:00	358	291
07/09/2010 10:00	302	300
07/09/2010 11:00	319	316
07/09/2010 12:00	269	364
07/09/2010 13:00	348	345
07/09/2010 14:00	476	452
07/09/2010 15:00	600	521
07/09/2010 16:00	696	644
07/09/2010 17:00	740	678
07/09/2010 18:00	494	466
07/09/2010 19:00	326	322
07/09/2010 20:00	208	263
07/09/2010 21:00	149	152
07/09/2010 22:00	95	102
07/09/2010 23:00	36	56

APPENDIX 5

MODIFIED *ENTICE* MODEL

```
<?php

//icemiser6.php

//ignore_user_abort(TRUE);// Previously left as ()
set_time_limit(600);// Important to prevent server timing out

// Sensitivity Analysis - 1 = ON, 0 = OFF
$LA = 1; $LW = 1; $SW = 1; $AL = 1; $RL = 1; $RC = 1; $TR = 1; $TOPO = 1; $PROX = 1; $TM = 0;

// Read in HOURLY forecast data

$IN = "ForecastData/".$SALTROUTE.".csv";
//echo $IN;

$HANDLE = fopen($IN, "r");
$DATA = fgetcsv($HANDLE, 1000, ",");
$JDAY = $DATA[0];$JMON = $DATA[1];$JYEAR = $DATA[2];

$DATA = fgetcsv($HANDLE, 1000, ",");
$RWIS = $DATA[0];

//$DATA = fgetcsv($HANDLE, 1000, ",");
//$SNOWLINE = $DATA[0];
$SNOWLINE = 1000;

$DATA = fgetcsv($HANDLE, 1000, ",");
$GROUND = $DATA[0];$SURF = $DATA[1];

$DATA = fgetcsv($HANDLE, 1000, ",");
$AT[0] = $DATA[0];$AT[1] = $DATA[1];$AT[2] = $DATA[2];$AT[3] = $DATA[3];$AT[4] = $DATA[4];
$AT[5] = $DATA[5];$AT[6] = $DATA[6];$AT[7] = $DATA[7];$AT[8] = $DATA[8];$AT[9] = $DATA[9];
$AT[10] = $DATA[10];$AT[11] = $DATA[11];$AT[12] = $DATA[12];$AT[13] = $DATA[13];$AT[14] =
$DATA[14];
$AT[15] = $DATA[15];$AT[16] = $DATA[16];$AT[17] = $DATA[17];$AT[18] = $DATA[18];$AT[19] =
$DATA[19];
$AT[20] = $DATA[20];$AT[21] = $DATA[21];$AT[22] = $DATA[22];$AT[23] = $DATA[23];$AT[24] =
$DATA[24];
//$AT[25] = $DATA[25];

$DATA = fgetcsv($HANDLE, 1000, ",");
$RF[0] = $DATA[0];$RF[1] = $DATA[1];$RF[2] = $DATA[2];$RF[3] = $DATA[3];$RF[4] = $DATA[4];
$RF[5] = $DATA[5];$RF[6] = $DATA[6];$RF[7] = $DATA[7];$RF[8] = $DATA[8];$RF[9] = $DATA[9];
$RF[10] = $DATA[10];$RF[11] = $DATA[11];$RF[12] = $DATA[12];$RF[13] = $DATA[13];$RF[14] =
$DATA[14];
$RF[15] = $DATA[15];$RF[16] = $DATA[16];$RF[17] = $DATA[17];$RF[18] = $DATA[18];$RF[19] =
$DATA[19];
$RF[20] = $DATA[20];$RF[21] = $DATA[21];$RF[22] = $DATA[22];$RF[23] = $DATA[23];$RF[24] =
$DATA[24];
//$RF[25] = $DATA[25];

$DATA = fgetcsv($HANDLE, 1000, ",");
$UI[0] = $DATA[0];$UI[1] = $DATA[1];$UI[2] = $DATA[2];$UI[3] = $DATA[3];
$UI[4] = $DATA[4];$UI[5] = $DATA[5];$UI[6] = $DATA[6];$UI[7] = $DATA[7];
$UI[8] = $DATA[8];$UI[9] = $DATA[9];$UI[10] = $DATA[10];$UI[11] = $DATA[11];
$UI[12] = $DATA[12];$UI[13] = $DATA[13];$UI[14] = $DATA[14];$UI[15] = $DATA[15];
$UI[16] = $DATA[16];$UI[17] = $DATA[17];$UI[18] = $DATA[18];$UI[19] = $DATA[19];
$UI[20] = $DATA[20];$UI[21] = $DATA[21];$UI[22] = $DATA[22];$UI[23] = $DATA[23];
$UI[24] = $DATA[24];
//$UI[25] = $DATA[25];

$DATA = fgetcsv($HANDLE, 1000, ",");
$RIN[0] = $DATA[0];$RIN[1] = $DATA[1];$RIN[2] = $DATA[2];$RIN[3] = $DATA[3];
$RIN[4] = $DATA[4];$RIN[5] = $DATA[5];$RIN[6] = $DATA[6];$RIN[7] = $DATA[7];
$RIN[8] = $DATA[8];$RIN[9] = $DATA[9];$RIN[10] = $DATA[10];$RIN[11] = $DATA[11];
$RIN[12] = $DATA[12];$RIN[13] = $DATA[13];$RIN[14] = $DATA[14];$RIN[15] = $DATA[15];
$RIN[16] = $DATA[16];$RIN[17] = $DATA[17];$RIN[18] = $DATA[18];$RIN[19] = $DATA[19];
$RIN[20] = $DATA[20];$RIN[21] = $DATA[21];$RIN[22] = $DATA[22];$RIN[23] = $DATA[23];
$RIN[24] = $DATA[24];
//$RIN[25] = $DATA[25];
```

```
$DATA = fgetcsv($HANDLE, 1000, ",");
$IA[0] = $DATA[0];$IA[1] = $DATA[1];$IA[2] = $DATA[2];$IA[3] = $DATA[3];
$IA[4] = $DATA[4];$IA[5] = $DATA[5];$IA[6] = $DATA[6];$IA[7] = $DATA[7];
$IA[8] = $DATA[8];$IA[9] = $DATA[9];$IA[10] = $DATA[10];$IA[11] = $DATA[11];
$IA[12] = $DATA[12];$IA[13] = $DATA[13];$IA[14] = $DATA[14];$IA[15] = $DATA[15];
$IA[16] = $DATA[16];$IA[17] = $DATA[17];$IA[18] = $DATA[18];$IA[19] = $DATA[19];
$IA[20] = $DATA[20];$IA[21] = $DATA[21];$IA[22] = $DATA[22];$IA[23] = $DATA[23];
$IA[24] = $DATA[24];
//$IA[25] = $DATA[25];

$DATA = fgetcsv($HANDLE, 1000, ",");
$IT[0] = $DATA[0];$IT[1] = $DATA[1];$IT[2] = $DATA[2];$IT[3] = $DATA[3];
$IT[4] = $DATA[4];$IT[5] = $DATA[5];$IT[6] = $DATA[6];$IT[7] = $DATA[7];
$IT[8] = $DATA[8];$IT[9] = $DATA[9];$IT[10] = $DATA[10];$IT[11] = $DATA[11];
$IT[12] = $DATA[12];$IT[13] = $DATA[13];$IT[14] = $DATA[14];$IT[15] = $DATA[15];
$IT[16] = $DATA[16];$IT[17] = $DATA[17];$IT[18] = $DATA[18];$IT[19] = $DATA[19];
$IT[20] = $DATA[20];$IT[21] = $DATA[21];$IT[22] = $DATA[22];$IT[23] = $DATA[23];
$IT[24] = $DATA[24];
//$IT[25] = $DATA[25];

$DATA = fgetcsv($HANDLE, 1000, ",");
$WINDIR[0] = $DATA[0];$WINDIR[1] = $DATA[1];$WINDIR[2] = $DATA[2];$WINDIR[3] = $DATA[3];
$WINDIR[4] = $DATA[4];$WINDIR[5] = $DATA[5];$WINDIR[6] = $DATA[6];$WINDIR[7] = $DATA[7];
$WINDIR[8] = $DATA[8];$WINDIR[9] = $DATA[9];$WINDIR[10] = $DATA[10];$WINDIR[11] = $DATA[11];
$WINDIR[12] = $DATA[12];$WINDIR[13] = $DATA[13];$WINDIR[14] = $DATA[14];$WINDIR[15] =
$DATA[15];
$WINDIR[16] = $DATA[16];$WINDIR[17] = $DATA[17];$WINDIR[18] = $DATA[18];$WINDIR[19] =
$DATA[19];
$WINDIR[20] = $DATA[20];$WINDIR[21] = $DATA[21];$WINDIR[22] = $DATA[22];$WINDIR[23] =
$DATA[23];
$WINDIR[24] = $DATA[24];


// Convert date to Julian day

$JUDY[0] = 31; $JUDY[1] = 59; $JUDY[2] = 90;
$JUDY[3] = 120; $JUDY[4] = 151; $JUDY[5] = 181;
$JUDY[6] = 212; $JUDY[7] = 243; $JUDY[8] = 273;
$JUDY[9] = 304; $JUDY[10] = 334;

$TOY = $JDAY;
for ($I = 1; $I<=11; $I++)
{
       $INDEX = $I - 1;
       if ($JMON == ($I+1)) {$TOY = $JUDY[$INDEX]+$JDAY;}
}
$MODRESULT = $JDAY % 4;
if (($JMON > 2) && ($MODRESULT == 0)) {$TOY = $TOY + 1;}
$LEAP = 12;
for ($I = 1950; $I<($JYEAR + 1); $I++)
{
        $MODRESULT = $I % 4;
        if ($MODRESULT == 0) {$LEAP = $LEAP + 1;}
}
$DAYS = (($JYEAR - 1900) * 365.0) + $LEAP + $TOY - 0.5;



// Interpolate wind, cloud and rain data
// Values are averaged linearly for the 20 minute intervals between input values.

for ($I = 1; $I<=72; $I++)
{

       if((($I+2)/3) == INTVAL(($I+2)/3)) // HOURLY DATA
       {
              $INDEX=(INTVAL(($I+2)/3))-1;
              $UA[$I]=($UI[$INDEX]*45)+90;
              $IC[$I]=$IA[$INDEX];
              $IH[$I]=$IT[$INDEX];
              $RFALL[$I]=$RIN[$INDEX];
              $WDIR[$I]=$WINDIR[$INDEX];
              $INDEX1=$INDEX+1;
       } ELSE {
                     if(($I/3) == INTVAL(($I+2)/3)) // 20 PAST HOUR
                     {
                            $UA[$I]=(($UI[$INDEX]+(($UI[$INDEX1]-$UI[$INDEX])/1.5))*45)+90;
                            $IC[$I]=INTVAL($IA[$INDEX]+(($IA[$INDEX1]-$IA[$INDEX])/1.5));
                            $IH[$I]=INTVAL($IT[$INDEX]+(($IT[$INDEX1]-$IT[$INDEX])/1.5));
```

```
                                $RFALL[$I]=INTVAL($RIN[$INDEX]+(($RIN[$INDEX1]-
$RIN[$INDEX])/1.5));
                                $WDIR[$I]=INTVAL($WINDIR[$INDEX]+(($WINDIR[$INDEX1]-
$WINDIR[$INDEX])/1.5));
                        } ELSE { //40 PAST HOUR
                                $UA[$I]=(($UI[$INDEX]+(($UI[$INDEX1]-$UI[$INDEX])/3))*45)+90;
                                $IC[$I]=INTVAL($IA[$INDEX]+(($IA[$INDEX1]-$IA[$INDEX])/3));
                                $IH[$I]=INTVAL($IT[$INDEX]+(($IT[$INDEX1]-$IT[$INDEX])/3));
                                $RFALL[$I]=INTVAL($RIN[$INDEX]+(($RIN[$INDEX1]-
$RIN[$INDEX])/3));
                                $WDIR[$I]=INTVAL($WINDIR[$INDEX]+(($WINDIR[$INDEX1]-
$WINDIR[$INDEX])/3));
                        }
        }

//echo "winddir=$WDIR[$I]<br>";

// Calculate stability class

        if (($IH[$I] == 3) && ($IC[$I] > 5)) {$IC[$I] = 4;}
        if (($UA[$I] < 181) && ($IC[$I] < 4))
        {
                $STABILITYCLASS[$I] = 1;
                $ELR[$I] = 0.0;
        } elseif (($UA[$I] < 226) && ($UA[$I] > 180) && ($IC[$I] < 5))
        {
                $STABILITYCLASS[$I] = 2;
                $ELR[$I] = 0.003;
        } elseif (($UA[$I] < 226) && ($IC[$I] > 4))
        {
                $STABILITYCLASS[$I] = 3;
                $ELR[$I] = 0.006;
        } elseif (($UA[$I] < 316) && ($UA[$I] > 225) && ($IC[$I] < 5))
        {
                $STABILITYCLASS[$I] = 3;
                $ELR[$I] = 0.006;
        } else
        {
                $STABILITYCLASS[$I] = 4;
                $ELR[$I] = 0.009;
        }
}



// Parameterise cloud data for use in the radiation balance

for ($J = 1; $J<=72; $J++)
{
        if (($IC[$J] >= 1) && ($IC[$J] <= 7))
        {
                if ($IH[$J] == 1)
                {
                        if (($IC[$J] >= 1) && ($IC[$J] <= 2)) {$X[$J] = 0.2; $Y[$J] = 0.6;
$Z[$J] = 0.87;}
                        if (($IC[$J] >= 3) && ($IC[$J] <= 5)) {$X[$J] = 0.5; $Y[$J] = 0.8;
$Z[$J] = 0.58;}
                        if ($IC[$J] > 5) {$X[$J] = 0.9; $Y[$J] = 1.0; $Z[$J] = 0.32;}
                } elseif ($IH[$J] == 2)
                {
                        if (($IC[$J] >= 1) && ($IC[$J] <= 2)) {$X[$J] = 0.1; $Y[$J] = 0.6;
$Z[$J] = 0.91;}
                        if (($IC[$J] >= 3) && ($IC[$J] <= 5)) {$X[$J] = 0.3; $Y[$J] = 0.8;
$Z[$J] = 0.72;}
                        if ($IC[$J] > 5) {$X[$J] = 0.9; $Y[$J] = 1.3; $Z[$J] = 0.54;}
                } else
                {
                        if (($IC[$J] >= 1) && ($IC[$J] <= 2)) {$X[$J] = 0.05; $Y[$J] = 0.5;
$Z[$J] = 0.96;}
                        if (($IC[$J] >= 3) && ($IC[$J] <= 5)) {$X[$J] = 0.1; $Y[$J] = 0.5;
$Z[$J] = 0.86;}
                        if ($IC[$J] > 5) {$X[$J] = 0.3; $Y[$J] = 0.6; $Z[$J] = 0.78;}
                }
        }
        if ($IC[$J] == 0) {$X[$J] = 0; $Y[$J] = 0.5; $Z[$J] = 1;}
        if ($IC[$J] == 8)
        {
                $X[$J] = 1; $Y[$J] = 1; $Z[$J] = 0.78;
                if ($IH[$J] == 1) {$Z[$J] = 0.32;}
                if ($IH[$J] == 2) {$Z[$J] = 0.54;}
```

```
        }

        $ALBED[$J] = $X[$J];
        $DPLUS[$J] = $Y[$J];
        $KCLOU[$J] = $Z[$J];
}



// Create empty route forecast database

$DBFNAME1 = "TemperatureDataQC/".$SALTROUTE.".dbf";
$DBFNAME2 = "ConditionDataQC/".$SALTROUTE.".dbf";
//$DBFNAME1 = "$OUT1.dbf";
//$DBFNAME2 = "$OUT2.dbf";
$DEF = array(
        array("X","N",12,2),
        array("Y","N",12,2),
        array("1200","N",12,2),
        array("1220","N",12,2),
        array("1240","N",12,2),
        array("1300","N",12,2),
        array("1320","N",12,2),
        array("1340","N",12,2),
        array("1400","N",12,2),
        array("1420","N",12,2),
        array("1440","N",12,2),
        array("1500","N",12,2),
        array("1520","N",12,2),
        array("1540","N",12,2),
        array("1600","N",12,2),
        array("1620","N",12,2),
        array("1640","N",12,2),
        array("1700","N",12,2),
        array("1720","N",12,2),
        array("1740","N",12,2),
        array("1800","N",12,2),
        array("1820","N",12,2),
        array("1840","N",12,2),
        array("1900","N",12,2),
        array("1920","N",12,2),
        array("1940","N",12,2),
        array("2000","N",12,2),
        array("2020","N",12,2),
        array("2040","N",12,2),
        array("2100","N",12,2),
        array("2120","N",12,2),
        array("2140","N",12,2),
        array("2200","N",12,2),
        array("2220","N",12,2),
        array("2240","N",12,2),
        array("2300","N",12,2),
        array("2320","N",12,2),
        array("2340","N",12,2),
        array("0000","N",12,2),
        array("0020","N",12,2),
        array("0040","N",12,2),
        array("0100","N",12,2),
        array("0120","N",12,2),
        array("0140","N",12,2),
        array("0200","N",12,2),
        array("0220","N",12,2),
        array("0240","N",12,2),
        array("0300","N",12,2),
        array("0320","N",12,2),
        array("0340","N",12,2),
        array("0400","N",12,2),
        array("0420","N",12,2),
        array("0440","N",12,2),
        array("0500","N",12,2),
        array("0520","N",12,2),
        array("0540","N",12,2),
        array("0600","N",12,2),
        array("0620","N",12,2),
        array("0640","N",12,2),
        array("0700","N",12,2),
        array("0720","N",12,2),
        array("0740","N",12,2),
        array("0800","N",12,2),
        array("0820","N",12,2),
```

```
        array("0840","N",12,2),
        array("0900","N",12,2),
        array("0920","N",12,2),
        array("0940","N",12,2),
        array("1000","N",12,2),
        array("1020","N",12,2),
        array("1040","N",12,2),
        array("1100","N",12,2),
        array("1120","N",12,2),
        array("1140","N",12,2)
      );
//dbase_create($DBF_RST_ROUTE_MAKE,$DEF);
//dbase_create($DBF_RSC_ROUTE_MAKE,$DEF);


$RSTDBF = dbase_create($DBFNAME1,$DEF);
$CONDBF = dbase_create($DBFNAME2,$DEF);


// Specify array - check if needed since $REC specified when data written to route database

//$REC = array($SITE[0], $SITE[1], $SITE[2], $SITE[3], $SITE[4], $SITE[5], $SITE[6], $SITE[7],
$SITE[8], $SITE[9], //$SITE[10], $SITE[11], $SITE[12], $SITE[13], $SITE[14], $SITE[15],
$SITE[16], $SITE[17], $SITE[18], $SITE[19], //$SITE[20], $SITE[21], $SITE[22], $SITE[23],
$SITE[24], $SITE[25]);



// Specify constants

$RDA = 0.00694;
$RDC = 0.012;
$RDS = 0.004;
//$ZG = 72.0; //commented out since $ZG is now variable based on GPR measurements
$PI = 3.141592654;
$RADEG = 360 / (2 * $PI);



// Start spatial loop
// Open the salting route database and read in data
if ($FETCH == 1)
{
        $IN = "SaltingRoutes/Bham_PhDzo100.dbf";
}
elseif ($FETCH == 2)
{
        $IN = "SaltingRoutes/Bham_PhDzo150.dbf";
}
elseif ($FETCH == 3)
{
        $IN = "SaltingRoutes/Bham_PhDzo200.dbf";
}
elseif ($FETCH == 4)
{
        $IN = "SaltingRoutes/Bham_PhDzo250.dbf";
}
elseif ($FETCH == 5)
{
        $IN = "SaltingRoutes/Bham_PhDzo500GPR.dbf";//added GPR to end of filename
}
else
{
        echo "error - no salting route databse found!";
}

//$IN = "SaltingRoutes/Bham_PhD.dbf";
//echo $IN;

$DB = dbase_open($IN,2);
$NR = dbase_numrecords($DB);

for ($M = 1; $M<=$NR; $M++)

{
        $SITE = dbase_get_record($DB,$M);
        $EASTING[$M] = $SITE[1];
        $NORTHING[$M] = $SITE[2];
        $LATITUDE[$M] = $SITE[3];
        //$LONGITUDE[$M] = $SITE[4];
```

```
        $SVF[$M] = $SITE[5];
        $ALTITUDE[$M] = $SITE[6];
        $SLOPE[$M] = $SITE[7];
        $ASPECT[$M] = $SITE[8];
        //$CAPI[$M] = $SITE[9];
        $LANDUSE[$M] = $SITE[10];
        $ROAD[$M] = $SITE[11];
        $SING[$M] = $SITE[12];
        $RESRST[$M] = $SITE[13];
        $ZONORTH[$M] = $SITE[14]; //14-21 New LIDAR based ZO values - added by DH 04/06/10
        $ZONEAST[$M] = $SITE[15];
        $ZOEAST[$M] = $SITE[16];
        $ZOSEAST[$M] = $SITE[17];
        $ZOSOUTH[$M] = $SITE[18];
        $ZOSWEST[$M] = $SITE[19];
        $ZOWEST[$M] = $SITE[20];
        $ZONWEST[$M] = $SITE[21];
        $GPR1[$M] = $SITE[22]; //22-24 New subsurface layer thicknesses based on GPR data -
added by DH 22/08/10
        $GPR2[$M] = $SITE[23];
        $GPR3[$M] = $SITE[24];
        $GPR4[$M] = $SITE[25]; //default 18cm
        $GPR5[$M] = $SITE[26]; //default 36cm

//echo "goat.$GPR1[$M],$SITE[22]<br>";

// Check projecting parameters

        if ($LA == 0)
        {
                $SLAT = 52.5;
        } else {
                $SLAT = $LATITUDE[$M];
        }
         if ($LW == 0)
                {
                $SVF[$M] = 1.0;
                $SING[$M] = 0;// added to ensure SVF isn't reset to zero in singularity
correction below during sensitivity analysis
                }
        if ($AL == 0) {$ALTITUDE[$M] = 10;}
                else {
//      if (($ALTITUDE[$M] < 10) && ($ALTITUDE[$M] > -10)) {$ALTITUDE[$M] = 10;}
//      if ($ALTITUDE[$M] == 0) {$ALTITUDE[$M] = 10;}
        $ALTITUDE[$M] = $ALTITUDE[$M]-$RWIS;}


        if ($SW == 0)
        {
                $ASPECT[$M] = 0;
                $SLOPE[$M] = 0;
        } else {
                $ASPECT[$M] *=  (1 / $RADEG);
        $SLOPE[$M] *=  (1 / $RADEG);
        }

// SINGULARITY CORRECTIONS

        IF ($SING[$M]==1){$ROAD[$M]=$ROAD[$M]+1;}
//      IF ($SING[$M]==2){$ROAD[$M]=$ROAD[$M]+1;}
        IF ($SING[$M]==3){$SVF[$M]=1.0;}
        IF ($SING[$M]==4){$SVF[$M]=0.0;}
//      IF ($SING[$M]==5){$ROAD[$M]=3000;}


// Thornes Model
// Parameterise the road surface

        $ZG[$M] = (54+($GPR1[$M]*100+$GPR2[$M]*100+$GPR3[$M]*100)); //Set new profile depth at
each point based on GPR measurements
//$ZG[$M] = 72;
        if ($RC == 1)
        {
                if ($ROAD[$M] == 2999) {$RKA[$M] = 0.0021;} //0.0027
                if ($ROAD[$M] == 3000) //{$RKA[$M] = 0.00438;}//0.0039;}
                {
                $RKA[$M] = ((($GPR1[$M]*100+$GPR2[$M]*100+$GPR3[$M]*100)*0.0019) +
(54*0.0052))/(54+($GPR1[$M]*100+$GPR2[$M]*100+$GPR3[$M]*100));
                }
                if ($ROAD[$M] == 3001) //{$RKA[$M] = 0.00410;}//0.0035;}
```

```
                {
                $RKA[$M] = ((($GPR1[$M]*100+$GPR2[$M]*100+$GPR3[$M]*100)*0.0019) + (18*0.0052)
+ ((36*0.8)*0.0052) + ((36*0.2)*0.0024))/(54+($GPR1[$M]*100+$GPR2[$M]*100+$GPR3[$M]*100));
                }
                if ($ROAD[$M] == 3002) //{$RKA[$M] = 0.00409;}//0.0029;} //0.0031
                {
                $RKA[$M] = ((($GPR1[$M]*100+$GPR2[$M]*100)*0.0019) +
(($GPR3[$M]*100)+18)*0.0052) + ((36*0.5)*0.0052) +
((36*0.5)*0.0024))/(54+($GPR1[$M]*100+$GPR2[$M]*100+$GPR3[$M]*100));
                }
                if ($ROAD[$M] == 3004) //{$RKA[$M] = 0.00359;}//0.0022;} //0.0027
                {
                $RKA[$M] = ((($GPR1[$M]*100)*0.0019) +
(($GPR2[$M]*100+$GPR3[$M]*100)+18)*0.0052) +
(36*0.0024))/(54+($GPR1[$M]*100+$GPR2[$M]*100+$GPR3[$M]*100));
                }
        } else {$RKA[$M] = ((($GPR1[$M]*100+$GPR2[$M]*100+$GPR3[$M]*100)*0.0019) +
(54*0.0052))/(54+($GPR1[$M]*100+$GPR2[$M]*100+$GPR3[$M]*100));}//0.00438;}//0.0039;}

        //$fi = fopen('gpr_depth.csv', 'w');
        //fputcsv($fi,$RKA,',');
        //fclose($fp);

  //$FRED[$M] = $GPR1[$M]*100+$GPR2[$M]*100+$GPR3[$M]*100;
  //echo "goat.$RKA[$M],$FRED[$M]<br>";


        if ($TR == 1)
        {
                if ($ROAD[$M] == 2999) {$TRAF = 0.85;}
                if ($ROAD[$M] == 3000) {$TRAF = 0.85;}
                if ($ROAD[$M] == 3001) {$TRAF = 0.9;}
                if ($ROAD[$M] == 3002) {$TRAF = 0.95;}
                if ($ROAD[$M] == 3004) {$TRAF = 1.0;}
                if ($LANDUSE[$M] > 3) {$TRAF = 0.85;}
        } else {$TRAF = 1.0;}

//      if ($RL == 1)
//      {
//      if ($LANDUSE[$M] == 1) {$ZO[$M] = 25;}
//              if ($LANDUSE[$M] == 2) {$ZO[$M] = 50;}
//              if ($LANDUSE[$M] == 3) {$ZO[$M] = 50;}
//              if ($LANDUSE[$M] == 4) {$ZO[$M] = 75;}
//              if ($LANDUSE[$M] == 5) {$ZO[$M] = 100;}
//              if (($LANDUSE[$M] == 1) && ($ROAD[$M] <= 3000)) {$ZO[$M] = 50;}
//      } else {$ZO[$M] = 15;}


if ($RL == 1)
{
// Select the correct LIDAR ZO dataset based on wind direction
//$ZO[$M] = 1;
        for ($I = 1; $I<=72; $I++)
        {
                if ($WDIR[$I] < 22.5 or $WDIR[$I] > 337.5)
                {
                $ZO[$M] = $ZONORTH[$M]*100;
                }
                elseif ($WDIR[$I] >= 22.5 and $WDIR[$I] < 67.5)
                {
                $ZO[$M] = $ZONEAST[$M]*100;
                }
                elseif ($WDIR[$I] >= 67.5 and $WDIR[$I] < 112.5)
                {
                $ZO[$M] = $ZOEAST[$M]*100;
                }
                elseif ($WDIR[$I] >= 112.5 and $WDIR[$I] < 157.5)
                {
                $ZO[$M] = $ZOSEAST[$M]*100;
                }
                elseif ($WDIR[$I] >= 157.5 and $WDIR[$I] < 202.5)
                {
                $ZO[$M] = $ZOSOUTH[$M]*100;
                }
                elseif ($WDIR[$I] >= 202.5 and $WDIR[$I] < 247.5)
                {
                $ZO[$M] = $ZOSWEST[$M]*100;
                }
                elseif ($WDIR[$I] >= 247.5 and $WDIR[$I] < 292.5)
                {
```

```
                $ZO[$M] = $ZOWEST[$M]*100;
                }
                elseif ($WDIR[$I] >= 292.5 and $WDIR[$I] <= 337.5)
                {
                $ZO[$M] = $ZONWEST[$M]*100;
                }
                else
                {
                $ZO[$M] = $ZOWEST[$M]*100;
                }
        }

        $ZO[$M] = $ZOWEST[$M] * 100;
//echo "$LANDUSE[$M],$ZO[$M]<br>";

        for ($I = 1; $I<=72; $I++)
        {

// Where LIDAR ZO values are missing (-999900), replace with original ZO value based on
ordinal classification

        if ($ZO[$M] == -999900)
        {
        if ($LANDUSE[$M] == 1)
        {
        $ZO[$M] = 15;
        }
        elseif ($LANDUSE[$M] == 2 or $LANDUSE[$M] == 3)
        {
        $ZO[$M] = 50;
        }
        elseif ($LANDUSE[$M] == 4)
        {
        $ZO[$M] = 70;
        }
        elseif ($LANDUSE[$M] == 5)
        {
        $ZO[$M] = 100;
        }
        elseif ($LANDUSE[$M] == 1 and $ROAD[$M] <= 3000)
        {
        $ZO[$M] = 50;
        }
        else
        {
        $ZO[$M] = 15;
        }
        }
        elseif ($ZO[$M] <= 15)
        {
        $ZO[$M] = 15;
        }
        elseif ($ZO[$M] > 15 and $ZO[$M] <= 25)////start of
extra////////////////////////////////////////////////
        {
        $ZO[$M] = 20;
        }
        elseif ($ZO[$M] > 25 and $ZO[$M] <= 35)
        {
        $ZO[$M] = 30;
        }
        elseif ($ZO[$M] > 35 and $ZO[$M] <= 45)
        {
        $ZO[$M] = 40;
        }
        elseif ($ZO[$M] > 45 and $ZO[$M] <= 55)
        {
        $ZO[$M] = 50;
        }
        elseif ($ZO[$M] > 55 and $ZO[$M] <= 65)
        {
        $ZO[$M] = 60;
        }
        elseif ($ZO[$M] > 65 and $ZO[$M] <= 75)
        {
        $ZO[$M] = 70;
        }
        elseif ($ZO[$M] > 75 and $ZO[$M] <= 85)
        {
        $ZO[$M] = 80;
```

```
        }
        elseif ($ZO[$M] > 85 and $ZO[$M] <= 95)
        {
        $ZO[$M] = 90;
        }
        elseif ($ZO[$M] > 95 and $ZO[$M] <= 105)
        {
        $ZO[$M] = 100;
        }
        elseif ($ZO[$M] > 105 and $ZO[$M] <= 115)
        {
        $ZO[$M] = 110;
        }
        elseif ($ZO[$M] > 115 and $ZO[$M] <= 125)
        {
        $ZO[$M] = 120;
        }
        elseif ($ZO[$M] > 125 and $ZO[$M] <= 135)
        {
        $ZO[$M] = 130;
        }
        elseif ($ZO[$M] > 135 and $ZO[$M] <= 145)
        {
        $ZO[$M] = 140;
        }
        elseif ($ZO[$M] > 145)
        {
        $ZO[$M] = 150;
        }
        else
        {
        $ZO[$M] = $ZO[$M];
        }
        }
        } else {$ZO[$M] = 15;}

//echo "$LANDUSE[$M],$ZO[$M]<br>";

//      $fi = fopen('lidar_zo.csv', 'w');
//      fputcsv($fi,$ZO,',');

// Convert temps to Kelvin scale and correct with ALTITUDE
// Looks inefficient - can temp and dew point be read in at the same time as cloud earlier in
code

        for ($I = 1; $I<=72; $I++)
        {
                if((($I+2)/3) == INTVAL(($I+2)/3))  // HOURLY DATA
                {
                        $INDEX=(INTVAL(($I+2)/3))-1;
                        $ATA[$I]=$AT[$INDEX];
                        $V[$I]=$RF[$INDEX];
                        $INDEX1=$INDEX+1;
                } ELSE {
                        if(($I/3) == INTVAL(($I+2)/3)) // 20 PAST HOUR DATA
                        {
                                $ATA[$I]=$AT[$INDEX]+(($AT[$INDEX1]-$AT[$INDEX])/1.5);
                                $V[$I]=$RF[$INDEX]+(($RF[$INDEX1]-$RF[$INDEX])/1.5);
                        } ELSE {  // 40 PAST HOUR DATA
                                $ATA[$I]=$AT[$INDEX]+(($AT[$INDEX1]-$AT[$INDEX])/3);
                                $V[$I]=$RF[$INDEX]+(($RF[$INDEX1]-$RF[$INDEX])/3);
                        }

                }

                $AELR = $ALTITUDE[$M] * $ELR[$I];
                $TA[$I] = $ATA[$I] - $AELR;
                $V[$I] = $V[$I] - $AELR;
                $TA[$I] = $TA[$I] + 273.16;
                $V[$I] = $V[$I] + 273.16;
                $DP[$I][$M] = $V[$I] - 273.16;
                $V[$I] = SHMB($V[$I],$TA[$I]);
                $RHF[$I] = $V[$I] / SHMB($TA[$I],$TA[$I]);
                $W[$I] = 1.5 * $V[$I] + 0.6;
//              if ($I == 1)
//              {
                $ZA[$I] = ZAIR($UA[$I],$ZO[$M]);
                $EXCO[$I] = ((POW(0.4,2)) * 0.001 * $UA[$I]) / (POW((LOG($ZA[$I] /
$ZO[$M])),2));
//              }
```

```
//              else
//              {
//              $ZA[$I] = $ZA[$I - 1];
//              $EXCO[$I]  = $EXCO[$I - 1];
//              }
        }


// Generate incoming radiation

        for ($I = 1; $I<=72; $I++)
        {
                $ALBED1 = $ALBED[$I];
                $DPLUS1 = $DPLUS[$I];

                $INDEX = $I + 36;
                $J = $INDEX % 72;
                if ($J == 0) {$J = 72;}
                $TIME[$I] = ($J-1)/3;
                $INDEX = $I-1;
                if (($INDEX % 3) == 0)
                {
                        $MIN=$I-1;
                        LIST($DEC,$R) = SUNDEC($DAYS,$TIME[1],$MIN,$RADEG);
                }
                list ($COSZ,$COSTHETA,$VFVAL) =
COSAZI($I,$J,$RADEG,$SLAT,$DEC,$SLOPE[$M],$ASPECT[$M]);
                //              $BUL = (($PI / 2) - ((($VFMAT($VFVAL, $M)) * $PI) / 100)) *
$RADEG;
                $BUL = (($PI / 2) - (($50 * $PI) / 100)) * $RADEG;
                list ($SUN[$I],$ALBEDO[$I],$COSZ,$COSTHETA,$ALT[$I]) =
SUNGEN($COSZ,$W[$I],$R,$ALBED1,$DPLUS1,$BUL,$COSTHETA,$RADEG);
        }



// Parameterise rainfall
// Note that as the original parameters were 500 and 1000 for light and heavy rain
respectively over 3 hour periods,
// the new parameters of 50 and 100 are applied to the new 20 minute forecast interval.
// These figures can be tweaked if needed.

        $RAIN = 0;
        $SHRF = 0;
        $SNO = 0;
        for ($I = 1; $I<=72; $I++)
        {
                if ($RFALL[$I] == 0) {$RAIN = $RAIN;}
                if (($I == 1) && ($RIN[1] == 1)) {$RAIN = 50;}
                if (($I == 1) && ($RIN[1] == 2)) {$RAIN = 100;}
                if (($I == 1) && ($RIN[1] == 3)) {$RAIN = 100;} // SNOW

                if ($RFALL[$I] == 1){$RAIN = $RAIN+50;$SNO = 0;}
                if ($RFALL[$I] == 2){$RAIN = $RAIN+100;$SNO = 0;}
                if ($RFALL[$I] == 3){$RAIN = $RAIN+100;$SNO = 1;}

                if ($RAIN > 0) {$SHRF = 1;}
                $PRECIPITATION = $RAIN;
                $SNOW = $SNO;



// Interval halving algorithm and longwave generation

                $K = 0;
                $Z1 = $TA[$I] - 10;
                $Z2 = $TA[$I] + 10;
                $SHWO[0] = 0;

                do
                {
                        $K=$K+1;
                        if ($K == 1) {$T[$I] = $Z1;}
                        if ($K == 2) {$T[$I] = $Z2;}
                        if ($K > 2)
                        {
                                $INDEX1 = $K-1;
                                $INDEX2 = $K-2;
                                $T[$I]= $TE[$INDEX1] - (($TE[$INDEX1] - $TE[$INDEX2]) *
$SHWO[$INDEX1]) / ($SHWO[$INDEX1] - $SHWO[$INDEX2]);
```

```
                        }

                        $TE[$K] = $T[$I];
                        $KCLOU1 = $KCLOU[$I];
                        $RNLONG = ((0.95*(BB($T[$I])))*$SVF[$M])-((BB($TA[$I]))*((0.82-
0.25*(POW(10,(-0.094*$V[$I])))))));
                        $RN[$I] = (1.0 - $ALBEDO[$I]) * $SUN[$I] - $RNLONG * $KCLOU1 * $TRAF;



// Road construction and introduce lag

                        if ($RC == 1)
                        {
                                $RCONS[$M] = $ROAD[$M];
                        } else {
                                $RCONS[$M] = 3000;
                        }
                        if ($I == 1)
                        {
                                $ZT = $ZG[$M] / ($ZG[$M]/($ZG[$M]-36));//2;
                                $ZZ = $ZT / ($ZT/($ZT-18));//2;
                                $ZX = $ZZ / ($ZZ/($ZZ-$GPR3[$M]*100));//2;
                                $ZU = $ZX / ($ZX/($ZX-$GPR2[$M]*100));//2;
//echo "$ZT,$ZZ,$ZX,$ZU,$LANDUSE[$M]<br>";
                                $TT[$I] = ($GROUND + 273.16); //$TA(I) THIS IS THE TEMP AT 36CM,
TZ IS 18CM
                                $TZ[$I] = ($TT[$I] + $T[$I]) / 2;//($ZT/$ZZ);//2;//18cm
                                $TX[$I] = ($TZ[$I] + $T[$I]) / 2;//($ZZ/$ZX);//2;//9cm
                                $TU[$I] = ($TX[$I] + $T[$I]) / 2;//($ZX/$ZU);//2;//5cm
                                $TG = $TU[$I];
//                              $vartz=($ZG[$M]/$ZT);
//                              $vartx=$ZZ/$ZX;
//                              $vartu=$ZX/$ZU;
//echo "$TT[$I],$TZ[$I],$TX[$I],$TU[$I],$T[$I]<br>";//,$vartx,$vartu,$TT<br>";
                                $S[$I] = (0.00438 / $ZG[$M]) * ($TU[$I] - $T[$I]) *
60000;//changed conductivity from 0.0039(original entice motorway av) to new motorway average
(0.00438)
                        } else {
                                $INDEX4 = $I-1;
                                if (($RCONS[$M] >= 3002) && ($LANDUSE[$M] == 1))
                                {
                                        $TT[$I] = $TT[$INDEX4] + $RDS * (($T[$INDEX4] - 2 *
$TT[$INDEX4] + $TG) / ($ZT * $ZT)) * 1.2E3;
                                } else {
                                        $TT[$I] = $TT[$INDEX4] + $RDC * (($T[$INDEX4] - 2 *
$TT[$INDEX4] + $TG) / ($ZT * $ZT)) * 1.2E3;
                                }
                                $TZ[$I] = $TZ[$INDEX4] + $RDC * (($T[$INDEX4] - 2 * $TZ[$INDEX4]
+ $TT[$INDEX4]) / ($ZZ * $ZZ)) * 1.2E3;
                                if (($RCONS[$M] == 3000) OR ($RCONS[$M] == 3001))
                                {
                                        $TX[$I] = $TX[$INDEX4] + $RDA * (($T[$INDEX4] - 2 *
$TX[$INDEX4] + $TZ[$INDEX4]) / ($ZX * $ZX)) * 1.2E3;
                                } else {
                                        $TX[$I] = $TX[$INDEX4] + $RDC * (($T[$INDEX4] - 2 *
$TX[$INDEX4] + $TZ[$INDEX4]) / ($ZX * $ZX)) * 1.2E3;
                                }
                                if ($RCONS[$M] == 2999)
                                {
                                        $TU[$I] = $TU[$INDEX4] + $RDC * (($T[$INDEX4] - 2 *
$TU[$INDEX4] + $TX[$INDEX4]) / ($ZU * $ZU)) * 1.2E3;
                                } else {
                                        $TU[$I] = $TU[$INDEX4] + $RDA * (($T[$INDEX4] - 2 *
$TU[$INDEX4] + $TX[$INDEX4]) / ($ZU * $ZU)) * 1.2E3;
                                }
                                $S[$I] = ($RKA[$M] / $ZU) * ($TU[$I] - $T[$I]) * 60000;
                        }
                        $EXXO[$I] = $EXCO[$I] * RIFIX($TA[$I], $T[$I], $ZA[$I], $ZO[$M],
$UA[$I]);
                        $H[$I] = $EXXO[$I] * 0.24 * ($TA[$I] + 0.0001 * $ZA[$I] - $T[$I]) *
60000;
                        $QGRAD = Q($TA[$I],$RHF[$I]) - Q($T[$I],1);
//echo "$TT[$I],$TZ[$I],$TX[$I],$TU[$I],$T[$I]<br>";


// Dew falls everywhere

                        if ($QGRAD > 0)
                        {
```

```
                        $LE[$I] = $EXXO[$I] * 590 * $QGRAD * 60000;
                } else {
                        $LE[$I] = $EXXO[$I] * 590 * $QGRAD * 60000 * $SHRF;
                }
                $SHWO[$K] = $RN[$I]+$S[$I]+$H[$I]+$LE[$I];
        } while (($SHWO[$K] > 1) OR ($SHWO[$K] < -1));

        $RAIN = $RAIN + $LE[$I];
//      if (($TA[$I] < $DP[$I]) && ($DP[$I] < 273.16)) {$RAIN = $RAIN + 500;} //HOAR
FROST
        if ($RAIN < 0)
        {
                $SHRF = 0;
                $RAIN = 0;
        }



// Convert surface temperature to Celsius

        $TC[$I] = $T[$I] - 273.16;
        $T18[$I] = $TZ[$I] - 273.16;
        $T9[$I] = $TX[$I] - 273.16;
        $T5[$I] = $TU[$I] - 273.16;
        $T35[$I] = $TT[$I] - 273.16;
        $TA[$I] = $TA[$I] - 273.16;
//      $TA[$I] -= 273.16;
        $TD[1] = $SURF;
        $INDEX5=($I-1);
        if ($I > 1)
        {
                $TD[$I] = $TC[$I] + ($TD[$INDEX5] - $TC[$I]) / 2;



//Traffic correction


                if (($TR == 1) && ($ROAD[$M] > 3000))
                {
                $TD[$I] = $TD[$I] - 1;
                        if ($LANDUSE[$M] == 5)
                        {
// DEAL WITH DIFFERENCE BTWN MWAY AND A ROAD DUAL CARRIAGEWAY (SING=5)
//                                      IF ($SING[$M]==5)
//                                      {$TD[$I] += 0.75;}ELSE{
                                        if ($ROAD[$M] == 3001) {$TD[$I] += 0.5;}
                                        if ($ROAD[$M] == 3002) {$TD[$I] += 0.5;}
                                        if ($ROAD[$M] == 3004) {$TD[$I] += 0.4;}
//                                      }
                        }
                        if ($LANDUSE[$M] == 4)
                        {
                                if ($ROAD[$M] == 3001) {$TD[$I] += 0.5;}
                                if ($ROAD[$M] == 3002) {$TD[$I] += 0.4;}
                                if ($ROAD[$M] == 3004) {$TD[$I] += 0.3;}
                        }
                        if ($LANDUSE[$M] == 3)
                        {
                                if ($ROAD[$M] == 3001) {$TD[$I] += 0.4;}
                                if ($ROAD[$M] == 3002) {$TD[$I] += 0.3;}
                                if ($ROAD[$M] == 3004) {$TD[$I] += 0.2;}
                        }
                        if ($LANDUSE[$M] == 2)
                        {
                                if ($ROAD[$M] == 3001) {$TD[$I] += 0.3;}
                                if ($ROAD[$M] == 3002) {$TD[$I] += 0.2;}
                                if ($ROAD[$M] == 3004) {$TD[$I] += 0.1;}
                        }
                        if ($LANDUSE[$M] == 1)
                        {
                                if ($ROAD[$M] == 3001) {$TD[$I] += 0.2;}
                                if ($ROAD[$M] == 3002) {$TD[$I] += 0.1;}
                        }
                }



// Topography correction
                if ($TOPO == 1) {}
```

```
// Proximity correction
                        if ($PROX == 1) {}
                }



// Condition parameters
                if ($PRECIPITATION == "0")
                {
                        $CONDITION[$I] = 0;
                } else {
                        $CONDITION[$I] = 1;
                }
                if ($TD[$I] < $DP[$I][$M]) {$CONDITION[$I] = 1;}
                if (($PRECIPITATION == "0") && ($RAIN > 0)) {$CONDITION[$I] = 1;}
                if (($TD[$I] < 0) && ($CONDITION[$I] = 1)) {$CONDITION[$I] = 2;}
//              if (($SNOW == 1) && ($TD[$I] < 2) && ($ALTITUDE[$M] > $SNOWLINE))
{$CONDITION[$I] = 3;}
                if (($SNOW == 1) && ($TD[$I] < 2)) {$CONDITION[$I] = 3;}



// Check for rounding error

                if (($TD[$I] < 0)&&($TD[$I] > -0.1)){$TD[$I]=-0.1;}
                if (($TD[$I] > 0)&&($TD[$I] < 0.1)){$TD[$I]=0.1;}
//echo "$WDIR[$I]<br>";

        } // End temporal loop



// Write RST to route database

        $REC = array($EASTING[$M], $NORTHING[$M], $TD[1], $TD[2], $TD[3], $TD[4], $TD[5],
$TD[6], $TD[7], $TD[8], $TD[9], $TD[10], $TD[11], $TD[12], $TD[13], $TD[14], $TD[15], $TD[16],
$TD[17], $TD[18], $TD[19], $TD[20], $TD[21], $TD[22], $TD[23], $TD[24], $TD[25], $TD[26],
$TD[27], $TD[28], $TD[29], $TD[30], $TD[31], $TD[32], $TD[33], $TD[34], $TD[35], $TD[36],
$TD[37], $TD[38], $TD[39], $TD[40], $TD[41], $TD[42], $TD[43], $TD[44], $TD[45], $TD[46],
$TD[47], $TD[48], $TD[49], $TD[50], $TD[51], $TD[52], $TD[53], $TD[54], $TD[55], $TD[56],
$TD[57], $TD[58], $TD[59], $TD[60], $TD[61], $TD[62], $TD[63], $TD[64], $TD[65], $TD[66],
$TD[67], $TD[68], $TD[69], $TD[70], $TD[71], $TD[72]);
        dbase_add_record($RSTDBF,$REC);


// Write RSC to route database

        $REC = array($EASTING[$M], $NORTHING[$M], $CONDITION[1], $CONDITION[2], $CONDITION[3],
$CONDITION[4], $CONDITION[5], $CONDITION[6], $CONDITION[7], $CONDITION[8], $CONDITION[9],
$CONDITION[10], $CONDITION[11], $CONDITION[12], $CONDITION[13], $CONDITION[14],
$CONDITION[15], $CONDITION[16], $CONDITION[17], $CONDITION[18], $CONDITION[19],
$CONDITION[20], $CONDITION[21], $CONDITION[22], $CONDITION[23], $CONDITION[24],
$CONDITION[25], $CONDITION[26], $CONDITION[27], $CONDITION[28], $CONDITION[29],
$CONDITION[30], $CONDITION[31], $CONDITION[32], $CONDITION[33], $CONDITION[34],
$CONDITION[35], $CONDITION[36], $CONDITION[37], $CONDITION[38], $CONDITION[39],
$CONDITION[40], $CONDITION[41], $CONDITION[42], $CONDITION[43], $CONDITION[44],
$CONDITION[45], $CONDITION[46], $CONDITION[47], $CONDITION[48], $CONDITION[49],
$CONDITION[50], $CONDITION[51], $CONDITION[52], $CONDITION[53], $CONDITION[54],
$CONDITION[55], $CONDITION[56], $CONDITION[57], $CONDITION[58], $CONDITION[59],
$CONDITION[60], $CONDITION[61], $CONDITION[62], $CONDITION[63], $CONDITION[64],
$CONDITION[65], $CONDITION[66], $CONDITION[67], $CONDITION[68], $CONDITION[69],
$CONDITION[70], $CONDITION[71], $CONDITION[72]);
        dbase_add_record($CONDBF,$REC);
//echo "$ZO[$M]<br>";
}
// End spatial loop

dbase_close($DB);
dbase_close($RSTDBF);
dbase_close($CONDBF);

echo "Route Forecast Complete<br><br>";

?>
```